UNIVERSIDADE ESTADUAL PAULISTA
"JÚLIO DE MESQUITA FILHO"
Campus de Botucatu

Instituto de Biociências de Botucatu - Unesp

INTEGRAÇÃO DE DADOS DE TRANSCRIPTOMA E MICRORNOMA PARA IDENTIFICAÇÃO DE REDES REGULATÓRIAS, MEDIADORES E BIOMARCADORES DA CAQUEXIA ASSOCIADA AO CÂNCER

PAULA PACCIELLI FREIRE

BOTUCATU- SP

2020

UNIVERSIDADE ESTADUAL PAULISTA

"Júlio de Mesquita Filho"

INSTITUTO DE BIOCIÊNCIAS DE BOTUCATU

INTEGRAÇÃO DE DADOS DE TRANSCRIPTOMA E MICRORNOMA PARA IDENTIFICAÇÃO DE REDES REGULATÓRIAS, MEDIADORES E BIOMARCADORES DA CAQUEXIA ASSOCIADA AO CÂNCER

PAULA PACCIELLI FREIRE

PROF. DR. ROBSON FRANCISCO CARVALHO

Tese apresentada ao Instituto de Biociências, Campus de Botucatu, UNESP, para a obtenção do título de Doutor no Programa de Pós-Graduação em Ciências Biológicas (Genética)

Orientador: *Prof. Dr. Robson Francisco Carvalho*

BOTUCATU-SP

2020

FICHA CATALOGRÁFICA ELABORADA PELA SEÇÃO TÉC. AQUIS. TRATAMENTO DA INFORM.
DIVISÃO TÉCNICA DE BIBLIOTECA E DOCUMENTAÇÃO - CÂMPUS DE BOTUCATU - UNESP
BIBLIOTECÁRIA RESPONSÁVEL: ROSEMEIRE APARECIDA VICENTE-CRB 8/5651

Freire, Paula Paccielli.
Integração de dados de transcriptoma e microRNoma para identificação de redes regulatórias, mediadores e biomarcadores da caquexia associada ao câncer / Paula Paccielli Freire. - Botucatu, 2020

Tese (doutorado) - Universidade Estadual Paulista "Júlio de Mesquita Filho", Instituto de Biociências de Botucatu
Orientador: Robson Francisco Carvalho
Capes: 20200005

1. Câncer. 2. Caquexia. 3. Marcadores bioquímicos. 4. Transcriptoma. 5. Músculo esquelético. 6. microRNA.

Palavras-chave: Biomarcadores; Caquexia; Músculo esquelético; Transcriptoma; microRNA.

Science works on the frontier between knowledge and ignorance.
We're not afraid to admit what we don't know. There's no shame in that.
The only shame is to pretend that we have all the answers.

Neil Degrasse Tyson

Dedico este trabalho às pessoas que mais me ajudaram nessa jornada e que me incentivaram para a materialização desse objetivo.

minha mãe, Silvia Aparecida Paccielli
e meu pai, Valter de Vasconcelos Freire

Muito obrigada por tudo.
Eu amo vocês.

Agradeço primeiramente ao Robson Francisco Carvalho, meu orientador e grande amigo, pessoa a qual admiro imensamente e tenho como exemplo de competência e profissionalismo. Obrigada por todos os ensinamentos, apoio, incentivo e confiança durante os últimos oito anos, sem os quais eu não chegaria até aqui. Minha vida profissional e pessoal sofreu grandes modificações após a sua entrada em minha vida. Sou muito grata por caminhar ao lado de alguém que possui princípios nobres e trabalha todos os dias por um propósito maior. Muito obrigada por tanto! O mérito desse trabalho também é todo seu.

Agradeço com muito carinho à professora Maeli Dal Pai, minha grande inspiração, que se tornou uma grande amiga durante o período do meu mestrado e doutorado. Obrigada por sempre estar disposta a ajudar e por ser um enorme exemplo de respeito e humildade para todos nós do departamento de morfologia.

Agradeço ao professor Da-Zhi Wang, meu supervisor nos Estados Unidos, com quem aprendi muito sobre respeito e honestidade na pesquisa científica e no ambiente de trabalho. Obrigada por permitir minha experiência internacional em um laboratório de ponta, por ter acreditado em mim e por me incentivar a buscar cada vez mais conhecimento.

Agradeço do fundo do meu coração aos meus pais, Valter de Vasconcelos Freire e Silvia Aparecida Paccielli, e aos meus irmãos, Carolina Paccielli Franco e José Vitor de Vasconcelos Freire. Obrigada por terem dedicado a mim tanto amor e paciência. Sei que vocês batalharam muito e se esforçaram ao máximo pensando no meu bem. Tenho muito orgulho de vocês e sou muito grata por ter escolhido vocês como minha família. Toda a minha dedicação, persistência no trabalho e na vida é para um dia poder retribuir tudo o que vocês fizeram por mim. Eu amo vocês mais que tudo.

Agradeço meus avós, José de Vasconcelos e Helena Pera, meus tios, Cecília Froner, Edemar Froner, Verginia Vasconcelos, Alexandre Tosetto, Nanci Paccielli e Denise Figueiredo, e meu cunhado Leandro Garcia. Obrigada pelo apoio e por todo o carinho que vocês sempre dedicaram a mim.

Agradeço muito ao meu namorado, João Marcos de Mattos Barguil, que foi a pessoa mais incrível que surgiu em minha vida nos últimos anos, me presenteando com seu amor, amizade e companheirismo. Muito obrigada por me ensinar o tempo todo e por me orientar nas horas mais difíceis. Você sempre foi um enorme exemplo de dedicação e discernimento. Sou uma pessoa melhor agora que tenho você comigo. Amo muito você e quero caminhar sempre ao seu lado na direção de um propósito maior. Agradeço também a Francisco Barguil e Ana Lúcia Barguil, pessoas maravilhosas que tive a sorte de conhecer e que agora são parte da minha família. Vocês são grandes exemplos para mim. Obrigada pelos ensinamentos, por tanto carinho e acolhimento.

Agradeço aos membros da banca de qualificação e de defesa, Patrícia Pintor dos Reis, Maeli Dal Pai Silva, Erick da Cruz Castelli, Edilamar Menezes de Oliveira, Rodrigo Wagner Alves de Souza, Luiz Gustavo de Almeida Chuffa e Luis Fernando Barbisan, pela disponibilidade, pelos valorosos conselhos e sugestões para a melhoria desse trabalho. Aproveito para agradecer o professor Luis Fernando Barbisan também pela supervisão durante o período de estágio docência, sua conduta me inspirou muito e aumentou ainda mais o meu desejo de me tornar professora universitária.

Agradeço a todos os docentes e funcionários do Departamento de Morfologia, especialmente os professores Wellerson Rodrigo Scarano (grande amigo), Luis Antonio Justulin Jr., Sérgio Luis Felisbino e Flávia Karina Delella. Obrigado por todo o aprendizado e pelo convívio diário.

Agradeço ao meu grande e eterno professor Antonio Carlos Cicogna, por ter me ensinado tanto sobre ética profissional e disciplina, por ter me preparado para o mundo acadêmico e por ser um incentivador de grandes mentes. Obrigada por me apoiar tanto e por estar sempre presente.

Agradeço a todos os amigos, novos e antigos, do Laboratório de Biologia do Músculo Estriado, Ana Omoto, Ana Carolina Alvarez, Bruna Zanella, Brunno Vivone, Bruno Fantinatti, Diogo Moraes, Douglas Marques, Erika Perez, Geysson Fernandez, Grasieli de Oliveira, Isabele Magiore, Jakeline Oliveira, Jefferson Souza, Jéssica Silvino, João Paulo Cunha, Juarez Ferreira, Leonardo de Moraes, Letícia Oliveira, Maria Laura Kuniyoshi, Mathias Chaves, Pedro Guilherme, Rafaela Nunes, Tassiana Gutierrez. Agradeço especialmente à Sarah Cury e Bruno Duran, que são meus grandes amigos e companheiros, os quais estiveram presentes em todos os meus melhores e piores dias durante a pós-graduação. Agradeço pelas risadas, pelo trabalho e por me ajudarem a crescer profissionalmente e pessoalmente.

Agradeço aos funcionários e colegas do Children's Hospital – Harvard Medical School, Xiaoyun Hu, Justin King, Yao Wei Lu, Vanessa Lima, Sumei Cui, Jing Lin, Katia Andrade, Yi Wang, Haipeng Guo, Cheng Fan, Erica Sousa, Tingting Wang e Panpan Hao. Agradeço especialmente ao Jianming Liu, meu amigo supervisor, que me auxiliou em todos os meus experimentos durante os seis meses de estágio no exterior. Obrigada pelos muitos ensinamentos. 謝謝你.

Agradeço aos meus amigos do Departamento de Morfologia, Ana Carolina Camargo, Ariana Musa, Bruno Martinucci, Caroline Barquilha, Caio Cesar, Cecilia Luvizutti, Cristiane Pinho, Elian Ribeiro, Flávia Bessi, Francielle Mosele, Helga Nunes, Isabela Barbosa, Jordana Oliveira, Ketlin Colombelli, Luiz Frediane, Maira Cucielo, Matheus Fioretto, Nilton Santos, Sérgio Alexandre dos Santos, Teng Fwu Shing e Vivian Cypriano. Obrigada pelo cafezinho diário, pelos encontros e por tornarem nosso ambiente de trabalho tão agradável. Nosso departamento possui uma harmonia inigualável.

Agradeço às minhas amigas Danielle Vileigas e Priscila Sales, por terem participado intensivamente desses meus dois últimos anos de doutorado. Obrigada pela amizade de vocês, pelas alegrias vividas, pelo apoio em todas as horas e, principalmente, pelos trabalhos desenvolvidos em conjunto.

Agradeço às minhas amigas de Botucatu, Vanessa Carvalho, Maria Carolina Vieira, Tainá Silva, Carolina Benato, Jéssica Nicolai e Isadora Tiegui, e aos meus amigos da universidade, Camila Pergentino, Claudia Diniz, Marcela Martins, Heloísa Bortolin, Mariane Gonçalves, André Sartori, Henrique Silva, Carlos Alves, Leandro Inson, Jonas Vieira e Danilo Hohne. Obrigada por estarem sempre do meu lado, comemorando minhas conquistas e me apoiando durantes os momentos difíceis. Não seria nada sem vocês.

Agradeço à seção técnica da Pós-Graduação, que sempre soube me auxiliar em tudo. Em especial, agradeço muito ao Davi Müller, um profissional excelente, paciente e muito prestativo. Obrigada por me ajudar durante esses seis anos de pós-graduação. Você é um grande exemplo para todos.

Agradeço ao Conselho Nacional de Desenvolvimento Científico e Tecnológico (CNPq) pela bolsa de doutorado: 141919/2016-7. Agradeço à Coordenação de Aperfeiçoamento de Pessoal de Nível Superior (CAPES) pelo auxílio financeiro para o desenvolvimento da pesquisa no exterior: programa PDSE processo 88881.187095/2018-01.

Sumário

Integração de dados de transcriptoma e microRNoma para identificação de redes regulatórias, mediadores e biomarcadores da caquexia associada ao câncer.

A caquexia associada ao câncer é uma síndrome metabólica complexa caracterizada pela perda de massa muscular, com ou sem perda de tecido adiposo, a qual não pode ser revertida por suporte nutricional. Pacientes com essa síndrome apresentam alterações funcionais em processos fisiológicos, metabólicos e imunológicos que resultam em um desequilíbrio energético e proteico. A caquexia associada ao câncer afeta até 80% dos pacientes em estágios avançados da doença, e representa a causa de morte de até 20% de todos os pacientes. Tipos específicos de tumores, como o de pâncreas, esôfago, estômago, cabeça e pescoço e pulmão apresentam uma alta prevalência de caquexia e, em contrapartida, os pacientes acometidos por câncer de mama ou próstata apresentam um menor risco de desenvolver a síndrome. As vias moleculares responsáveis pela caquexia não estão completamente esclarecidas, entretanto, evidências sugerem que citocinas pró-inflamatórias possuem um papel fundamental no desenvolvimento de alterações metabólicas que resultam na perda de função e massa muscular. A complexidade dessas alterações também sugere o envolvimento de moléculas reguladoras pós-transcricionais, como os microRNAs (miRNAs). Essas moléculas trabalham de forma orquestrada para controlar uma via ou função biológica comum, sendo consideradas ferramentas eficientes para determinação de vias específicas envolvidas em doenças ou processos biológicos. O presente trabalho realizou três estratégias diferentes para identificar redes regulatórias, mediadores e biomarcadores da caquexia associada ao câncer. No primeiro capítulo, avaliamos o perfil de expressão de miRNAs na atrofia de células musculares esqueléticas induzida por IL-6, uma importante molécula indutora de caquexia. Essa análise identificou o miR-497 associado a um potencial mecanismo anti-atrófico em resposta à IL-6. No segundo capítulo, como há uma diversidade de modelos experimentais, heterogeneidade entre pacientes e tipos tumorais nos estudos de caquexia, realizamos uma revisão sistemática e meta-análise para integrar dados de mRNAs e miRNAs do músculo esquelético na caquexia associada ao câncer. Essa estratégia identificou vias moleculares, novas interações entre mRNAs e miRNAs e potenciais alvos de drogas para a síndrome. No último capítulo, considerando que a prevalência da caquexia varia de acordo com o tipo tumoral, avaliamos dados de transcriptoma de 12 tipos tumorais humanos (4.651 amostras) comparadas com os respectivos tecidos não doentes (2.737 amostras). Nossos dados mostram um perfil tumor-específico de mediadores de caquexia e observamos que os tumores que apresentam uma alta prevalência de caquexia possuem um número elevado de fatores indutores de caquexia. Além disso, a expressão desses mediadores está associada a um pior prognóstico (sobrevida). Em conjunto, esses resultados poderão servir de base para estudos funcionais e desenvolvimento de futuras estratégias terapêuticas visando a minimização da perda de massa muscular, aumentando assim a sobrevida e a melhora da qualidade de vida dos pacientes com caquexia.

Transcriptome and microRNome integration to identify regulatory networks, mediators and biomarkers of cancer cachexia

Cancer cachexia is a complex metabolic syndrome characterized by muscle mass loss, with or without loss of adipose tissue, which cannot be reversed by nutritional support and leads to progressive functional impairment. Patients with this syndrome have functional changes in physiological, metabolic and immunological processes that result in energy and protein imbalances. Cachexia affects up to 80% of patients in advanced stages of cancer, and represents the cause of death for up to 20% of all cancer patients. Specific types of tumors, such as pancreas, esophagus, head and neck, stomach, and lung, have a high prevalence of cachexia and, similarly, patients with these neoplasms have greater weight loss. In contrast, patients with breast or prostate cancer have a lower risk of developing the syndrome. The molecular pathways responsible for cancer cachexia are not completely understood, but evidence suggests that pro-inflammatory cytokines play a fundamental role in the development of metabolic changes that result in function and muscle mass loss. The complexity of these changes also suggests the involvement of post-transcriptional regulatory molecules, such as microRNAs (miRNAs). These molecules work in an orchestrated way to control a common biological pathway or function, being considered efficient tools for determining specific pathways involved in diseases or biological processes. The present work carried out three different strategies to identify regulatory networks, mediators and biomarkers of cachexia associated with cancer. In the first approach, we evaluate the expression profile of miRNAs in skeletal muscle cells atrophy induced by IL-6, an important cachexia-inducing molecule. This analysis identified miR-497 as a miRNA associated with a potential anti-atrophic mechanism in response to IL-6. In the second strategy, as there is a diversity of experimental models and heterogeneity between patients and tumor types in cachexia associated with cancer, we integrate data from skeletal muscle mRNAs and miRNAs in this syndrome, obtained in the literature from a systematic review and meta-analysis. This strategy identified molecular pathways, new interactions between mRNAs and miRNAs, and potential drug targets for the syndrome. In the last approach, considering that the prevalence of cachexia varies according to the tumor type, we evaluated transcriptome data from 12 human tumor types (4,651 samples) compared with the respective non-diseased tissues (2,737 samples). Our data show a tumor-specific profile of cachexia mediators, and that tumors that have a high prevalence of cachexia have a high number of cachexia-inducing factors. In addition, the expression of these mediators is associated with a worse prognosis. Together, these results may be useful as a basis for functional studies and to the development of future therapeutic strategies aimed at minimizing the loss of muscle mass, thus increasing survival and improving the patients' quality of life.

Introdução

Atrofia do músculo esquelético

O músculo esquelético compreende aproximadamente 40-50 % da massa corpórea em humanos e é responsável por funções básicas como locomoção, metabolismo e respiração, além de apresentar uma alta plasticidade em resposta às mudanças nas demandas funcionais; exercícios de resistência induzem a hipertrofia do músculo esquelético, a qual é caracterizada por aumento na síntese de proteínas, no diâmetro fibra e na produção de força [1,2]. Contrariamente, condições de desuso, imobilização, repouso prolongado em leito, desnervação, microgravidade, envelhecimento e restrição alimentar resultam em perda de massa muscular, conhecida como atrofia do músculo esquelético [3–6].

Em condições catabólicas como câncer, sepse, queimadura, insuficiência cardíaca e AIDS, o tecido muscular, por ser um reservatório de proteína do corpo, atua como fonte de aminoácidos que podem ser utilizados para a produção de energia por vários órgãos (incluindo o coração, fígado e cérebro). No entanto, a degradação excessiva de proteínas e a perda de músculo resultante são altamente prejudiciais e podem levar à morte desses pacientes [7]. Além disso, a perda exacerbada de massa muscular é um indicador de prognóstico desfavorável e pode prejudicar a eficácia de muitos tratamentos terapêuticos [7,8]. Assim, a atrofia muscular agrava as doenças, aumentando a morbidade e a mortalidade. Portanto, a manutenção de músculos saudáveis é crucial para prevenir distúrbios metabólicos, manter um envelhecimento saudável e fornecer energia aos órgãos vitais durante condições de estresse (para revisão, ver Bonaldo e Sandri 2013) [7].

Estudos demonstram que a atrofia do músculo esquelético é controlada pela ação coordenada de vias reguladoras chaves envolvendo IGF1-AKT-FoxO, miostatina, citocinas inflamatórias e o fator transcricional NF-kappa B (NF-kB) [3,9] [para revisão, ver Braun & Gautel 2011[10]]. Posteriormente, vários sistemas de proteólise, tais como o que envolve as proteases lisossomais (catepsinas), as calpaínas dependente de cálcio e o proteassomal dependente de ubiquitina são ativados para degradação da maioria das proteínas musculares [4,5,11].

Caquexia

A atrofia do músculo esquelético é um fenômeno comum em várias condições sistêmicas crônicas como septicemia, insuficiência cardíaca crônica, doença pulmonar obstrutiva crônica, doença renal crônica, diabetes, AIDS e câncer [12–14]. Essas condições podem ser acompanhadas de uma síndrome metabólica complexa caracterizada pela diminuição de massa muscular, com ou sem diminuição de massa gorda, denominada de caquexia [12,14–16]. A característica clínica mais proeminente

da caquexia é a perda de peso nos adultos (corrigida pela retenção fluídica) ou o distúrbio de crescimento nas crianças (excluindo desordens endócrinas) [15,16]; além disso, sabe-se que esta síndrome não pode ser revertida por suporte nutricional convencional [16].

A caquexia emerge a partir de alterações metabólicas do organismo em resposta a uma dessas condições crônicas, como por exemplo, o câncer. Nessa condição, as citocinas liberadas pelo tumor ganham a circulação sanguínea e são responsáveis por gerar uma inflamação sistêmica que afeta diversos órgãos como o cérebro e o fígado, e tecidos como o adiposo e muscular, com consequente indução de anorexia, fadiga, anemia, aumento da termogênese e, principalmente, perda de massa muscular, a qual pode ou não ser acompanhada de perda do tecido adiposo (**Figura 1**) [16–18].

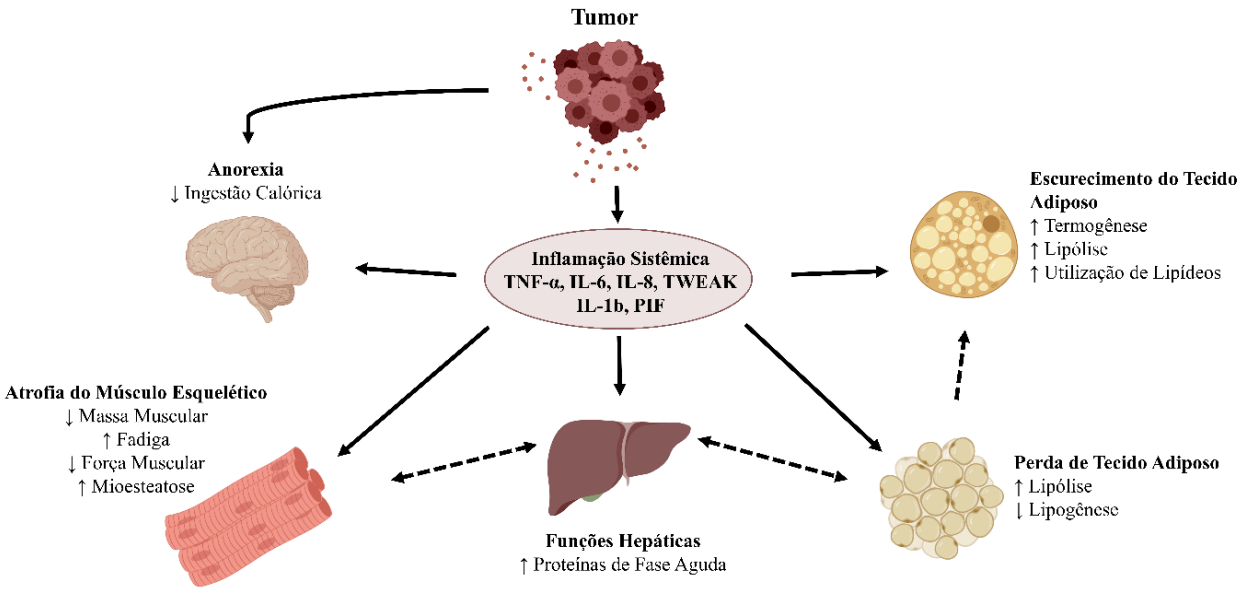

Figura 1. Alterações metabólicas na caquexia associada ao câncer. Citocinas são secretadas pelo tumor e levam a alterações metabólicas em diversos tecidos, tais como: modificação do controle neuroendócrino do apetite; redução da função e massa muscular; escurecimento e perda do tecido adiposo; e aumento da síntese de proteínas de fase aguda no fígado [adaptado de Tsoli & Robertson [19]].

A diminuição na ingestão do alimento e perda de massa corpórea resultam numa condição de astenia, imobilidade e insuficiência respiratória ou cardíaca [12]. O estado caquético é particularmente importante no câncer, representando pobre prognóstico e diminuição da resposta ao tratamento rádio e quimioterápico [13]. Além disso, sabe-se que a caquexia afeta cerca de 50% dos pacientes quando todos os tipos de tumores são considerados [20]; até 83% dos pacientes com câncer gástrico ou pancreático desenvolvem caquexia [13,17,19,21] (**Tabela 1).**

Tabela 1. Incidência de perda de peso em diferentes tipos de tumores (adaptado de Laviano 2005 [20])

Tumor	Incidência de Perda de Peso (%)
Pâncreas	83
Gástrico	83
Esôfago	79
Cabeça e Pescoço	72
Colorretal	55-60
Pulmão	50-60
Próstata	56
Mama	10-35
Outros	63

A etiologia da caquexia associada ao câncer em diferentes tipos tumorais envolve interações tumor-hospedeiro muito complexas e específicas que ainda precisam ser completamente elucidadas. A ação combinatória de mediadores solúveis (mediadores caquéticos) secretados por células tumorais e células não-tumorais do microambiente tumoral (MAT), incluindo citocinas pró-inflamatórias, contribuem para uma inflamação sistêmica, e atuam diretamente no músculo esquelético, induzindo a perda de massa muscular [19,22–24].

Secretoma tumoral

Recentes avanços na genômica, transcriptômica e proteômica tem auxiliado a esclarecer os efeitos de citocinas e fatores solúveis do MAT através da análise do secretoma tumoral [22]. O secretoma representa o conjunto de macromoléculas secretadas por células, as quais permitem a comunicação celular [25,26]. O termo secretoma foi cunhado por Tjalsma *et al.*[27] para denotar todos os fatores secretados por uma célula e, também, os constituintes da via secretória. A definição de secretoma foi posteriormente revisada para incluir apenas proteínas secretadas no espaço extracelular [24, 25].

O secretoma tumoral apresenta um papel importante em processos biológicos do câncer tais como proliferação celular, apoptose, angiogênese, alterações no metabolismo energético e desenvolvimento de resistência contra a terapias anticâncer [25]. O secretoma pode ser avaliado pela análise do meio condicionado de linhagens celulares, de líquidos intersticiais do tecido ou tumor, e de fluídos corporais (revisado por Schaaij-Visser *et al.*[28]). Portanto, a análise do secretoma tem grande pontencial para revelar mediadores, biomarcadores e alvos para tratamento da caquexia associada ao câncer.

Algumas abordagens transcriptômicas e algoritmos emergentes para predição de sequências peptídeo-sinal tornaram-se ferramentas úteis para identificar o perfil do secretoma [29] e também revelaram que uma grande fração de proteínas enriquecidas nos tecidos humanos é secretada [30]. Utilizando essa abordagem, um estudo recente apresentou uma análise *Pan-Cancer* da expressão gênica de componentes do secretoma, a qual resultou em candidatos a biomarcadores diagnósticos detectáveis em fluidos biológicos [31]. Essa investigação também revelou os padrões e as funções biológicas associadas às alterações na expressão de proteínas secretadas em diferentes tipos tumorais.

Com o avanço de tecnologias para a análise de expressão gênica na última década e os experimentos em larga escala, grandes quantidades de dados estão gerados e estão sendo depositados em bancos públicos, tornando-se acessíveis para toda comunidade científica [32]. A integração de dados ômicos disponíveis em bancos de dados é capaz de gerar respostas biológicas, que, talvez, em estudos individuais não pudessem ser obtidos [32]. A reutilização dos dados disponíveis em bancos públicos podem auxiliar na identificação de novas vias moleculares e mediadores caquéticos que são potencialmente secretados pelas células tumorais.

Vias moleculares e citocinas associadas à caquexia

As vias moleculares responsáveis pela caquexia não estão completamente esclarecidas, entretanto, evidências sugerem que citocinas pró-inflamatórias como interleucina-1β (IL-1β), fator de necrose tumoral (TNF)-α, interferon (INF)-γ e interleucina-6 (IL-6) possuem um papel fundamental, principalmente no desenvolvimento de alterações celulares e moleculares em células musculares [33,34]. Essas citocinas acarretam a ativação de diferentes vias, tais como: *Nuclear Factor Kappa-light-chain-enhancer of activated B cells* (NF-kB), *Signal Transducer and Activator of Transcription* (STAT), MAP kinase family (MAPKs) e *Activator Protein 1* (AP-1). A transdução de sinal para os fatores de transcrição NF-kB e STAT tem um papel fundamental, especialmente durante as alterações celulares e moleculares que resultam na regulação de genes envolvidos em três principais vias moleculares: a) sistema proteossomal dependente ubiquitina, b) Via de sinalização IGF1-AKT-FoxO e c) sistema autofágico-lisossomal; que resultam em um desequilíbrio entre a síntese e a degradação das proteínas musculares, acarretando diminuição na massa e função muscular [35].

Via ubiquina-proteassomal: a degradação de proteínas através do sistema proteossomal dependente de ubiquitina é a principal via de proteólise, não lisossômica, de proteínas intracelulares. As proteínas são direcionadas para a degradação, por modificação covalente com a ubiquitina. Essa ativação requer ações coordenadas de três enzimas: enzimas ativadoras de ubiquitina (E1), enzimas

conjugadoras de ubiquitina (E2) e ubiquitina ligases (E3) que reconhecem a proteína específica que será ligada à ubiquitina para posterior degradação nos proteossomos [36]. O papel central das ligases de ubiquitina E3 na atrofia do músculo esquelético geralmente é devido à redução da síntese proteica, aumento da degradação, ou um desequilíbrio relativo entre os dois processos [36,37]. Esses mediadores de sinalização regulam a expressão das ligases E3, como o *Tripartite Motif Containing 63-E3 Ubiquitin Protein Ligase*, TRIM63 (MuRF1, na Figura 2) e *F-Box Protein 32*, FBXO32 (Atrogin-1, na Figura 2), que atuam na degradação das proteínas sarcoméricas e na inibição da síntese proteica [7,36]. Atrogin-1 induz a ubiquitinação de um eIF3f, que faz atua principalmente na maquinaria de tradução de proteínas [38].

Via de sinalização IGF1-AKT-FOXO: O conteúdo total de proteínas no interior da fibra muscular é regulada por uma interação entre os processos de síntese e degradação de proteínas [39]. Um dos mecanismos mais caracterizados de síntese proteica é o da sinalização de IGF1 (*insulin-like growth factor 1*). A via que acarreta a hipertrofia durante a ativação do IGF1 é IRS1/PI3K/AKT/mTOR [40] (**Figura 2**). O AKT induz a ativação da síntese proteica bloqueando a repressão do mTOR, que por sua vez mantém a massa muscular através de dois complexos distintos, conhecidos como TORC1 e TORC2 [40]. A TORC1 estimula a via da p70S6 quinase e 4E-BP, que ativam a formação do complexo ribossomal, com consequente indução da síntese de proteínas [41].

Sistema autofágico-lisossomal: Em condições de atrofia, além da proteólise mediada por ubiquitina, há a indução da autofagia que contribui para a degradação de proteínas musculares e, consequentemente, para a atrofia muscular [42]. Na autofagia, as organelas são sequestradas em vacúolos autofágicos que se fundem com lisossomos e tornam-se digeridas por enzimas lisossômicas [43]. Os genes de autofagia e o sistema proteolítico lisossômico são ativados durante a desnervação e câncer e, em ambos os casos, contribuem para a atrofia através da atividade de FOXO [44] (**Figura 2**). Estudos demonstraram que o análogo à proteína AKT, a FOXO3 é regulada negativamente pela PGC-1α. O PGC-1α é regulada negativamente nos músculos de ratos portadores de tumor e em outras condições de perda de massa muscular, e o aumento da expressão gênica de PGC-1α é capaz de amenizar a perda de músculo, através da inibição de FOXO3 e pela produção de produtos metabólicos [45].

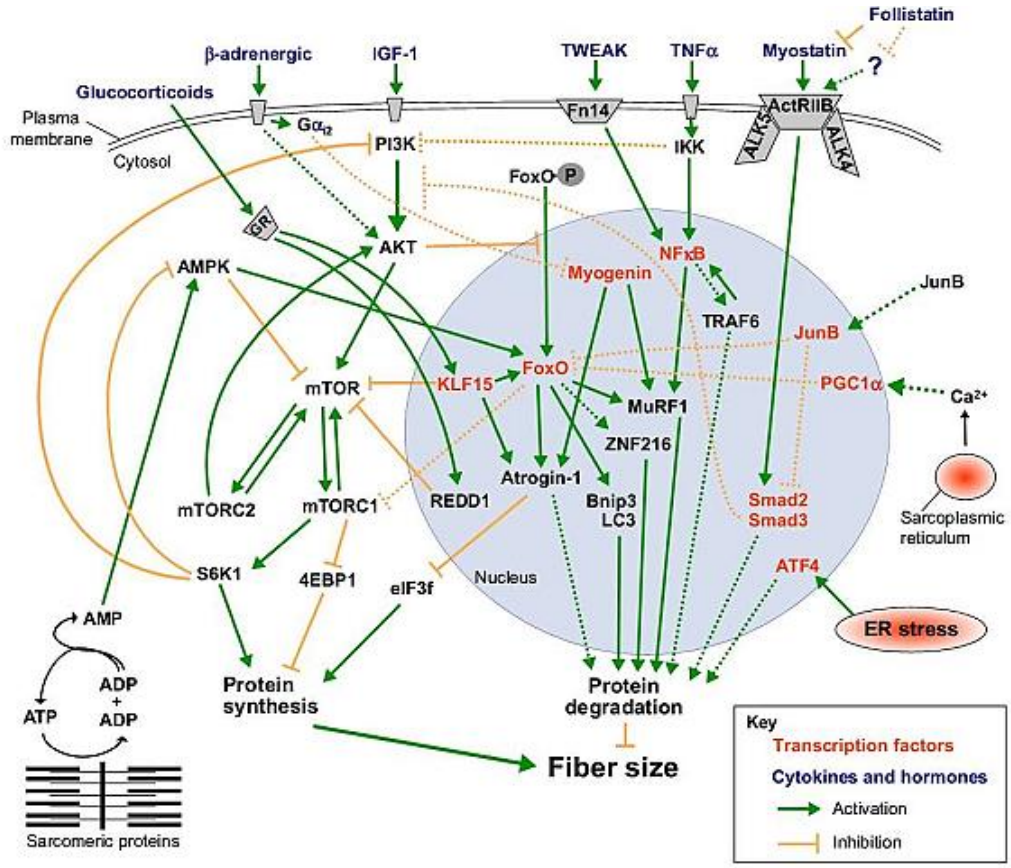

Figura 2. Principais vias que controlam a massa proteica da fibra muscular. A síntese e a degradação de proteínas são reguladas por vários estímulos diferentes, que ativam múltiplas vias de sinalização, muitas das quais convergem em elementos intermediários comuns. Linhas pontilhadas descrevem vias nas quais os mecanismos moleculares ainda não foram completamente esclarecidos no músculo esquelético adulto [adaptado de Bonaldo et al, 2013 [7]].

Além das vias mencionadas acima, destacamos que diversos autores já avaliaram os mecanismos pelos quais as citocinas pro-inflamatórias induzem isoladamente a degradação de proteínas em células musculares [46–51]. Também já foi descrito que altos níveis de citocinas inflamatórias causam alterações na matriz extracelular que impedem a regeneração de fibras musculares [52,53]. Um estudo demonstrou que as citocinas catabólicas IL-1α, TWEAK, IL-1β e TNF-α induzem efeitos catabólicos mediada pelo fator transcricional p65 em cultura de miotubos [51]; ainda segundo esses autores, a atrofia de miotubos induzida isoladamente pela IL-6 é a única independente do p65 e os mecanismos moleculares ainda não estão completamente esclarecidos. Além disso, foi descrito uma correlação inversa entre altos níveis de IL-6 e o tempo de sobrevida de pacientes com câncer em estágio avançado, sugerindo que essa citocina possui um valor prognóstico importante em pacientes com caquexia associada ao câncer [54].

IL-6 é uma citocina pleiotrópica e, além do seu papel na atrofia de células musculares, também é essencial para cicatrização e regeneração de tecidos, tumorigênese, produção de proteínas de fase aguda do fígado [55,56] e hipertrofia do tecido muscular [57]. Durante o exercício físico, há um aumento na concentração circulante de diversas citocinas, incluindo a IL-6, a qual é produzida pelo próprio músculo esquelético em regeneração e em condições hipertróficas [58,59]. Além disso, a IL-6 apresenta uma importante função como um regulador da ativação de células satélites, uma vez que a deficiência de IL-6 prejudica a ativação da STAT3 e a expressão de seu alvo Ciclina D1 e, consequentemente, deprime a proliferação de células satélites [60]. Esses efeitos paradoxais da IL-6, a qual atua em processos distintos, como hipertrofia e atrofia muscular, tem sido atribuídos a uma função temporal dessa citocina, e pode estar relacionado às respostas distintas entre as exposições aguda ou crônica à IL-6 [61].

A função da IL-6 envolve ativação dos leucócitos, particularmente através da diferenciação de macrófagos para um fenótipo anti-inflamatório [62]. A família da citocina IL-6 compartilha o receptor secundário glicoproteína 130 (gp130). O complexo IL-6 / mIL-6R (receptor de membrana IL-6R) recruta duas subunidades gp130 para induzir a ativação da via JAK/STAT (Janus Kinase/ Signal Transducer and Activator of Transcription) e da sinalização da via ERK (Extracellular Signal-Regulated Kinases). A fosforilação da STAT-3 conduz à transcrição de SPE-3, um regulador negativo da sinalização de IL-6 [63,64]. A sinalização clássica da IL-6, limitada pela expressão celular de mIL-6R leva à proliferação, regeneração e resposta de fase aguda (APR) em tecidos-alvos [65]. No entanto, em condições crônicas como caquexia associada ao câncer, a ativação prolongada da proliferação e APR pode levar a tumorigênese e hipermetabolismo, conduzindo ao recrutamento adaptativo do sistema imune e da sinalização de IL-6R (sIL-6R) solúvel.

IL-6 na caquexia associada ao câncer

Diversos trabalhos demonstraram que a perda muscular durante a caquexia associada ao câncer possui dois mecanismos: um envolvendo a supressão da síntese de proteínas e outro relacionado à ativação de diversas vias de degradação de proteínas [66–68]. Adicionalmente, os níveis de IL-6 estão elevados em pacientes com câncer e modelos experimentais de caquexia [69–71] e, dentre esses, a IL-6 está envolvida com a perda de massa muscular de camundongos com caquexia associada ao câncer de cólon-26 (C26) e a caquexia associada ao carcinoma cervical uterino [70–79]. A suramina, um antagonista da IL-6 ao seu receptor, diminui acentuadamente a taxa de caquexia em camundongos portadores de tumores C26 [70], enquanto que a utilização de anticorpos neutralizadores contra IL-6 levam a uma diminuição da perda de massa muscular em ratos com carcinoma cervical uterino [71]. A inibição da IL-6 utilizando o anticorpo contra o receptor solúvel (sIL-6R) também reduz a atrofia muscular em

modelo de câncer intestinal utilizando camundongos com câncer colorretal [80]. Em humanos, estudos demonstraram que a IL-6 é um indicador muito sensível para perda de massa muscular em pacientes com câncer de cólon [81,82] e câncer de pulmão [83]. Assim, a citocina IL-6 permanece como uma estratégia terapêutica promissora para atenuar a progressão da caquexia em diversos tipos de câncer. No entanto, ainda é necessária uma melhor compreensão dos efeitos diretos e indiretos da IL-6, bem como entender melhor suas funções em diferentes tecidos, incluindo tecido muscular, de pacientes com câncer.

Embora alguns componentes das vias moleculares envolvidas na atrofia de células pela IL-6 já tenham sido descritos, ainda é necessário elucidar os mecanismos globais de controle da expressão gênica responsáveis pelas alterações moleculares na atrofia muscular induzida por essa citocina durante a caquexia. A complexidade desses mecanismos de controle da expressão gênica nesse processo sugere o envolvimento de moléculas reguladoras adicionais, como os microRNAs (miRNAs); essas pequenas moléculas de RNA não codificantes regulam a função do músculo esquelético durante o desenvolvimento e estão envolvidas em diversas doenças musculares [84].

MicroRNAs e a regulação da expressão gênica

MiRNAs são pequenos RNAs reguladores não codificantes com tamanho variando de 17 a 25 nucleotídeos (ver miRBase, http://microrna.sanger.ac.uk/). A definição de miRNA é baseada na sua formação pela ação da enzima RNase III (Dicer), uma RNase que processa precursores com estrutura de *hairpin* (conhecidos como pré-miRNA) originando o miRNA maduro [85]. Essas moléculas reprimem pós-transcricionalmente a expressão proteica pelo reconhecimento de locais complementares na região 3’ não traduzida (3’ UTR) de seus RNAs mensageiros (mRNA) alvos.

Atualmente, estão registrados no banco de dados miRBase (miRBase v. 22.1, outubro 2018) mais de 50492 miRNAs de 285 organismos e são conhecidos atualmente 2883 miRNAs maduros humanos e 2110 miRNAs maduros em camundongos. Os miRNAs são nomeados como miR- mais números (ex: miR-133), entretanto, existem algumas exceções. Os miRNAs de sequências similares são geralmente distinguidos por uma letra adicional seguida do número do miRNA (ex: miR-133a). Um miRNA com uma sequência madura idêntica pode aparecer em diferentes *loci* genômicos com diferentes sequências precursoras, nesses casos, os diferentes genes de miRNA são usualmente distinguidos por outro número adicional no final da sequência (ex: miR-133a-1).

A biogênese de um miRNA começa com a síntese de um longo transcrito primário conhecido como pri-miRNA. Os pri-miRNAs são preferencialmente transcritos pela RNA polimerase II e possuem estrutura de *cap* na sua região *5’* e a cauda de poli (A) na sua região 3’UTR [86–88]. Entretanto, a RNA polimerase III é responsável por gerar um conjunto menor de miRNAs, a partir da transcrição

de miRNAs localizados em repetições genômicas do tipo Alu [89]. No núcleo, o pri-miRNA é processado para pré-miRNA pela enzima RNAse III (Drosha), a qual requer um cofator, a proteína DGCR8 (*DiGeorge Syndrome critical region gene 8*) em humanos (Pasha em *D. Melagonaster* e *C. Elegans*) [90–93]. A DGCR8 forma com a Drosha um grande complexo conhecido como complexo microprocessador, que em humanos possui ~650 kDa [91–93]. Esse complexo microprocessador reconhece e cliva o pri-miRNA, originando uma molécula com estrutura de *hairpin* de aproximadamente 70 pb, o pré-miRNA [94,95]. Um subconjunto de miRNAs, conhecidos como miRtrons utiliza uma via alternativa, na qual os pré-miRNA são derivados como produto secundário de um evento de *splicing*, sem a necessidade de processamento pela Drosha [96–98]. Após o processamento nuclear, cada pré-miRNAs é exportado para o citoplasma pela exportina-5 (EXP5), membro da família de receptores de transporte sendo convertido para miRNAs maduro e funcional pela Dicer nuclear [99–101]. Após a clivagem pela Dicer, a molécula de dupla fita de RNA com aproximadamente 22 nucleotídeos associa-se à proteína Argonauta para formar o complexo de silenciamento induzido por RNA (RISC) [102]. Uma das fitas de aproximadamente 22 nucleotídeos do RNA dupla fita permanece na proteína Argonauta como o miRNA maduro (fita guia ou miRNA), enquanto a outra fita (fita passageiro ou miRNA) pode ser degradada ou, em algumas situações, ambas as fitas podem atuar como fita guia e/ou passageiro [103–105]. Da mesma maneira como ocorre a seleção de um siRNA [106,107], a fita que possui sua extremidade 5’ formando o duplex mais instável com sua fita parceira parece preferencialmente sobreviver como o miRNA no RISC [95,106,107]. O complexo miRNA-RISC interage com sítios ligantes da região 3' UTR do RNA mensageiro alvo inibindo a expressão ou degradando o RNA mensageiro alvo [108,109]. A interação entre o RNA mensageiro alvo e o complexo miRNA-RISC ocorre devido à complementaridade total ou parcial de uma sequência de 5-7 nucleotídeos do miRNA e do RNA mensageiro alvo [108,110].

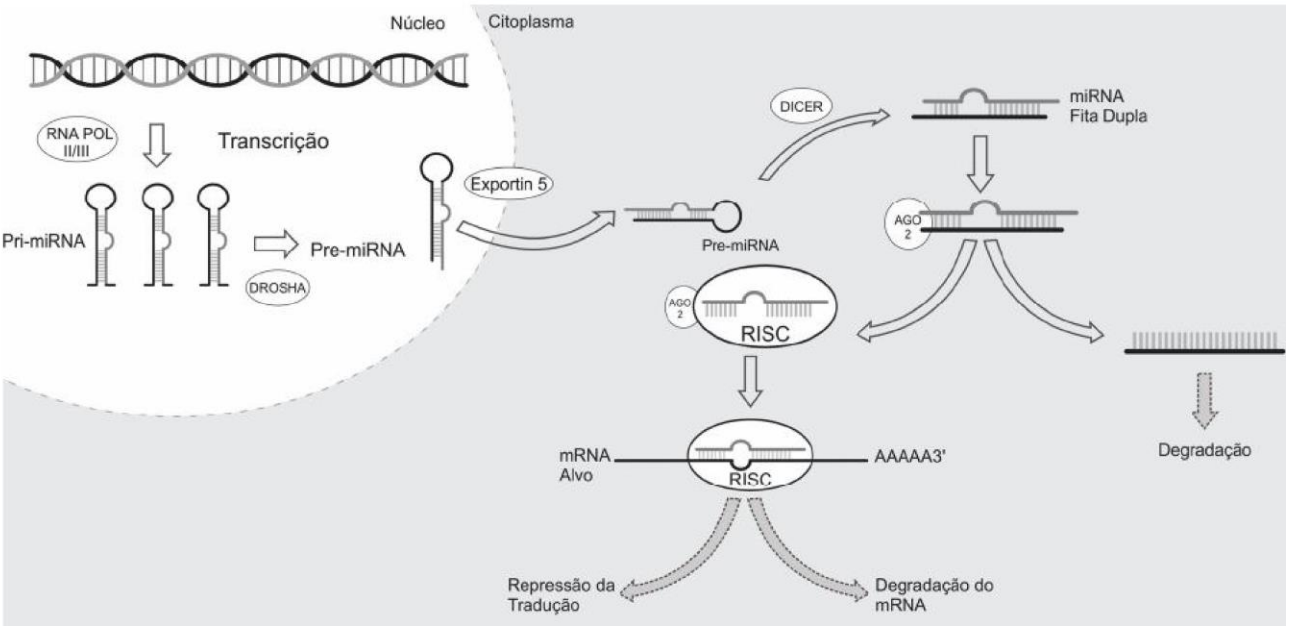

Figura 3. Biogênese e principais mecanismos de ação dos miRNAs. A enzima RNA polimerase II realiza a transcrição dos miRNAs primários (pri-miRNA). O complexo enzimático *Drosha* cliva os grampos formando precursores do miRNA (pre-miRNA), os quais são carreados ao citoplasma e associados ao complexo *Exportin-5-Ran-GTP-dependent (Exportin 5)*. No citoplasma, o pre-miRNA é clivado pelo complexo *Dicer*, perdendo a configuração em grampo. O miRNA fita-dupla formado associa-se à proteína Argonauta 2 e uma das fitas é acoplada ao complexo de proteínas que reprime a expressão do gene alvo (RISC), enquanto a outra é degradada. O RISC, contendo o miRNA, liga-se ao mRNA-alvo, reprimindo a sua tradução ou promovendo a sua degradação [Adaptado de Campos et al.2011 [111]].

Estima-se que cada miRNA possa se ligar a muitos RNAs mensageiros, e que os RNAs mensageiros podem ter sua estabilidade ou tradução regulada por mais de um miRNAs [112]. Os miRNAs trabalham de forma orquestrada para controlar uma via ou função biológica comum [113,114]; essa característica única dos miRNAs os tornam ferramentas eficientes para determinação de vias específicas envolvidas em doenças ou processos biológicos.

MicroRNAs em doenças do músculo esquelético

Atualmente, embora o número de genes relacionados com o desenvolvimento de doenças musculares aumente a cada ano e a patologia histológica do tecido esteja bem documentada, as vias moleculares envolvidas permanecem pouco compreendidas [115]. Porém, importantes estudos indicam que a expressão de miRNAs está alterada em doenças do músculo esquelético e, em alguns casos, um único miRNA pode causar a doença [116,117]. Um importante miRNA para o músculo esquelético, o miR-206, encontra-se elevado no músculo diafragma do camundongo mdx (também conhecido como Dmd),

modelo animal de distrofia muscular [118]. De maneira semelhante, foi demonstrado em um modelo de atrofia muscular em ratos, que o nível de expressão do miRNA músculo específico miR-499 também está aumentado, sugerindo a ativação da rede MyomiR, codificada por genes de cadeia pesada de miosina, nessa condição [119]. Por outro lado, os níveis de expressão do miR-1 e do miR-133a estão diminuídos num modelo de hipertrofia do músculo esquelético em camundongos [116]. Em adição a esses estudos da expressão de miRNAs em doenças musculares, uma ligação genética direta conectou o miRNA com a hipertrofia muscular [120]. Uma mutação que é responsável pela excepcional muscularização da ovelha *Texel* foi mapeada como uma única mutação G/T dentro da região 3' UTR do RNA mensageiro que codifica a proteína miostatina, um membro da família do fator de crescimento transformante (TGFβ); a miostatina é regulador negativo do crescimento muscular. Essa mutação cria um sítio de ligação para os miRNAs miR-1 e miR-206, levando à repressão da tradução da miostatina, a qual origina um fenótipo semelhante à "dupla musculatura" resultante da perda da miostatina em camundongos, ratos e humanos [121,122]. Também foi demonstrado um mecanismo envolvendo interações genéticas entre os fatores transcricionais NF-κB e YYI e o miR-29; esse miRNA regula a diferenciação de mioblastos e funciona como um supressor tumoral em rabdomiosarcomas, um tumor resultante da desregulação da proliferação de células progenitoras musculares [123]. Além disso, estudos recentes realizados em nosso laboratório demonstraram o papel do miR-29b na atrofia muscular de ratos com insuficiência cárdica [124] e do miR-155 durante os processos de proliferação e diferenciação da miogênese [125]. Esses estudos demonstram a importância da regulação mediada por miRNAs para o controle de expressão de transcritos, em diferentes condições associadas com a manutenção e desenvolvimento do tecido muscular. Entretanto, considerando-se a complexidade desses mecanismos de regulação, muitos estudos envolvendo os perfis de expressão de miRNAs e mRNAs em escala global têm auxiliado na identificação das principais vias moleculares relacionadas com a perda de massa muscular, como descrito na **Tabela 2**.

Tabela 2. Estudos do perfil genômico global de miRNA e/ou mRNAs na atrofia muscular.

Condição Experimental de Atrofia	Pefil Gênomico	Plataforma	Vias identificadas	Ref.
Imobilização muscular (ratos)	mRNA	DD	A	[36]
Restrição alimentar (ratos)	mRNA	Microarray	A	[126]
Suspensão dos membros (ratos)	mRNA	Microarray	A,B,C,D,E,F	[127]
Sarcopenia (humanos)	mRNA	Microarray	G,H,I,J,K,L	[128]
Privação do meio de cultura (células C2C12)	mRNA	Microarray	A,C,F,I	[129]
Tratamento com TNF-α/INF-γ (células C2C12)	mRNA	Microaray	A,F,M,N	[130]
Suspensão dos membros (ratos)	miRNA	Microarray	O,P	[119]
Tratamento com TNF-α (células C2C12)	mRNA	Microarray	A,I,M,N,Q	[131]
Tratmento com TWEAK (células C2C12)	mRNA e miRNA	Microarray e TLDA	A,C,F,G,I,L,M,O	[132]
Tratamento com TNF e IGF (células C2C12)	mRNA e miRNA	Microarray e TLDA	M, Q, R	[50]
Modelo de cancer-caquexia (camundongos)	mRNA	Illumina HiSeq	F, I, J, S	[74]
Modelo de cancer-caquexia (camundongos)	mRNA	Illumina HiSeq	A, E, I, S	[75]
Modelo de cancer-caquexia (camundongos)	mRNA	Microarray	I, S	[76]
Caquexia associada ao câncer (humanos)	miRNA	TaqMan MiRNA Array	A, I, M, T	[133]
Caquexia associada ao câncer (humanos)	miRNA	Truseq Small RNA	D, I, M, Q	[134]
Modelos de atrofia muscular (camundongos)	miRNA	Microarray	A, T	[135]

Tabela 2. As principais vias/genes identificados foram: A) Sistema Proteassomal Dependente de Ubiquitina, B) Chaperonas, C) Estresse Oxidativo, D) Calpaínas, E) Proteases Lisossomais, F) Myod, G) MyhC, H) Transportador de Glutamina, I) Resposta imune e Citocinas Inflamatórias, J) Apoptose, K) Sistema de *Splicing*, L) Sinalização Wnt, M) Sinalização NFkB , N) Sistema iNOS, O) Rede MyomiR, P) miR-23, miR-221, miR-148b e miR-338, Q) Miogênese, R) miR-155, miR-206, miR-322, miR-335, miR-351 e miR-532 S) Sinalização JAK-STAT. T) Insulin signaling pathway. TLDA*: TaqMan low density array (Life Technologies,EUA);* DD: *Differential Display.*

Justificativas e Objetivos

Justificativa Capítulo 1 – "MicroRNA-regulated networks in skeletal muscle cells treated with interleukin-6: the potential role of miR-497 in muscle wasting"

Buscamos identificar novos fatores que pudessem estar envolvidos com a atrofia muscular durante a caquexia associada ao câncer. Embora alguns componentes regulados pela IL-6 já tenham sido descritos, o perfil global de expressão de miRNA e/ou mRNAs na atrofia de células musculares tratadas com IL-6 ainda é pouco explorado. Até o presente momento, não existem estudos que realizaram a integração dos resultados de miRNAs e mRNAs para elucidar os mecanismos moleculares envolvidos na atrofia de células musculares esqueléticas induzida por IL-6. Considerando que: 1) os níveis plasmáticos de IL-6 se encontram elevados durante a atrofia do músculo esquelético na caquexia associada ao câncer; 2) a IL-6 induz a atrofia de miotubos musculares e está associada à menor sobrevida de pacientes com câncer; e 3) os miRNAs controlam a expressão gênica em diferentes vias moleculares relacionadas ao processo de atrofia de células musculares, a hipótese do presente trabalho é que a atrofia de células musculares induzida por IL-6 possui um perfil específico de expressão de miRNAs que permite a identificação de redes reguladas por miRNAs e vias moleculares envolvidas nesse processo.

Objetivo Geral 1

Analisar se a atrofia de células musculares induzida por IL-6 possui um perfil específico de expressão de miRNAs que se são responsáveis pela regulação vias moleculares na atrofia muscular.

Objetivos Específicos 1

1. Identificar a capacidade pró-atrófica da IL-6 em células musculares;
2. Caracterizar o microRNoma na atrofia de células musculares induzida por IL-6;
3. Integrar o perfil global de expressão de miRNAs e mRNAs-alvos para identificação das vias moleculares envolvidas com a atrofia dos miotubos;
4. Validar a expressão do miRNA identificado e os potenciais mRNA alvos desse miRNA na atrofia de células musculares;
5. Realizar a análise funcional desse miRNA e a sua influência nos processos proliferação e atrofia das células musculares.

Justificativa Capítulo 2 – "The pathway to cancer cachexia: microRNA-regulated networks in muscle wasting based on integrative meta-analysis"

Diversos estudos analisaram o perfil de expressão global de mRNAs em modelos experimentais com caquexia associada ao câncer, visando identificar os mecanismos moleculares envolvidos na atrofia muscular, incluindo a identificação de novos potenciais biomarcadores para essa síndrome. Embora estudos transcriptômicos tenham contribuído para uma melhor compreensão dos mecanismos moleculares subjacentes à perda de músculo na caquexia do câncer, poucos trabalhos avaliaram, de maneira integrativa, os conjuntos de miRNAs e mRNAs em uma mesma amostra de músculo esquelético. Entretanto, estratégias para melhorar a identificação de novas vias reguladoras baseadas em miRNAs devem considerar: 1) a realização de análises de expressão de miRNAs e mRNA em uma única amostra de músculo, ou 2) a realização de uma meta-análise para coletar e integrar os dados de miRNA e mRNA mais relevantes disponíveis na literatura. Tais estratégias integrativas são importantes para identificar a funcionalidade dos genes desregulados, miRNAs e vias moleculares envolvidas na atrofia muscular durante a caquexia. Considerando que há uma como há uma diversidade de modelos experimentais e heterogeneidade entre pacientes e tipos tumorais na caquexia associada ao câncer, integramos dados de mRNAs e miRNAs do músculo esquelético nessa síndrome, obtidos na literatura a partir de uma revisão sistemática e meta-análise. Essa estratégia identificou vias moleculares, novas interações entre mRNAs e miRNAs, e potenciais alvos de drogas para a síndrome.

Objetivo Geral 2

O objetivo deste estudo foi realizar uma meta-análise, a partir de dados de expressão globais previamente publicados, para identificação de novas redes moleculares reguladas por miRNAs na atrofia muscular na caquexia associada ao câncer.

Objetivos Específicos 2

1. Identificar o perfil global de mRNAs descritos e validados em diferentes modelos experimentais e pacientes na caquexia associada ao câncer, utilizando revisão sistemática e meta-análise;
2. Identificar o perfil global de miRNAs envolvidos na regulação dos mRNAs identificados, utilizando revisão sistemática e meta-análise;

3. Integrar o perfil global de expressão de miRNAs e mRNAs-alvos na atrofia do músculo esquelético durante a caquexia associada ao câncer para identificar potenciais novas interações miRNAs-mRNAs;
4. Identificar potenciais novos alvos de drogas a partir dos dados obtidos na meta-análise.

Justificativa Capítulo 3 – "The landscape of cachexia-inducing factors in human cancers"

A caquexia é uma síndrome associada a tipos específicos de tumores, mas as causas desta variação na prevalência e gravidade da caquexia ainda são desconhecidas. Neste capítulo, nossa hipótese foi que o perfil da expressão gênica tumoral de fatores indutores de caquexia em cânceres humanos com diferentes prevalências de caquexia pode revelar mediadores e biomarcadores da caquexia específicos para cada tipo tumoral. Além disso, considerando a ausência de estudos que mostram quais as principais células que são responsáveis pela expressão desses mediadores de caquexia, buscamos avaliamos se a pureza tumoral também está associada à expressão gênica de mediadores da caquexia.

Objetivo Geral 3

O objetivo deste estudo foi caracterizar o perfil de expressão gênica de fatores indutores de caquexia em 12 cânceres humanos com diferentes prevalências de caquexia para identificar mediadores e biomarcadores da síndrome.

Objetivos Específicos 3

1. Investigar sistematicamente os dados transcriptômicos para caracterizar o perfil de expressão do secretoma tumoral em 12 tipos tumorais que apresentam diferentes prevalência de caquexia;
2. Identificar os processos biológicos e vias moleculares associadas ao perfil do secretoma específico de cada tipo tumoral;
3. Avaliar a correlação entre o perfil dos fatores indutores de caquexia e a prevalência da caquexia;
4. Identificar a associação entre os fatores indutores de caquexia e a pureza tumoral em adenocarcinomas pancreáticos;
5. Investigar o valor prognóstico de fatores indutores de caquexia em pacientes com diferentes tipos tumorais.

Referências

1. Miyazaki, M. & Esser, K. a. Cellular mechanisms regulating protein synthesis and skeletal muscle hypertrophy in animals. *J. Appl. Physiol.* **106,** 1367–73 (2009).
2. Rennie, M. J., Wackerhage, H., Spangenburg, E. E. & Booth, F. W. Control of the size of the human muscle mass. *Annu. Rev. Physiol.* **66,** 799–828 (2004).
3. Kandarian, S. C. & Jackman, R. W. Intracellular signaling during skeletal muscle atrophy. *Muscle Nerve* **33,** 155–65 (2006).
4. Lecker, S. H. *et al.* Multiple types of skeletal muscle atrophy involve a common program of changes in gene expression. *FASEB J.* **18,** 39–51 (2004).
5. Jackman, R. W. & Kandarian, S. C. The molecular basis of skeletal muscle atrophy. *Am. J. Physiol. Cell Physiol.* **287,** C834–43 (2004).
6. Glass, D. J. Skeletal muscle hypertrophy and atrophy signaling pathways. *Int. J. Biochem. Cell Biol.* **37,** 1974–84 (2005).
7. Bonaldo, P. & Sandri, M. Cellular and molecular mechanisms of muscle atrophy. *Dis. Model. Mech.* **6,** 25–39 (2013).
8. Fearon, K. *et al.* Definition and classification of cancer cachexia: an international consensus. *Lancet Oncol.* **12,** 489–95 (2011).
9. Dogra, C. *et al.* TNF-related weak inducer of apoptosis (TWEAK) is a potent skeletal muscle-wasting cytokine. *FASEB J.* **21,** 1857–69 (2007).
10. Braun, T. & Gautel, M. Transcriptional mechanisms regulating skeletal muscle differentiation, growth and homeostasis. *Nat. Rev. Mol. Cell Biol.* **12,** 349–61 (2011).
11. Cao, P. R., Kim, H. J. & Lecker, S. H. Ubiquitin-protein ligases in muscle wasting. *Int. J. Biochem. Cell Biol.* **37,** 2088–97 (2005).
12. Tisdale, M. J. Biology of cachexia. *J. Natl. Cancer Inst.* **89,** 1763–73 (1997).
13. Tisdale, M. J. Cachexia in cancer patients. *Nat. Rev. cancer* **3,** 883–9 (2002).
14. Morley, J. E., Thomas, D. R. & Wilson, M.-M. G. Cachexia: pathophysiology and clinical relevance. *Am. J. Clin. Nutr.* **83,** 735–43 (2006).
15. Evans, W. J. *et al.* Cachexia: a new definition. *Clin. Nutr.* **27,** 793–9 (2008).
16. Donohoe, C. L., Ryan, A. M. & Reynolds, J. V. Cancer Cachexia: Mechanisms and Clinical Implications. *Gastroenterol. Res. Pract.* **2011,** 1–13 (2011).
17. Fearon, K. C. H. Cancer cachexia: developing multimodal therapy for a multidimensional problem. *Eur. J. Cancer* **44,** 1124–32 (2008).
18. Das, S. K. *et al.* Adipose triglyceride lipase contributes to cancer-associated cachexia. *Science* **333,** 233–8 (2011).
19. Tsoli, M. & Robertson, G. Cancer cachexia: malignant inflammation, tumorkines, and metabolic mayhem. *Trends Endocrinol. Metab.* **24,** 174–83 (2013).
20. Laviano, A., Meguid, M. M., Inui, A., Muscaritoli, M. & Rossi-Fanelli, F. Therapy insight: Cancer anorexia-cachexia syndrome--when all you can eat is yourself. *Nat. Clin. Pract. Oncol.* **2,** 158–65 (2005).
21. Tisdale, M. J. Reversing cachexia. *Cell* **142,** 511–2 (2010).

22. Twelkmeyer, B., Tardif, N. & Rooyackers, O. Omics and cachexia. *Curr. Opin. Clin. Nutr. Metab. Care* **20,** 181–185 (2017).

23. Argilés, J. M., Stemmler, B., López-Soriano, F. J. & Busquets, S. Inter-tissue communication in cancer cachexia. *Nat. Rev. Endocrinol.* (2018). doi:10.1038/s41574-018-0123-0

24. Baracos, V. E., Martin, L., Korc, M., Guttridge, D. C. & Fearon, K. C. H. Cancer-associated cachexia. *Nat. Rev. Dis. Prim.* **4,** 17105 (2018).

25. Patel, S., Ngounou Wetie, A., Darie, C. & Clarkson, B. Cancer secretomes and their place in supplementing other hallmarks of cancer. *Adv Exp Med Biol* **806,** 409–42 (2014).

26. Makridakis, M. & Vlahou, A. Secretome proteomics for discovery of cancer biomarkers. *Proteomics, J* **73,** 2291–305 (2010).

27. Tjalsma, H., Bolhuis, A., Jongbloed, J., Bron, S. & van Dijl, J. Signal peptide-dependent protein transport in Bacillus subtilis: a genome-based survey of the secretome. *Microbiol Mol Biol Rev* **64,** 515–547 (2000).

28. Schaaij-Visser, T. B. M., de Wit, M., Lam, S. W. & Jiménez, C. R. The cancer secretome, current status and opportunities in the lung, breast and colorectal cancer context. *Biochim. Biophys. Acta* **1834,** 2242–58 (2013).

29. Mukherjee, P. & Mani, S. Methodologies to decipher the cell secretome. *Biochim. Biophys. Acta - Proteins Proteomics* **1834,** 2226–2232 (2013).

30. Uhlen, M. *et al.* Tissue-based map of the human proteome. *Science (80-.).* **347,** 1260419–1260419 (2015).

31. Robinson, J. L., Feizi, A., Uhlén, M. & Nielsen, J. A Systematic Investigation of the Malignant Functions and Diagnostic Potential of the Cancer Secretome. *Cell Rep.* **26,** 2622–2635.e5 (2019).

32. Rung, J. & Brazma, A. Reuse of public genome-wide gene expression data. *Nat. Rev. Genet.* **14,** 89–99 (2013).

33. Onesti, J. K. & Guttridge, D. C. Inflammation based regulation of cancer cachexia. *Biomed Res. Int.* **2014,** 168407 (2014).

34. Keller, U. Pathophysiology of cancer cachexia. *Support. Care Cancer* **1,** 290–4 (1993).

35. Banerjee, A. & Guttridge, D. C. Mechanisms for maintaining muscle. *Curr. Opin. Support. Palliat. Care* **6,** 451–6 (2012).

36. Bodine, S. C. *et al.* Identification of ubiquitin ligases required for skeletal muscle atrophy. *Science* **294,** 1704–8 (2001).

37. Shaid, S., Brandts, C. H., Serve, H. & Dikic, I. Ubiquitination and selective autophagy. *Cell Death Differ.* **20,** 21–30 (2013).

38. Csibi, A., Leibovitch, M. P., Cornille, K., Tintignac, L. A. & Leibovitch, S. A. MAFbx/Atrogin-1 controls the activity of the initiation factor eIF3-f in skeletal muscle atrophy by targeting multiple C-terminal lysines. *J. Biol. Chem.* **284,** 4413–21 (2009).

39. Samuels, S. E. *et al.* Higher skeletal muscle protein synthesis and lower breakdown after chemotherapy in cachectic mice. *Am. J. Physiol. Regul. Integr. Comp. Physiol.* **281,** R133–9 (2001).

40. Rommel, C. *et al.* Mediation of IGF-1-induced skeletal myotube hypertrophy by PI(3)K/Akt/mTOR and PI(3)K/Akt/GSK3 pathways. *Nat. Cell Biol.* **3,** 1009–13 (2001).

41. Bentzinger, C. F. *et al.* Skeletal muscle-specific ablation of raptor, but not of rictor, causes metabolic changes and results in muscle dystrophy. *Cell Metab.* **8,** 411–24 (2008).

42. Mammucari, C. *et al.* FoxO3 controls autophagy in skeletal muscle in vivo. *Cell Metab.* **6,** 458–71 (2007).

43. Lum, J. J., DeBerardinis, R. J. & Thompson, C. B. Autophagy in metazoans: cell survival in the land of plenty. *Nat. Rev. Mol. Cell Biol.* **6,** 439–48 (2005).

44. Zhao, J. *et al.* FoxO3 coordinately activates protein degradation by the autophagic/lysosomal and proteasomal pathways in atrophying muscle cells. *Cell Metab.* **6,** 472–83 (2007).

45. Sandri, M. *et al.* PGC-1alpha protects skeletal muscle from atrophy by suppressing FoxO3 action and atrophy-specific gene transcription. *Proc. Natl. Acad. Sci. U. S. A.* **103,** 16260–5 (2006).

46. Li, Y. P., Schwartz, R. J., Waddell, I. D., Holloway, B. R. & Reid, M. B. Skeletal muscle myocytes undergo protein loss and reactive oxygen-mediated NF-kappaB activation in response to tumor necrosis factor alpha. *FASEB J.* **12,** 871–80 (1998).

47. Li, Y. P. & Reid, M. B. NF-kappaB mediates the protein loss induced by TNF-alpha in differentiated skeletal muscle myotubes. *Am. J. Physiol. Regul. Integr. Comp. Physiol.* **279,** R1165–70 (2000).

48. Reid, M. B. & Li, Y. P. Tumor necrosis factor-alpha and muscle wasting: a cellular perspective. *Respir. Res.* **2,** 269–72 (2001).

49. Haddad, F., Zaldivar, F., Cooper, D. M. & Adams, G. R. IL-6-induced skeletal muscle atrophy. *J. Appl. Physiol.* **98,** 911–7 (2005).

50. Meyer, S. U. *et al.* Integrative Analysis of MicroRNA and mRNA Data Reveals an Orchestrated Function of MicroRNAs in Skeletal Myocyte Differentiation in Response to TNF-α or IGF1. *PLoS One* **10,** e0135284 (2015).

51. Yamaki, T. *et al.* Rel A/p65 is required for cytokine-induced myotube atrophy. *Am. J. Physiol. Cell Physiol.* **303,** C135–42 (2012).

52. Srivastava, A. K. *et al.* Tumor necrosis factor-alpha augments matrix metalloproteinase-9 production in skeletal muscle cells through the activation of transforming growth factor-beta-activated kinase 1 (TAK1)-dependent signaling pathway. *J. Biol. Chem.* **282,** 35113–24 (2007).

53. Acharyya, S. *et al.* Cancer cachexia is regulated by selective targeting of skeletal muscle gene products. *Regulation* **114,** (2004).

54. Suh, S.-Y. *et al.* Interleukin-6 but not tumour necrosis factor-alpha predicts survival in patients with advanced cancer. *Support. Care Cancer* **21,** 3071–7 (2013).

55. Wang, K., Grivennikov, S. I. & Karin, M. Implications of anti-cytokine therapy in colorectal cancer and autoimmune diseases. *Ann. Rheum. Dis.* **72 Suppl 2,** ii100–3 (2013).

56. Taniguchi, K. & Karin, M. IL-6 and related cytokines as the critical lynchpins between inflammation and cancer. *Semin. Immunol.* **26,** 54–74 (2014).

57. Begue, G. *et al.* Early activation of rat skeletal muscle IL-6/STAT1/STAT3 dependent gene expression in resistance exercise linked to hypertrophy. *PLoS One* **8,** e57141 (2013).

58. Pedersen, B. K. & Febbraio, M. A. Muscle as an endocrine organ: focus on muscle-derived interleukin-6. *Physiol. Rev.* **88,** 1379–406 (2008).

59. Peake, J. M., Della Gatta, P., Suzuki, K. & Nieman, D. C. Cytokine expression and secretion by skeletal muscle cells: regulatory mechanisms and exercise effects. *Exerc. Immunol. Rev.* **21,** 8–25 (2015).

60. Serrano, A. L., Baeza-Raja, B., Perdiguero, E., Jardí, M. & Muñoz-Cánoves, P. Interleukin-6 is an essential regulator of satellite cell-mediated skeletal muscle hypertrophy. *Cell Metab.* **7,** 33–44 (2008).

61. Puppa, M. J. *et al.* The effect of exercise on IL-6-induced cachexia in the Apc (Min/+) mouse. *J.*

Cachexia. Sarcopenia Muscle **3,** 117–37 (2012).

62. Zhang, C. *et al.* Interleukin-6/signal transducer and activator of transcription 3 (STAT3) pathway is essential for macrophage infiltration and myoblast proliferation during muscle regeneration. *J. Biol. Chem.* **288,** 1489–99 (2013).

63. Carow, B. & Rottenberg, M. E. SOCS3, a Major Regulator of Infection and Inflammation. *Front. Immunol.* **5,** 58 (2014).

64. White, U. A. & Stephens, J. M. The gp130 receptor cytokine family: regulators of adipocyte development and function. *Curr. Pharm. Des.* **17,** 340–6 (2011).

65. Scheller, J., Garbers, C. & Rose-John, S. Interleukin-6: from basic biology to selective blockade of pro-inflammatory activities. *Semin. Immunol.* **26,** 2–12 (2014).

66. Puppa, M. J., Murphy, E. A., Fayad, R., Hand, G. A. & Carson, J. A. Cachectic skeletal muscle response to a novel bout of low-frequency stimulation. *J. Appl. Physiol.* **116,** 1078–87 (2014).

67. Suzuki, H., Asakawa, A., Amitani, H., Nakamura, N. & Inui, A. Cancer cachexia--pathophysiology and management. *J. Gastroenterol.* **48,** 574–94 (2013).

68. Gordon, B. S., Kelleher, A. R. & Kimball, S. R. Regulation of muscle protein synthesis and the effects of catabolic states. *Int. J. Biochem. Cell Biol.* **45,** 2147–57 (2013).

69. Moses, A. G. W., Maingay, J., Sangster, K., Fearon, K. C. H. & Ross, J. A. Pro-inflammatory cytokine release by peripheral blood mononuclear cells from patients with advanced pancreatic cancer: relationship to acute phase response and survival. *Oncol. Rep.* **21,** 1091–5 (2009).

70. Strassmann, G. *et al.* Suramin interferes with interleukin-6 receptor binding in vitro and inhibits colon-26-mediated experimental cancer cachexia in vivo. *J. Clin. Invest.* **92,** 2152–9 (1993).

71. Tamura, S. *et al.* Involvement of human interleukin 6 in experimental cachexia induced by a human uterine cervical carcinoma xenograft. *Clin. Cancer Res.* **1,** 1353–8 (1995).

72. Soda, K., Kawakami, M., Kashii, A. & Miyata, M. Manifestations of cancer cachexia induced by colon 26 adenocarcinoma are not fully ascribable to interleukin-6. *Int. J. Cancer* **62,** 332–6 (1995).

73. Strassmann, G., Fong, M., Kenney, J. S. & Jacob, C. O. Evidence for the involvement of interleukin 6 in experimental cancer cachexia. *J. Clin. Invest.* **89,** 1681–4 (1992).

74. Tseng, Y.-C. *et al.* Preclinical Investigation of the Novel Histone Deacetylase Inhibitor AR-42 in the Treatment of Cancer-Induced Cachexia. *J. Natl. Cancer Inst.* **107,** djv274 (2015).

75. Bonetto, A. *et al.* STAT3 activation in skeletal muscle links muscle wasting and the acute phase response in cancer cachexia. *PLoS One* **6,** e22538 (2011).

76. Gilabert, M. *et al.* Pancreatic cancer-induced cachexia is Jak2-dependent in mice. *J. Cell. Physiol.* **229,** 1437–43 (2014).

77. Martinelli, G. B. *et al.* Activation of the SDF1/CXCR4 pathway retards muscle atrophy during cancer cachexia. *Oncogene* **35,** 6212–6222 (2016).

78. Fukawa, T. *et al.* Excessive fatty acid oxidation induces muscle atrophy in cancer cachexia. *Nat. Med.* **22,** 666–71 (2016).

79. Constantinou, C. *et al.* Nuclear magnetic resonance in conjunction with functional genomics suggests mitochondrial dysfunction in a murine model of cancer cachexia. *Int. J. Mol. Med.* **27,** 15–24 (2011).

80. White, J. P. *et al.* The regulation of skeletal muscle protein turnover during the progression of cancer cachexia in the Apc(Min/+) mouse. *PLoS One* **6,** e24650 (2011).

81. Carson, J. A. & Baltgalvis, K. A. Interleukin 6 as a key regulator of muscle mass during cachexia.

Exerc. Sport Sci. Rev. **38,** 168–76 (2010).

82. Fearon, K. C. *et al.* Elevated circulating interleukin-6 is associated with an acute-phase response but reduced fixed hepatic protein synthesis in patients with cancer. *Ann. Surg.* **213,** 26–31 (1991).

83. Scott, H. R., McMillan, D. C., Crilly, A., McArdle, C. S. & Milroy, R. The relationship between weight loss and interleukin 6 in non-small-cell lung cancer. *Br. J. Cancer* **73,** 1560–2 (1996).

84. Güller, I. & Russell, A. P. MicroRNAs in skeletal muscle: their role and regulation in development, disease and function. *J. Physiol.* **588,** 4075–87 (2010).

85. Ambros, V. A uniform system for microRNA annotation. *Rna* **9,** 277–279 (2003).

86. Lee, Y. *et al.* MicroRNA genes are transcribed by RNA polymerase II. *EMBO J.* **23,** 4051–60 (2004).

87. Cai, X., Hagedorn, C. H. & Cullen, B. R. Human microRNAs are processed from capped, polyadenylated transcripts that can also function as mRNAs. *RNA* **10,** 1957–66 (2004).

88. Kim, V. N. MicroRNA biogenesis: coordinated cropping and dicing. *Nat. Rev. Mol. Cell Biol.* **6,** 376–85 (2005).

89. Borchert, G. M., Lanier, W. & Davidson, B. L. RNA polymerase III transcribes human microRNAs. *Nat. Struct. Mol. Biol.* **13,** 1097–101 (2006).

90. Landthaler, M., Yalcin, A. & Tuschl, T. The human DiGeorge syndrome critical region gene 8 and Its D. melanogaster homolog are required for miRNA biogenesis. *Curr. Biol.* **14,** 2162–7 (2004).

91. Gregory, R. I. *et al.* The Microprocessor complex mediates the genesis of microRNAs. *Nature* **432,** 235–40 (2004).

92. Han, J. *et al.* The Drosha-DGCR8 complex in primary microRNA processing. *Genes Dev.* **18,** 3016–27 (2004).

93. Denli, A. M., Tops, B. B. J., Plasterk, R. H. a, Ketting, R. F. & Hannon, G. J. Processing of primary microRNAs by the Microprocessor complex. *Nature* **432,** 231–5 (2004).

94. Zeng, Y. & Cullen, B. R. Efficient processing of primary microRNA hairpins by Drosha requires flanking nonstructured RNA sequences. *J. Biol. Chem.* **280,** 27595–603 (2005).

95. Han, J. *et al.* Molecular basis for the recognition of primary microRNAs by the Drosha-DGCR8 complex. *Cell* **125,** 887–901 (2006).

96. Berezikov, E., Chung, W., Willis, J., Cuppen, E. & Lai, E. C. Mammalian mirtron genes. *Mol. Cell* **28,** 328–36 (2007).

97. Okamura, K., Hagen, J. W., Duan, H., Tyler, D. M. & Lai, E. C. The mirtron pathway generates microRNA-class regulatory RNAs in Drosophila. *Cell* **130,** 89–100 (2007).

98. Ruby, J. G., Jan, C. H. & Bartel, D. P. Intronic microRNA precursors that bypass Drosha processing. *Nature* **448,** 83–6 (2007).

99. Yi, R., Qin, Y., Macara, I. G. & Cullen, B. R. Exportin-5 mediates the nuclear export of pre-microRNAs and short hairpin RNAs. *Genes Dev.* **17,** 3011–6 (2003).

100. Bohnsack, M. T. Exportin 5 is a RanGTP-dependent dsRNA-binding protein that mediates nuclear export of pre-miRNAs. *RNA* **10,** 185–191 (2004).

101. Lund, E., Güttinger, S., Calado, A., Dahlberg, J. E. & Kutay, U. Nuclear export of microRNA precursors. *Science* **303,** 95–8 (2004).

102. Kim, V. N., Han, J. & Siomi, M. C. Biogenesis of small RNAs in animals. *Nat. Rev. Mol. Cell Biol.* **10,** 126–39 (2009).

103. Meijer, H. A., Smith, E. M. & Bushell, M. Regulation of miRNA strand selection: follow the leader? *Biochem. Soc. Trans.* **42,** 1135–40 (2014).

104. Miyoshi, K., Miyoshi, T. & Siomi, H. Many ways to generate microRNA-like small RNAs: non-canonical pathways for microRNA production. *Mol. Genet. Genomics* **284,** 95–103 (2010).

105. Potla, R., Singh, I. S., Atamas, S. P. & Hasday, J. D. Shifts in temperature within the physiologic range modify strand-specific expression of select human microRNAs. *RNA* **21,** 1261–73 (2015).

106. Schwarz, D. S. *et al.* Asymmetry in the assembly of the RNAi enzyme complex. *Cell* **115,** 199–208 (2003).

107. Salzman, D. W., Shubert-Coleman, J. & Furneaux, H. P68 RNA helicase unwinds the human let-7 microRNA precursor duplex and is required for let-7-directed silencing of gene expression. *J. Biol. Chem.* **282,** 32773–9 (2007).

108. Lim, L. P. *et al.* Microarray analysis shows that some microRNAs downregulate large numbers of target mRNAs. *Nature* **433,** 769–73 (2005).

109. Lee, Y. S. & Dutta, A. MicroRNAs in cancer. *Annu. Rev. Pathol.* **4,** 199–227 (2009).

110. Sen, G. L. & Blau, H. M. Argonaute 2/RISC resides in sites of mammalian mRNA decay known as cytoplasmic bodies. *Nat. Cell Biol.* **7,** 633–6 (2005).

111. Campos, V. F., Urtiaga, G., Gonçalves, B., Deschamps, J. C. & Collares, T. MicroRNAs e seu papel no desenvolvimento embrionário. *Ciência Rural* **41,** 85–93 (2011).

112. Doench, J. G. & Sharp, P. A. Specificity of microRNA target selection in translational repression. *Genes Dev.* **18,** 504–11 (2004).

113. Esau, C. *et al.* miR-122 regulation of lipid metabolism revealed by in vivo antisense targeting. *Cell Metab.* **3,** 87–98 (2006).

114. Leung, A. K. L. & Sharp, P. a. microRNAs: a safeguard against turmoil? *Cell* **130,** 581–5 (2007).

115. Davies, K. E. & Nowak, K. J. Molecular mechanisms of muscular dystrophies: old and new players. *Nat. Rev. Mol. Cell Biol.* **7,** 762–73 (2006).

116. McCarthy, J. J. & Esser, K. a. MicroRNA-1 and microRNA-133a expression are decreased during skeletal muscle hypertrophy. *J. Appl. Physiol.* **102,** 306–13 (2007).

117. Eisenberg, I. *et al.* Distinctive patterns of microRNA expression in primary muscular disorders. *Proc. Natl. Acad. Sci. U. S. A.* **104,** 17016–21 (2007).

118. McCarthy, J. J., Esser, K. a & Andrade, F. H. MicroRNA-206 is overexpressed in the diaphragm but not the hindlimb muscle of mdx mouse. *Am. J. Physiol. Cell Physiol.* **293,** C451–7 (2007).

119. McCarthy, J. J., Esser, K. a, Peterson, C. a & Dupont-Versteegden, E. E. Evidence of MyomiR network regulation of beta-myosin heavy chain gene expression during skeletal muscle atrophy. *Physiol. Genomics* **39,** 219–26 (2009).

120. Clop, A. *et al.* A mutation creating a potential illegitimate microRNA target site in the myostatin gene affects muscularity in sheep. *Nat. Genet.* **38,** 813–8 (2006).

121. Lee, S.-J. Regulation of muscle mass by myostatin. *Annu. Rev. Cell Dev. Biol.* **20,** 61–86 (2004).

122. Tobin, J. F. & Celeste, A. J. Myostatin, a negative regulator of muscle mass: implications for muscle degenerative diseases. *Curr. Opin. Pharmacol.* **5,** 328–32 (2005).

123. Wang, H. *et al.* NF-kappaB-YY1-miR-29 regulatory circuitry in skeletal myogenesis and rhabdomyosarcoma. *Cancer Cell* **14,** 369–81 (2008).

124. Moraes, L. N. *et al.* Integration of miRNA and mRNA expression profiles reveals microRNA-regulated networks during muscle wasting in cardiac cachexia. *Sci. Rep.* **7,** (2017).

125. Freire, P. P. *et al.* Osteoglycin inhibition by microRNA miR-155 impairs myogenesis. *PLoS One* **12,** e0188464 (2017).

126. Gomes, M. D., Lecker, S. H., Jagoe, R. T., Navon, A. & Goldberg, A. L. Atrogin-1, a muscle-specific F-box protein highly expressed during muscle atrophy. *Proc. Natl. Acad. Sci. U. S. A.* **98,** 14440–5 (2001).

127. Stevenson, E. J., Giresi, P. G., Koncarevic, A. & Kandarian, S. C. Global analysis of gene expression patterns during disuse atrophy in rat skeletal muscle. *J. Physiol.* **551,** 33–48 (2003).

128. Giresi, P. G. *et al.* Identification of a molecular signature of sarcopenia. *Physiol. Genomics* **21,** 253–63 (2005).

129. Stevenson, E. J., Koncarevic, A., Giresi, P. G., Jackman, R. W. & Kandarian, S. C. Transcriptional profile of a myotube starvation model of atrophy. *J. Appl. Physiol.* **98,** 1396–406 (2005).

130. Di Marco, S. *et al.* NF-kappa B-mediated MyoD decay during muscle wasting requires nitric oxide synthase mRNA stabilization, HuR protein, and nitric oxide release. *Mol. Cell. Biol.* **25,** 6533–45 (2005).

131. Bhatnagar, S. *et al.* Tumor necrosis factor-α regulates distinct molecular pathways and gene networks in cultured skeletal muscle cells. *PloS one* **5,** e13262 (2010).

132. Panguluri, S. K. *et al.* Genomic profiling of messenger RNAs and microRNAs reveals potential mechanisms of TWEAK-induced skeletal muscle wasting in mice. *PLoS One* **5,** e8760 (2010).

133. van de Worp, W. R. P. H. *et al.* Identification of microRNAs in skeletal muscle associated with lung cancer cachexia. *J. Cachexia. Sarcopenia Muscle* (2019). doi:10.1002/jcsm.12512

134. Narasimhan, A. *et al.* Small RNAome profiling from human skeletal muscle: novel miRNAs and their targets associated with cancer cachexia. *J. Cachexia. Sarcopenia Muscle* **8,** 405–416 (2017).

135. Soares, R. J. *et al.* Involvement of microRNAs in the regulation of muscle wasting during catabolic conditions. *J. Biol. Chem.* **289,** 21909–25 (2014).

Capítulo I

MICRORNA-REGULATED NETWORKS IN SKELETAL MUSCLE CELLS TREATED WITH INTERLEUKIN-6: THE POTENTIAL ROLE OF MIR-497 IN MUSCLE WASTING

Paula P. Freire[1], Geysson J. Fernandez[1,2], Jianming Liu[3], Sarah S. Cury[1], Grasieli de Oliveira[1], Letícia O. Lopes[1], Diogo de Moraes[1], Leonardo N. Moraes[1], Maeli Dal-Pai-Silva[1], Xiaoyun Hu[3], Da-Zhi Wang[3,4], Robson F. Carvalho[1*].

[1]. Department of Morphology, Institute of Biosciences, São Paulo State University, UNESP, Botucatu, SP, Brazil

[2]. Faculty of Medicine, University of Antioquia, UdeA, Medellín, Colombia

[3]. Department of Cardiology, Boston Children's Hospital, Harvard Medical School, Boston, MA, 02115, USA

[4]. Harvard Stem Cell Institute, Harvard University, Cambridge, MA 02138, USA

* Corresponding author
Robson Francisco Carvalho
Department of Morphology, São Paulo State University, Botucatu-SP Brazil
Telephone: +55 14 3880 0473
CEP: 18.618-689
Email address: rcarvalho@ibb.unesp.br

(*To be submitted to the Journal of Molecular Biology*)

Abstract

Systemic inflammation contributes to the development of cachexia, and the pro-inflammatory cytokine interleukin-6 (IL-6) has emerged as a critical factor related to muscle wasting in this condition. Regulation of gene expression by microRNAs (miRNAs) in skeletal muscle wasting involves thousands of transcripts through different regulatory mechanisms. Our objective was to analyze the global miRNA expression profile in skeletal muscle cells with atrophy induced by IL-6 to uncover potential miRNAs involved with this catabolic condition. Genome-wide gene expression profiles of miRNAs were performed by using TaqMan Low-Density Arrays in C2C12 myotubes treated with IL-6, followed by *in silico* predictions of miRNA targets. High concentrations of IL-6 induced myotube atrophy, decreased the levels of Myh7 and e-MHC, and deregulated 20 miRNAs (5 up-regulated, and 15 down-regulated). Gene Ontology analysis of the predicted targets of these miRNAs revealed potential posttranscriptional regulation of genes involved in cell differentiation, apoptosis, migration, and catabolic processes. The treatment with IL-6 suppressed the miRNA miR-497, and it was found in the literature to be down-regulated in other different muscle-wasting conditions. Thus, we used miR-497 mimics and inhibitors to explore the function of this miRNA. The miRNA miR-497 changed cell cycle target-genes, such as Ccnd2 and Ccne1, but did not alter myoblast proliferation, as assessed by the EdU assay. Also, miR-497-mimic induced myotubes atrophy. The miR-497 inhibitor did not change myotubes diameters but resulted in overexpression of the miR-497 target genes *Insr* and *Igf1r*. These genes are involved with the insulin-like growth factor pathway and are over-expressed in muscle samples of different cancer cachexia models (GSE48363, GSE63032, GSE24111, and GSE51931). Our miRNA analysis identified miRNA-regulated networks and suggests that miR-497 is involved in a compensatory mechanism of muscle atrophy in response to IL-6.

Keywords: Interleukin 6; C2C12, microRNAs, miR-497; atrophy.

Introduction

Cancer cachexia is a wasting syndrome that affects approximately 50% of all cancer patients, depending on the tumor type, and is the first cause of death of all cancer patients [1]. The major problem related to cancer-cachexia prevention is that patients are only diagnosed with cachexia when they lose around 7-15% of body mass [2,3]. The treatments used in cancer patients, as radiochemotherapy, can aggravate cachexia progression in some cases [4] and entails in diminishing quality of life owing to a high loss of skeletal muscle mass [1,5].

Cancer cachexia is also characterized by chronic inflammation, and several tumor-derived factors have been implicated in inducing the cachectic state and muscle wasting [6]. Proinflammatory cytokines such as interleukin-1β (IL-1β), tumor necrosis factor (TNF)-α, interferon (INF)-γ and interleukin-6 (IL-6) play a key role, mainly in the development of cellular and molecular changes in muscle cells [7–9]. Several authors have evaluated the mechanisms by which these proinflammatory cytokines independently induce the degradation of proteins in muscle cells [10–15]. IL-6 has emerged as a major player in cancer cachexia progression with its levels correlating to survival time in advanced cancer patients [16]. Also, IL-6 is a cytokine able to induced atrophy of skeletal muscle cells per se [15], but the molecular mechanisms regulated by IL-6 during muscle wasting are still not fully understood.

Several studies demonstrated that IL-6 display a pleiotropic role in skeletal muscles (reviewed by Munoz Canovez 2013 [17]). Skeletal muscle has been shown to produce and secrete significant levels of IL-6 after exercise [18]. Increases in IL-6 levels and consequent activation of the JAK/STAT pathway were associated with stimulation of hypertrophic muscle growth and myogenesis by regulating the proliferative capacity of muscle satellite cells [19,20]. In response to exercise-induced muscle stress, satellite cells are activated, proliferate, differentiate, and fuse to form new muscle fibers [20,21]. This IL-6 promyogenic effect is usually associated with the transient production and short-term action of this cytokine [20]. In addition, IL-6 has other beneficial effects, such as the regulation of energy metabolism [22,23]. Thus, in a healthy state, IL-6 can act as a strong metabolic signal instead of directly controlling the rates of protein turnover in muscle [24]. Paradoxically, detrimental functions of IL-6 have also been described, such as promoting atrophy and loss of muscle during prolonged exposure to high levels of IL-6 [13,25,26]. It is important to note the differential effects of IL-6 on muscle are dependent on the dose applied, exposure time, and the administration way [13,27]. For example, high concentrations of IL-6 significantly reduced the skeletal muscle weight by 15% and reduced the myofibers area of fast and slow fiber types, affecting particularly the gastrocnemius muscle [28]. Although some molecules have

been proposed for these pro-atrophic effects, the specific role IL-6 on muscle atrophy has not been characterized.

Overexpression of IL-6 is also involved with the loss of muscle mass in a mice model of cachexia associated with colon cancer (C26) and with uterine cancer [29–38]. Suramin, an antagonist of the IL-6 receptor, markedly decreases the cachexia rate in mice bearing C26 tumors [30], whereas the use of neutralizing antibodies against IL-6 caused a decrease in the wasting muscle in rats with cancer-cachexia [32]. Inhibition of IL-6 using soluble receptor antibody (sIL-6R) also reduces muscle atrophy in intestinal cancer mice [39]. In addition, it has been shown that in humans, IL-6 is a very sensitive indicator of muscle mass loss in patients with colon cancer [40,41] and lung cancer [42]. Therefore, IL-6 remains a promising therapeutic strategy to attenuate the progression of cachexia in several types of cancer. However, a better understanding of the direct and indirect effects of IL-6 is necessary.

Although some molecular components and pathways involved in IL-6 induced muscle atrophy are well characterized, the post-transcriptional mechanism responsible for regulating these molecular changes in muscle atrophy induced by IL-6 during cachexia is unknown. The complexity that controls gene expression suggests the involvement of additional regulatory molecules, such as microRNAs (miRNAs). These small non-coding RNAs regulate the function of skeletal muscle during development and are involved in various muscle diseases [43]. Specifically, miRNAs in cachexia were associated with chronic inflammation that induces some catabolic conditions and, ultimately, leads to muscle wasting [44–46]. Currently, little is known about the miRNA deregulated in skeletal muscle cell atrophy induced by IL-6. Thus, the purpose of this study is to identify the miRNA expression profile in muscle wasting caused by high levels of IL-6 to clarify the regulatory networks and molecular pathways involved in atrophy of skeletal muscle cells.

Material and Methods

TCGA and GTEx transcriptomics datasets

We used the transcriptional profiles from TCGA (https://portal.gdc.cancer.gov/) of 6 human cancers and compared with matched normal tissues from TCGA and GTEx [47] (http://www.gtexportal.org/). Further, we used the web-based tool *Gene Expression Profiling Analysis* [48] (http://gepia.cancerpku.cn/) to uniform and unify the RNA sequencing data according to Toil Pipeline [49]. Differentially expressed genes (DEGs) between tumor and normal samples were determined by one-way ANOVA applying the statistical cutoffs of log2 fold-change > 1 and q-value < 0.01.

Cell Culture and Muscle Differentiation

C2C12 mouse myoblasts (ATCC® CRL-1772™) were cultured in a growth medium (GM) consisting of Dulbecco's modified Eagle's medium (DMEM, Thermo Fisher Scientific, USA) supplemented with 1% Penicillin–Streptomycin (Thermo Fisher Scientific, USA) and 10% fetal bovine serum (Thermo Fisher Scientific, USA) at 37°C and 5% CO2. Near-confluent cells (80% to 90%) were induced to differentiate in a differentiation medium (DM), consisting of DMEM plus 2% horse serum (Thermo Fisher Scientific, USA) and 1% Penicillin–Streptomycin solution for 5 days. Three concentration of recombinant Interleukin-6 (PMC0065, Thermo Fisher Scientific, USA) was added in differentiated myotubes to induce muscle wasting (Suppl Fig. 1A). All the experiments were carried out using at least three independent replicates per group.

Oligonucleotides and transfection

The mimic miR-497 (miRIDIAN microRNA mmu-miR-497-5p mimic, C310724-01-0002, Dharmacon), the inhibitor miR-497 (miRIDIAN microRNA mmu-miR-497-5p hairpin inhibitor, IH310724-03-0002), and the respective negative controls (miRIDIAN microRNA Mimic Negative Control #1 CN-001000-01-05 and miRIDIAN microRNA Hairpin Inhibitor Negative Control #1 IN-001005-01-05, Dharmacon, USA) were combined with Opti-MEM reduced serum medium and RNAiMAX lipofectamine (Thermo Fisher Scientific, USA) to form a complex before transfection. This complex, carried with 30 nM of each oligonucleotide, was incubated for 15 hours in 5-day differentiated C2C12 myotubes (Suppl Fig. 1B). All the experiments were carried out using at least three independent replicates per group.

Immunofluorescence

C2C12 myotubes cultured in 6-well plates were fixed in 4% paraformaldehyde for 15 mins, washed with PBS and 0.1% TritonX-100 (Sigma, USA), and blocked with 3% BSA, 1% glycine, 8% fetal bovine serum in PBS, and 0.1% TritonX-100 for 1 hour at room temperature. Subsequently, the cells were incubated with primary (Myh2) antibody overnight at 4°C and, after washing, the cells were incubated with secondary antibodies for 1 hour at room temperature and counterstained with DAPI. All images were acquired at room temperature from scanning confocal microscope TCS SP5 (Leica Microsystems, UK). The myotubes area and diameters were measured using NIH ImageJ software (https://imagej.nih.gov/ij/). To do these measurements, 15 fields were randomly selected in each group, and at least 100 myotubes were analyzed per field. We determined the average diameter calculating

the mean of the measures taken along the length of the myotubes, as previously described by Rommel et al. [50].

EdU assay

The EdU incorporation assay was performed using an EdU assay kit (Click-iT™ EdU Cell Proliferation Kit for Imaging – Thermo Fisher Scientific, USA) following the manufacturer's instructions. EdU labeling was conducted for 4 h for the C2C12 myoblasts with miR-497 mimic or IL-6 (100 ng/ml), and the respective controls. The proportions of EdU- and DAPI-positive cells were measured using ImageJ software.

RNA isolation

The total RNA was extracted from C2C12 cells using a TRIzol reagent (Thermo Fisher Scientific, USA), as recommended by the manufacturer. The RNA concentration and quality were assessed using a NanoVue Plus Spectrophotometer (GE Healthcare, USA). The RNA quality was also assured by the RNA integrity number (RIN) obtained from an analysis of ribosomal RNAs based on microfluidics using the 2100 Bioanalyzer system (Agilent, USA). Only RNA samples with A260/280 ratio of 1.8-2.0, A260/230 ratio > 2.0, and we used samples with RIN > 9 for subsequent analysis.

Expression profiling of microRNAs

MicroRNA samples were reverse transcribed using the Megaplex RT Primers Pools A (Thermo Fisher Scientific, USA). Global microRNA profiling of myotubes treated with IL-6 (n = 3) and control (n = 3) samples was performed with the TaqMan® Array Rodent MicroRNA Cards A v3.0 (Thermo Fisher Scientific, USA) for 373 mature microRNAs following the manufacturer's instructions. The samples ran on the QuantStudio™ 12K Flex System (Thermo Fisher Scientific, USA) using the following cycle conditions: 95 °C for 10 mins followed by 40 cycles of 95 °C for 15 secs and 60 °C for 1 min. Small RNA MammU6 was used as a reference to normalize the microRNA data. This reference microRNA was selected based on geNorm calculations [51]. Finally, raw data from each card set was retrieved and imported into Expression Suite Software v1.0.3 (Thermo Fisher Scientific, USA). Relative quantification of microRNA expression was evaluated using the $2^{-\Delta\Delta CT}$ method [52]. Cutoffs for significant changes were set at fold-change >1.5 and p-value ≤ 0.05.

mRNA gene expression

mRNA samples were reverse transcribed using the High Capacity RNA-to-cDNA master mix (Thermo Fisher Scientific, USA). The mRNAs qPCR analysis was performed in 15 µl reaction with Power SYBR™ Green Master Mix for mRNAs (Thermo Fisher Scientific, USA), as described by the manufacturer. The samples ran on QuantStudio™ 12K Flex System (Thermo Fisher Scientific, USA) using the following cycle conditions: 95 °C for 10 mins followed by 40 cycles of 95 °C for 15 secs and 60 °C for 1 min. The oligonucleotides used for mRNA analyses are listed in Supplementary Table 1. Rpl13a was used as a reference gene to normalize the mRNA data. This reference gene was selected based on geNorm calculations [51]. Relative quantification of mRNA expression was evaluated using the $2^{-\Delta\Delta CT}$ method [52]. Cutoffs for significant changes were set at fold-change >1.5 and p-value < 0.05.

Identification of miRNA-targets and pathway analysis

Using miRNA target prediction algorithm TargetScan 7.1 [53] and MirWalk [54], the deregulated miRNAs in myotubes treated with IL-6 were used for the prediction of mRNAs targets. Targeted gene pathways for differentially expressed miRNAs were explored by EnrichR [55,56] (http://amp.pharm.mssm.edu/Enrichr/), and the enrichment result is represented by p-value (Fisher exact test) and Z-score (correction to the test) in a combined score computed by EnrichR [55,56]. Protein-protein interaction (PPI) networks were then generated using Metasearch STRING v10.5.1 [57,58], and visualization and annotation data of PPI and miRNA-gene interaction networks were generated using Cytoscape v3.4.0 [59].

Validation Sets of Cancer Cachexia Models

To confirm whether miR-497 targets are indeed deregulated in the skeletal muscle of cancer cachexia models, we compared muscle gene expression profiles publicly available with our gene expression data after inhibition of miR-497 in C2C12 myotubes. The gene expression profiling data reanalyzed in the present study have been deposited in the NCBI Gene Expression Omnibus (GEO, https://www.ncbi.nlm.nih.gov/geo/) and are accessible through GEO Series accession number GSE48363 (C26 colon adenocarcinoma) [60], GSE63032 (C26 colon adenocarcinoma) [61], GSE51931 (mice with pancreatic cancer) [35], and GSE24111 (C26 colon adenocarcinoma) [34]. We analyzed each dataset individually by using GEO2R (http://www.nci.nlm.nih.gov/geo/geo2r/). GEO2R is an interactive online tool for R-based analysis of GEO data that allows the identification of genes that are differentially expressed across different experimental conditions [62]. The adjusted P-value was used to identify a list of deregulated genes from each dataset (fold-change > 2.0 and adjusted p-value < 0.05).

Statistical analysis and data visualization

All experimental data were normally distributed and expressed as the mean ± standard deviation (SD). Data were analyzed using the Student's t-test (using GraphPad Prism 6) to establish a significant value between data points. P-value < 0.05 were considered statistically significant. The Venn graph was created using the software Lucidchart (https://www.lucidchart.com/). The heatmaps were created using the web tool Morpheus [63] (https://software.broadinstitute.org/morpheus).

Results

High concentrations of IL-6 induce C2C12 myotubes atrophy

First, to confirm whether IL-6 is highly expressed in cachexia-associated tumor types, we sought to evaluate the IL-6 expression levels in four different tumor types with different prevalence of cachexia. Gene expression profiles were obtained of 1,938 tumors comprising from TCGA, and 900 corresponding normal tissues (TCGA and GTEx). These tumors were selected to allow an analysis of cancer types presenting different prevalence of cachexia [64,65]. We found that in cancer types with a high prevalence of cachexia, such as PAAD (Pancreatic Adenocarcinoma) and ESCA (Esophageal Carcinoma), IL-6 levels were higher when compared with normal tissue. On the other hand, in cancer types with a low prevalence of cachexia, as BRCA (Breast Invasive Carcinoma) and PRAD (Prostate Adenocarcinoma), the levels of IL-6 were lower or did not have difference when compared with normal tissue (Fig. 1A). Then, to test if the IL-6 could induce myotubes atrophy in vitro, three different concentrations of IL-6 were tested in 5-day differentiated C2C12 myotubes: 10 ng/ml, 50 ng/ml, and 100 ng/ml. The differentiated myotubes treated with exogenous IL-6 (50 ng/ml and 100 ng/ml) resulted in increased transcription of endogenous IL-6, while lower doses did not induce this effect (Fig. 1B-D). Myosin gene expression was not changed in myotubes with 10 ng/ml and 50 ng/ml of IL-6 but was decreased in the myotubes treated with 100 ng/ml of IL-6. We observed no differences in the myotubes diameter after the treatment with 10 ng/ml of IL-6 (Fig. 1E), while a significant reduction in the myotubes diameter and area was observed after the treatment with 50 ng/ml and 100 ng/ml of IL-6 (Fig. 1F-I). Also, the expression of embryonic myosin (Myh-emb), a typical and abundant myosin of C2C12myotubes, decreased in myotubes treated with IL-6 100 ng/ml (Fig. 1J). Moreover, the percentage of small myotubes were higher when differentiated myotubes were treated with high

concentrations of IL-6 (Suppl Fig. 2). These results indicated that high concentrations of IL-6 are sufficient to induce atrophy in differentiated myotubes.

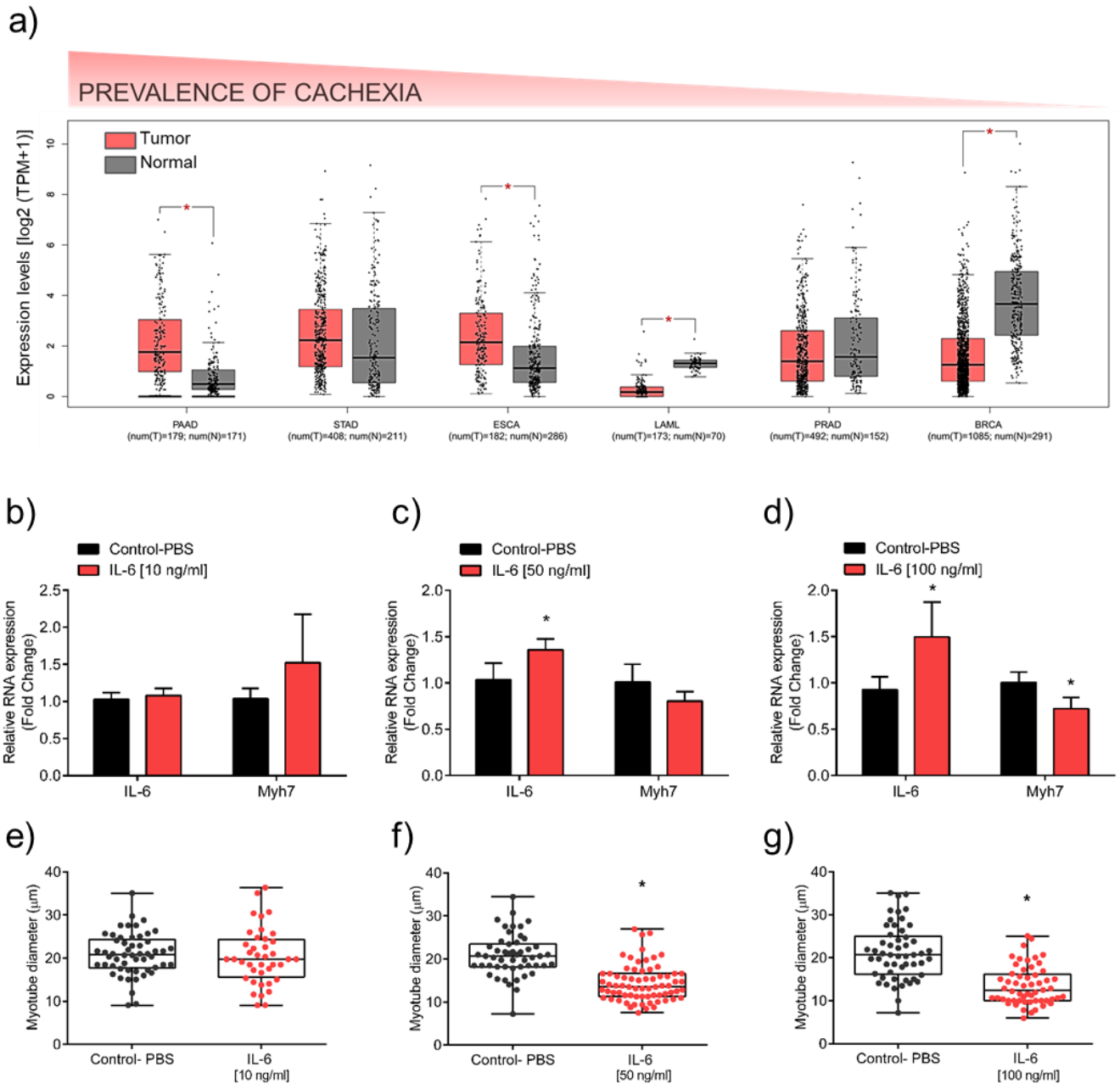

h)

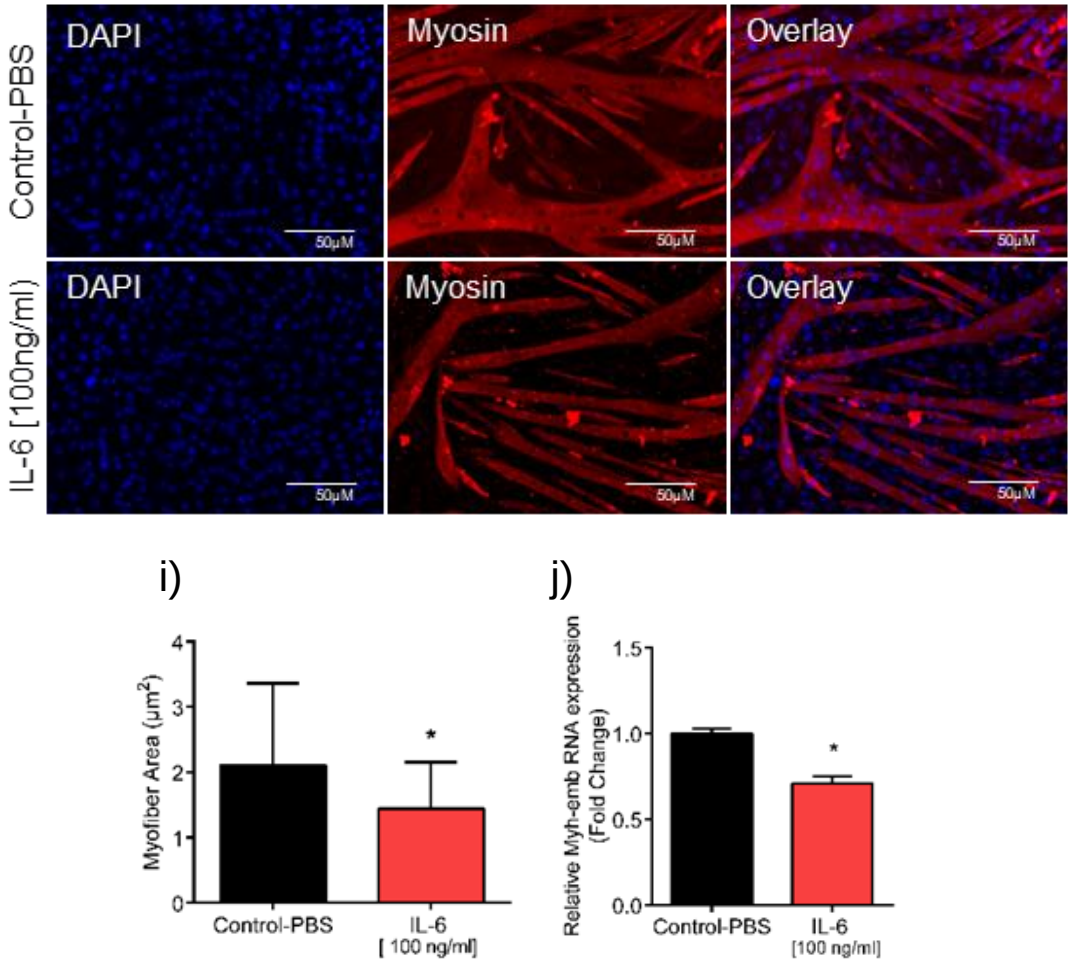

Figure 1. High concentrations of IL-6 induce C2C12 myotubes atrophy. A, Box-plot showing the mean expression levels [log2 (TPM+1)] of IL-6 in four different cancer types compared with normal tissues. Differential expression levels were calculated using the web-based tool Gene Expression Profiling Analysis (GEPIA, http://gepia.cancerpku.cn/)[48], using the dataset of PAAD (Pancreatic Adenocarcinoma), STAD, ESCA (Esophageal Carcinoma), LAML, PRAD (Prostate Adenocarcinoma) e BRCA (Breast Invasive Carcinoma). **B-D,** mRNA levels of IL-6 and Myh7 in differentiated C2C12 myotubes treated with three different concentrations of IL-6. RT-qPCR data are presented as fold change (2^-ΔΔCt) relative to Rpl13a. Data represent the average of three independent experiments with standard deviation. **E-G,** Myotubes diameter of control and treated with IL-6 (B, 10 ng/ml; D, 50 ng/ml; F 100 ng/ml). **H,** Representative images of myotubes from the control group and treated with IL-6 (100 ng/ml). The immunofluorescence was performed using the antibody against Myh2 and Dapi (4',6-Diamidine-2'-phenylindole dihydrochloride). **I,** Quantitative analysis of myotubes area. **J,** mRNA levels of embryonic myosin (Myh-emb) in differentiated C2C12 myotubes treated with IL-6 (100 ng/ml). RT-qPCR data are presented as fold change (2^-ΔΔCt) relative to Rpl13a. Statistical difference was analyzed by Student's t-test. * $P < 0.05$ vs. Control.

Global miRNA expression analysis identified miR-497as a miRNA involved in muscle atrophy

Twenty miRNAs, 5 upregulated and 15 downregulated, were differentially expressed in myotubes treated with IL-6 (100 ng/ml) (Fig. 2A and Sup Table 2). This analysis could identify some miRNAs already related to skeletal muscle atrophy, such as miR-23a, miR-146a, and miR-29c [66–68]. To understand which biological processes these miRNAs are potentially involved in, we predicted the targets for each miRNA identified. The over-represented Gene Ontology categories of biological processes included miRNA-target genes regulating cyclic nucleotide catabolic process, activation of NFkappaB-inducing kinase activity, insulin-like growth factor signaling, JAK-STAT cascade, and regulation of cell cycle (Fig. 2B). These results indicate an implicated combination of target multiplicity and miRNA cooperativeness on muscle wasting under high concentration of IL-6.

Next, we performed a comparison between our miRNA expression profile and previous studies that reported alterations in miRNA expression in muscle atrophy conditions [45,69]. This analysis revealed miRNAs in our study that are shared with these previous studies. The miRNAs miR-23a and miR-497 are deregulated in cancer cachexia [45]; miR-146, miR-151, and miR-497 in primary disorders [69]; and miR-23a, miR-29c, miR-499, and miR-497 in different catabolic conditions [45] (Fig. 2C). We identified miR-497 as differentially expressed in all conditions analyzed. Consequently, we validated by RT-qPCR that miR-497 is down-regulated in myotubes treated with higher concentrations of IL-6 (50 ng/ml and 100 ng/ml) (Fig. 2D). To elucidate post-transcriptional mechanisms of the miR-497 that potentially affect myotubes size, the targets of this miRNA were predicted using TargetScan 7.1 (http://www.targetscan.org/). The miR-497 targets interaction network shows several proteins involved insulin signaling pathway, cell cycle, ubiquitin-mediated proteolysis, and apoptosis. Complex interactome analysis of miR-497 target genes and its respective functional annotations is illustrated in Fig. 2E.

a)

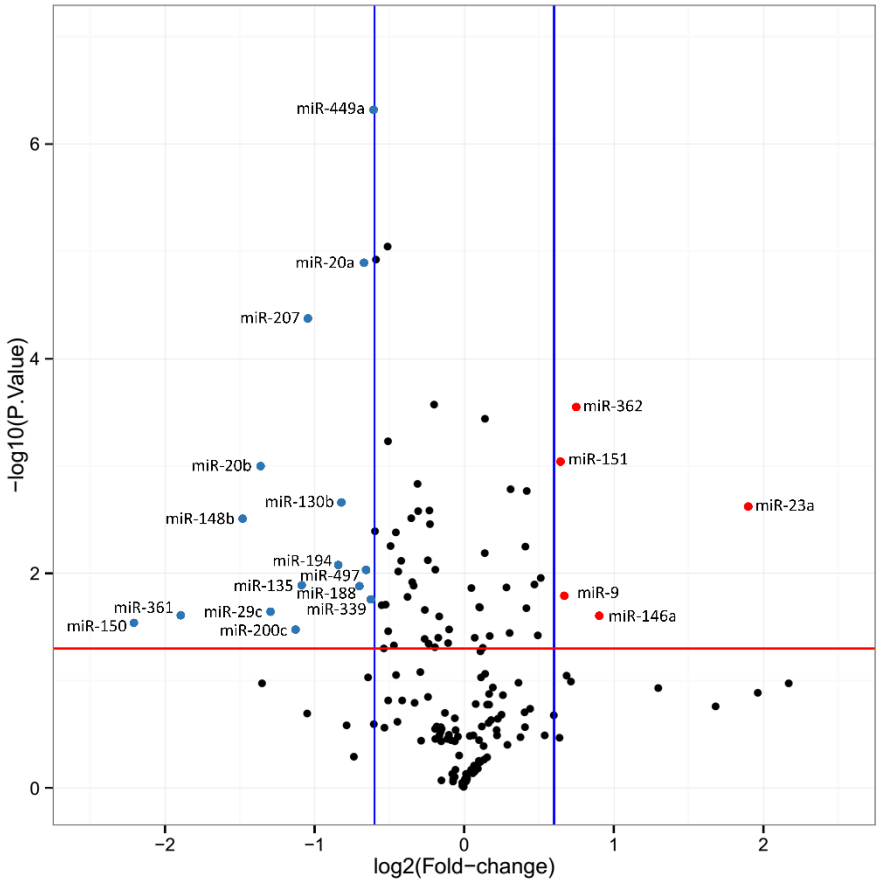
miR-449a
miR-20a
miR-207
miR-362
miR-151
miR-20b
miR-130b
miR-148b
miR-23a
miR-194
miR-497
miR-135
miR-188
miR-9
miR-361
miR-29c
miR-339
miR-146a
miR-150
miR-200c
−log10(P.Value)
log2(Fold−change)

b)

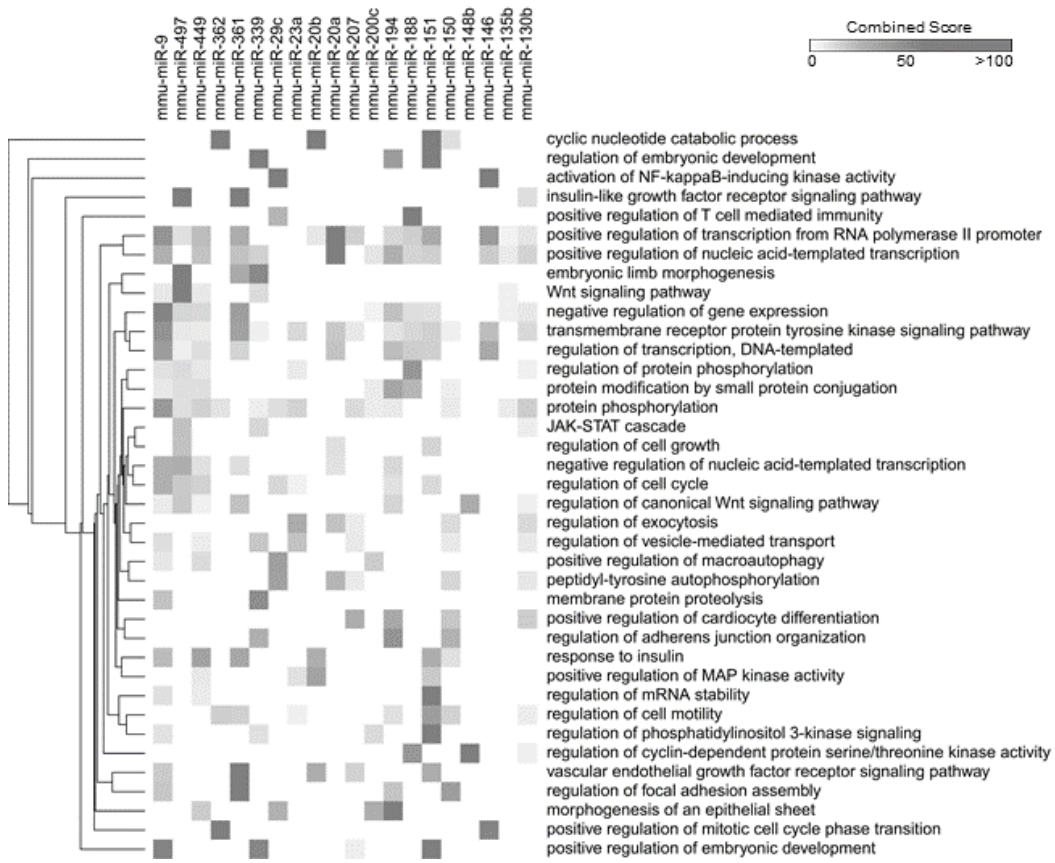
mmu-miR-9
mmu-miR-497
mmu-miR-449
mmu-miR-362
mmu-miR-361
mmu-miR-339
mmu-miR-29c
mmu-miR-23a
mmu-miR-20b
mmu-miR-20a
mmu-miR-207
mmu-miR-200c
mmu-miR-194
mmu-miR-188
mmu-miR-151
mmu-miR-150
mmu-miR-148b
mmu-miR-146
mmu-miR-135b
mmu-miR-130b
Combined Score
0
50
>100
cyclic nucleotide catabolic process
regulation of embryonic development
activation of NF-kappaB-inducing kinase activity
insulin-like growth factor receptor signaling pathway
positive regulation of T cell mediated immunity
positive regulation of transcription from RNA polymerase II promoter
positive regulation of nucleic acid-templated transcription
embryonic limb morphogenesis
Wnt signaling pathway
negative regulation of gene expression
transmembrane receptor protein tyrosine kinase signaling pathway
regulation of transcription, DNA-templated
regulation of protein phosphorylation
protein modification by small protein conjugation
protein phosphorylation
JAK-STAT cascade
regulation of cell growth
negative regulation of nucleic acid-templated transcription
regulation of cell cycle
regulation of canonical Wnt signaling pathway
regulation of exocytosis
regulation of vesicle-mediated transport
positive regulation of macroautophagy
peptidyl-tyrosine autophosphorylation
membrane protein proteolysis
positive regulation of cardiocyte differentiation
regulation of adherens junction organization
response to insulin
positive regulation of MAP kinase activity
regulation of mRNA stability
regulation of cell motility
regulation of phosphatidylinositol 3-kinase signaling
regulation of cyclin-dependent protein serine/threonine kinase activity
vascular endothelial growth factor receptor signaling pathway
regulation of focal adhesion assembly
morphogenesis of an epithelial sheet
positive regulation of mitotic cell cycle phase transition
positive regulation of embryonic development

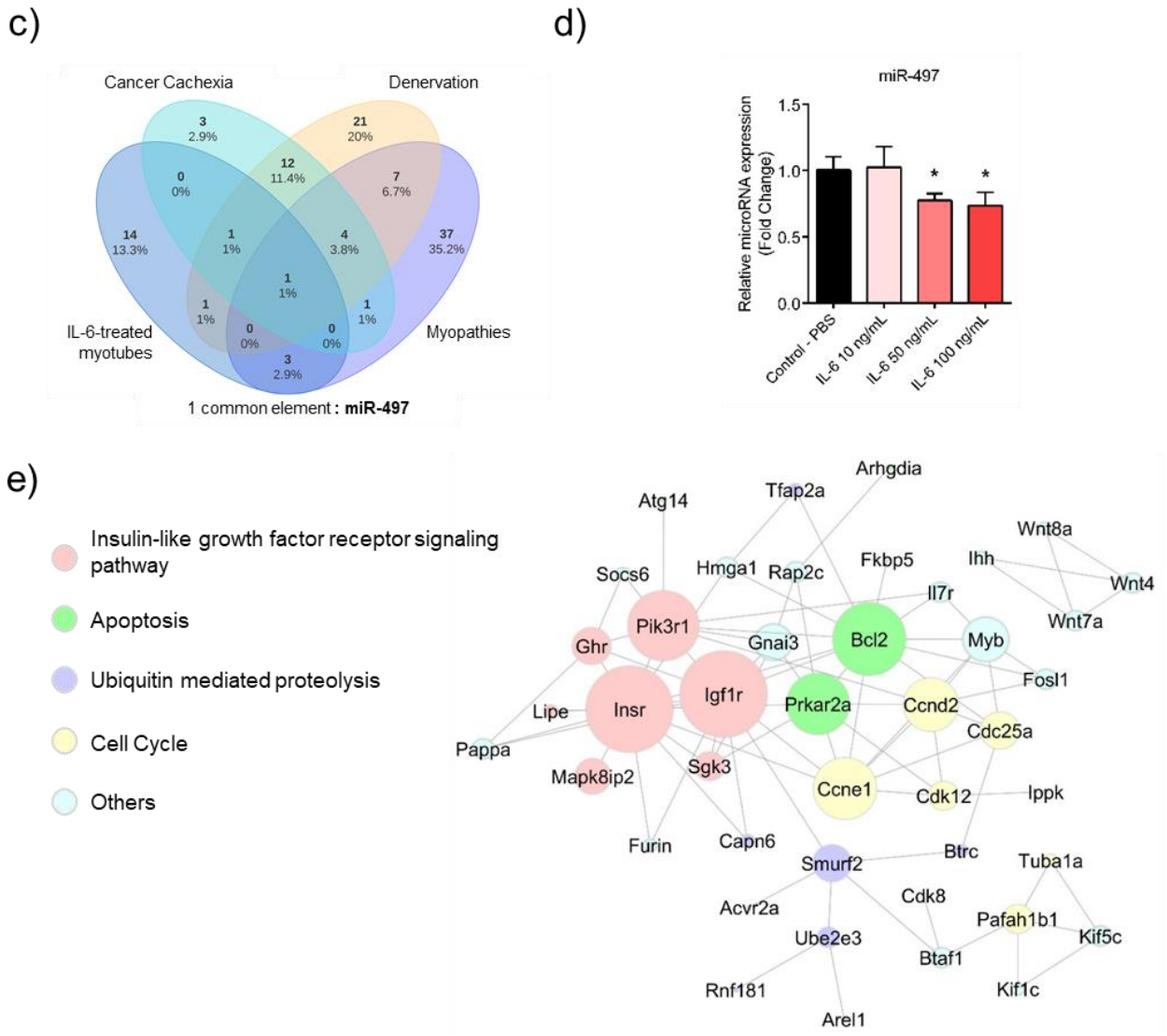

Figure 2. miR-497 is deregulated in skeletal muscle cells in different atrophic conditions. A, Volcano plot representing the log 2-fold change and p-value of all microRNA differentially expressed. A set of 20 miRNAs displayed significant changes (p-value < 0.05 and fold change ≥ 1.5). **B,** Heatmap presents the Biological Process enriched by a predicted set of targets for each miRNA. The top five ranked annotations of GO and enriched in at least two datasets were shown and illustrated. The enriched terms are clustered according to Euclidean distance. **C,** Venn diagram showing the miR-497 as a common element between our data, cancer cachexia, primary muscle disorders, and other catabolic conditions. **D,** MiR-497 expression levels in differentiated C2C12 myotubes treated with three different concentrations of IL-6. RT-qPCR data are presented as fold change ($2^{-\Delta\Delta Ct}$) relative to MammU6. **E,** Interactome between predicted miR-497 target genes. Nodes represent miR-497 target genes according to the biological process. The larger the nodes, the higher the degree of interactions identified. Nodes with no connections were excluded. STRING v10.5.1 was used to generate protein interactions, and the network interactions were visualized using Cytoscape v3.4.0.

MiR-497 overexpression induces myotubes atrophy

Considering that miR-497 is a miRNA affected by IL-6, we next asked whether miR-497 may induce atrophy of skeletal muscle cells. There is evidence that this miRNA is involved in atrophic conditions, such as in cancer cachexia [45,46], denervation [45], and in several myopathies [69]. Here, we confirmed the pro-atrophic capacity of miR-497 in vitro by transfecting miRNA mimics in C2C12 myotubes. RT-qPCR confirmed the efficiency of miRNA mimics or inhibitors on miR-497 expression in myotubes (Fig. 3A and B). Therefore, we next examined whether the overexpression or underexpression of miR-497 is accompanied by a change in the myotubes size. We observed large differences in gene expression for some regulators of myotubes growth. The expression of myogenin (Myog) was increased in myotubes overexpressing miR-497, but no differences were observed in myotubes that underexpressed this miRNA (Suppl Fig. 4). Moreover, we investigated the gene expression of *Myh7*, *Hmga1*, and *Id3*, but were observed no differences in *Myh7* and *Id3* expression even with mimics or inhibitors. The *Hmga1* expression was downregulated with miR-497 mimic and inhibitor transfections (Suppl Fig. 4). Immunofluorescence analysis revealed that the transfection with miR-497 mimic decreased myotubes diameter (Fig. 3C and D) while miR-497 inhibitor did not change the myotubes size (Fig. 3E and F). Thus, the pro-atrophic capacity of miR-497 is regulated by mechanisms that are predominant in myotubes overexpressing miR-497 but not in myotubes with low levels of miR-497.

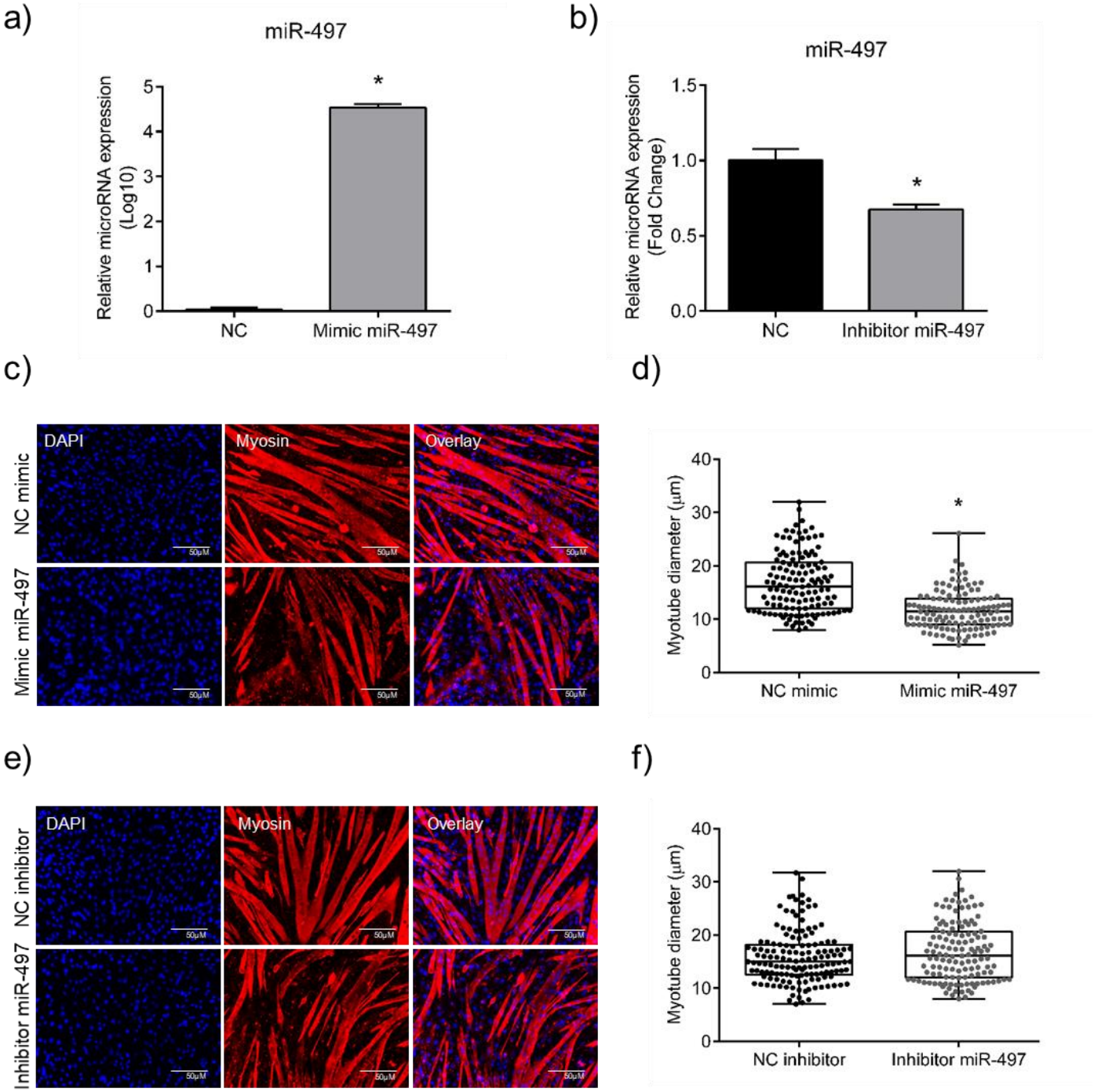

Figure 3. miR-497 effects in differentiated C2C12 myotubes. A, Relative log10 transformed miR-497 levels measured by RT-qPCR in C2C12 myotubes transfected with miRNA mimics of miR-497, compared with mimic control. **B,** RT-qPCR is showing decreased expression of miR-497 in C2C12 myotubes transfected with miRNA inhibitor against miR-497. **C,** Representative images of myotubes from the negative control group and transfected with mimic miR-497. **D,** Myotubes diameter of transfected with negative control and with mimic miR-497. **E,** Representative images of myotubes from the negative control group and transfected with inhibitor miR-497. **F,** Myotubes diameter of transfected with negative control and with inhibitor miR-497. The

immunofluorescence was performed using the antibody against Myh2 (red) and Dapi (blue). Statistical difference was analyzed by Student's t-test. * P < 0.05. NC: negative control.

The insulin signaling pathway is enriched with miR-497 targets genes

We sought to identify which biological functions miR-497 targets regulated in muscle cells. The list of miR-497 target genes highlights the insulin-growth factor receptor pathway as the most overrepresented (enriched) biological annotation, according to Gene Ontology analysis (Fig. 4A). Moreover, through other biological annotation databases, we analyzed several terms enriched by the mir-497 target genes. Ubiquitin mediated proteolysis, cell cycle, apoptosis, and JAK-STAT signaling pathway were other terms identified as overrepresented in different databases. The insulin pathway is enriched in almost all databases analyzed. (Suppl. Fig 4). Among the genes that enriched the insulin-signaling pathway, *Insr*, *Igf1r*, *Pik3r1*, and *Mapk8ip2* were further analyzed by RT-qPCR. The myotubes transfected with miR-497 mimic decreased the expression of *Insr* and *Mapk8ip2*, while the effect of miR-497 inhibitor increased the *Insr* and *Igf1r*. The *Pik3r1* did not change in both conditions. Together, these results suggest that miR-497 regulates genes involved with the insulin-growth factor receptor pathway, playing a role in compensatory mechanism during the skeletal muscle atrophy caused by IL-6.

a)

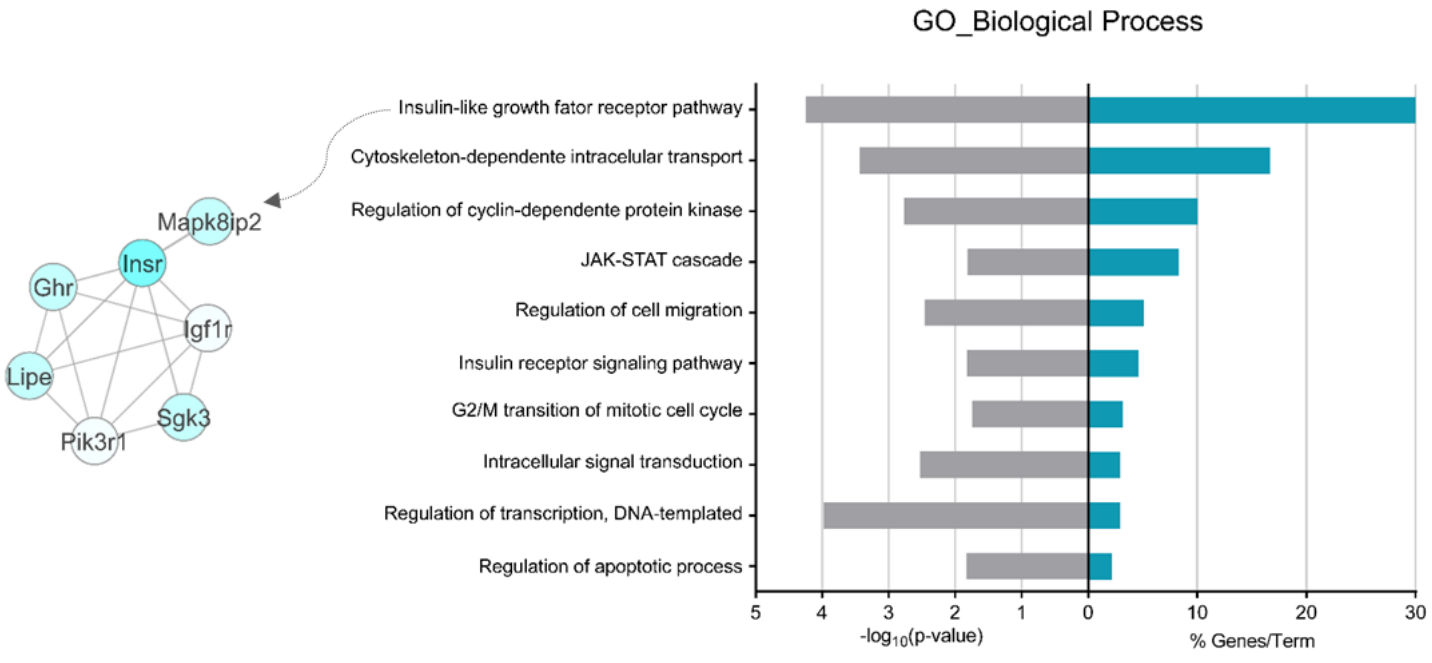

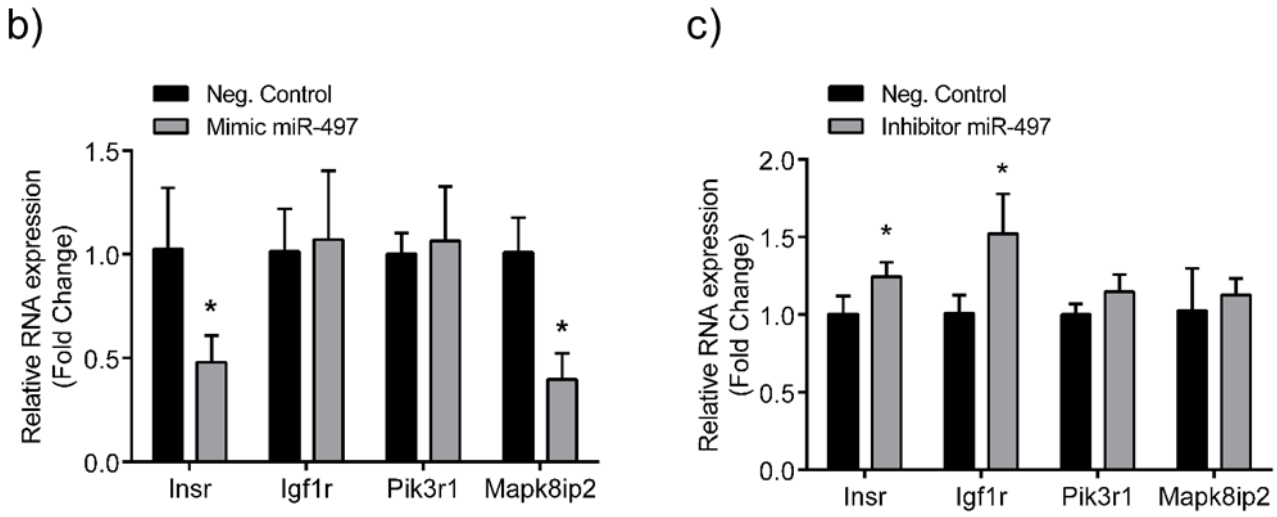

Figure 4. miR-497 target genes enriched the insulin-growth factor pathway. A, Biological analysis of miR-497 target genes showing the overrepresented (enriched) terms according to Gene Ontology (p-value ≤ 1.82E-02). **B,** mRNA levels of *Insr*, *Igf1r*, *Pik3r1*, and *Mapk8ip2* in differentiated C2C12 myotubes transfected with mimic miR-497. **C,** mRNA levels of *Insr*, *Igf1r*, *Pik3r1*, and Mapk8ip2 in differentiated C2C12 myotubes transfected with inhibitor miR-497. RT-qPCR data are presented as fold change ($2^{\wedge-\Delta\Delta Ct}$) relative to Rpl13a. Data represent the average of three independent experiments with standard deviation. Statistical difference was analyzed by Student's t-test. * $P < 0.05$. Insr: insulin receptor; *Igf1r*: insulin-like growth factor 1 receptor; *Pik3r1*: phosphoinositide-3-kinase regulatory subunit 1; *Mapk8ip2*: mitogen-activated protein kinase 8 interacting protein 2.

Neither IL-6 or miR-497 affect the myoblast proliferation rate

Cell cycle appeared among the pathways enriched in our ontology analysis. The mir-497 has already been reported to play an important role in regulating skeletal muscle cell proliferation. Cyclins CcnD2 and CcnE1 are predicted as potential targets of miR-497, and there is evidence that miR-497 acts on muscle cell proliferation by regulating CcnD2 and CcnE1 [70]. The transfection with miR-497 mimic decreases significant *CcnD2* and *CcnE1* expression, while inhibition of miR-497 and treatment with IL-6 showed no change in expression levels of these cyclins. We sought to evaluate cellular proliferation in myoblasts treated with miR-497 mimetic molecules or IL-6. We found no alteration on proliferation rate in myoblasts treated with mimic miR-497 or with IL-6. Thus, our results show that miR-497 affects *CcnD2* and *CcnE1* expression but does not affect myoblast proliferation rate.

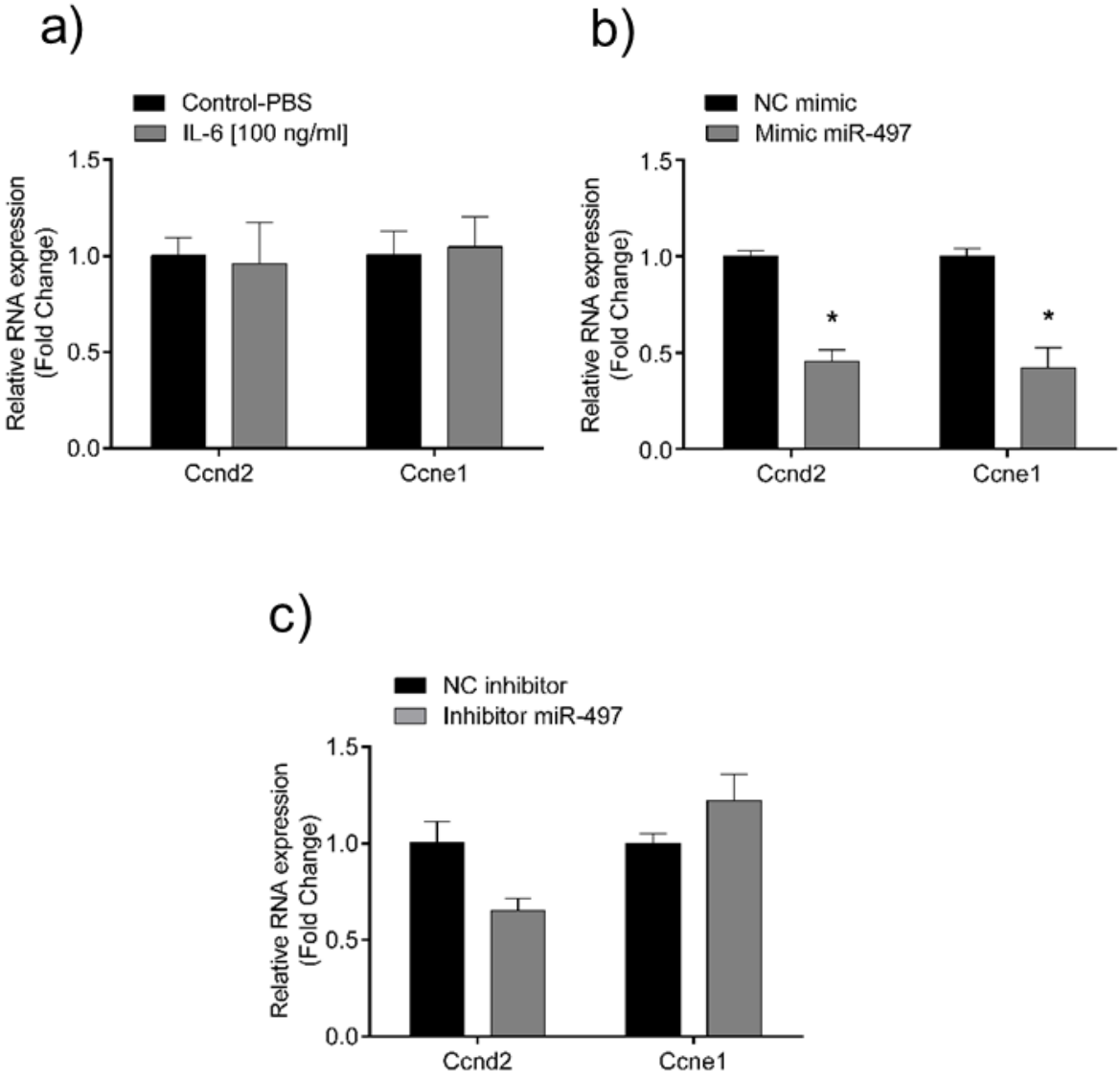
a)
Control-PBS
IL-6 [100 ng/ml]
Relative RNA expression (Fold Change)
1.5
1.0
0.5
0.0
Ccnd2
Ccne1
b)
NC mimic
Mimic miR-497
Relative RNA expression (Fold Change)
1.5
1.0
0.5
0.0
*
*
Ccnd2
Ccne1
c)
NC inhibitor
Inhibitor miR-497
Relative RNA expression (Fold Change)
1.5
1.0
0.5
0.0
Ccnd2
Ccne1

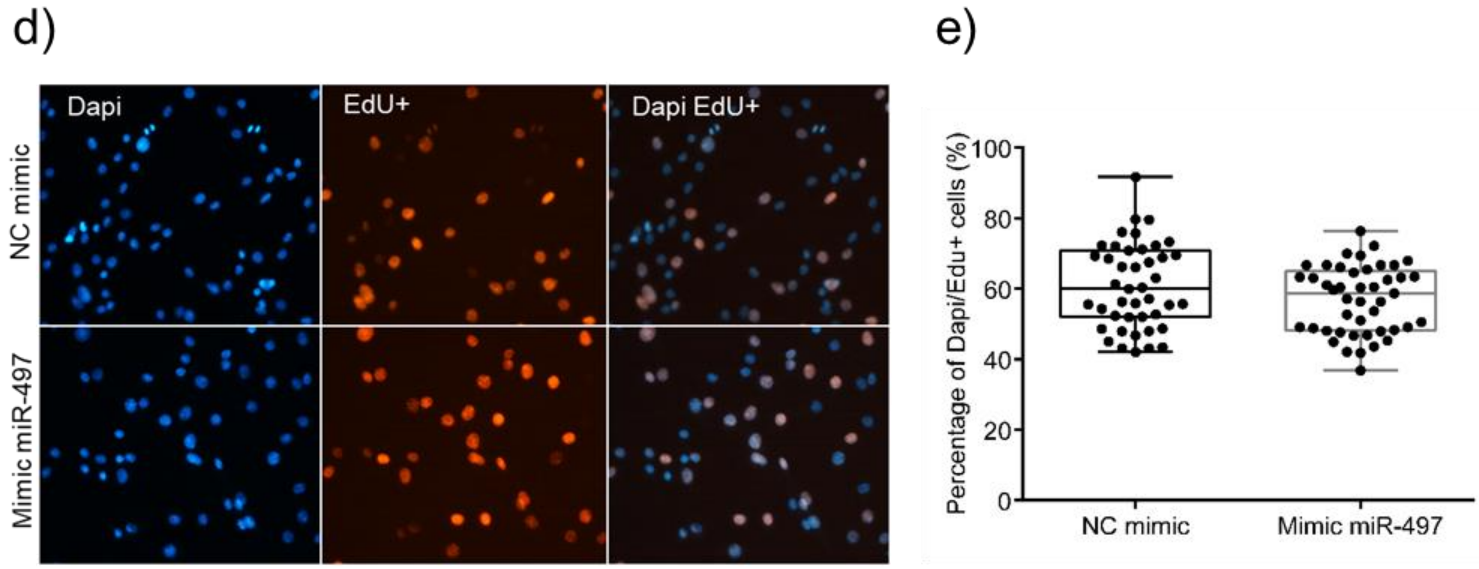
d)
Dapi
EdU+
Dapi EdU+
NC mimic
Mimic miR-497
e)
Percentage of Dapi/Edu+ cells (%)
100
80
60
40
20
0
NC mimic
Mimic miR-497

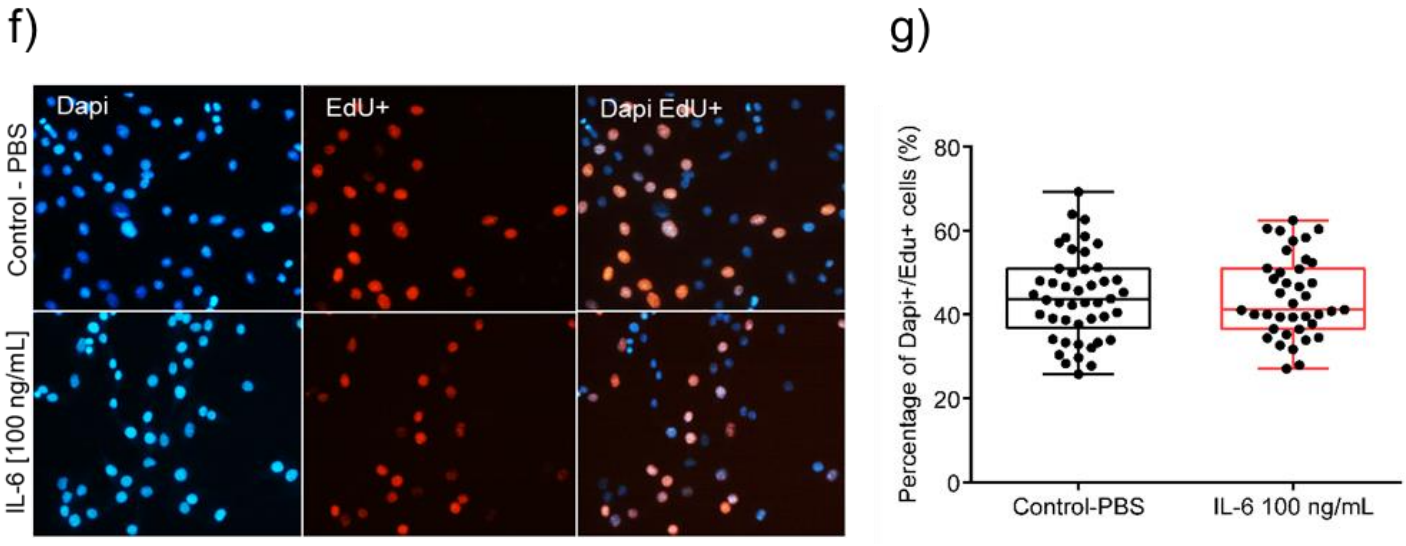

Figure 5. miR-497 and proliferation. mRNA levels of the cyclins *CcnD2* and *CcnE1in* C2C12 myoblasts treated with IL-6 [100 ng/ml] and PBS (**A**), transfected with mimic miR-497 and negative control (**B**), and with transfected with inhibitor miR-497 and negative control (**C**). RT-qPCR data are presented as fold change (2^-ΔΔCt) relative to Rpl13a. **D,** Representative images of myoblasts transfected with mimic miR-497 and negative control, cells were stained with EdU (red). **E,** Percentage of Dapi (blue) and Edu+ cells out of the total number of Dapi cells was determined. **F,** Representative images of myoblasts treated with IL-6 [100 ng/ml] and PBS as control, cells were stained with EdU (red). **G,** Percentage of Dapi (blue), and Edu+ cells out of the total number of Dapi cells were determined. Data represent the average of three independent experiments with standard deviation. Statistical difference was analyzed by Student's t-test. * $P < 0.05$. NC: negative control.

In silico validation using cancer cachexia models

To verify how consistent our findings are with those observed in cancer cachexia models, we reanalyzed transcriptomic data of muscle from cachectic animals with different cancer types, all of them available at NCBI Gene Expression Omnibus. The miR-497 targets analyzed in the heatmap, as well as the graphs showing these results, are presented in Suppl. Fig. 4. Notably, the expression of the *Igf1*, *Insr*, and *Pik3r1* genes was similar to that observed in the miR-497 inhibitor-treated myotubes, while the expression pattern of several miRNA targets was not consistent with that observed in the models.

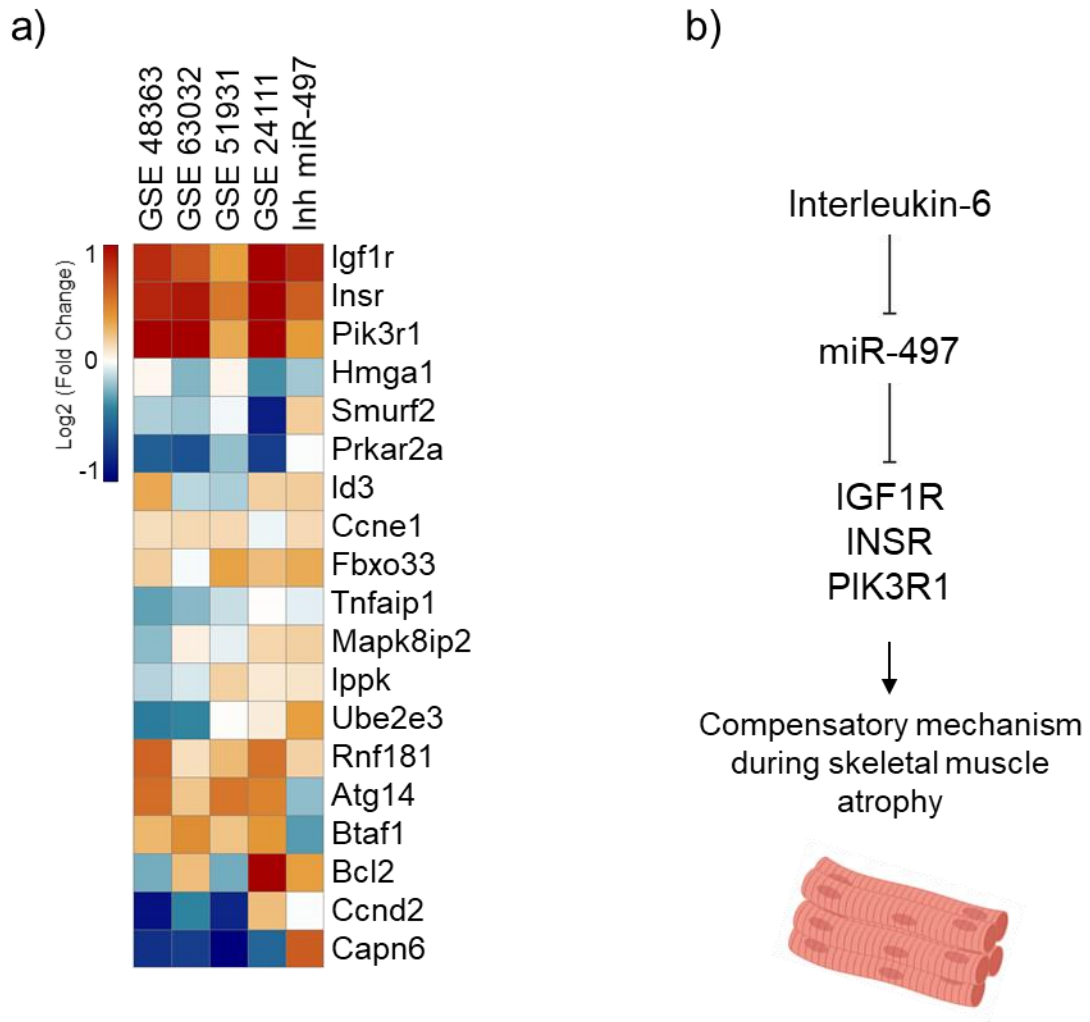

Figure 6. miR-497 involves the regulation of *Igf1r* and *Insr* genes and the potential activation of a compensatory mechanism. A, Heatmap of the expression levels [Log2 Fold Change] of miR-497 target genes in four different cancer cachexia datasets and in myotubes transfected with inhibitor miR-497. Both rows (target genes) and columns (datasets) were clustered using Euclidian distance. **B,** Schematic diagram of the IL-6–miR-497–Igf1r/Insr pathway and its role in a compensatory mechanism during skeletal muscle atrophy.

Discussion

Although many studies have shown the involvement of IL-6 in skeletal muscle atrophy due to systemic inflammation in cancer patients, little is known about the intracellular mechanisms that are induced by this cytokine. The present study aimed to identify miRNAs that are dysregulated during muscle cell atrophy upon high concentrations of IL-6. We identified a profile of 20 differentially expressed miRNAs, which are responsible for the regulation of genes involved with activation of NFkappaB-inducing kinase activity, insulin-like growth factor signaling, JAK-STAT cascade, and cell cycle.

Among then, miR-497 appeared to be promising as it was also downregulated in other atrophic conditions such as cancer cachexia, denervation, and myopathies [45,69]. Our results showed that IL-6 decreases the expression of miR-497, which regulates the insulin pathway genes such as *Insr* and *Igf1r*. This constitutes a potential compensatory mechanism during muscle cell atrophy.

Several studies have indicated IL-6 with an important regulatory role in skeletal muscle plasticity [71]. The effects of this cytokine in the muscle are paradoxes, and this divergence between catabolism or anabolism is due to conditions such as the level of IL-6, acute or chronic exposure, and the type of administration [40]. Our results show that in cancer types more likely to develop muscle wasting, IL-6 is significantly overexpressed in tumor tissue as compared to respective normal tissue. Although the increased circulating levels of IL-6 have been well established in cancer patients, our findings showed evidence that IL-6 expression is tumor-specific, and indeed appears to be associated with tumor types with a higher prevalence of cachexia. Due to the importance of IL-6 and its regulatory role in muscle wasting during cachexia, we mimicked chronic effects and high concentration using different doses of IL-6 in C2C12 myotubes to understand the inducing effects of muscle atrophy. Our results showed that supraphysiological dose of 100 ng/ml can be preferentially used to induce catabolic effects in myotubes. These results are consistent with Bonetto *et al.*(2012) who found a decrease of 36% in the myotubes diameter when these cells were treated with 100 ng/ml of IL-6 [9].

We also found that this supraphysiological dose of IL-6 leads to myotubes atrophy and deregulates the expression of 20 miRNAs. Some of these miRNAs were previously described as deregulated in skeletal muscle atrophy conditions [66–68]. We observed that biological processes for these target transcripts are enriched for activation of NFkappaB-inducing kinase activity, JAK-STAT cascade, regulation of T cell-mediated immunity, insulin-like growth factor, and cell cycle. To better understand which microRNA could be crucial during the atrophy process induced by IL-6, we performed a comparative analysis that allowed us to identify miR-23a and miR-497 as deregulated miRNAs in cancer cachexia models [45]. However, although miR-23a was found in common, the directions of expression were divergent; Soares et al. demonstrated that miR-23a is downregulated in cancer cachexia mice and our myotubes atrophied by IL6 increased the expression of miR-23a. Several other studies have pointed out that miR-23a is an important miRNA involved with muscle plasticity (reviewed by [72]). For instance, some studies showed the increase of miR-23a associated with muscle atrophy, suggesting that miR-23a could be the key regulatory factor in the denervated atrophy process [73,74]. On the other hand, studies also pointed out that increased expression of this miRNA is important to attenuate muscle loss [75,76]. Due to this divergence, we chose not to investigate miR-23a further; in

contrast, while comparing other miRNAs datasets across different atrophy conditions, the miR-497 appeared to have lower expression in our model, in cancer cachexia and in denervation-induced atrophy [45].

There is evidence showing miR-497 as a key player in skeletal muscle development [70,77]. Previous research showed a regulatory axis for myogenesis in which miR-195/497 promotes myogenic differentiation by repressing the HMGA1–Id3 pathway [77]. To validate this role of miR-497 in proliferation, we performed in vitro assays to confirm this antiproliferative effect on myoblasts. Although miR-497 had some influence on Hmga1 gene expression, we observed no significant effect on Id3 expression (Suppl Fig 5), and our functional results showed no alteration in the proliferation rate of myoblasts. These divergent results may have occurred due to the different protocols used to evaluate proliferation. Another study showed the increase of mir-497, decreasing the expression of Ccnd2 and CcnE1 cyclins, which leads to less proliferation of myoblasts [70]. In our results, we observed a miR-497 effect on inhibition of these cyclins; however, our functional studies do not corroborate with the data found by these authors. Although these studies have already shown the role of miR-497 during skeletal muscle development, there is no knowledge about the mechanisms by which miR-497 acts during muscle cell atrophy. In order to understand the effects of miR-497 in skeletal muscle cells, we analyzed the overexpression and the inhibition of miR-497 in differentiated myotubes. The inhibition of miR-497 did not affect the size of myotubes, and this means that the atrophic effect observed in IL-6-treated myotubes was probably not caused due to lower miR-497 expression levels. Additionally, the overexpression of miR-497 caused a decrease in myotubes size, showing that the high expression of miR-497 may not be beneficial to differentiated myotubes. Our findings suggest that miR-497 regulates important genes of the insulin-like growth factor pathway, like *Igf1r* and *Insr*. Muscle mass is controlled by several different signaling pathways, and the insulin-like growth factor is a positive signaling pathway, as it increases muscle mass upon increasing protein synthesis and decreasing protein degradation.

Our data reanalysis showed overexpression of growth-related genes was also observed in cachexia cancer model datasets [34,35,60,61]. The proteins IGF1, INSR, PI3KR1 have an important role in inducing skeletal muscle hypertrophy, both by increasing protein synthesis and by blocking protein degradation [78]. Although intriguing, the high expression of these factors in the context of atrophy is reasonable to understand that muscle strives to maintain muscle homeostasis, even during atrophy conditions. By activating the expression of *Insr*, *Igf1*, and *Pik3r1*, the anabolic pathway is activated in order to balance the catabolic process. Thus, inhibition of miR-497 after IL-6 treatment, with

consequent increased expression of *Igf1* and *Insr*, may suggest activation of the compensatory mechanism by miR-497 during IL-6-induced muscle cell atrophy.

In summary, we identified a specific miRNA expression profile from skeletal muscle cell atrophied by high levels of IL-6. In addition, our study suggests that IL-6 leads to a decrease in miR-497 as a potential compensatory mechanism during skeletal muscle atrophy. The mechanism underlying this activation of the compensatory mechanism by miR-497 involves the regulation of *Igf1r* and *Insr* genes. Finally, our data indicate a novel signaling pathway that involves IL-6–miR-497–Igf1r/Insr during muscle cells atrophy. Our findings provide insight into the mechanisms that occur in muscle atrophy and might have great significance for understanding cancer cachexia.

Funding

This study was supported by the São Paulo Research Foundation – FAPESP (grants #12/13961-6, #13/50343-1, and #14/13941-0); National Council of Technological and Scientific Development (CNPq 141919/2016-7); and CAPES-PDSE grant 88881.187095/2018-01.

Acknowledgments

We would like to thank Justin King from Children's Hospital of Harvard Medical School for helping us during immunofluorescence experiments. The results shown here are in part based upon data generated by the TCGA Research Network (http://cancergenome.nih.gov/), and by the Genotype-Tissue Expression project (GTEx) (https://gtexportal.org/).

References

1. Fearon, K. C. H., Glass, D. J. & Guttridge, D. C. Cancer cachexia: mediators, signaling, and metabolic pathways. *Cell Metab.* **16,** 153–66 (2012).
2. Gallagher, I. J. *et al.* Suppression of skeletal muscle turnover in cancer cachexia: evidence from the transcriptome in sequential human muscle biopsies. *Clin. Cancer Res.* **18,** 2817–27 (2012).
3. Muscaritoli, M., Rossi Fanelli, F. & Molfino, A. Perspectives of health care professionals on cancer cachexia: results from three global surveys. *Ann. Oncol. Off. J. Eur. Soc. Med. Oncol.* **27,** 2230–2236 (2016).
4. Laine, A., Iyengar, P. & Pandita, T. K. The role of inflammatory pathways in cancer-associated cachexia and radiation resistance. *Mol. Cancer Res.* **11,** 967–72 (2013).
5. Fearon, K. *et al.* Definition and classification of cancer cachexia: an international consensus. *Lancet Oncol.* **12,** 489–95 (2011).
6. Porporato, P. E. Understanding cachexia as a cancer metabolism syndrome. *Oncogenesis* **5,** e200 (2016).
7. Onesti, J. K. & Guttridge, D. C. Inflammation based regulation of cancer cachexia. *Biomed Res. Int.*

2014, 168407 (2014).

8. Keller, U. Pathophysiology of cancer cachexia. *Support. Care Cancer* **1,** 290–4 (1993).

9. Bonetto, A. *et al.* JAK/STAT3 pathway inhibition blocks skeletal muscle wasting downstream of IL-6 and in experimental cancer cachexia. *Am. J. Physiol. Metab.* **303,** E410–E421 (2012).

10. Li, Y. P., Schwartz, R. J., Waddell, I. D., Holloway, B. R. & Reid, M. B. Skeletal muscle myocytes undergo protein loss and reactive oxygen-mediated NF-kappaB activation in response to tumor necrosis factor alpha. *FASEB J.* **12,** 871–80 (1998).

11. Li, Y. P. & Reid, M. B. NF-kappaB mediates the protein loss induced by TNF-alpha in differentiated skeletal muscle myotubes. *Am. J. Physiol. Regul. Integr. Comp. Physiol.* **279,** R1165–70 (2000).

12. Reid, M. B. & Li, Y. P. Tumor necrosis factor-alpha and muscle wasting: a cellular perspective. *Respir. Res.* **2,** 269–72 (2001).

13. Haddad, F., Zaldivar, F., Cooper, D. M. & Adams, G. R. IL-6-induced skeletal muscle atrophy. *J. Appl. Physiol.* **98,** 911–7 (2005).

14. Meyer, S. U. *et al.* Integrative Analysis of MicroRNA and mRNA Data Reveals an Orchestrated Function of MicroRNAs in Skeletal Myocyte Differentiation in Response to TNF-α or IGF1. *PLoS One* **10,** e0135284 (2015).

15. Yamaki, T. *et al.* Rel A/p65 is required for cytokine-induced myotube atrophy. *Am. J. Physiol. Cell Physiol.* **303,** C135–42 (2012).

16. Suh, S.-Y. *et al.* Interleukin-6 but not tumour necrosis factor-alpha predicts survival in patients with advanced cancer. *Support. Care Cancer* **21,** 3071–7 (2013).

17. Muñoz-Cánoves, P., Scheele, C., Pedersen, B. K. & Serrano, A. L. Interleukin-6 myokine signaling in skeletal muscle: a double-edged sword? *FEBS J.* **280,** 4131–4148 (2013).

18. Pedersen, B. K. & Febbraio, M. A. Muscle as an endocrine organ: focus on muscle-derived interleukin-6. *Physiol. Rev.* **88,** 1379–406 (2008).

19. Sun, L. *et al.* JAK1-STAT1-STAT3, a key pathway promoting proliferation and preventing premature differentiation of myoblasts. *J. Cell Biol.* **179,** 129–38 (2007).

20. Serrano, A. L., Baeza-Raja, B., Perdiguero, E., Jardí, M. & Muñoz-Cánoves, P. Interleukin-6 is an essential regulator of satellite cell-mediated skeletal muscle hypertrophy. *Cell Metab.* **7,** 33–44 (2008).

21. Guerci, A. *et al.* Srf-dependent paracrine signals produced by myofibers control satellite cell-mediated skeletal muscle hypertrophy. *Cell Metab.* **15,** 25–37 (2012).

22. Pedersen, B. K. Muscular interleukin-6 and its role as an energy sensor. *Med. Sci. Sports Exerc.* **44,** 392–6 (2012).

23. Ruderman, N. B. *et al.* Interleukin-6 regulation of AMP-activated protein kinase. Potential role in the systemic response to exercise and prevention of the metabolic syndrome. *Diabetes* **55 Suppl 2,** S48–54 (2006).

24. van Hall, G. *et al.* Interleukin-6 markedly decreases skeletal muscle protein turnover and increases nonmuscle amino acid utilization in healthy individuals. *J. Clin. Endocrinol. Metab.* **93,** 2851–8 (2008).

25. Tsujinaka, T. *et al.* Muscle undergoes atrophy in association with increase of lysosomal cathepsin activity in interleukin-6 transgenic mouse. *Biochem. Biophys. Res. Commun.* **207,** 168–74 (1995).

26. De Benedetti, F. *et al.* Interleukin 6 causes growth impairment in transgenic mice through a decrease in insulin-like growth factor-I. A model for stunted growth in children with chronic inflammation. *J. Clin. Invest.* **99,** 643–50 (1997).

27. Bodell, P. W. *et al.* Skeletal muscle growth in young rats is inhibited by chronic exposure to IL-6 but preserved by concurrent voluntary endurance exercise. *J. Appl. Physiol.* **106,** 443–53 (2009).

28. Janssen, S. P. M. *et al.* Interleukin-6 causes myocardial failure and skeletal muscle atrophy in rats. *Circulation* **111,** 996–1005 (2005).

29. Soda, K., Kawakami, M., Kashii, A. & Miyata, M. Manifestations of cancer cachexia induced by colon 26 adenocarcinoma are not fully ascribable to interleukin-6. *Int. J. Cancer* **62,** 332–6 (1995).

30. Strassmann, G. *et al.* Suramin interferes with interleukin-6 receptor binding in vitro and inhibits colon-26-mediated experimental cancer cachexia in vivo. *J. Clin. Invest.* **92,** 2152–9 (1993).

31. Strassmann, G., Fong, M., Kenney, J. S. & Jacob, C. O. Evidence for the involvement of interleukin 6 in experimental cancer cachexia. *J. Clin. Invest.* **89,** 1681–4 (1992).

32. Tamura, S. *et al.* Involvement of human interleukin 6 in experimental cachexia induced by a human uterine cervical carcinoma xenograft. *Clin. Cancer Res.* **1,** 1353–8 (1995).

33. Tseng, Y.-C. *et al.* Preclinical Investigation of the Novel Histone Deacetylase Inhibitor AR-42 in the Treatment of Cancer-Induced Cachexia. *J. Natl. Cancer Inst.* **107,** djv274 (2015).

34. Bonetto, A. *et al.* STAT3 activation in skeletal muscle links muscle wasting and the acute phase response in cancer cachexia. *PLoS One* **6,** e22538 (2011).

35. Gilabert, M. *et al.* Pancreatic cancer-induced cachexia is Jak2-dependent in mice. *J. Cell. Physiol.* **229,** 1437–43 (2014).

36. Martinelli, G. B. *et al.* Activation of the SDF1/CXCR4 pathway retards muscle atrophy during cancer cachexia. *Oncogene* **35,** 6212–6222 (2016).

37. Fukawa, T. *et al.* Excessive fatty acid oxidation induces muscle atrophy in cancer cachexia. *Nat. Med.* **22,** 666–71 (2016).

38. Constantinou, C. *et al.* Nuclear magnetic resonance in conjunction with functional genomics suggests mitochondrial dysfunction in a murine model of cancer cachexia. *Int. J. Mol. Med.* **27,** 15–24 (2011).

39. White, J. P. *et al.* The regulation of skeletal muscle protein turnover during the progression of cancer cachexia in the Apc(Min/+) mouse. *PLoS One* **6,** e24650 (2011).

40. Carson, J. A. & Baltgalvis, K. A. Interleukin 6 as a key regulator of muscle mass during cachexia. *Exerc. Sport Sci. Rev.* **38,** 168–76 (2010).

41. Fearon, K. C. *et al.* Elevated circulating interleukin-6 is associated with an acute-phase response but reduced fixed hepatic protein synthesis in patients with cancer. *Ann. Surg.* **213,** 26–31 (1991).

42. Scott, H. R., McMillan, D. C., Crilly, A., McArdle, C. S. & Milroy, R. The relationship between weight loss and interleukin 6 in non-small-cell lung cancer. *Br. J. Cancer* **73,** 1560–2 (1996).

43. Güller, I. & Russell, A. P. MicroRNAs in skeletal muscle: their role and regulation in development, disease and function. *J. Physiol.* **588,** 4075–87 (2010).

44. Marinho, R., Alcântara, P. S. M., Ottoch, J. P. & Seelaender, M. Role of Exosomal MicroRNAs and myomiRs in the Development of Cancer Cachexia-Associated Muscle Wasting. *Front. Nutr.* **4,** 69 (2017).

45. Soares, R. J. *et al.* Involvement of microRNAs in the regulation of muscle wasting during catabolic conditions. *J. Biol. Chem.* **289,** 21909–25 (2014).

46. Narasimhan, A. *et al.* Small RNAome profiling from human skeletal muscle: novel miRNAs and their targets associated with cancer cachexia. *J. Cachexia. Sarcopenia Muscle* **8,** 405–416 (2017).

47. Lonsdale, J. *et al.* The Genotype-Tissue Expression (GTEx) project. *Nat. Genet.* **45,** 580–585 (2013).

48. Tang, Z. *et al.* GEPIA: a web server for cancer and normal gene expression profiling and interactive analyses. *Nucleic Acids Res.* **45,** W98–W102 (2017).

49. Vivian, J. *et al.* Toil enables reproducible, open source, big biomedical data analyses. *Nat. Biotechnol.* **35,** 314–316 (2017).

50. Rommel, C. *et al.* Mediation of IGF-1-induced skeletal myotube hypertrophy by PI(3)K/Akt/mTOR and PI(3)K/Akt/GSK3 pathways. *Nat. Cell Biol.* **3,** 1009–13 (2001).

51. Vandesompele, J. *et al.* Accurate normalization of real-time quantitative RT-PCR data by geometric averaging of multiple internal control genes. *Genome Biol.* **3,** RESEARCH0034 (2002).

52. Livak, K. J. & Schmittgen, T. D. Analysis of relative gene expression data using real-time quantitative PCR and the 2(-Delta Delta C(T)) Method. *Methods* **25,** 402–8 (2001).

53. Agarwal, V., Bell, G. W., Nam, J.-W. & Bartel, D. P. Predicting effective microRNA target sites in mammalian mRNAs. *Elife* **4,** (2015).

54. Chou, C.-H. *et al.* miRTarBase 2016: updates to the experimentally validated miRNA-target interactions database. *Nucleic Acids Res.* **44,** D239–47 (2016).

55. Kuleshov, M. V *et al.* Enrichr: a comprehensive gene set enrichment analysis web server 2016 update. *Nucleic Acids Res.* **44,** W90–7 (2016).

56. Chen, E. Y. *et al.* Enrichr: interactive and collaborative HTML5 gene list enrichment analysis tool. *BMC Bioinformatics* **14,** 128 (2013).

57. Szklarczyk, D. *et al.* The STRING database in 2017: quality-controlled protein–protein association networks, made broadly accessible. *Nucleic Acids Res.* **45,** D362–D368 (2017).

58. Snel, B., Lehmann, G., Bork, P. & Huynen, M. A. STRING: a web-server to retrieve and display the repeatedly occurring neighbourhood of a gene. *Nucleic Acids Res.* **28,** 3442–4 (2000).

59. Shannon, P. *et al.* Cytoscape: a software environment for integrated models of biomolecular interaction networks. *Genome Res.* **13,** 2498–504 (2003).

60. Cornwell, E. W., Mirbod, A., Wu, C.-L., Kandarian, S. C. & Jackman, R. W. C26 cancer-induced muscle wasting is IKKβ-dependent and NF-kappaB-independent. *PLoS One* **9,** e87776 (2014).

61. Shum, A. M. Y. *et al.* Cardiac and skeletal muscles show molecularly distinct responses to cancer cachexia. *Physiol. Genomics* **47,** 588–99 (2015).

62. Davis, S. & Meltzer, P. S. GEOquery: a bridge between the Gene Expression Omnibus (GEO) and BioConductor. *Bioinformatics* **23,** 1846–7 (2007).

63. Starruß, J., de Back, W., Brusch, L. & Deutsch, A. Morpheus: a user-friendly modeling environment for multiscale and multicellular systems biology. *Bioinformatics* **30,** 1331–2 (2014).

64. Hébuterne, X. *et al.* Prevalence of malnutrition and current use of nutrition support in patients with cancer. *J. Parenter. Enter. Nutr.* **38,** 196–204 (2014).

65. Pressoir, M. *et al.* Prevalence, risk factors and clinical implications of malnutrition in french comprehensive cancer centres. *Br. J. Cancer* **102,** 966–971 (2010).

66. Panguluri, S. K. *et al.* Genomic profiling of messenger RNAs and microRNAs reveals potential mechanisms of TWEAK-induced skeletal muscle wasting in mice. *PLoS One* **5,** e8760 (2010).

67. Wang, F. *et al.* Serum miRNAs miR-23a, 206, and 499 as Potential Biomarkers for Skeletal Muscle Atrophy. *Biomed Res. Int.* **2017,** 8361237 (2017).

68. Silva, W. J. *et al.* miR-29c improves skeletal muscle mass and function throughout myocyte proliferation and differentiation and by repressing atrophy-related genes. *Acta Physiol. (Oxf).* **226,**

e13278 (2019).

69. Eisenberg, I. *et al.* Distinctive patterns of microRNA expression in primary muscular disorders. *Proc. Natl. Acad. Sci. U. S. A.* **104,** 17016–21 (2007).

70. Wei, W. *et al.* The NF-κB-modulated microRNAs miR-195 and miR-497 inhibit myoblast proliferation by targeting Igf1r, Insr and cyclin genes. *J. Cell Sci.* **129,** 39–50 (2016).

71. Narsale, A. A. & Carson, J. A. Role of interleukin-6 in cachexia: therapeutic implications. *Curr. Opin. Support. Palliat. Care* **8,** 321–7 (2014).

72. Wang, X. H. MicroRNA in myogenesis and muscle atrophy. *Curr. Opin. Clin. Nutr. Metab. Care* **16,** 258–266 (2013).

73. Li, G. *et al.* miRNA targeted signaling pathway in the early stage of denervated fast and slow muscle atrophy. *Neural Regen. Res.* **11,** 1293–303 (2016).

74. Hsieh, C.-H. *et al.* Altered Expression of the MicroRNAS and Their Potential Target Genes in the Soleus Muscle After Peripheral Denervation and Reinnervation in Rats. *J. Trauma Inj. Infect. Crit. Care* **70,** 472–480 (2011).

75. Zhang, A. *et al.* miRNA-23a/27a attenuates muscle atrophy and renal fibrosis through muscle-kidney crosstalk. *J. Cachexia. Sarcopenia Muscle* **9,** 755–770 (2018).

76. Wang, B. *et al.* MicroRNA-23a and MicroRNA-27a Mimic Exercise by Ameliorating CKD-Induced Muscle Atrophy. *J. Am. Soc. Nephrol.* **28,** 2631–2640 (2017).

77. Qiu, H. *et al.* Regulatory Axis of miR-195/497 and HMGA1-Id3 Governs Muscle Cell Proliferation and Differentiation. *Int. J. Biol. Sci.* **13,** 157–166 (2017).

78. Shi, J., Luo, L., Eash, J., Ibebunjo, C. & Glass, D. J. The SCF-Fbxo40 Complex Induces IRS1 Ubiquitination in Skeletal Muscle, Limiting IGF1 Signaling. *Dev. Cell* **21,** 835–847 (2011).

Supplementary Material

Supplementary Figure 1

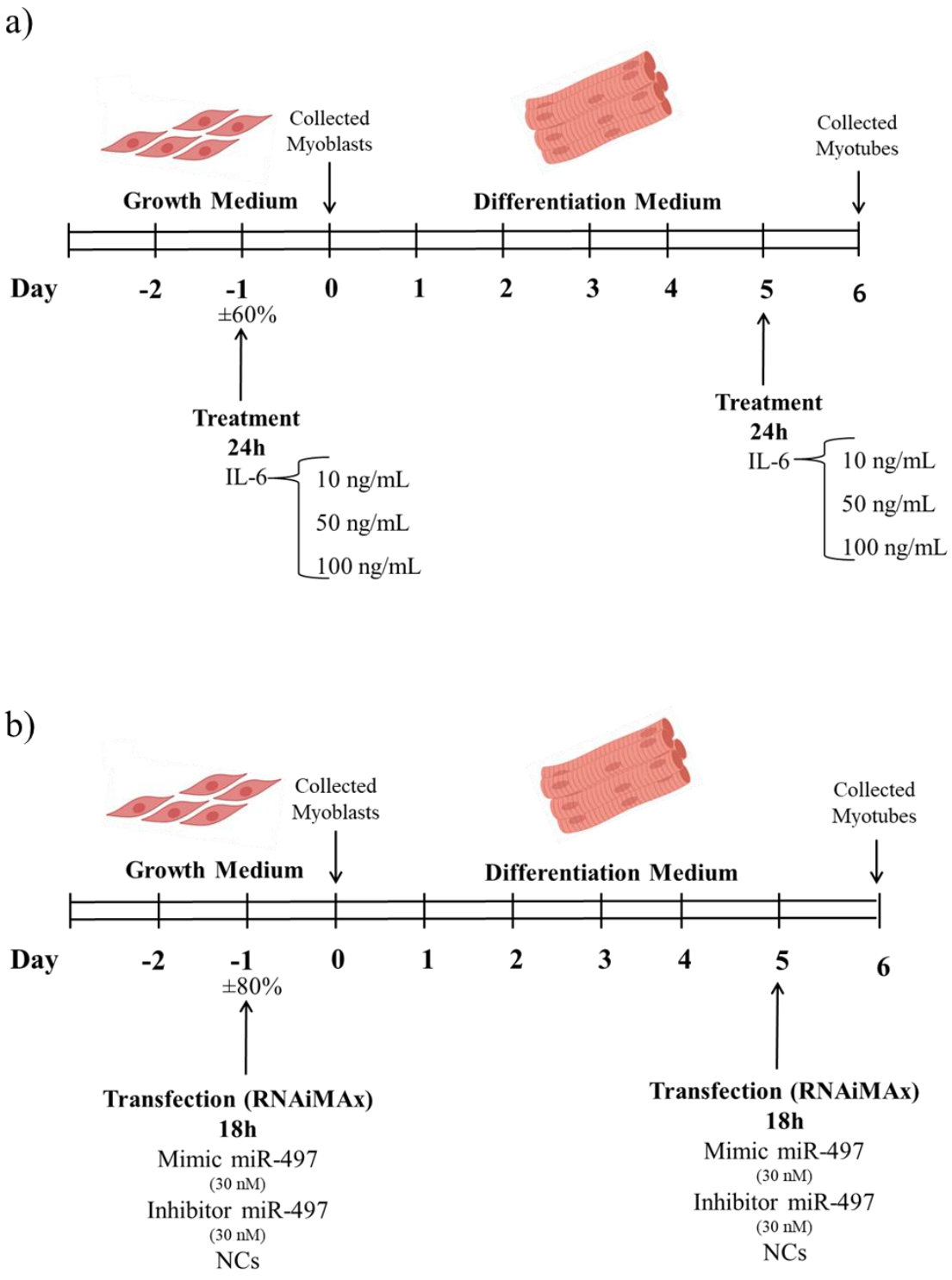

Supplementary Figure 2

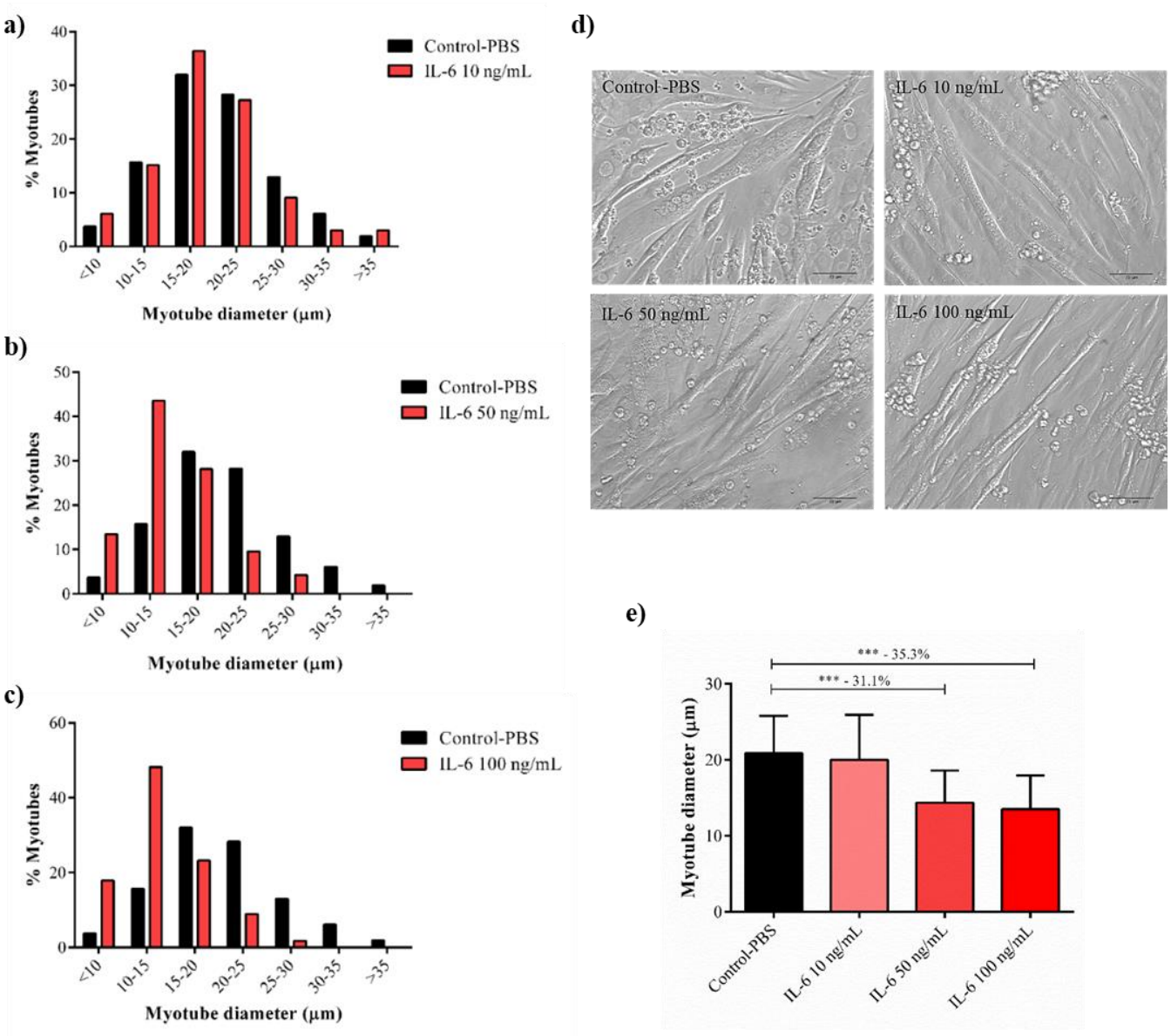

Supplementary Figure 3

a)

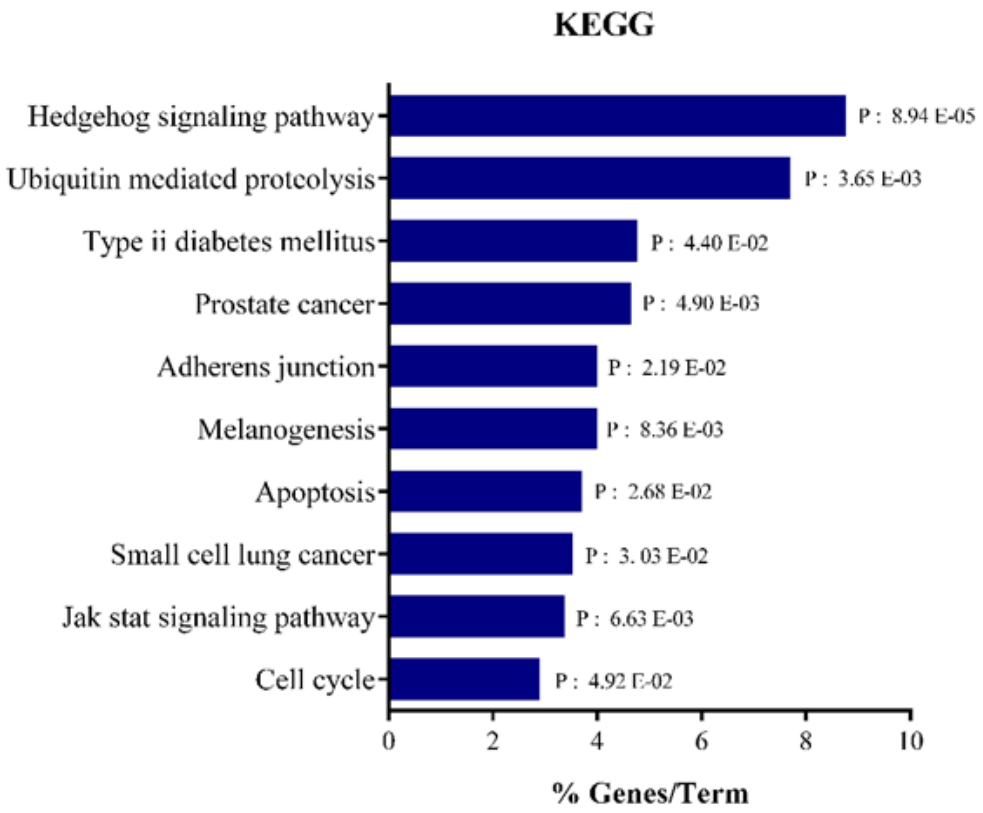

b)

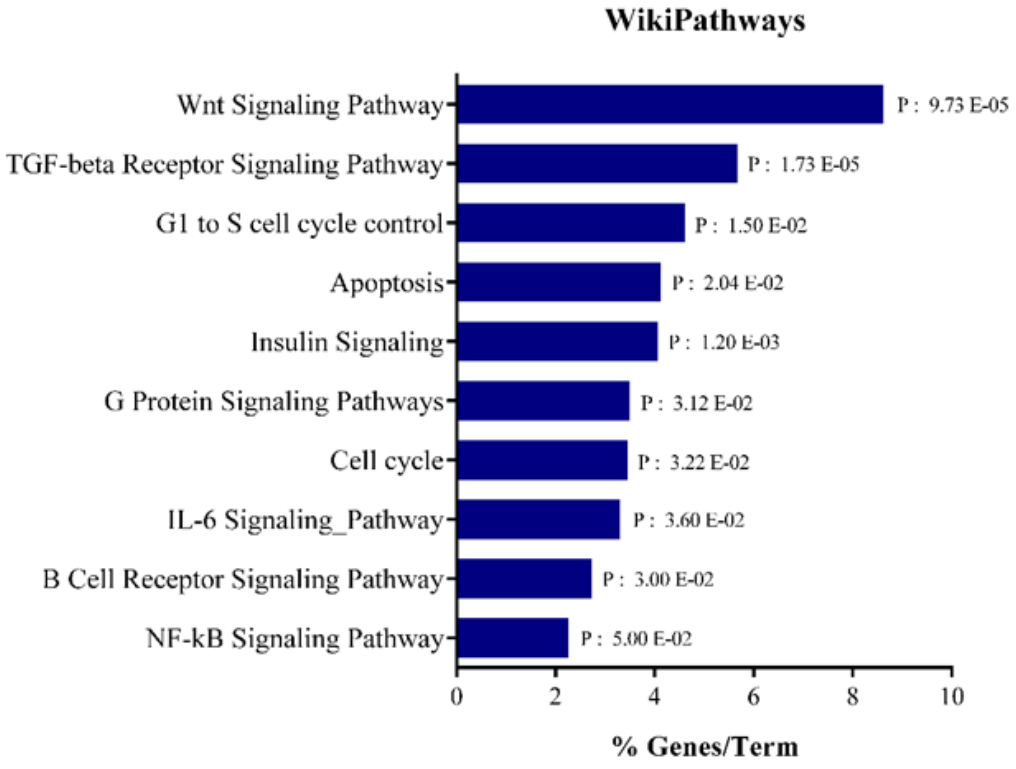

c)

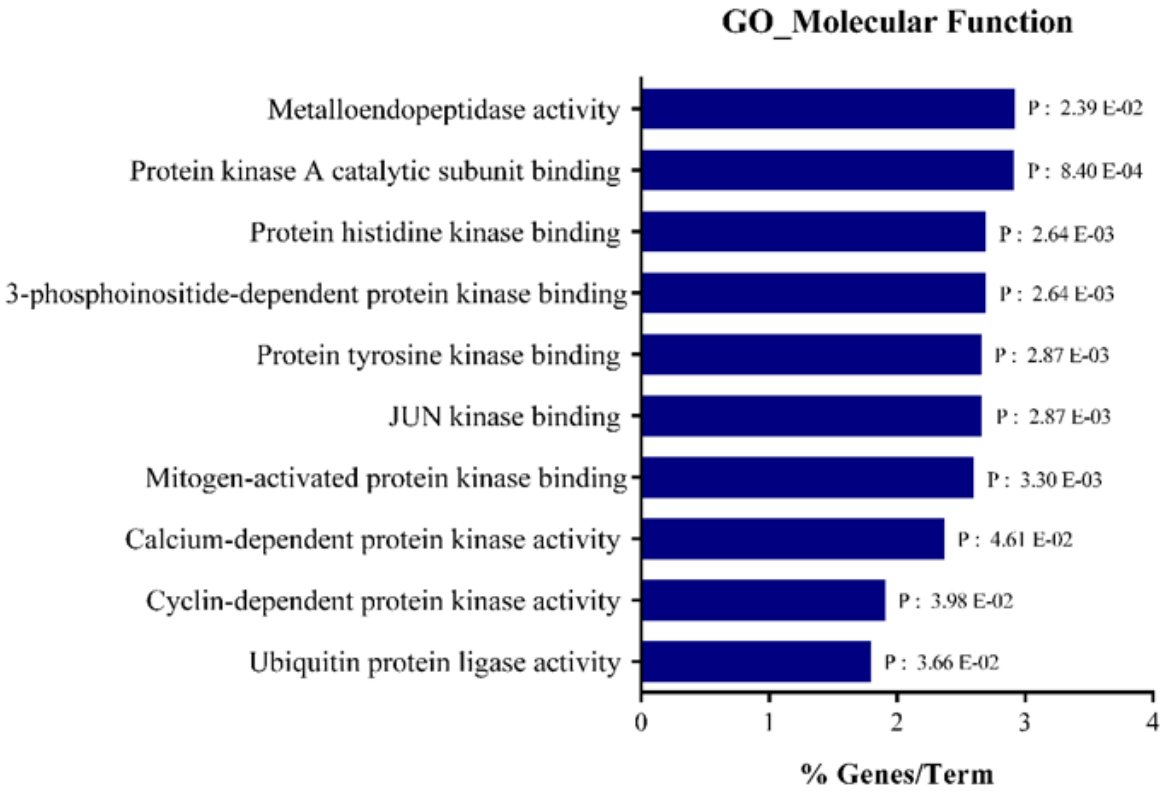
GO_Molecular Function
Metalloendopeptidase activity
P : 2.39 E-02
Protein kinase A catalytic subunit binding
P : 8.40 E-04
Protein histidine kinase binding
P : 2.64 E-03
3-phosphoinositide-dependent protein kinase binding
P : 2.64 E-03
Protein tyrosine kinase binding
P : 2.87 E-03
JUN kinase binding
P : 2.87 E-03
Mitogen-activated protein kinase binding
P : 3.30 E-03
Calcium-dependent protein kinase activity
P : 4.61 E-02
Cyclin-dependent protein kinase activity
P : 3.98 E-02
Ubiquitin protein ligase activity
P : 3.66 E-02
0
1
2
3
4
% Genes/Term

Supplementary Figure 3

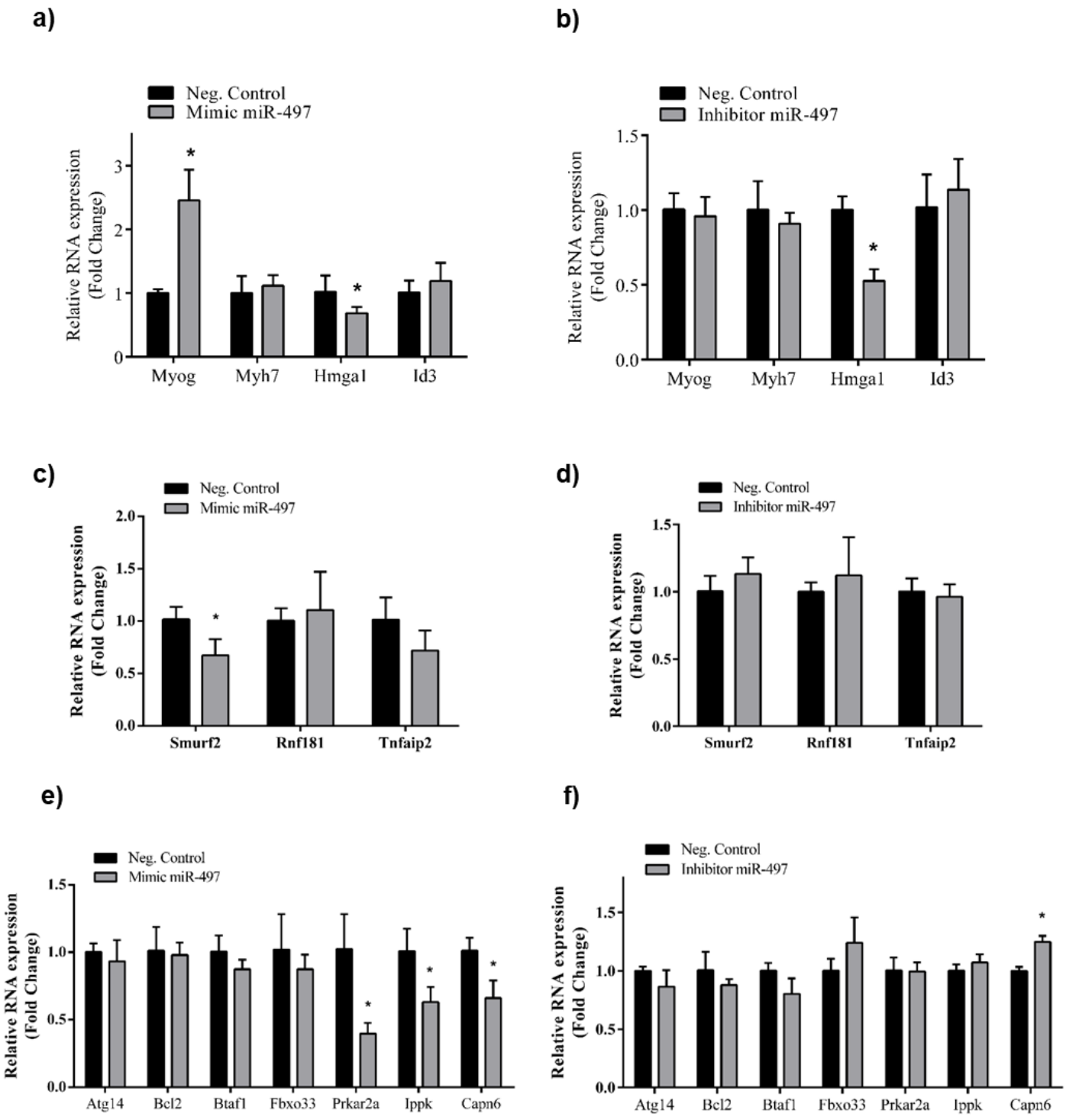

Supplementary Figure 4

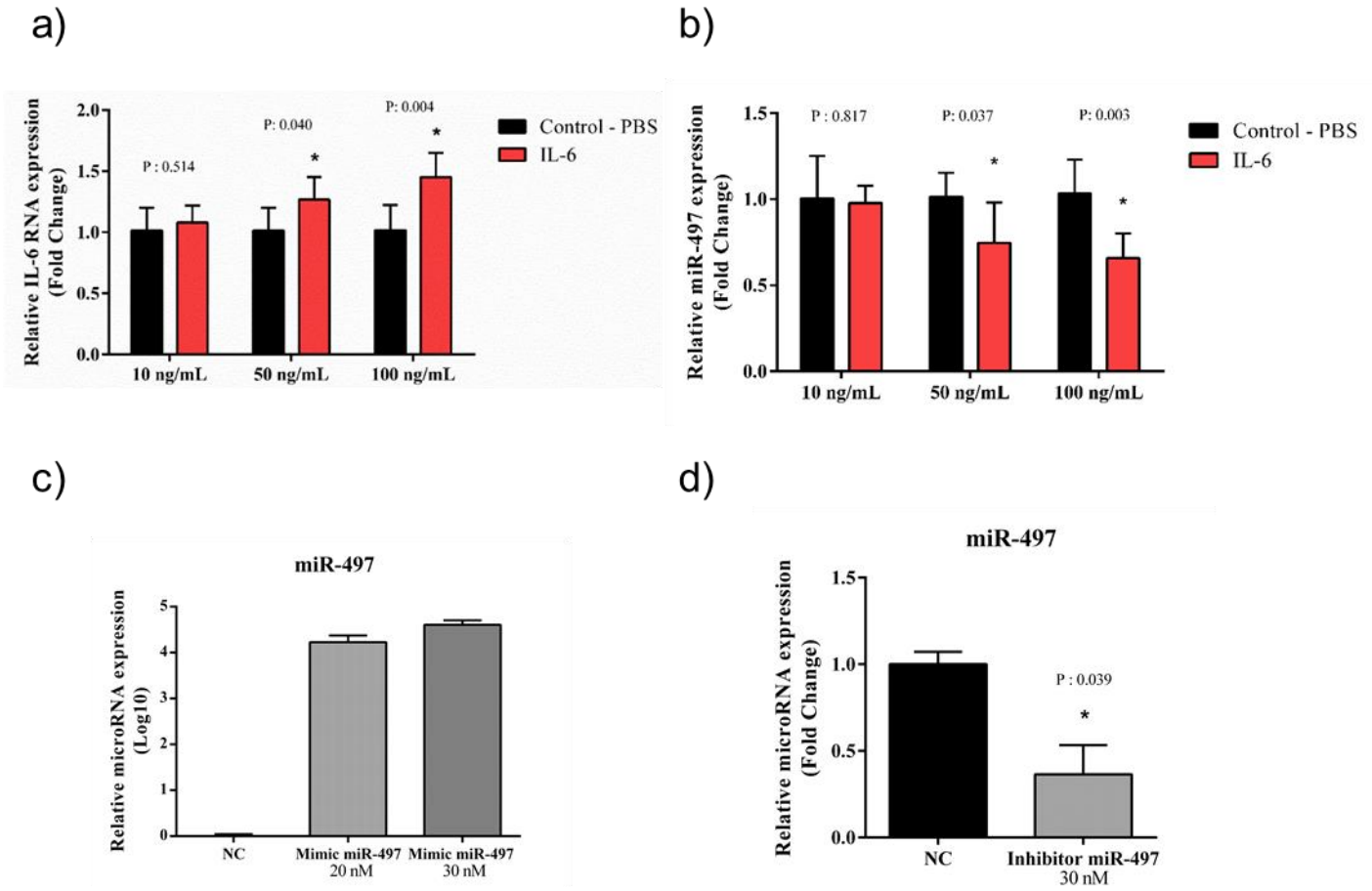

Supplementary Table 1. Primers for the expression analysis by RT-qPCR of the mRNAs indicated.

Gene	Official Name	NCBI REF Seq	Sequence (5'-3')
Rpl13a	*Mus musculus ribosomal protein L13A*	NM_009438.5	AACGGACTCCTGGTGTGAAC TGGTCCCCACTTCCCTAGTT
Rnf181	*Mus musculus ring finger protein 181*	NM_001331167.1	GGGAGTAGGTGGAACATGCAG CGCCGGTTTCTAGAAGTGCC
IL-6	*Mus musculus interleukin 6*	NM_031168.2	TCCAGTTGCCTTCTTGGGAC AGTCTCCTCTCCGGACTTGT
Myh7	*Mus musculus myosin, heavy polypeptide 7*	NM_080728.3	ACTCTTCATTCAGGCCCTTGGCG GGCAGAGGAGAGGGCGGACA
Capn6	*Mus musculus calpain 6*	NM_007603.3	CATTTTTGACACGCAGGCCA TGGGGTCAGCATCGAGAGTA
Ippk	*Mus musculus inositol 1,3,4,5,6-pentakisphosphate 2-kinase*	NM_199056.3	CTTTTCTTCAGACGGCTGCG TTGCCTTCGCCATGGTAACT
Atg14	*Mus musculus autophagy related 14*	NM_172599.4	ACCACATGGGCTGCTTTACA TTGCAGCTTTCCCAATGCAC
Dlk2	*Mus musculus delta like non-canonical Notch ligand 2*	NM_001286013.1	TCGGATCCGGTTTGACTCTG GATGAACGGCCAGACGTGTA
Myog	*Mus musculus myogenin*	NM_031189.2	AGCGCAGGCTCAAGAAAGTGA CTGTAGGCGCTCAATGTACTG
Btaf1	*Mus musculus B-TFIID TATA-box associated factor 1*	NM_001080706.1	CGTGCAGACGCTAAGTCCG CTGACCCGCACCACTTCAAA
Smurf2	*Mus musculus SMAD specific E3 ubiquitin protein ligase 2*	NM_025481.3	CGCCTGACAGTACTCTGTGC AGAATGGCACTGCCCAGAAC
Tnfaip1	*Mus musculus tumor necrosis factor, alpha-induced protein 1*	NM_001159392.1	TGAGCTCACAGCCGAGATTG CATACTCTCAGTGCCGTCCG
Pik3r1	*Mus musculus phosphoinositide-3-kinase regulatory subunit 1*	NM_001024955.2	GAGCCGGCGTGACATGTAG ACACCCCAGCCAATCAAGTC
Prkar2a	*Mus musculus protein kinase, cAMP dependent regulatory, type II alpha*	NM_008924.2	TCCAAAGCGTAACACCCTCC CAAACGAGACGGAAGGCTCT
Fbxo33	*Mus musculus F-box protein 33*	NM_001033156.4	TGCTCAGCATCCGGAACAAC AATCTTCTTGCCGTCAGGGT
Mapk8ip2	*Mus musculus mitogen-activated protein kinase 8 interacting protein 2*	NM_021921.3	GCCTTAGCTACGACTCGGAC AAATAGGGTGTGGCTGCTCC
Igf1r	*Mus musculus insulin-like growth factor I receptor*	NM_010513.2	GACTTCGGACCAGTCTCGC GAGGAGCAAAGCCCAAATCG
Bcl2	*Mus musculus B cell leukemia/lymphoma 2*	NM_009741.5	GCGTCAACAGGGAGATGTCA GCATGCTGGGGCCATATAGT

NCBI REF Seq NCBI (http://www.ncbi.nlm.nih.gov/)

Supplementary Table 2. Differentially expressed microRNAs in skeletal muscle cells treated with IL-6 ranked by a combination of p-value < 0.05 and fold change ≥ 1.5.

Direction of Fold Change	MicroRNA	MirBase ID	Fold Change	Log2 Fold Change	P-value
Up	mmu-miR-23a-5p	MIMAT0017019	3.77	1.92	0.002
	mmu-miR-146a-5p	MIMAT0000158	1.91	0.93	0.025
	mmu-miR-362-3p	MIMAT0004684	1.68	0.75	0.000
	mmu-miR-9-5p	MIMAT0000142	1.60	0.68	0.016
	mmu-miR-151-3p	MIMAT0000161	1.57	0.65	0.001
Down	mmu-miR-20a-5p	MIMAT0000529	0.66	-0.60	0.000
	mmu-miR-339-3p	MIMAT0004649	0.66	-0.60	0.017
	mmu-miR-449a-3p	MIMAT0017180	0.66	-0.61	0.000
	mmu-miR-497-5p	MIMAT0003453	0.64	-0.64	0.009
	mmu-miR-188-5p	MIMAT0000217	0.63	-0.67	0.013
	mmu-miR-130b-5p	MIMAT0004583	0.57	-0.80	0.002
	mmu-miR-194-5p	MIMAT0000224	0.57	-0.81	0.008
	mmu-miR-135b-3p	MIMAT0017044	0.50	-1.00	0.013
	mmu-miR-200c-5p	MIMAT0004663	0.50	-1.00	0.033
	mmu-miR-207	MI0003479	0.49	-1.04	0.000
	mmu-miR-29c-5p	MIMAT0004632	0.45	-1.14	0.023
	mmu-miR-20b-5p	MIMAT0003187	0.40	-1.32	0.001
	mmu-miR-148b-5p	MIMAT0017036	0.38	-1.39	0.003
	mmu-miR-361-5p	MIMAT0000704	0.35	-1.50	0.024
	mmu-miR-150-3p	MIMAT0004535	0.23	-2.13	0.027

Capítulo II

THE PATHWAY TO CANCER CACHEXIA: MICRORNA-REGULATED NETWORKS IN MUSCLE WASTING BASED ON INTEGRATIVE META-ANALYSIS

Paula Paccielli Freire [1], Geysson Javier Fernandez [1], Sarah Santiloni Cury [1], Diogo de Moraes [1], Jakeline Santos Oliveira [1], Grasieli de Oliveira [1], Maeli Dal-Pai-Silva [1], Patrícia Pintor dos Reis [2,3] and Robson Francisco Carvalho [1,*]

[1] Department of Morphology, Institute of Biosciences, São Paulo State University (UNESP), Botucatu, São Paulo, 18.618-619, Brazil;

[2] Department of Surgery and Orthopedics, Faculty of Medicine, São Paulo State University (UNESP), Botucatu, São Paulo, 18.618-687, Brazil;

[3] Experimental Research Unity, Faculty of Medicine, São Paulo State University (UNESP), Botucatu, São Paulo, 18.618-687, Brazil

***** Correspondence: robson.carvalho@unesp.br; Tel.: +55-14-3880-0473

Published in International Journal of Molecular Science

Received: 12 March 2019; Accepted: 11 April 2019; Published: 22 April 2019

Abstract

Cancer cachexia is a multifactorial syndrome that leads to significant weight loss. Cachexia affects 50%–80% of cancer patients, depending on the tumor type, and is associated with 20%–40% of cancer patient deaths. Besides the efforts to identify molecular mechanisms of skeletal muscle atrophy—a key feature in cancer cachexia—no effective therapy for the syndrome is currently available. MicroRNAs are regulators of gene expression, with therapeutic potential in several muscle wasting disorders. We performed a meta-analysis of previously published gene expression data to reveal new potential microRNA–mRNA networks associated with muscle atrophy in cancer cachexia. We retrieved 52 differentially expressed genes in nine studies of muscle tissue from patients and rodent models of cancer cachexia. Next, we predicted microRNAs targeting these differentially expressed genes. We also include global microRNA expression data surveyed in atrophying skeletal muscles from previous studies as background information. We identified deregulated genes involved in the regulation of apoptosis, muscle hypertrophy, catabolism, and acute phase response. We further predicted new microRNA–mRNA interactions, such as miR-27a/*Foxo1*, miR-27a/*Mef2c*, miR-27b/*Cxcl12*, miR-27b/*Mef2c*, miR-140/*Cxcl12*, miR-199a/*Cav1*, and miR-199a/*Junb*, which may contribute to muscle wasting in cancer cachexia. Finally, we found drugs targeting *MSTN*, *CXCL12*, and *CAMK2B*, which may be considered for the development of novel therapeutic strategies for cancer cachexia. Our study has broadened the knowledge of microRNA-regulated networks that are likely associated with muscle atrophy in cancer cachexia, pointing to their involvement as potential targets for novel therapeutic strategies.

Keywords: cancer cachexia; microRNAs; transcriptome; protein-protein interaction networks

1. Introduction

Cachexia is a syndrome associated with pathological conditions, including sepsis, chronic obstructive pulmonary disease, heart failure, and cancer [1,2]. Notably, cachexia is the leading cause of death for 20%–40% of cancer patients [3], and affects around 60% of patients when all cancer types are considered [4]. Cachexia is more prevalent in gastric or pancreatic cancer, as up to 80% of patients may develop the syndrome [5,6].

Cachexia occurs in all cancer stages, and is associated with poor prognosis, decreased treatment tolerance, and a significant reduction in quality of life [7]. International consensus defines the diagnostic for cancer cachexia based on weight loss greater than 5% over six months, or weight loss greater than 2% in individuals with a body mass index lower than 20 kg/m^2 or with sarcopenia [7]. Other features associated with cancer cachexia are a reduction in food intake, an increase of systemic inflammation markers like C-reactive protein, and decreased response to chemotherapy [7]. These features may increase surgical risk in cachectic patients [7,8]. Thus, the conservation of lean body mass is critical for cancer patients' survival. Although there are some advances in therapeutic strategies for muscle wasting in cancer cachexia (reviewed in [4]), effective targets to treat the syndrome are still lacking.

Many studies have been conducted to identify the molecular mechanisms related to muscle wasting in cancer cachexia. These studies have already lead to important advances through the recognition of the association between cachexia and high levels of pro-inflammatory cytokines, such as interleukin (IL)-1β, IL-6, IL-8, tumor necrosis factor alpha (TNF), and interferon gamma (IFN) [9–14]. These cytokines activate different molecular axes in skeletal muscle cells by the nuclear factor kappa-light-chain-enhancer of activated B cells (NF-κB), signal transducer and activator of transcription (STAT), MAP kinase family (MAPKs), and activator protein 1 (AP1) [15–18]. Signal transductions to NF-κB and STAT transcription factors have key roles, especially in altering three major effector biological systems: the ubiquitin–proteasome system, the IGF1–AKT–FOXO signaling pathway, and the autophagy–lysosome system [19–21]. Together, these systems contribute to an imbalance between protein synthesis and degradation that results in loss of muscle mass and function [19–21]. Given the complexity of these processes leading to muscle atrophy, the identification and characterization of new genes and signaling pathways based on global analysis will likely contribute to the understanding of the underlying molecular mechanisms of muscle wasting in cancer cachexia.

In fact, global gene expression studies of muscle wasting conditions, such as glucocorticoid treatment, immobilization, unloading, diabetes, sarcopenia, starvation, and denervation [22–27], have helped to shed light on the molecular mechanisms of muscle atrophy, including the identification of new potential biomarkers of cancer cachexia [28,29]. The identification of microRNAs has also broadened the knowledge about global gene expression regulation in conditions that induce skeletal muscle atrophy [30–33], including cancer cachexia [34,35]. However, there is a lack of integration of global microRNA and mRNA expression data from the same set of muscle samples in previous cancer cachexia studies [28,29,34–41]. Furthermore, to our knowledge, no study has integrated the most relevant microRNA and mRNA data available in the literature. Such integrative strategies are important for identifying the functional significance of key deregulated genes, microRNAs, and molecular pathways involved in muscle wasting in cachexia.

Moreover, the high diversity among human and animal models with cancer cachexia, the complexity of the syndrome, the difficulties in recruiting patients for studies, and the heterogeneity of cancer cells and muscle phenotypes leads to low translatability from experimental systems to clinical practice [42]. We performed a systematic integration of validated gene expression data derived from global mRNA and microRNA expression profiles in muscle wasting in cancer cachexia, to capture the most relevant microRNA-regulated networks across multiple human and rodent studies. Our analysis identified new molecular pathways potentially involved in skeletal muscle atrophy in cancer cachexia. These data have also proven useful for identifying new, potentially molecular-targeted treatment strategies for the syndrome.

2. Results

2.1. Study Selection and Characteristics

The meta-analysis resulted in nine studies reporting skeletal muscle gene expression data in cancer cachexia [28,29,36–41,43]. The process to select the studies is summarized in Figure 1. We present the description of publicly available cancer cachexia studies included in the meta-analysis in Table 1. These studies report muscle gene expression data from patients and mouse models with different cancer types (gastrointestinal, colon, and pancreatic cancers). The expression data were obtained in distinct muscles: three studies present data from the gastrocnemius, three from the quadriceps, one from the rectus abdominis, one from the biceps femoris, and one from the extensor digitorum longus. This variability in skeletal muscle phenotype expands the transcript profiles, increasing the number of

possibilities for identification of key common molecular pathways in muscle wasting triggered by different cancer types. Most of these studies were performed in a limited number of samples (3–21 samples/group), and therefore, a comprehensive and integrative analysis of these data may reveal new molecular components that are not identified when these studies are analyzed individually.

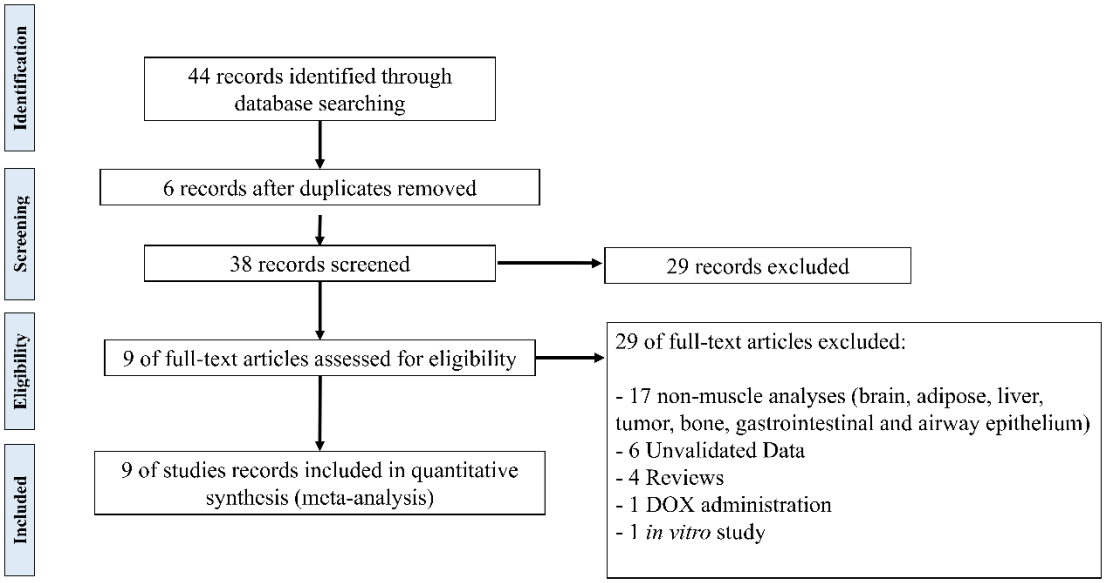

Figure 1. Flow chart of literature search in the meta-analysis.

Table 1. Description of publicly available studies used in the meta-analysis.

Authors	Gene Expression Platforms	Validation Platforms	Muscle	Cancer Cachexia Study (Rodent Model or Cancer Type)	Number of Samples (Cachectic/Control)	Ref.
Mus Musculus						
Tseng et al. 2015	Illumina HiSeq 2500	RT	Gastrocnemius	Colon-26 adenocarcinoma tumor-bearing mice	3/3	[36]
Roberts et al. 2013	Illumina Genome Analyzer II	RT, WB	Quadriceps	Pancreatic adenocarcinoma-bearing mice	2/2	[37]
Bonetto et al. 2011	Illumina MouseWG-6 v2.0 expression beadchip	RT, WB	Quadriceps	Colon-26 adenocarcinoma tumor-bearing mice	4/4	[38]
Gilabert et al. 2014	Affymetrix Mouse Gene 1.0 ST Array	RT	Biceps femoris	Pancreatic adenocarcinoma-bearing mice	3/3	[39]
Shum et al. 2015	Affymetrix Mouse Gene 1.0 ST Array	RT	Gastrocnemius	Colon-26 carcinoma tumor-bearing mice	3/3	[40]
Fontes-Oliveira et al. 2014	Affymetrix RAE230Plus	RT	Extensor Digitorum Longus	Rats injected with AH-130 Yoshida ascites hepatoma cells	7/6	[41]
Homo Sapiens						
Martinelli et al. 2016	Agilent-014850 Whole Human Genome Microarray	RT, WB	Rectus abdominis	Pancreatic, colorectal, Hepatic, and renal cancers	115	[43]
Stephens et al. 2010	Affymetrix GeneChip Human Genome U133 Plus 2.0 Array	RT	Rectus abdominis	Gastrointestinal cancer	18/3	[28]
Gallagher et al. 2012	Affymetrix Human Genome U133 Plus 2.0 Array	RT	Quadriceps	Upper gastrointestinal cancer	12/6	[29]

RT: quantitative reverse transcription polymerase chain reaction (RT-qPCR); WB: western blot; Ref: reference.

2.2. Validated Data Selection of Differentially Expressed Genes in Cancer Cachexia

We filtered the genes with differential expression that were validated by western blotting and/or quantitative reverse transcription polymerase chain reaction (RT-qPCR) techniques. This strategy allowed us to use the transcripts selected as more relevant by the authors in the global analysis, and therefore, specifically investigate those that may be directly related to molecular alterations in muscle wasting in cancer cachexia. These studies reported, excluding duplicates, 52 differentially expressed genes in 59 samples of muscle tissue from patients and rodent models of cancer cachexia. A list of the validated data for differentially expressed genes in cancer cachexia, with their respective functions and location, is summarized in Table 2 and Table S1. We highlight that the atrogenes *Fbxo32* and *Trim63* appeared in six out of the nine selected studies, and *Cebpd* and *Cxcl12* are dysregulated in two studies. Notably, 10 over-expressed genes (*Comp, Mmp3, Adipoq, Angptl7, Fgg, Hp, Mstn, Saa1, Serpina3n,* and *Cxcl12*) are translated into secreted proteins, and therefore, can be further explored as potential cancer cachexia biomarkers.

Table 2. List of 52 differentially expressed genes of skeletal muscle in cancer cachexia samples.

Official Symbol	Species	Function	Location
Up-Regulated			
TIE1	H	Regulation of angiogenesis	Cell Membrane
EIF3I	H	Cell proliferation, including cell cycling, differentiation and apoptosis	Cytoplasm
HGS	H	Intracellular signal transduction mediated by cytokines and growth factors	Cytoplasm
NUDC	H	Neurogenesis and neuronal migration	Cytoplasm
PCK1	H	Metabolic pathway that produces glucose	Cytoplasm
TSC2	H	Negatively regulating mTORC1 signaling and playing a role in microtubule-mediated protein transport	Cytoplasm
CAMK2B	H	Regulation of sarcoplasmic reticulum Ca2+ transport in skeletal muscle	Cytoplasm; Sarcoplasmic reticulum membrane
POLRMT	H	Transcription of mitochondrial DNA into RNA	Mitochondrion
COMP	H	Suppressor of apoptosis; interact with extracellular matrix proteins such as the collagens and fibronectin	Secreted - ECM
MMP3	H	Degrade fibronectin, laminin, gelatins, collagens, and cartilage proteoglycans	Secreted - ECM
ADIPOQ	H	Control of fat metabolism, insulin sensitivity, cell growth, angiogenesis and tissue remodeling	Secreted - ER
ANGPTL7	H	Anti-angiogenic protein and play a role in extracellular matrix formation	Secreted - ER
Kcnip4	M	Modulates channel expression at the cell membrane	Cell Membrane
Pnpla2	M	Response of the organism to starvation, enhancing hydrolysis of triglycerides and providing free fatty acids to other tissues	Cell Membrane
Socs3	M	Negative regulation of cytokines that signal through the JAK/STAT pathway	Cytoplasm

Foxo1	M	Autophagic cell death induction in response to starvation or oxidative stress	Cytoplasm and Nucleus
Stat3	M	Signal transducer and transcription activator that mediates cellular responses to interleukins and growth factors	Cytoplasm and Nucleus
Ufd1	M	Promote ubiquitination and degradation	Cytoplasm and Nucleus
C1s1	M	Serine protease	Extracellular exosome; Extracellular space
Ucp3	M	Thermogenesis and energy balance	Mitochondrion
Cebpd	M	Immune and inflammatory responses. Transcriptional activator that enhances IL6 transcription	Nucleus
Junb	M	Regulate gene activity following the primary growth factor response	Nucleus
Fgg	M	Guide cell migration during re-epithelialization	Secreted
HP	M	Antibacterial activity and plays a role in modulating many aspects of the acute phase response	Secreted
Mstn	M	Acts specifically as a negative regulator of skeletal muscle growth	Secreted
Saa1	M	Major acute phase protein	Secreted
Serpina3n	M	Response to cytokine	Secreted
FBXO32	H, M	Proteasomal degradation of target proteins during skeletal muscle atrophy	Cytoplasm and Nucleus
TRIM63	H, M	Regulates the proteasomal degradation of muscle proteins and inhibits de novo skeletal muscle protein synthesis	Cytoplasm and Nucleus
Down-Regulated			
APCDD1	H	Negative regulator of the Wnt signaling pathway	Cell Membrane
ADCY7	H	Membrane-bound, calcium-inhibitable adenylyl cyclase	Cell Membrane
GABARAPL1	H	Autophagosome maturation	Cytoplasm
HINT3	H	Hydrolyzes phosphoramidate and acyl-adenylate substrates	Cytoplasm and Nucleus
NR3C1	H	Affects inflammatory responses, cellular proliferation, and differentiation in target tissues	Cytoplasm and Nucleus
RCAN1	H	Central nervous system development	Cytoplasm and Nucleus
HSP90AB1	H	Maturation, structural maintenance, and proper regulation of specific target proteins involved, for instance in cell cycle control and signal transduction	Cytoplasm, nucleus, cell membrane and secreted
HSD11B1	H	Reversibly catalyzes the conversion of cortisol to the inactive metabolite cortisone	Endoplasmic reticulum membrane
BNIP3	H	Mitochondrial protein catabolic process; cell death pathway	Mitochondrion
SLC25A37	H	Mitochondrial iron transporter that specifically mediates iron uptake	Mitochondrion
PAK1	H	Cell adhesion, migration, proliferation, apoptosis, mitosis, and vesicle-mediated transport processes	Cytoplasm and Cell Membrane
PROX1	H	Cell fate determination, gene transcriptional regulation, and progenitor cell regulation	Nucleus
Cav1	M	T-cell proliferation and NF-kappa-B activation	Cell Membrane
Fap	M	Extracellular matrix degradation, tissue remodeling, fibrosis, wound healing, inflammation and tumor growth	Cell Membrane
Actc1	M	Cell motility	Cytoplasm
Myh8	M	Muscle contraction	Cytoplasm
Tuba1a	M	Constituent of microtubules	Cytoplasm
Tuba4a	M	Constituent of microtubules	Cytoplasm
Mef2c	M	Controls cardiac morphogenesis and myogenesis, and is also involved in vascular development	Nucleus
Tfcp2	M	Binds a variety of cellular promoters, including fibrinogen and alpha-globin promoters	Nucleus
Lama2	M	Attachment, migration, and organization of cells by interacting with extracellular matrix components	Secreted (ECM)

Fst	M	Specific inhibitor of the biosynthesis and secretion of pituitary follicle stimulating hormone (FSH)	Secreted (ER)
CXCL12	H, M	Immune surveillance, inflammation response, tissue homeostasis, and tumor growth and metastasis	Secreted

H: human samples; M: mouse samples; ER: endoplasmic reticulum; ECM: extracellular matrix; SR: sarcoplasmic reticulum.

2.3. Gene Ontology Enrichment Analysis of Differentially Expressed Genes in Muscle Wasting in Cancer Cachexia

Gene ontology (GO) analysis shows information on the biological role of differentially expressed genes involved in muscle wasting in cancer cachexia. We used gene ontology hierarchically structured categories to identify proteins encoded by the up- and down-expressed genes. This analysis revealed over-represented GO categories of biological processes that included structural and development genes (e.g., negative regulation of muscle hypertrophy, anatomical structure morphogenesis, epithelial cell proliferation, muscle organ development, muscle cell differentiation, and tissue development), metabolic process, acute-phase response, and apoptotic process. Other relevant terms enriched in our dataset included response to insulin and response to hormone stimulus. The statistically significant enriched GO terms are shown in Figure 2.

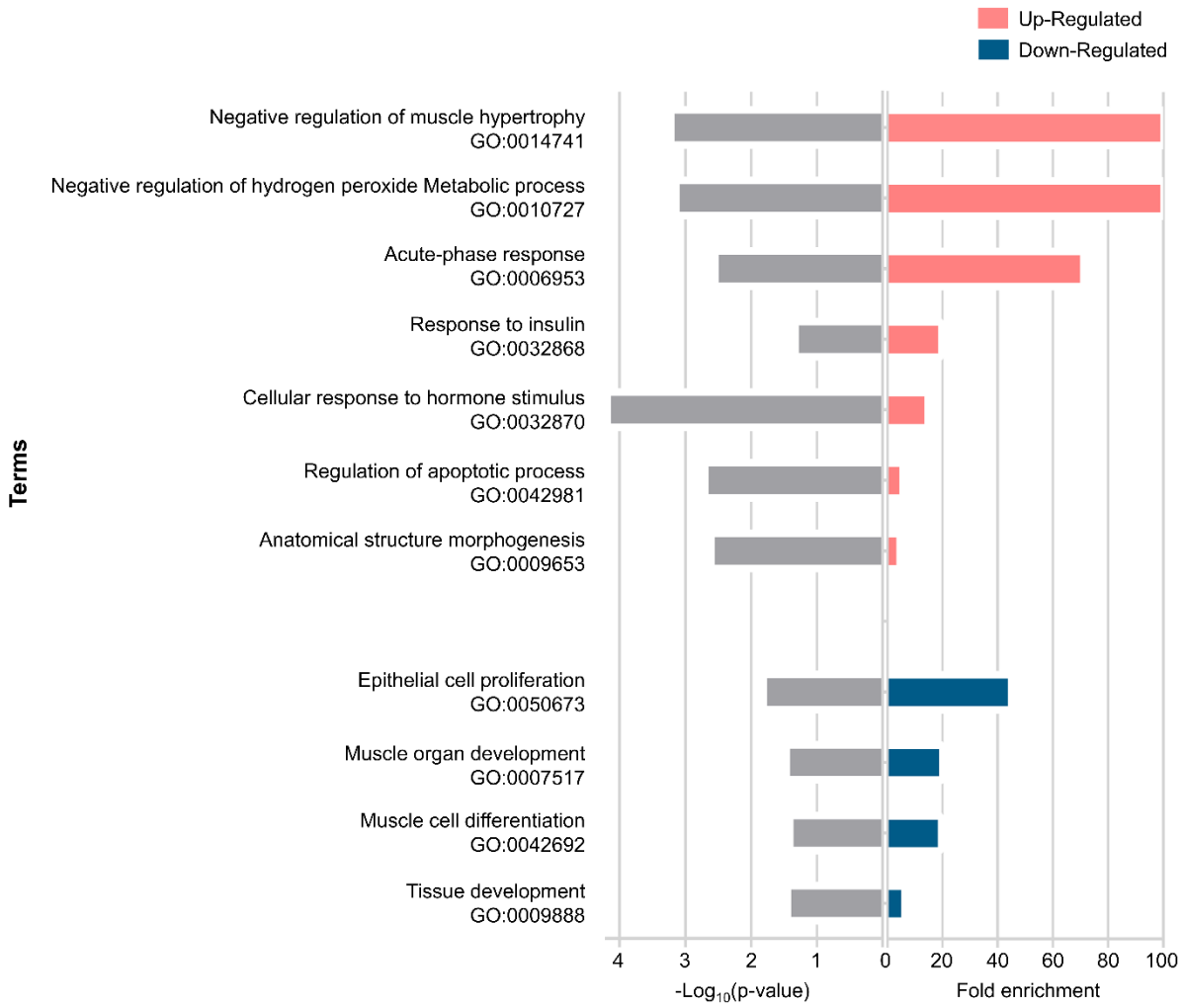

Figure 2. Enrichment pathway analysis of differentially expressed genes in muscle wasting during cancer cachexia. Biological processes identified with up-regulated genes (p-value ≤ 0.00253) and down-regulated genes (p-value ≤ 0.0364).

2.4. Protein–Protein Interaction Network in Muscle Wasting in Cancer Cachexia

The integrated protein–protein interaction (PPI) network shows a higher number of interactions between proteins of the inflammatory response, catabolism and anabolism, fat metabolism, apoptotic process, and transcriptional control. Complex interactome analysis of deregulated genes in cancer cachexia, with respective functional annotations, is illustrated in Figure 3.

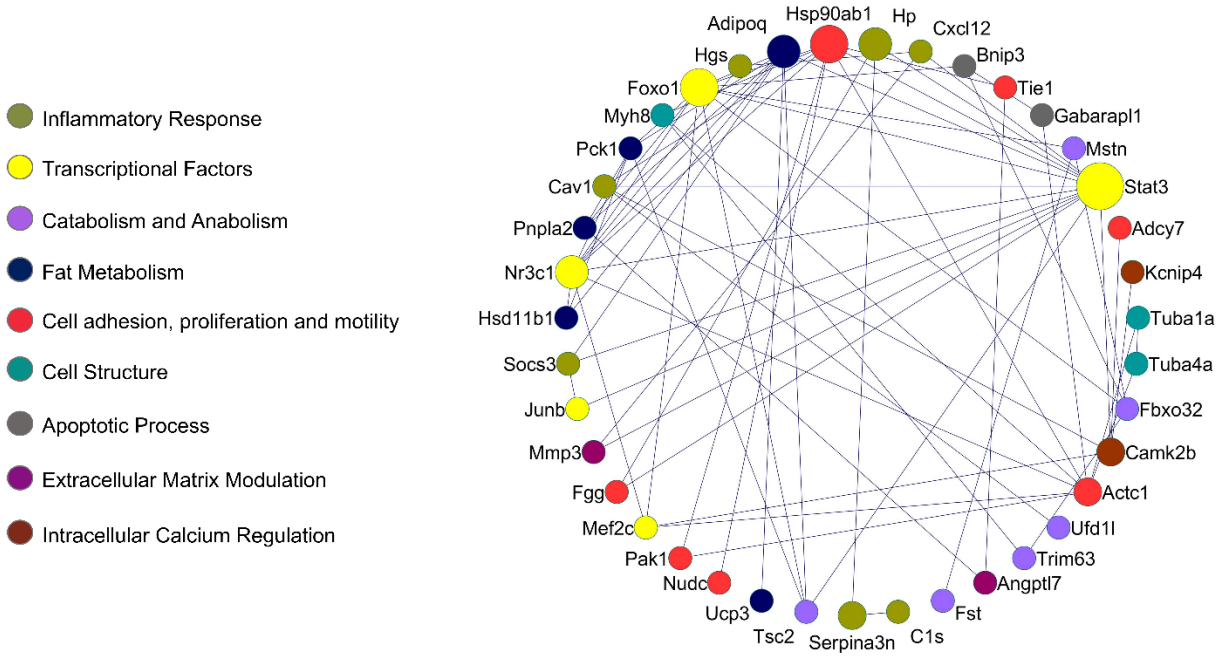

Figure 3. Protein–protein interaction (PPI) network in muscle wasting in cancer cachexia. Lines highlight PPI, with Stat3, Foxo1, Camk2b, Adipoq, Nr3c1, and Actc1 presenting the highest number of interactions. Colors highlight biological processes or molecular function of the circle network components. The larger the circle, the higher the number of interactions identified. STRING v10.5.1 was used to generate protein interactions, and the resulting network was visualized using Cytoscape v3.4.0.

2.5. Identification of New Potential microRNA-Regulated Networks in Muscle Wasting in Cancer Cachexia

The miRNA-mRNA target prediction identified 3150 non-validated and 98 validated interactions (Tables S2 and S3). The validated interactions were used to construct a microRNA-target mRNA interaction network for up- and down-regulated genes (Figures 4A and 4B, respectively). Networks were constructed with our list of microRNAs predicted in silico as targeting the mRNAs retrieved by our meta-analysis, and with microRNAs found as deregulated in two previous microRNAs studies on muscle wasting in cancer cachexia [34,35] (Table S2). Interestingly, the intersection of all the microRNA data showed that our list of predicted microRNAs shares five microRNAs with one study [35] (miR-27a, miR-27b, miR-140, miR-24, and miR-15) and the microRNA miR-199 with another [34] (Figure 5A).

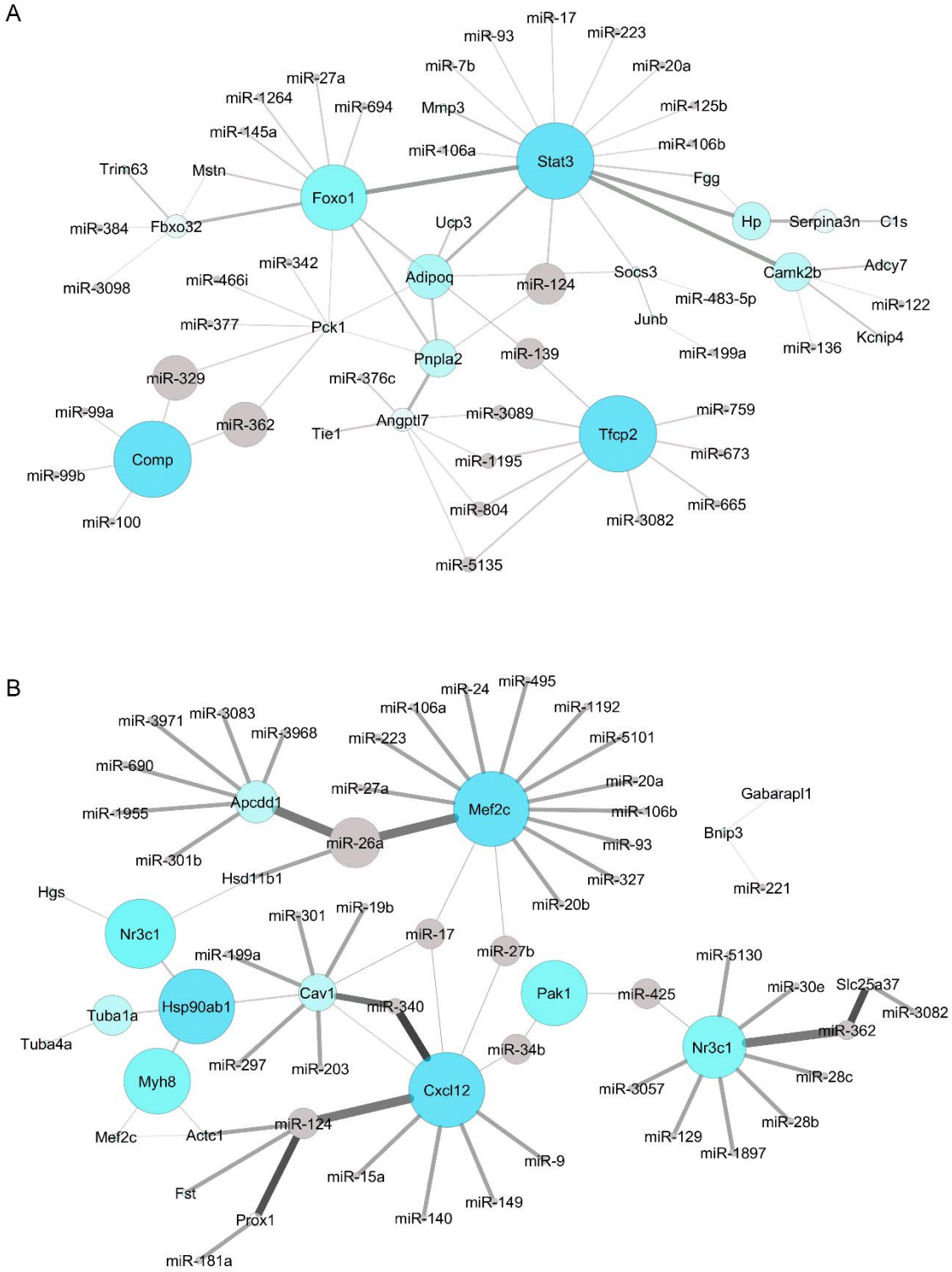

Figure 4. The miRNA–mRNA target interaction network in muscle wasting in cancer cachexia. (**A**) Interactome between up-regulated genes and the respective potential regulatory microRNAs. The larger the circles, the higher the number of interactions identified. Gray lines highlight the interactions; line thickness reflects the betweenness centrality. (**B**) Interactome between down-regulated genes and the potential regulatory microRNAs. The larger the circles, the higher the number of interactions identified. Gray lines highlight the

interactions; line thickness refers to the betweenness centrality. MicroRNA–gene interactions were visualized using Cytoscape v3.4.0.

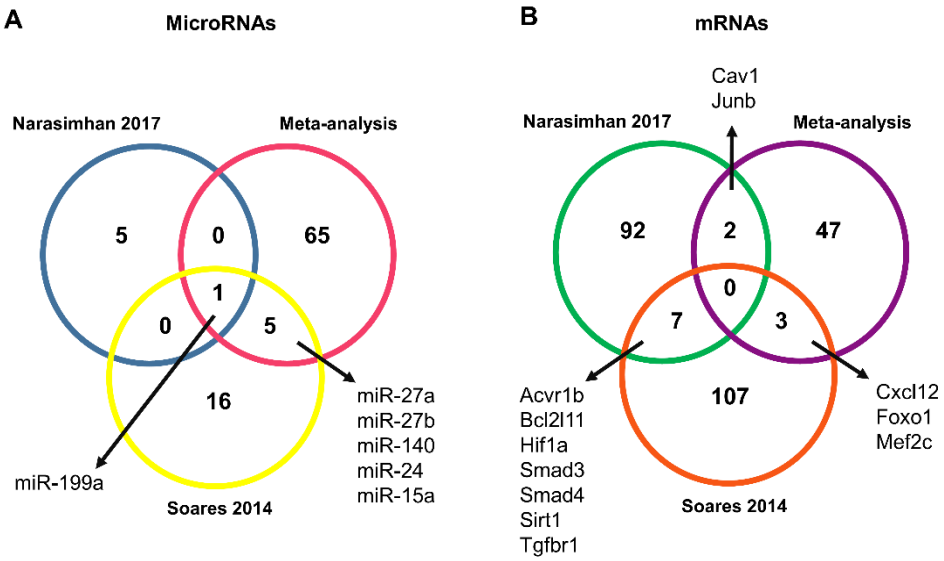

Figure 5. MicroRNAs and mRNAs identified in muscle wasting in cancer cachexia. (**A**) MicroRNAs predicted in silico as targeting mRNAs retrieved by our meta-analysis (pink circle) were further compared with microRNAs identified as differentially expressed in previous studies of muscle wasting in cancer cachexia, performed by Soares et al. [35] (yellow circle) and Narasimhan et al. [34] (blue circle). (**B**) Venn Diagram comparing the predicted microRNA target for Soares et al. [35] (red circle) and Narasimhan et al. [34] (green circle) with the list of 52 deregulated genes in muscle wasting in cancer cachexia identified in our meta-analysis (purple circle).

Next, we predicted genes targeted by the differentially expressed microRNAs by both these previous studies. These genes were further compared with the list of 52 deregulated genes identified in our meta-analysis. We found a total of five shared transcripts (*Cav1*, *Cxcl12*, *Foxo1*, *Mef2c*, and *Junb*) (Figure 5B), and most importantly, these five transcripts revealed seven new microRNA-mRNA interactions in muscle wasting in cancer cachexia (miR-27a/*Foxo1*, miR-27a/*Mef2c*, miR-27b/*Cxcl12*, miR-27b/*Mef2c*, miR-140/*Cxcl12*, miR-199a/*Cav1*, and miR-199a/*Junb*) (Table 3). Notably, three interactions—miR-27a/*Foxo1*, miR-140/*Cxcl12*, and miR-199a/*Cav1*—showed an opposite direction of expression between microRNAs (identified in the previous studies [34,35]) and mRNAs (identified in the meta-analysis) (Table 3).

Table 3. Identification of new relevant microRNA–mRNA interaction in muscle wasting in cancer cachexia.

Study	microRNA/mRNA Interactions	
	microRNA	**mRNA***
Soares et al. [35]	↓ miR-27b	↓ *Cxcl12*
	↑ miR-140	↓ *Cxcl12*
	↓ miR-27a	↑ *Foxo1*
	↓ miR-27a	↓ *Mef2c*
	↓ miR-27b	↓ *Mef2c*
Narasimhan et al. [34]	↑ miR-199a	↑ *Junb*
	↑ miR-199a	↓ *Cav1*

Up arrow: up-regulated genes; down arrow: down-regulated genes; *mRNAs identified in our meta-analysis.

Table 4. Potential target agents identified based on protein–protein interaction networks of deregulated genes in cancer cachexia.

Gene Symbol	Gene Name	Selected Target Agent	Activity	Clinical Relevance	Ref.
ADIPOQ	Adiponectin	Spironolactone, Fenofibrate, Nevirapine	Aldosterone blocker; anti-diabetic and anti-atherosclerotic; antiretroviral therapy	Type 2 diabetes mellitus; cardiovascular disease; HIV infection	[44–46]
CAMK2B	Calcium/calmodulin-dependent protein kinase II, beta	Mibefradil, Nifedipine, Nisoldipine	Block T-type calcium channel	Smooth muscle; cardiac muscle	[47–49]
COMP	Cartilage oligomeric matrix protein	Tadalafil	Tumor cell growth inhibitory	Breast cancer	[50]
CXCL12	Chemokine ligand 12	Tinzaparin Sodium	Regulate the proteoglycan core proteins	Breast cancer	[51]
MSTN	Myostatin	Stamulumab	Growth/differentiation factor 8 inhibitor	Myopathies	[52,53]

2.6. Identification of Potential Target Agents for the Treatment of Muscle Wasting in Cancer Cachexia

Interestingly, Drug–Gene Interaction Database (DGIdb) data revealed *ADIPOQ*, *CAMK2B*, *COMP*, *CXCL12*, and *MSTN* as drug-targetable genes, using chemical compounds such as Spironolactone, Fenofibrate, Nevirapine, Mibefradil, Nifedipine, Nisoldipine, Tadalafil, Tinzaparin Sodium, and Stamulumab (Table 4). The above drugs have been demonstrated as clinically useful in Type 2 diabetes mellitus, cardiovascular disease, HIV infection, smooth muscle, cardiac muscle, breast cancer, and myopathies [44–53]. Outstandingly, the potential drugs found here have not been tested yet for the treatment of muscle wasting in cancer cachexia.

3. Discussion

Researchers have conducted several studies on molecular mechanisms of muscle wasting in cancer cachexia. However, the complexity of the syndrome and the insufficient knowledge of pathogenic mechanisms hinder the design of effective therapeutic strategies. Most cancer cachexia studies rely on a single, thorough, standardized model or specific cancer types, rarely integrating and comparing their datasets with those from other experimental systems. The present meta-analysis allowed us to select relevant mRNA expression data from different cancer cachexia studies. This is the first study integrating the most relevant literature data from global gene expression profiling studies in muscle wasting in cancer cachexia, in order to find common regulatory networks and molecular pathways. We identify new potential microRNA-regulated gene networks involved in muscle wasting in cancer cachexia (Scheme I). Specifically, our results suggest that microRNA/mRNA interactions miR-27a/*Foxo1*, miR-27a/*Mef2c*, miR-27b/*Cxcl12*, miR-27b/*Mef2c*, miR-140/*Cxcl12*, miR-199a/*Cav1*, and miR-199a/*Junb* may contribute to muscle wasting in cancer cachexia.

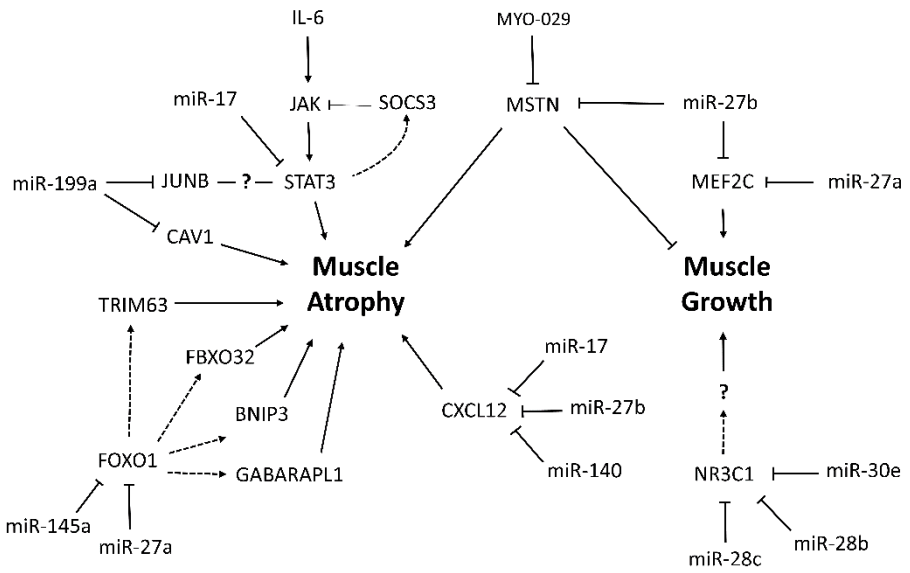

Scheme I. MicroRNA-regulated networks in muscle wasting during cancer cachexia based on meta-analysis data.

Among the 52 deregulated genes identified in our analysis, six of the nine studies included in the meta-analysis have evaluated the expression of *Trim63* and *Fbxo32* as molecular markers of muscle atrophy in cancer cachexia. In 2001, *Trim63* and *Fbxo32* were first identified as two important muscle-specific E3 ubiquitin ligases that are transcriptionally increased in skeletal muscle under atrophy-inducing conditions, making them excellent markers of muscle atrophy [54]. The transcription of enzymes *Trim63* and *Fbxo32* is dependent on transcriptional factors *FoxO1* and *FoxO*3, which are thought to regulate both the ubiquitin/proteasome [27] and autophagy [20,55,56] pathways. Interestingly, our enrichment analysis also showed alteration in the regulation of the apoptotic process induced by changes in the expression of *FoxO1*, *BNIP3*, and *GABARAPL1*. These results are in agreement with the fact that skeletal muscle wasting is the result of an imbalance between synthesis and degradation of protein pathways, together with the instability of regenerative capacity and myocyte apoptosis [57,58].

Moreover, we showed miR-145a as a new potential *FoxO1* regulator during muscle wasting in cancer cachexia. Indeed, the increase of miR-145 decreases *FoxO1* expression in metastatic T24T bladder cancer cells [59]. Conversely, in non-metastatic bladder transitional cell carcinoma T24 cells, miR-145 overexpression inhibited cell growth, which correlates with upregulation of *FoxO1* [59]. These opposite results are probably associated with different cell types and experimental conditions, raising the necessity to further explore miR-145-*FoxO1*. One of the most important findings of our

study was that *FoxO1* is a validated target of the microRNA miR-27a. Besides, Soares et al. [35] identified the down-regulation of miR-27a in cancer-cachexia. Although the miR-27a–*FoxO1* interaction is not validated in skeletal muscle cells, the overexpression of miR-27a in mice with chronic kidney disease attenuated muscle loss, improved grip strength, and decreased the expression of FoxO1, Trim63, and Fbxo32 proteins [60].

Besides these molecular markers of muscle atrophy, our meta-analysis also identified *Nr3c1* as down-regulated in the skeletal muscle of cachectic patients with upper gastrointestinal cancer [29]. *Nr3c1* has a function in the regulation of muscle hypertrophy and strength in response to resistance training [61]; however, the role of *Nr3c1* in the development of muscle wasting associated with cancer is still unknown. Furthermore, our microRNA target prediction analysis identified nine microRNAs that potentially modulate *Nr3c1* expression, including microRNAs miR-28b and miR-28c. We also identified that the *Nr3c1* transcript is potentially regulated by miR-30e, which is upregulated in the skeletal muscle of *Mstn*-/- mice, and its expression was associated with glycolytic myofiber formation [62]. Considering that microRNAs miR-28b, miR-28c, and miR-30e potentially target the *Nr3c1* transcript, and that both microRNAs and their target transcripts have important functions previously described in skeletal muscle tissue, our integrative analysis reveals these new microRNA–mRNA interactions as potential targets for future exploratory analysis of muscle wasting in cancer cachexia.

Our prediction analyses also revealed microRNA miR-17 as an important regulator of transcripts, such as *Cxcl12*, *Mef2c*, *Stat3*, and *Cav1*, that are translated into proteins with a role in cancer cachexia. MicroRNA miR-17 is involved in oncogenic events in different cancer types with a high incidence of cachexia (hepatocellular carcinoma [63], pancreatic cancer [64], and non-small lung cancer [65,66]). Among the miR-17 target genes, *Mef2c* is involved in the regulation of skeletal muscle regeneration and myogenesis (reviewed in Dong et al. [67]). Also, two studies have identified miR-27b as a regulator of *Mef2c* [68,69]; notably, one of these studies shows that miR-27b is involved in the regulation of mitochondrial biogenesis in myocytes by regulating *Mef2c* [69]. Importantly, miR-27b also negatively regulates myostatin (*Mstn*) to promote satellite cell activation and myoblast proliferation, and to prevent muscle wasting [70]. *Mstn*, a member of the *TGFβ* superfamily of growth factors, is a highly conserved negative regulator of skeletal muscle mass upregulated in muscle wasting conditions, including cancer cachexia [37,71,72]. Accordingly, *Mstn* deficiency increase skeletal muscle mass and strength and counterattacks muscle wasting conditions [73]. Several studies have demonstrated the therapeutic potential of *Mstn* inhibition under muscle wasting conditions as cancer

[74,75]; consequently, the identification of *Mstn* as a putative target of miR-27b has potential therapeutic and biological implications in muscle wasting conditions.

Moreover, our results showed that the drug Stamulumab (MYO-029), known as a potential *MSTN* inhibitor, was previously tested in clinical studies of subjects with myopathies. This trial showed a potential increase in the muscle size of the subjects, but the researchers observed no improvements in muscle strength or function [52,53]. Considering that there are no studies testing MYO-029 on cancer cachexia, further studies are needed to demonstrate whether this drug may improve muscle mass and function in this syndrome.

It is also important to highlight that our enrichment analysis identified genes associated with the acute-phase response. Systemic inflammation is a hallmark of cancer cachexia, and this inflammatory response is the main driving force that leads to the metabolic alterations observed in cancer patients [7]. The literature points out several origins of inflammation, including tumor cells and activated immune cells that release cytokines, chemokines, and other inflammatory mediators [76]. *Cxcl12* was one of the top transcripts, with the highest number of microRNA interactions identified in our meta-analysis (nine interactions in total). The identification of microRNAs that target *CXCL12* is important, because it has been demonstrated that *CXCR4* pathway is consistently downregulated in skeletal muscles from mice and patients with cancer-associated cachexia, and the activation of the *Cxcl12/Cxcr4* pathway protects muscle from wasting in mice with the syndrome [43]. This inflammatory chemokine is also relevant in skeletal muscle regeneration by increasing the activity of metalloproteases, which are crucial to the remodeling of the extracellular matrix [77]. Our results also show protein–protein interactions of *Cxcl12* with the metalloprotease *Mmp*, suggesting that this interaction could affect muscle regeneration and extracellular matrix remodeling in cancer cachexia. Indeed, we identified that miR-27b and miR-140 are two potential microRNAs involved in *Cxcl12* regulation. Importantly, it has been previously demonstrated that miR-140 transfection decreases *Cxcl12* expression and release in human airway smooth muscle cells, with a reduction in inflammatory response [78]. Thus, our data also suggest a response that compromises inflammatory response through the mir-140/*Cxcl12* axis in muscle wasting during cancer cachexia.

Furthermore, among the acute phase response genes identified by ontology analysis, *Stat3* was the most notorious factor of our interaction network. The role of this transcriptional factor is widely studied in cancer cachexia. The increase of interleukin-6 in cachectic patients triggers the activation of JAK (Janus kinase), with consequent STAT3 phosphorylation that acts at the nucleus; this leads to

transcription activation of several genes associated with skeletal muscle cells growth, atrophy, proliferation, differentiation, survival, and apoptosis [38,79,80]. Moreover, STAT3 contributes to cancer cachexia enhancing tumorigenesis, metastasis, and immune suppression, mostly in tumors associated with a high prevalence of cachexia [80]. Given the diversity of activated genes obtained through the JAK/STAT pathway, it is essential to better characterize *Stat3* downstream target genes in the skeletal muscle cells in wasting conditions. The SOCS3 is a classic inhibitor of the JAK/STAT pathway and several cytokines, and pathogenic mediators induce the expression of SOCS3, which acts in a negative feedback loop to further inhibit signal transduction [81,82]. In a murine model of pancreatic cancer cachexia, the JAK/STAT/SOCS3-dependent intracellular pathway plays an essential role in pathogenesis, since its pharmacological inhibition attenuates cachexia progression in a lethal pancreatic cancer model [39].

Our predicted molecular network also revealed a *Stat3/Junb* interaction. *Junb* is a transcriptional factor that regulates gene expression on multiple levels [83], but the functionality of this *Stat3/Junb* interaction deserves future study in relation to cancer cachexia. Our study identified miR-199a as a potential microRNA that modulates *Junb* expression in muscle wasting in this syndrome. In addition, we found an inverse correlation between miR-199a and *Cav1* expression. Since many inflammatory mediators are activated in cancer cachexia, and the miR199a/*Cav1* axis was previously described in several chronic inflammatory lung diseases as an important regulatory pathway [84], this axis should also be considered for further investigations in muscle wasting in cancer cachexia.

The main contribution of the present investigation is that we identify new potential microRNA-regulated mRNAs in cancer cachexia. Nevertheless, our study has some limitations due to the nature of our analysis, which consists of the reuse of transcriptomic data from different studies and in silico analysis. Further studies are needed to validate the microRNA–mRNA interactions described herein, as well as to validate the efficiency of the identified potential drugs. Furthermore, the deregulated genes selected in our analysis were restricted to those further validated by RT-qPCR or Western Blot. We considered this strategy to increase the possibility of rescuing truly deregulated targets, or with a potential impact on protein levels. Finally, due to the small number of studies evaluating muscle transcriptome of patients with cachexia, we used data from humans and mice together to identify a higher range of transcripts.

In conclusion, we identified new microRNA–mRNA interactions, such as miR-27a/*Foxo1*, miR-27a/*Mef2c*, miR-27b/*Cxcl12*, miR-27b/*Mef2c*, miR-140/*Cxcl12*, miR-199a/*Cav1*, and miR-199a/*Junb*,

that may contribute to muscle wasting in cancer cachexia. Finally, we found drugs targeting *MSTN*, *CXCL12*, and *CAMK2B*, which may be considered for the development of novel therapeutic strategies for cancer-related cachexia.

4. Methods

4.1. Meta-Analysis of Global Gene Expression Data in Muscle Wasting in Cancer Cachexia

We performed a meta-analysis design following the stages of the PRISMA Statement [85] (Figure 1), by searching PubMed (http://www.ncbi.nlm.nih.gov/pubmed) to find the collection of previously published gene expression data of skeletal muscles in cancer cachexia. The keywords used were: "cancer cachexia AND global gene expression", "cancer cachexia AND transcriptome", "cancer cachexia AND transcriptomics", "cancer cachexia AND microarray", and "cancer cachexia AND RNAseq". These meta-analysis searches comprised studies published between January 2005 and February 2019. Our inclusion criteria were (1) gene expression data in muscle samples of patients with cancer cachexia or animal models of cancer cachexia, (2) all types of cancer were considered, (3) all types of muscle were considered, (4) the inclusion of normal tissues for comparison, (5) all gene expression analysis platforms were considered, and (6) only data further validated by RT-qPCR or Western Blot were included for the integrative analyses. Our exclusion criteria were (1) non-muscle samples, (2) treatment before molecular genetic analysis, and (3) review studies. The deregulated genes reported in selected studies were further used for bioinformatics prediction of microRNAs as potential regulators of gene expression, as described below.

4.2. Meta-Analysis of Global microRNA Expression Data in Muscle Wasting in Cancer Cachexia

To search previously published global microRNA expression data for skeletal muscle in cancer cachexia, we used the following keywords in PubMed: "cancer cachexia AND global microRNA expression", "cancer cachexia AND microRNome", and "cancer cachexia AND microRNA profiling". This search only retrieved four studies: (1) microRNA profiling in adipocyte lipolysis [86]; (2) integrative microRNAs and mRNAs expression analysis during skeletal muscle wasting in cardiac cachexia [87]; (3) microRNA profiling in muscle wasting during catabolic conditions, including cancer cachexia [35]; and (4) microRNA profiling from human skeletal muscle in cancer cachexia [34]. The microRNA data of these last two studies were included for the identification of regulatory networks, in addition to the microRNAs that were identified in an in silico, mRNA-based target prediction described subsequently.

4.3. Identification of Muscle microRNAs as Potential Modulators of Deregulated Genes in Cancer Cachexia

The deregulated genes identified in our meta-analysis were used for microRNA prediction by multiple algorithms (TargetScan [88], MiRTarBase [89], and miRWalk [90]) to identify potential regulators (predicted and validated interactions) of the expressed genes in cancer cachexia. Next, to generate the interaction networks, we filtered all microRNAs found by these computational tools, considering only those identified by MiRTarBase as presenting the "reporter assay" as a validation method. We selected MiRTarBase [89] due to its different validation methods of interaction between mRNAs and microRNAs, ranging from strong to weak evidence of interaction (accordingly, "reporter assay" has the strongest evidence of microRNA–target gene interaction). We also used MiRTarBase to identify microRNA-target transcripts from global microRNA expression in cancer cachexia studies [34,35]. The deregulated genes were used to identify over-represented gene ontology categories of biological processes with the Gene Ontology Consortium tool, powered by PANTHER v11.0 [91–93] (available at http://www.pantherdb.org/). We considered the GO categories with p-value ≤ 0.05 to be significant. The UniProtKB database (available at http://www.uniprot.org/) was used to access functional information of components identified through the meta-analysis. Protein–protein interaction (PPI) networks were then generated using Metasearch STRING v10.5.1 [94,95]. Visualization and annotation data of PPI and microRNA-gene interaction networks were generated using Cytoscape v3.4.0 [96].

4.4. Identification of Candidate Drug Targets Based on microRNA-Regulated Networks in Cancer Cachexia

We used the Drug–Gene Interaction Database (DGIdb), a database and web interface for finding known and potential drug–gene relationships. Genes were defined by Entrez Gene and Ensembl and were matched with genes from drug–gene interactions and druggable gene categories. The drugs were defined by searching PubChem, and were then matched with drugs from drug–gene interaction data. The source guide to pharmacology interaction was obtained from the DrugBank [97,98].

Funding: The following grants supported the development of this study: National Council of Technological and Scientific Development (CNPq 141919/2016-7), São Paulo Research Foundation (FAPESP grants #14/13783-6 and #12/13961-6), and Coordenação de Aperfeiçoamento Pessoal de Nível Superior-Brasil (CAPES)-grant 88881.187095/2018-01.

Acknowledgments: We wish to acknowledge Vanessa M. Lima and João M. Barguil from the University of São Paulo for helping us with comments that improved our manuscript.

Conflicts of Interest: The authors declare no conflicts of interest.

References

1. Argilés, J.M.; Busquets, S.; Stemmler, B.; López-Soriano, F.J. Cancer cachexia: Understanding the molecular basis. *Nat. Rev. Cancer* **2014**, *14*, 754–762.
2. Holecek, M. Muscle wasting in animal models of severe illness. *Int. J. Exp. Pathol.* **2012**, *93*, 157–171.
3. Hauser, C.A.; Stockler, M.R.; Tattersall, M.H.N. Prognostic factors in patients with recently diagnosed incurable cancer: A systematic review. *Support. Care Cancer* **2006**, *14*, 999–1011.
4. Laviano, A.; Meguid, M.M.; Inui, A.; Muscaritoli, M.; Rossi-Fanelli, F. Therapy insight: Cancer anorexia-cachexia syndrome--when all you can eat is yourself. *Nat. Clin. Pract. Oncol.* **2005**, *2*, 158–165.
5. Fearon, K.C.H. Cancer cachexia: Developing multimodal therapy for a multidimensional problem. *Eur. J. Cancer* **2008**, *44*, 1124–1132.
6. Tisdale, M.J. Cachexia in cancer patients. *Nat. Rev. Cancer* **2002**, *3*, 883–889.
7. Fearon, K.; Strasser, F.; Anker, S.D.; Bosaeus, I.; Bruera, E.; Fainsinger, R.L.; Jatoi, A.; Loprinzi, C.; MacDonald, N.; Mantovani, G.; et al. Definition and classification of cancer cachexia: An international consensus. *Lancet Oncol.* **2011**, *12*, 489–495.
8. Morley, J.E.; Thomas, D.R.; Wilson, M.-M.G. Cachexia: Pathophysiology and clinical relevance. *Am. J. Clin. Nutr.* **2006**, *83*, 735–743.
9. Penafuerte, C.A.; Gagnon, B.; Sirois, J.; Murphy, J.; Macdonald, N.; Tremblay, M.L. Identification of neutrophil-derived proteases and angiotensin II as biomarkers of cancer cachexia. *Br. J. Cancer* **2016**, *114*, 680–687.
10. Kuroda, K.; Nakashima, J.; Kanao, K.; Kikuchi, E.; Miyajima, A.; Horiguchi, Y. Interleukin 6 is associated with cachexia in patients with prostate cancer. *Urology* **2007**, *69*, 113–117.
11. Hou, Y.-C.; Wang, C.-J.; Chao, Y.-J.; Chen, H.-Y.; Wang, H.-C.; Tung, H.-L.; Lin, J.-T.; Shan, Y.-S. Elevated Serum Interleukin-8 Level Correlates with Cancer-Related Cachexia and Sarcopenia: An Indicator for Pancreatic Cancer Outcomes. *J. Clin. Med.* **2018**, *7*, 502.
12. Kandarian, S.C.; Nosacka, R.L.; Delitto, A.E.; Judge, A.R.; Judge, S.M.; Ganey, J.D.; Moreira, J.D.; Jackman, R.W. Tumour-derived leukaemia inhibitory factor is a major driver of cancer cachexia and morbidity in C26 tumour-bearing mice. *J. Cachexia Sarcopenia Muscle* **2018**, *9*, 1109–1120.
13. Moldawer, L.L.; Georgieff, M.; Lundholm, K. Interleukin 1, tumour necrosis factor-alpha (cachectin) and the pathogenesis of cancer cachexia. *Clin. Physiol.* **1987**, *7*, 263–274.
14. Argilés, J.M.; López-Soriano, F.J. The role of cytokines in cancer cachexia. *Med. Res. Rev.* **1999**, *19*, 223–248.

15. Ait-Ali, D.; Turquier, V.; Grumolato, L.; Yon, L.; Jourdain, M.; Alexandre, D.; Eiden, L.E.; Vaudry, H.; Anouar, Y. The proinflammatory cytokines tumor necrosis factor-alpha and interleukin-1 stimulate neuropeptide gene transcription and secretion in adrenochromaffin cells via activation of extracellularly regulated kinase 1/2 and p38 protein kinases, and activator pro. *Mol. Endocrinol.* **2004**, *18*, 1721–1739.
16. Yao, X.; Huang, J.; Zhong, H.; Shen, N.; Faggioni, R.; Fung, M.; Yao, Y. Targeting interleukin-6 in inflammatory autoimmune diseases and cancers. *Pharmacol. Ther.* **2014**, *141*, 125–139.
17. Zhang, C.; Li, Y.; Wu, Y.; Wang, L.; Wang, X.; Du, J. Interleukin-6/signal transducer and activator of transcription 3 (STAT3) pathway is essential for macrophage infiltration and myoblast proliferation during muscle regeneration. *J. Biol. Chem.* **2013**, *288*, 1489–1499.
18. Heinrich, P.C.; Behrmann, I.; Haan, S.; Hermanns, H.M.; Müller-Newen, G.; Schaper, F. Principles of interleukin (IL)-6-type cytokine signalling and its regulation. *Biochem. J.* **2003**, *374*, 1–20.
19. Cao, P.R.; Kim, H.J.; Lecker, S.H. Ubiquitin-protein ligases in muscle wasting. *Int. J. Biochem. Cell Biol.* **2005**, *37*, 2088–2097.
20. Zhao, J.; Brault, J.J.; Schild, A.; Cao, P.; Sandri, M.; Schiaffino, S.; Lecker, S.H.; Goldberg, A.L. FoxO3 coordinately activates protein degradation by the autophagic/lysosomal and proteasomal pathways in atrophying muscle cells. *Cell Metab.* **2007**, *6*, 472–483.
21. Samuels, S.E.; Knowles, A.L.; Tilignac, T.; Debiton, E.; Madelmont, J.C.; Attaix, D. Higher skeletal muscle protein synthesis and lower breakdown after chemotherapy in cachectic mice. *Am. J. Physiol. Regul. Integr. Comp. Physiol.* **2001**, *281*, R133–9.
22. Gomes, M.D.; Lecker, S.H.; Jagoe, R.T.; Navon, A.; Goldberg, A.L. Atrogin-1, a muscle-specific F-box protein highly expressed during muscle atrophy. *Proc. Natl. Acad. Sci. USA* **2001**, *98*, 14440–14445.
23. Stevenson, E.J.; Giresi, P.G.; Koncarevic, A.; Kandarian, S.C. Global analysis of gene expression patterns during disuse atrophy in rat skeletal muscle. *J. Physiol.* **2003**, *551*, 33–48.
24. Giresi, P.G. Identification of a molecular signature of sarcopenia. *Physiol. Genom.* **2005**, *21*, 253–263.
25. Stevenson, E.J.; Koncarevic, A.; Giresi, P.G.; Jackman, R.W.; Kandarian, S.C. Transcriptional profile of a myotube starvation model of atrophy. *J. Appl. Physiol.* **2005**, *98*, 1396–1406.
26. Hasselgren, P.O. Glucocorticoids and muscle catabolism. *Curr. Opin. Clin. Nutr. Metab. Care* **1999**, *2*, 201–205.
27. Sacheck, J.M.; Hyatt, J.-P.K.; Raffaello, A.; Jagoe, R.T.; Roy, R.R.; Edgerton, V.R.; Lecker, S.H.; Goldberg, A.L. Rapid disuse and denervation atrophy involve transcriptional changes similar to those of muscle wasting during systemic diseases. *FASEB J.* **2007**, *21*, 140–155.
28. Stephens, N.A.; Gallagher, I.J.; Rooyackers, O.; Skipworth, R.J.; Tan, B.H.; Marstrand, T.; Ross, J.A.; Guttridge, D.C.; Lundell, L.; Fearon, K.C.; et al. Using transcriptomics to identify and validate novel biomarkers of human skeletal muscle cancer cachexia. *Genome Med.* **2010**, *2*, 1.

29. Gallagher, I.J.; Stephens, N.A.; MacDonald, A.J.; Skipworth, R.J.E.; Husi, H.; Greig, C.A.; Ross, J.A.; Timmons, J.A.; Fearon, K.C.H. Suppression of skeletal muscle turnover in cancer cachexia: Evidence from the transcriptome in sequential human muscle biopsies. *Clin. Cancer Res.* **2012**, *18*, 2817–2827.
30. Güller, I.; Russell, A.P. MicroRNAs in skeletal muscle: Their role and regulation in development, disease and function. *J. Physiol.* **2010**, *588*, 4075–4087.
31. Eisenberg, I.; Alexander, M.S.; Kunkel, L.M. miRNAS in normal and diseased skeletal muscle. *J. Cell. Mol. Med.* **2009**, *13*, 2–11.
32. Eisenberg, I.; Eran, A.; Nishino, I.; Moggio, M.; Lamperti, C.; Amato, A.A.; Lidov, H.G.; Kang, P.B.; North, K.N.; Mitrani-Rosenbaum, S.; et al. Distinctive patterns of microRNA expression in primary muscular disorders. *Proc. Natl. Acad. Sci. USA* **2007**, *104*, 17016–17021.
33. van de Worp, W.R.P.H.; Theys, J.; van Helvoort, A.; Langen, R.C.J. Regulation of muscle atrophy by microRNAs: "AtromiRs" as potential target in cachexia. *Curr. Opin. Clin. Nutr. Metab. Care* **2018**, *21*, 423–429.
34. Narasimhan, A.; Ghosh, S.; Stretch, C.; Greiner, R.; Bathe, O.F.; Baracos, V.; Damaraju, S. Small RNAome profiling from human skeletal muscle: Novel miRNAs and their targets associated with cancer cachexia. *J. Cachexia Sarcopenia Muscle* **2017**, *8*, 405–416.
35. Soares, R.J.; Cagnin, S.; Chemello, F.; Silvestrin, M.; Musaro, A.; De Pitta, C.; Lanfranchi, G.; Sandri, M. Involvement of microRNAs in the regulation of muscle wasting during catabolic conditions. *J. Biol. Chem.* **2014**, *289*, 21909–21925.
36. Tseng, Y.-C.; Kulp, S.K.; Lai, I.-L.; Hsu, E.-C.; He, W.A.; Frankhouser, D.E.; Yan, P.S.; Mo, X.; Bloomston, M.; Lesinski, G.B.; et al. Preclinical Investigation of the Novel Histone Deacetylase Inhibitor AR-42 in the Treatment of Cancer-Induced Cachexia. *J. Natl. Cancer Inst.* **2015**, *107*, djv274.
37. Roberts, E.W.; Deonarine, A.; Jones, J.O.; Denton, A.E.; Feig, C.; Lyons, S.K.; Espeli, M.; Kraman, M.; McKenna, B.; Wells, R.J.B.; et al. Depletion of stromal cells expressing fibroblast activation protein-α from skeletal muscle and bone marrow results in cachexia and anemia. *J. Exp. Med.* **2013**, *210*, 1137–1151.
38. Bonetto, A.; Aydogdu, T.; Kunzevitzky, N.; Guttridge, D.C.; Khuri, S.; Koniaris, L.G.; Zimmers, T.A. STAT3 activation in skeletal muscle links muscle wasting and the acute phase response in cancer cachexia. *PLoS ONE* **2011**, *6*, e22538.
39. Gilabert, M.; Calvo, E.; Airoldi, A.; Hamidi, T.; Moutardier, V.; Turrini, O.; Iovanna, J. Pancreatic cancer-induced cachexia is Jak2-dependent in mice. *J. Cell. Physiol.* **2014**, *229*, 1437–1443.
40. Shum, A.M.Y.; Fung, D.C.Y.; Corley, S.M.; McGill, M.C.; Bentley, N.L.; Tan, T.C.; Wilkins, M.R.; Polly, P. Cardiac and skeletal muscles show molecularly distinct responses to cancer cachexia. *Physiol. Genom.* **2015**, *47*, 588–599.
41. Fontes-Oliveira, C.C.; Busquets, S.; Fuster, G.; Ametller, E.; Figueras, M.; Olivan, M.; Toledo, M.; López-Soriano, F.J.; Qu, X.; Demuth, J.; et al. A differential pattern of gene expression in skeletal muscle of

tumor-bearing rats reveals dysregulation of excitation–contraction coupling together with additional muscle alterations. *Muscle Nerve* **2014**, *49*, 233–248.

42. Penna, F.; Busquets, S.; Argilés, J.M. Experimental cancer cachexia: Evolving strategies for getting closer to the human scenario. *Semin. Cell Dev. Biol.* **2016**, *54*, 20–27.
43. Martinelli, G.B.; Olivari, D.; Re Cecconi, A.D.; Talamini, L.; Ottoboni, L.; Lecker, S.H.; Stretch, C.; Baracos, V.E.; Bathe, O.F.; Resovi, A.; et al. Activation of the SDF1/CXCR4 pathway retards muscle atrophy during cancer cachexia. *Oncogene* **2016**, *35*, 6212–6222.
44. Matsumoto, S.; Takebayashi, K.; Aso, Y. The effect of spironolactone on circulating adipocytokines in patients with type 2 diabetes mellitus complicated by diabetic nephropathy. *Metabolism* **2006**, *55*, 1645–1652.
45. Hiuge, A.; Tenenbaum, A.; Maeda, N.; Benderly, M.; Kumada, M.; Fisman, E.Z.; Tanne, D.; Matas, Z.; Hibuse, T.; Fujita, K.; et al. Effects of peroxisome proliferator-activated receptor ligands, bezafibrate and fenofibrate, on adiponectin level. *Arterioscler. Thromb. Vasc. Biol.* **2007**, *27*, 635–641.
46. Petit, J.M.; Duong, M.; Masson, D.; Buisson, M.; Duvillard, L.; Bour, J.B.; Brindisi, M.C.; Galland, F.; Guiguet, M.; Gambert, P.; et al. Serum adiponectin and metabolic parameters in HIV-1-infected patients after substitution of nevirapine for protease inhibitors. *Eur. J. Clin. Investig.* **2004**, *34*, 569–575.
47. Martin, R.L.; Lee, J.H.; Cribbs, L.L.; Perez-Reyes, E.; Hanck, D.A. Mibefradil block of cloned T-type calcium channels. *J. Pharmacol. Exp. Ther.* **2000**, *295*, 302–308.
48. Liao, P.; Yu, D.; Li, G.; Yong, T.F.; Soon, J.L.; Chua, Y.L.; Soong, T.W. A smooth muscle Cav1.2 calcium channel splice variant underlies hyperpolarized window current and enhanced state-dependent inhibition by nifedipine. *J. Biol. Chem.* **2007**, *282*, 35133–35142.
49. Splawski, I.; Timothy, K.W.; Sharpe, L.M.; Decher, N.; Kumar, P.; Bloise, R.; Napolitano, C.; Schwartz, P.J.; Joseph, R.M.; Condouris, K.; et al. Ca(V)1.2 calcium channel dysfunction causes a multisystem disorder including arrhythmia and autism. *Cell* **2004**, *119*, 19–31.
50. Mohamed, H.A.; Girgis, N.M.R.; Wilcken, R.; Bauer, M.R.; Tinsley, H.N.; Gary, B.D.; Piazza, G.A.; Boeckler, F.M.; Abadi, A.H. Synthesis and molecular modeling of novel tetrahydro-β-carboline derivatives with phosphodiesterase 5 inhibitory and anticancer properties. *J. Med. Chem.* **2011**, *54*, 495–509.
51. Koo, C.-Y.; Sen, Y.-P.; Bay, B.-H.; Yip, G.W. Targeting heparan sulfate proteoglycans in breast cancer treatment. *Recent Pat. Anticancer Drug Discov.* **2008**, *3*, 151–158.
52. Bogdanovich, S.; Krag, T.O.B.; Barton, E.R.; Morris, L.D.; Whittemore, L.-A.; Ahima, R.S.; Khurana, T.S. Functional improvement of dystrophic muscle by myostatin blockade. *Nature* **2002**, *420*, 418–421.
53. Wagner, K.R.; Fleckenstein, J.L.; Amato, A.A.; Barohn, R.J.; Bushby, K.; Escolar, D.M.; Flanigan, K.M.; Pestronk, A.; Tawil, R.; Wolfe, G.I.; et al. A phase I/IItrial of MYO-029 in adult subjects with muscular dystrophy. *Ann. Neurol.* **2008**, *63*, 561–571.

54. Bodine, S.C.; Latres, E.; Baumhueter, S.; Lai, V.K.; Nunez, L.; Clarke, B.A.; Poueymirou, W.T.; Panaro, F.J.; Na, E.; Dharmarajan, K.; et al. Identification of ubiquitin ligases required for skeletal muscle atrophy. *Science* **2001**, *294*, 1704–1708.
55. Mammucari, C.; Milan, G.; Romanello, V.; Masiero, E.; Rudolf, R.; Del Piccolo, P.; Burden, S.J.; Di Lisi, R.; Sandri, C.; Zhao, J.; et al. FoxO3 controls autophagy in skeletal muscle in vivo. *Cell Metab.* **2007**, *6*, 458–471.
56. Sin, T.K.; Yu, A.P.; Yung, B.Y.; Yip, S.P.; Chan, L.W.; Wong, C.S.; Ying, M.; Rudd, J.A.; Siu, P.M. Modulating effect of SIRT1 activation induced by resveratrol on Foxo1-associated apoptotic signalling in senescent heart. *J. Physiol.* **2014**, *592*, 2535–2548.
57. Penna, F.; Costamagna, D.; Pin, F.; Camperi, A.; Fanzani, A.; Chiarpotto, E.M.; Cavallini, G.; Bonelli, G.; Baccino, F.M.; Costelli, P. Autophagic degradation contributes to muscle wasting in cancer cachexia. *Am. J. Pathol.* **2013**, *182*, 1367–1378.
58. Argilés, J.M.; Busquets, S.; Stemmler, B.; López-Soriano, F.J. Cachexia and sarcopenia: Mechanisms and potential targets for intervention. *Curr. Opin. Pharmacol.* **2015**, *22*, 100–106.
59. Jiang, G.; Huang, C.; Li, J.; Huang, H.; Jin, H.; Zhu, J.; Wu, X.-R.; Huang, C. Role of STAT3 and FOXO1 in the Divergent Therapeutic Responses of Non-metastatic and Metastatic Bladder Cancer Cells to miR-145. *Mol. Cancer Ther.* **2017**, *16*, 924–935.
60. Wang, B.; Zhang, C.; Zhang, A.; Cai, H.; Price, S.R.; Wang, X.H. MicroRNA-23a and MicroRNA-27a Mimic Exercise by Ameliorating CKD-Induced Muscle Atrophy. *J. Am. Soc. Nephrol.* **2017**, *28*, 2631–2640.
61. Ash, G.I.; Kostek, M.A.; Lee, H.; Angelopoulos, T.J.; Clarkson, P.M.; Gordon, P.M.; Moyna, N.M.; Visich, P.S.; Zoeller, R.F.; Price, T.B.; et al. Glucocorticoid Receptor (NR3C1) Variants Associate with the Muscle Strength and Size Response to Resistance Training. *PLoS ONE* **2016**, *11*, e0148112.
62. Jia, H.; Zhao, Y.; Li, T.; Zhang, Y.; Zhu, D. miR-30e is negatively regulated by myostatin in skeletal muscle and is functionally related to fiber-type composition. *Acta Biochim. Biophys. Sin. (Shanghai)* **2017**, *49*, 392–399.
63. Zhu, H.; Han, C.; Wu, T. MiR-17-92 cluster promotes hepatocarcinogenesis. *Carcinogenesis* **2015**, *36*, 1213–1222.
64. Cioffi, M.; Trabulo, S.M.; Sanchez-Ripoll, Y.; Miranda-Lorenzo, I.; Lonardo, E.; Dorado, J.; Reis Vieira, C.; Ramirez, J.C.; Hidalgo, M.; Aicher, A.; et al. The miR-17-92 cluster counteracts quiescence and chemoresistance in a distinct subpopulation of pancreatic cancer stem cells. *Gut* **2015**, *64*, 1936–1948.
65. Chatterjee, A.; Chattopadhyay, D.; Chakrabarti, G. miR-17-5p downregulation contributes to paclitaxel resistance of lung cancer cells through altering beclin1 expression. *PLoS ONE* **2014**, *9*, e95716.
66. Zhao, J.; Fu, W.; Liao, H.; Dai, L.; Jiang, Z.; Pan, Y.; Huang, H.; Mo, Y.; Li, S.; Yang, G.; et al. The regulatory and predictive functions of miR-17 and miR-92 families on cisplatin resistance of non-small cell lung cancer. *BMC Cancer* **2015**, *15*, 731.

67. Dong, C.; Yang, X.-Z.; Zhang, C.-Y.; Liu, Y.-Y.; Zhou, R.-B.; Cheng, Q.-D.; Yan, E.-K.; Yin, D.-C. Myocyte enhancer factor 2C and its directly-interacting proteins: A review. *Prog. Biophys. Mol. Biol.* **2017**, *126*, 22–30.
68. Chinchilla, A.; Lozano, E.; Daimi, H.; Esteban, F.J.; Crist, C.; Aranega, A.E.; Franco, D. MicroRNA profiling during mouse ventricular maturation: A role for miR-27 modulating Mef2c expression. *Cardiovasc. Res.* **2011**, *89*, 98–108.
69. Shen, L.; Chen, L.; Zhang, S.; Du, J.; Bai, L.; Zhang, Y.; Jiang, Y.; Li, X.; Wang, J.; Zhu, L. MicroRNA-27b Regulates Mitochondria Biogenesis in Myocytes. *PLoS ONE* **2016**, *11*, e0148532.
70. McFarlane, C.; Vajjala, A.; Arigela, H.; Lokireddy, S.; Ge, X.; Bonala, S.; Manickam, R.; Kambadur, R.; Sharma, M. Negative auto-regulation of myostatin expression is mediated by Smad3 and microRNA-27. *PLoS ONE* **2014**, *9*, e87687.
71. Rodriguez, J.; Vernus, B.; Chelh, I.; Cassar-Malek, I.; Gabillard, J.C.; Hadj Sassi, A.; Seiliez, I.; Picard, B.; Bonnieu, A. Myostatin and the skeletal muscle atrophy and hypertrophy signaling pathways. *Cell. Mol. Life Sci.* **2014**, *71*, 4361–4371.
72. Argilés, J.M.; Orpí, M.; Busquets, S.; López-Soriano, F.J. Myostatin: More than just a regulator of muscle mass. *Drug Discov. Today* **2012**, *17*, 702–709.
73. Han, H.Q.; Mitch, W.E. Targeting the myostatin signaling pathway to treat muscle wasting diseases. *Curr. Opin. Support. Palliat. Care* **2011**, *5*, 334–341.
74. Smith, R.C.; Lin, B.K. Myostatin inhibitors as therapies for muscle wasting associated with cancer and other disorders. *Curr. Opin. Support. Palliat. Care* **2013**, *7*, 352–360.
75. Gallot, Y.S.; Durieux, A.-C.; Castells, J.; Desgeorges, M.M.; Vernus, B.; Plantureux, L.; Rémond, D.; Jahnke, V.E.; Lefai, E.; Dardevet, D.; et al. Myostatin gene inactivation prevents skeletal muscle wasting in cancer. *Cancer Res.* **2014**, *74*, 7344–7356.
76. Argiles, J.M.; Lopez-Soriano, F.J.; Busquets, S. Counteracting inflammation: A promising therapy in cachexia. *Crit. Rev. Oncog.* **2012**, *17*, 253–262.
77. Brzoska, E.; Kowalewska, M.; Markowska-Zagrajek, A.; Kowalski, K.; Archacka, K.; Zimowska, M.; Grabowska, I.; Czerwińska, A.M.; Czarnecka-Góra, M.; Stremińska, W.; et al. Sdf-1 (CXCL12) improves skeletal muscle regeneration via the mobilisation of Cxcr4 and CD34 expressing cells. *Biol. Cell* **2012**, *104*, 722–737.
78. Dileepan, M.; Sarver, A.E.; Rao, S.P.; Panettieri, R.A.; Subramanian, S.; Kannan, M.S. MicroRNA Mediated Chemokine Responses in Human Airway Smooth Muscle Cells. *PLoS ONE* **2016**, *11*, e0150842.
79. Bonetto, A.; Aydogdu, T.; Jin, X.; Zhang, Z.; Zhan, R.; Puzis, L.; Koniaris, L.G.; Zimmers, T.A. JAK/STAT3 pathway inhibition blocks skeletal muscle wasting downstream of IL-6 and in experimental cancer cachexia. *Am. J. Physiol. Endocrinol. Metab.* **2012**, *303*, E410–E421.
80. Zimmers, T.A.; Fishel, M.L.; Bonetto, A. STAT3 in the systemic inflammation of cancer cachexia. *Semin. Cell Dev. Biol.* **2016**, *54*, 28–41.

81. Diao, Y.; Wang, X.; Wu, Z. SOCS1, SOCS3, and PIAS1 promote myogenic differentiation by inhibiting the leukemia inhibitory factor-induced JAK1/STAT1/STAT3 pathway. *Mol. Cell. Biol.* **2009**, *29*, 5084–5093.
82. Lieskovska, J.; Guo, D.; Derman, E. Growth impairment in IL-6-overexpressing transgenic mice is associated with induction of SOCS3 mRNA. *Growth Horm. IGF Res.* **2003**, *13*, 26–35.
83. Mehic, D.; Bakiri, L.; Ghannadan, M.; Wagner, E.F.; Tschachler, E. Fos and jun proteins are specifically expressed during differentiation of human keratinocytes. *J. Investig. Dermatol.* **2005**, *124*, 212–220.
84. Zhang, P.; Cheng, J.; Zou, S.; D'Souza, A.D.; Koff, J.L.; Lu, J.; Lee, P.J.; Krause, D.S.; Egan, M.E.; Bruscia, E.M. Pharmacological modulation of the AKT/microRNA-199a-5p/CAV1 pathway ameliorates cystic fibrosis lung hyper-inflammation. *Nat. Commun.* **2015**, *6*, 6221.
85. Moher, D.; Liberati, A.; Tetzlaff, J.; Altman, D.G. Preferred Reporting Items for Systematic Reviews and Meta-Analyses: The PRISMA Statement. *PLoS Med.* **2009**, *6*, e1000097.
86. Kulyté, A.; Lorente-Cebrián, S.; Gao, H.; Mejhert, N.; Agustsson, T.; Arner, P.; Rydén, M.; Dahlman, I. MicroRNA profiling links miR-378 to enhanced adipocyte lipolysis in human cancer cachexia. *Am. J. Physiol. Endocrinol. Metab.* **2014**, *306*, E267–E274.
87. Moraes, L.N.; Fernandez, G.J.; Vechetti-Júnior, I.J.; Freire, P.P.; Souza, R.W.A.; Villacis, R.A.R.; Rogatto, S.R.; Reis, P.P.; Dal-Pai-Silva, M.; Carvalho, R.F. Integration of miRNA and mRNA expression profiles reveals microRNA-regulated networks during muscle wasting in cardiac cachexia. *Sci. Rep.* **2017**, *7*, 6998.
88. Agarwal, V.; Bell, G.W.; Nam, J.-W.; Bartel, D.P. Predicting effective microRNA target sites in mammalian mRNAs. *Elife* **2015**, *4*, e05005.
89. Chou, C.-H.; Chang, N.-W.; Shrestha, S.; Hsu, S.-D.; Lin, Y.-L.; Lee, W.-H.; Yang, C.-D.; Hong, H.-C.; Wei, T.-Y.; Tu, S.-J.; et al. miRTarBase 2016: Updates to the experimentally validated miRNA-target interactions database. *Nucleic Acids Res.* **2016**, *44*, D239–D247.
90. Dweep, H.; Sticht, C.; Pandey, P.; Gretz, N. miRWalk–database: Prediction of possible miRNA binding sites by "walking" the genes of three genomes. *J. Biomed. Inform.* **2011**, *44*, 839–847.
91. Mi, H.; Huang, X.; Muruganujan, A.; Tang, H.; Mills, C.; Kang, D.; Thomas, P.D. PANTHER version 11: Expanded annotation data from Gene Ontology and Reactome pathways, and data analysis tool enhancements. *Nucleic Acids Res.* **2017**, *45*, D183–D189.
92. Mi, H.; Dong, Q.; Muruganujan, A.; Gaudet, P.; Lewis, S.; Thomas, P.D. PANTHER version 7: Improved phylogenetic trees, orthologs and collaboration with the Gene Ontology Consortium. *Nucleic Acids Res.* **2010**, *38*, D204–D210.
93. Mi, H.; Lazareva-Ulitsky, B.; Loo, R.; Kejariwal, A.; Vandergriff, J.; Rabkin, S.; Guo, N.; Muruganujan, A.; Doremieux, O.; Campbell, M.J.; et al. The PANTHER database of protein families, subfamilies, functions and pathways. *Nucleic Acids Res.* **2005**, *33*, D284–D288.

94. Szklarczyk, D.; Morris, J.H.; Cook, H.; Kuhn, M.; Wyder, S.; Simonovic, M.; Santos, A.; Doncheva, N.T.; Roth, A.; Bork, P.; et al. The STRING database in 2017: Quality-controlled protein–protein association networks, made broadly accessible. *Nucleic Acids Res.* **2017**, *45*, D362–D368.
95. Snel, B.; Lehmann, G.; Bork, P.; Huynen, M.A. STRING: A web-server to retrieve and display the repeatedly occurring neighbourhood of a gene. *Nucleic Acids Res.* **2000**, *28*, 3442–3444.
96. Shannon, P.; Markiel, A.; Ozier, O.; Baliga, N.S.; Wang, J.T.; Ramage, D.; Amin, N.; Schwikowski, B.; Ideker, T. Cytoscape: A software environment for integrated models of biomolecular interaction networks. *Genome Res.* **2003**, *13*, 2498–2504.
97. Wagner, A.H.; Coffman, A.C.; Ainscough, B.J.; Spies, N.C.; Skidmore, Z.L.; Campbell, K.M.; Krysiak, K.; Pan, D.; McMichael, J.F.; Eldred, J.M.; et al. DGIdb 2.0: Mining clinically relevant drug-gene interactions. *Nucleic Acids Res.* **2016**, *44*, D1036–D1044.
98. Griffith, M.; Griffith, O.L.; Coffman, A.C.; Weible, J. V.; McMichael, J.F.; Spies, N.C.; Koval, J.; Das, I.; Callaway, M.B.; Eldred, J.M.; et al. DGIdb: Mining the druggable genome. *Nat. Methods* **2013**, *10*, 1209–1210.

Supplementary Tables

S1 Table. Gene List.

List with ID, symbol, full name, and synonyms of the 52 differentially expressed genes validated in the skeletal muscles from cancer cachexia samples.

ID	Official Symbol	Official Full Name	Synonyms
11459	Actc1	actin, alpha 1	Acts; Acta-2; Actsk-1
11513	Adcy7	adenylate cyclase 7	AA407758
11450	Adipoq	adiponectin, C1Q and collagen domain containing	Ad; APN; Acdc; apM1; adipo; Acrp30
654812	Angptl7	angiopoietin-like 7	Angl7
494504	Apcdd1	adenomatosis polyposis coli down-regulated 1	Drapc1
12176	Bnip3	BCL2/adenovirus E1B interacting protein 3	Nip3; Bcl2
50908	C1s1	complement component 1, s subcomponent 1	C1s; C1sa
12323	Camk2b	calcium/calmodulin-dependent protein kinase II, beta	KCC2B
12389	Cav1	caveolin 1	Cav; Cav-1
12609	Cebpd	CCAAT/enhancer binding protein (C/EBP), delta	c/EBPdelta
12845	Comp	cartilage oligomeric matrix protein	TSP5
20315	Cxcl12	chemokine (C-X-C motif) ligand 12	Pbsf; Sdf1; Tlsf; Tpar1; Scyb12
54709	Eif3i	eukaryotic translation initiation factor 3, subunit I	Trip1; Eif3s2
14089	Fap	fibroblast activation protein	SIMP ; SEPR
67731	Fbxo32	F-box protein 32	MAFbx; ATROGIN1;
99571	Fgg	fibrinogen gamma chain	FIBG
56458	Foxo1	forkhead box O1	Afxh; FKHR; Fkhr1; Foxo1a
14313	Fst	follistatin	FS
57436	Gabarapl1	gamma-aminobutyric acid A receptor-associated protein-like 1	GECI; Apg8l; Atg8l; GBRL1
15239	Hgs	HGF-regulated tyrosine kinase substrate	tn; Hgr; Hrs
66847	Hint3	histidine triad nucleotide binding protein 3	HINT-3; HINT-4
15439	HP	haptoglobin	HP-1; hpt; preHP2
15483	Hsd11b1	hydroxysteroid 11-beta dehydrogenase 1	DHI1
15516	Hsp90ab1	heat shock protein 90 alpha, class B member 1	Hsp84; Hsp90; Hspcb; Hsp84-1
16477	Junb	jun B proto-oncogene	MyD21

80334	Kcnip4	Kv channel interacting protein 4	Calp; KChIP4; Calp250; KChIP4a
16773	Lama2	laminin, alpha 2	dy; mer; merosin
17260	Mef2c	myocyte enhancer factor 2C	Mef2
17392	Mmp3	matrix metallopeptidase 3	SL-1; EMS-2; SLN-1; STR-1; Stmy1
17700	Mstn	myostatin	Cmpt; Gdf8
17885	Myh8	myosin, heavy polypeptide 8, skeletal muscle	MHCp; Myhsp; Myhs-p; MyHC-pn
14815	Nr3c1	nuclear receptor subfamily 3, group C, member 1	GCR; Grl1; Grl-1
18221	Nudc	nudC nuclear distribution protein	SIG-92; Silg92
18479	Pak1	p21 protein (Cdc42/Rac)-activated kinase 1	Paka; PAK-1
18534	Pck1	phosphoenolpyruvate carboxykinase 1, cytosolic	PEPCK; Pck-1
66853	Pnpla2	patatin-like phospholipase domain containing 2	Atgl; TTS-2.2
216151	Polrmt	polymerase (RNA) mitochondrial	Q8BKF1
19130	Prox1	prospero homeobox 1	P48437
54720	Rcan1	regulator of calcineurin 1	CSP1; DSC1; RCN1; Dscr1; MCIP1; CALP1L; Adapt78
20208	Saa1	serum amyloid A 1	Saa2; Saa-1
20716	Serpina3n	serine peptidase inhibitor, clade A, member 3N	Spi2-2; Spi2.2; Spi2/eb.4
67712	Slc25a37	solute carrier family 25, member 37	Mfrn; Mscp; Mfrn1; frascati; mitoferrin
12702	Socs3	suppressor of cytokine signaling 3	Cis3; Ef10; Ssi3; Cish3; EF-10; SSI-3
20848	Stat3	signal transducer and activator of transcription 3	Aprf
21422	Tfcp2	transcription factor CP2	CP2; LSF; CP-2; LBP1; UBP-1; LBP-1c; LBP-1d; Tcfcp2;
21846	Tie1	tyrosine kinase with immunoglobulin-like and EGF-like domains 1	TIE; tie-1
433766	Trim63	tripartite motif-containing 63	RF1; MuRF1; Rnf28
22084	Tsc2	tuberous sclerosis 2	Tcs2; Nafld
22142	Tuba1a	tubulin, alpha 1A	Tuba1; Tuba-1
22145	Tuba4a	tubulin, alpha 4A	M[a]4; Tuba4
22229	Ucp3	uncoupling protein 3	UCP-3
22230	Ufd1	ubiquitin fusion degradation 1 like	UB

S2 Table. Predicted and validated microRNAs.

Number of predicted and validated microRNA-mRNA interactions

	microRNAs (n)			
mRNA Target	**Predicted**	**Validated**	**Soares et al. 2014; Narasimhan et al. 2017**	**Total**
Actc1	36	1	0	37
Adcy7	87	0	0	87
Adipoq	37	0	0	37
Angptl7	12	5	0	17
Apcdd1	61	7	0	68
Bnip3	29	1	0	30
C1s1	12	0	0	12
Camk2b	108	2	0	110
Cav1	66	6	1	73
cEBP	37	0	0	37
Comp	17	5	0	22
Cxcl12	197	8	2	207
Eif3i	1	0	0	1
Fap	37	0	0	37
Fbxo32	57	2	0	59
Fgg	28	0	0	28
Foxo1	133	4	1	138
Fst	48	1	0	49
Gabarapl1	45	0	0	45
Hgs	66	0	0	66
Hint3	28	0	0	28
HP	35	0	0	35
Hsd11b1	69	1	0	70
Hsp90ab1	62	0	0	62
Junb	76	0	1	77
Kcnip4	52	0	0	52
Lama2	20	0	0	20
Mef2c	33	14	2	49
Mmp3	40	0	0	40
Mstn	65	0	0	65
Myh8	26	0	0	26
Nr3c1	50	9	0	59
Nudc	38	0	0	38
Pak	60	2	0	62

Pck1	86	5	0	91
Pnpla2	66	1	0	67
Polrmt	9	0	0	9
Prox1	62	2	0	64
Rcan1	85	1	0	86
Saa1	44	0	0	44
Serpina3n	139	0	0	139
Slc25a37	133	2	0	135
Socs3	75	1	0	76
Stat3	124	9	0	133
Tfcp2	78	9	0	87
Tie1	50	0	0	50
Trim63	121	0	0	121
Tsc2	99	0	0	99
Tuba1a	32	0	0	32
Tuba4a	97	0	0	97
Ucp3	82	0	0	82
Ufd1	0	0	0	0
TOTAL	**3150**	**98**	**7**	**3255**

S3 Table. microRNA-mRNA interactions.

List of predicted and validated microRNA-mRNA interactions

	Target	Validated microRNA
Up-regulated	Stat3	miR-106a-5p, miR-93-5p, miR-20a-5p, miR-17-5p, let-7b-5p, miR-125b-5p, miR-106b-5p, miR-223-3p, miR-124-3p
	Tfcp2	miR-3089-5p, miR-3082-5p, miR-804, miR-759, miR-1195, miR-665-3p, miR-673-3p, miR-5135, miR-139-5p
	Angptl7	miR-1195, miR-804, miR-3089-5p, miR-5135, miR-376c-3p,
	Comp	miR-329-3p, miR-362-3p, miR-100-5p, miR-99a-5p, miR-99b-5p
	Foxo1	miR-139-5p, miR-145a-5p, miR-694, miR-27a, miR-1264-3p
	Pck1	miR-342-3p, miR-377-3p, miR-362-3p, miR-329-3p, miR-466i-3p
	Camk2b	miR-122-5p, miR-136-5p
	Fbxo32	miR-3098-5p, miR-384-3p
	Pak1	miR-425-5p, miR-34b-5p
	Pnpla2	miR-124-3p
	Socs3	miR-483-5p
	Mstn	miR-27b
	Junb	miR-199a
Down- regulated	Mef2c	miR-223-3p, miR-24-3p, miR-26a-5p, miR-27a, miR-27b, miR-327, miR-495-3p, miR-1192, miR-5101, miR-106b-5p, miR-20a-5p, miR-20b-5p, miR-93-5p, miR-17-5p, miR-106a-5p
	Nr3c1	miR-425-5p, miR-362-5p, miR-30e-5p, miR-129-5p, miR-1897-5p, miR-3057-5p, miR-5130, miR-28b, miR-28c
	Cxcl12	miR-124-3p, miR-140-5p, miR-17-5p, miR-340-5p, miR-27b, miR-15a-5p, miR-34b-5p, miR-149-5p, miR-9-5p
	Cav1	miR-340-5, miR-301-3p, miR-17-5p, miR-19b-3p, miR-199a, miR-297-5p, miR-203-3p
	Apcdd1	miR-301b-3p, miR-26a-5p, miR-3968, miR-3971, miR-1955-3p, miR-690
	Slc25a37	miR-362-5p, miR-3082-3p
	Prox1	miR-181a-5, miR-124-3p
	Rcan1	miR-122-5p
	Bnip3	miR-221-3p
	Hsd11b1	miR-26a-5p
	Fst	miR-124-3p
	Actc1	miR-124-3p

International Journal of
Molecular Sciences

MDPI

Review

The Pathway to Cancer Cachexia: MicroRNA-Regulated Networks in Muscle Wasting Based on Integrative Meta-Analysis

Paula Paccielli Freire [1], Geysson Javier Fernandez [1], Sarah Santiloni Cury [1], Diogo de Moraes [1], Jakeline Santos Oliveira [1], Grasieli de Oliveira [1], Maeli Dal-Pai-Silva [1], Patrícia Pintor dos Reis [2,3] and Robson Francisco Carvalho [1,*]

1 Department of Morphology, Institute of Biosciences, São Paulo State University (UNESP), Botucatu, São Paulo 18.618-619, Brazil; paula.freire@unesp.br (P.P.F.); jasonfergar@hotmail.com (G.J.F.); sarahscury@gmail.com (S.S.C.); demoraesdiogo2017@gmail.com (D.d.M.); jakoliveira.jo@gmail.com (J.S.O.); oliveira.grase@gmail.com (G.d.O.); maeli.dal-pai@unesp.br (M.-D.-P.-S.)
2 Department of Surgery and Orthopedics, Faculty of Medicine, São Paulo State University (UNESP), Botucatu, São Paulo 18.618-687, Brazil; patricia.reis@unesp.br
3 Experimental Research Unity, Faculty of Medicine, São Paulo State University (UNESP), Botucatu, São Paulo 18.618-687, Brazil
* Correspondence: robson.carvalho@unesp.br; Tel.: +55-14-3880-0473

Received: 12 March 2019; Accepted: 11 April 2019; Published: 22 April 2019

Abstract: Cancer cachexia is a multifactorial syndrome that leads to significant weight loss. Cachexia affects 50%–80% of cancer patients, depending on the tumor type, and is associated with 20%–40% of cancer patient deaths. Besides the efforts to identify molecular mechanisms of skeletal muscle atrophy—a key feature in cancer cachexia—no effective therapy for the syndrome is currently available. MicroRNAs are regulators of gene expression, with therapeutic potential in several muscle wasting disorders. We performed a meta-analysis of previously published gene expression data to reveal new potential microRNA–mRNA networks associated with muscle atrophy in cancer cachexia. We retrieved 52 differentially expressed genes in nine studies of muscle tissue from patients and rodent models of cancer cachexia. Next, we predicted microRNAs targeting these differentially expressed genes. We also include global microRNA expression data surveyed in atrophying skeletal muscles from previous studies as background information. We identified deregulated genes involved in the regulation of apoptosis, muscle hypertrophy, catabolism, and acute phase response. We further predicted new microRNA–mRNA interactions, such as miR-27a/*Foxo1*, miR-27a/*Mef2c*, miR-27b/*Cxcl12*, miR-27b/*Mef2c*, miR-140/*Cxcl12*, miR-199a/*Cav1*, and miR-199a/*Junb*, which may contribute to muscle wasting in cancer cachexia. Finally, we found drugs targeting *MSTN*, *CXCL12*, and *CAMK2B*, which may be considered for the development of novel therapeutic strategies for cancer cachexia. Our study has broadened the knowledge of microRNA-regulated networks that are likely associated with muscle atrophy in cancer cachexia, pointing to their involvement as potential targets for novel therapeutic strategies.

Keywords: cancer cachexia; microRNAs; transcriptome; protein-protein interaction networks

1. Introduction

Cachexia is a syndrome associated with pathological conditions, including sepsis, chronic obstructive pulmonary disease, heart failure, and cancer [1,2]. Notably, cachexia is the leading cause of death for 20%–40% of cancer patients [3], and affects around 60% of patients when all cancer types are

Capítulo III

THE EXPRESSION LANDSCAPE OF CACHEXIA-INDUCING FACTORS IN HUMAN CANCERS

Paula Paccielli Freire[1*], Geysson Javier Fernandez [1,2*], Diogo de Moraes[1], Sarah Santiloni Cury[1], Maeli Dal Pai-Silva[1], Patrícia Pintor dos Reis[3,4], Silvia Regina Rogatto[5#] & Robson Francisco Carvalho[1#].

1. Department of Morphology, Institute of Biosciences, São Paulo State University, UNESP, Botucatu, SP, Brazil.
2. Faculty of Medicine, University of Antioquia, UdeA, Medellín, Colombia.
3. Department of Surgery and Orthopedics, Faculty of Medicine, São Paulo State University, UNESP, Botucatu, São Paulo, Brazil.
4. Experimental Research Unity, Faculty of Medicine, São Paulo State University, UNESP, Botucatu, São Paulo, Brazil.
5. Department of Clinical Genetics, University Hospital, Institute of Regional Health Research, University of Southern Denmark, Vejle, Denmark.

* These authors contributed equally to this study

Corresponding authors

Corresponding authors
Professor Robson Francisco Carvalho
Department of Morphology
Institute of Biosciences, São Paulo State University
CEP: 18.618-689, Botucatu, São Paulo – Brazil
Telephone number: +55 14 3880 0473
robson.carvalho@unesp.br

Professor Silvia Regina Rogatto
Department of Clinical Genetics, University Hospital, Vejle
Institute of Regional Health Research, University of Southern Denmark
Beriderbakken 4, 7100 Vejle – Denmark
Telephone number: +45 -7940 6669
silvia.regina.rogatto@rsyd.dk

(Submitted to Journal of Cachexia, Sarcopenia and Muscle)

Abstract

Background: Cachexia is a multifactorial syndrome highly associated with specific tumor types, but the causes of variation in cachexia prevalence and severity are unknown. While circulating plasma mediators (soluble cachectic factors) derived from tumors have been implicated with the pathogenesis of the syndrome, these associations were generally based on plasma concentration rather than tissue-specific gene expression levels. Here, we hypothesized that tumor gene expression profiling of cachexia-inducing factors (CIF) in human cancers with different prevalence of cachexia could reveal potential cancer-specific cachexia mediators and biomarkers of clinical outcome.

Methods: First, we combined uniformly processed RNA sequencing data from The Cancer Genome Atlas (TCGA) and Genotype-Tissue Expression (GTEx) databases to characterize the expression profile of secretome genes in 12 cancer types (4,651 samples) compared to their matched normal tissues (2,737 samples). We systematically investigated the transcriptomic data to assess the tumor expression profile of 25 known CIF and their predictive values for patient survival. We used Xena Functional Genomics tool to analyze the gene expression of CIF according to neoplastic cellularity in pancreatic adenocarcinoma, which is known to present the highest prevalence of cachexia.

Results: A comprehensive characterization of the expression profiling of secreted genes in different human cancers revealed pathways and mediators with a potential role in cachexia within the tumor microenvironment. Cytokine and chemokine related-pathways were enriched in tumor types frequently associated with the syndrome. Cachexia-inducing factors presented a tumor-specific expression profile, in which the number of upregulated genes was correlated with the cachexia prevalence (r square: 0.80; p-value: 0.002) and weight loss (r square: 0.81; p-value: 0.002). The distinct gene expression profile, according to tumor type, was significantly associated with prognosis (p-value $\leq$ 1.96 E-06). In pancreatic adenocarcinoma, the upregulated CIF genes were associated with tumors presenting low neoplastic cellularity and high leukocyte fraction, and not with tumor grade.

Conclusion: Our results present a biological dimension of tumor-secreted elements that are potentially useful to explain why specific cancer types are more likely to develop cachexia. The tumor-specific profile of CIF may help the future development of better-targeted therapies to treat cancer types highly associated with the syndrome.

Key words: Cachexia-inducing factors, Cancer Genomics, GTEx, Omics, Pan-Cancer, TCGA.

Introduction

Cancer cachexia is a multifactorial syndrome characterized by muscle wasting, leading to a significant weight loss that impacts patient's quality of life, tolerance to treatment, response to therapy, and survival[1–5]. The syndrome affects up to 80% of advanced **cancer** patients, and it represents the cause of 20% of all cancer deaths[6]. Cachexia is highly associated with specific tumor types such as pancreatic, esophageal, gastric, lung and liver, and similarly, patients with these malignancies have the highest degree of weight loss[7–12]. The etiology of cancer cachexia in different tumor types involves complex and specific tumor-host interactions that remain to be completely elucidated. The combinatorial action of soluble secreted mediators (secretome) by cancer cells and cells within the tumor microenvironment, including many pro-inflammatory cytokines, contribute to systemic inflammation and directly act on skeletal muscle to induce wasting[12–15]. Consequently, the efforts to identify mediators and biomarkers have been centered on the levels of cachectic factors from plasma[16–21]. However, it remains unclear whether these factors circulating in the blood are derived from the host or tumor secretome. In addition, the extent to which these secreted factors associated with cachexia are expressed by different tumor types, and which are the most ubiquitously expressed in different cancer sites, have yet to be determined. A comprehensive characterization of the gene expression profile of cachexia-inducing factors (CIF) has the potential to reveal tumor secretome transcriptional patterns, which may help to explain the variation on prevalence and severity of cachexia within and across human cancers.

Transcriptomic approaches have been applied to unravel the secretome of a specific cell or tissue types[22]. In a pioneer genome-wide study based on microarrays, Welsh *et al.*[23] described 74 overexpressed genes encoding secreted proteins in human cancers. Despite the reduced number of genes predicted as encoding secreted proteins and the relatively low number of tissue samples surveyed in this study, a significant fraction of these overexpressed secretome genes in carcinomas were found to be dysregulated in cancer or having demonstrated applications in cancer diagnosis and therapy. The advent of RNA sequencing (RNA-Seq) has revolutionized the transcriptomic studies and enabled researchers a better understanding of the genetic mechanisms underlying human diseases, especially in cancer[24–26]. Therefore, RNA-Seq followed by newly emerging algorithms for signal-peptide predictions have become useful tools for profiling the secretome [22], and have revealed that a larger fraction of human tissue-enriched proteins are secreted[27]. Based on this knowledge, Robinson *et al.*[28] conducted a Pan-Cancer analysis of secretome gene expression that resulted in ranked lists of candidate diagnostic biomarkers detectable in biological fluids. This investigation also revealed the patterns and biological functions associated with changes in secreted protein expression in different tumor types,

focusing mainly on a "core" secretome. This strategy reduced the complexity of the secretome by narrowing the range of secreted molecules necessary to explore fundamental questions underlying altered secretome expression in different cancer types. However, the secretome complexity is still far from being completely understood and selecting different methodological strategies or specific tumor types might lead to new insights into its biological function.

The Pan-Cancer studies integrate different levels of molecular data to comprehensively identify the similarities and differences in single or different tumor types [29]. Here, we compared the expression profiles and functions of secreted proteins in 12 tumor types with different prevalence of cachexia. We hypothesized that tumor gene expression profiling of CIF could reveal potential cancer-specific mediators and biomarkers of clinical outcome. To test this, we first combined uniformly processed RNA sequencing data from The Cancer Genome Atlas (TCGA) and Genotype-Tissue Expression (GTEx) databases to characterize the expression profile of secretome genes. These datasets allowed us to comprehensively characterize the expression landscape of genes encoding predicted secreted proteins in human cancers and revealed potential mediators of cachexia within the tumor microenvironment. Next, we focused on the transcriptomic data to assess the tumor expression profile of 25 known CIF and their prognostic value in terms of predicting patient survival. Interestingly, we detected a tumor-specific expression profile of CIF. The number of upregulated cachectic factor genes in tumor compared to normal tissues was strongly correlated with the prevalence of cachexia and weight loss. We identified the expression of tumor cachectic factors genes relevant to cancer biology, which may help to elucidate why specific cancer types are more prone to develop cachexia.

Methods

TCGA and GTEx transcriptomics datasets

Transcriptional profiles from TCGA (https://portal.gdc.cancer.gov/) of 12 human cancers were compared with matched normal tissues from TCGA and GTEx[30] (http://www.gtexportal.org/). We used RNA sequencing data uniformly processed and unified by the Toil Pipeline[31], via the web-based tool *Gene Expression Profiling Analysis*[32] (GEPIA, http://gepia.cancerpku.cn/). A similar strategy was previously described in pan-cancer studies[33,34], and their comparability findings demonstrated that TCGA and GTEx expression profiles could be collectively analyzed. Differentially expressed genes (DEGs) between tumor and normal samples were determined by one-way ANOVA applying the statistical cutoffs of log2 fold-change > 1 and q-value < 0.01.

Transcriptome-based secretome analysis

DEGs were further filtered for secreted protein-coding genes based on the human secretome list available at The Human Protein Atlas[27] (https://www.proteinatlas.org/humanproteome/secretome), which was predicted by a whole-proteome scan using at least two of the three following methods for signal peptide prediction: SignalP4.0, Phobius, and SPOCTOPUS. Shared upregulated secretome genes among all tumor types were displayed using Circos[35] (http://circos.ca/). The Kyoto Encyclopedia of Genes and Genomes (KEGG) pathway and Biological Process (Gene Ontology) analyses of the deregulated secretome genes were performed with EnrichR links[36,37] (http://amp.pharm.mssm.edu/Enrichr/), and the enrichment result is represented by p-value (Fisher exact test) and Z-score (correction to the test) in a combined score computed by EnrichR[36,37]. The KEGG pathway and Biological Process terms were included in an integrative analysis using the criterion of over-representation (Log2 combined score > 2) in at least one tumor type. The set of CIF detected and enriched in the top 10 Biological Process terms are displayed through an Alluvial Graph generated using the online tool: http://sankeymatic.com/.

Cachectic soluble factors gene expression profile in 12 tumor types

For mRNA profiling of cachectic soluble factors, we selected 25 transcripts coding for soluble factors associated with cachexia. These transcripts were previously selected for blood screening by a multiplex array platform in pancreatic cachectic patients[16] (Supplementary Table 1). The number of upregulated transcripts were correlated with the prevalence of cachexia and average weight loss for each tumor type obtained from previous studies[8,11]. Although our dataset may not represent the entire range of cachexia variation for all the 12 cancer types analyzed, these selected data provided numbers with potential correspondence in cachexia studies. We calculated the Pearson's correlations coefficient (r) with corresponding p-values for the covariation between the number of differentially expressed CIF from TCGA datasets (tumor tissues vs. matched normal TCGA and GTEx data) with the prevalence of cachexia and percentage of weight loss. We considered significant correlation when p-value < 0.01 and r square value ≥ 0.8. The correlation analysis was performed using the software GraphPad Prism (GraphPad Prism 6).

Tumor purity analysis

We collected the pancreatic adenocarcinoma (PAAD) clinical and tumor purity information from The Cancer Genome Atlas Research Network[38]. The expression levels of 25 CIF genes were analyzed using unsupervised clustering approaches, according to the neoplastic cellularity of PAAD (high purity *vs.* low purity tumors). Xena Functional Genomics Explorer tool was used to collect the gene expression

information, using normalized data by the upper quartile method represented as log2 norm_count+1 (http://xenabrowser.net/). Morpheus (https://software.broadinstitute.org/morpheus)[39] was used to cluster the expression profile of the 25 CIF in PAAD samples according to neoplastic cellularity data (leukocyte methylation percentage, tumor DNA hypermethylation, and purity class) and tumor grade.

Survival analysis and risk assessment

SurvExpress[40] (http://bioinformatica.mty.itesm.mx/SurvExpress) was used to determine the risk assessment and perform a survival analysis of 12 TCGA cancer datasets. This online tool allowed us to assess the tumor gene expression of all 25 pro-cachectic factors simultaneously and analyzed their association with the survival of cancer patients by Cox Proportional Hazard regression in high- and low-risk groups, as determined through the SurvExpress optimization algorithm. This analysis was performed without considering other clinical characteristics rather than survival.

Data representation and analysis

Correlation analysis and bar plots were constructed with GraphPad Prism (GraphPad Software). Venn diagrams were plotted using the webserver http://bioinformatics.psb.ugent.be/webtools/Venn/. Heatmaps and PCA plots were created using the web tools ClustVis[41] (http://biit.cs.ut.ee/clustvis/) and Morpheus [39] (https://software.broadinstitute.org/morpheus).

Results

The secretome genes show differential expression profiles across human cancers.

Gene expression profiles were obtained of 4,743 tumors comprising 12 cancer types (TCGA), and 2,737 corresponding normal tissues (TCGA and GTEx). These tumors were selected to allow a comparison between cancer types ranging from high to low prevalence of cachexia and weight loss[8,11,12]. The summary of the number of TCGA and GTEx samples is described in Supplementary Table 2.

Differentially expressed genes were filtered for those genes previously predicted to have at least one secreted protein by the Human Protein Atlas (HPA)[27] (Supplementary Data 1). This analysis revealed 2,162 out of 2,933 HPA differentially expressed secretome genes in at least one cancer type compared with normal samples (Log2 fold change > 1 and q-value cutoff = 0.01; Supplementary Data 2). The clustering analyses based on Euclidian distance revealed that PAAD displays a gene expression profile that is distinct from other cancers (Fig. 1a). Also, this analysis grouped cancer types originating from the same anatomical sites, such as lung adenocarcinoma (LUAD) and lung squamous cell

carcinoma (LUSC), as well as colon adenocarcinoma (COAD) and rectum adenocarcinoma (READ) (Fig. 1a). Similarly, Esophageal squamous cell carcinoma (ESCA) and head and neck squamous cell carcinoma (HNSC) also presented similar expression profiles (Fig. 1a). To test whether our transcriptome-based secretome analysis defines tumor types, we performed principal component analysis (PCA) that revealed that PAAD, acute myeloid leukemia (LAML), LUSC, and the cluster composed by COAD and READ, are distinguished among the 12 cancer types based on the expression profile of the secretory protein-coding genes (Fig. 1b).

We investigated the diversity and complexity of the cancer transcriptome-based secretome in these selected 12 cancer types. We found that tumors differed highly in the number of dysregulated secretome genes in comparison to normal tissues. For instance, PAAD presented 1365 dysregulated genes, while hepatocellular liver carcinoma (LIHC) had 380 (Fig. 1c, Supplementary Table 3). The proportions of up and downregulated secretome genes also showed wide distribution among malignant tissues. PAAD, stomach adenocarcinoma (STAD), ESCA, and HNSC presented 72% to 93% of upregulated secretome genes, whereas LUSC, LUAD, and prostate adenocarcinoma (PRAD) showed 24% to 27% (Fig. 1c, Supplementary Tables 3-5).

Secretome genes reveal potential mediators of cachexia within and across human cancers.

Given that many secreted soluble factors have been associated with cachexia in different tumor types, significantly upregulated genes coding for secreted proteins shared among these tumors have the potential to reveal key players towards the pathogenesis of the syndrome. PAAD, which is associated with a severe form of cachexia, shared the highest number of upregulated genes in all tumor types tested (Fig. 1d, Supplementary Table 6). Other tumor types highly associated with cachexia, including STAD, READ, COAD, ESCA, and HNSC, had in common a high number of upregulated secretome genes. STAD shared 515 common upregulated genes with PAAD, while ESCA, COAD, READ, and HNSC presented 305-366. Among the cancer types, PRAD had the lowest number (n=69) of overlapping upregulated genes with PAAD. Fig. 1d and Supplementary Fig. 1 are representatives of these findings. Importantly, the shared upregulated genes for secreted proteins revealed potential mediators of cachexia within the tumor microenvironment, especially in tumors highly associated with the syndrome.

Upregulated secretome genes exclusively detected in a single cancer type, particularly in those highly associated with cachexia, are tumor-specific candidates (Supplementary Table 7). In PAAD, we found exclusive upregulation of 371 genes encoding mainly for cytokine-cytokine receptor

interaction, complement and coagulation cascades, and Rap1 signaling pathways (Fig. 1e, Supplementary Tables 7 and 8). Interestingly, many of these exclusively upregulated genes in PAAD were dysregulated in opposite directions in tumors originating from lung and large intestine (Supplementary Fig. 2, Supplementary Table 9). A total of 103 genes were exclusively upregulated in LAML, and these genes were related to coagulation cascades and pyruvate metabolism and downregulated 180 unique secretome genes involved in arginine and proline metabolism, ribosome, and metabolic pathways (Supplementary Tables 10 and 11). Together, these results show that tumor-specific factors have the potential to explain the variation in the prevalence and severity of cancer cachexia.

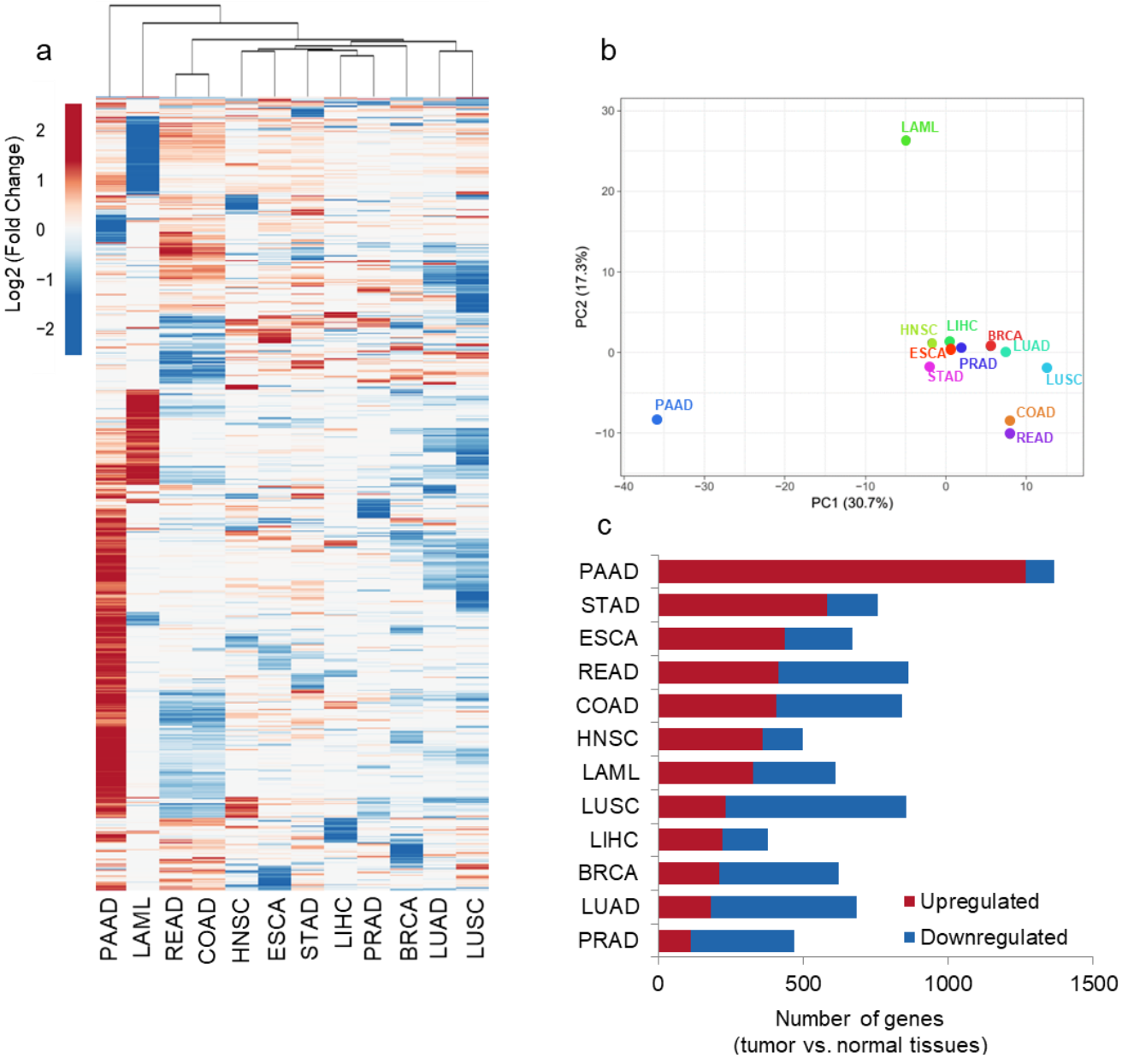

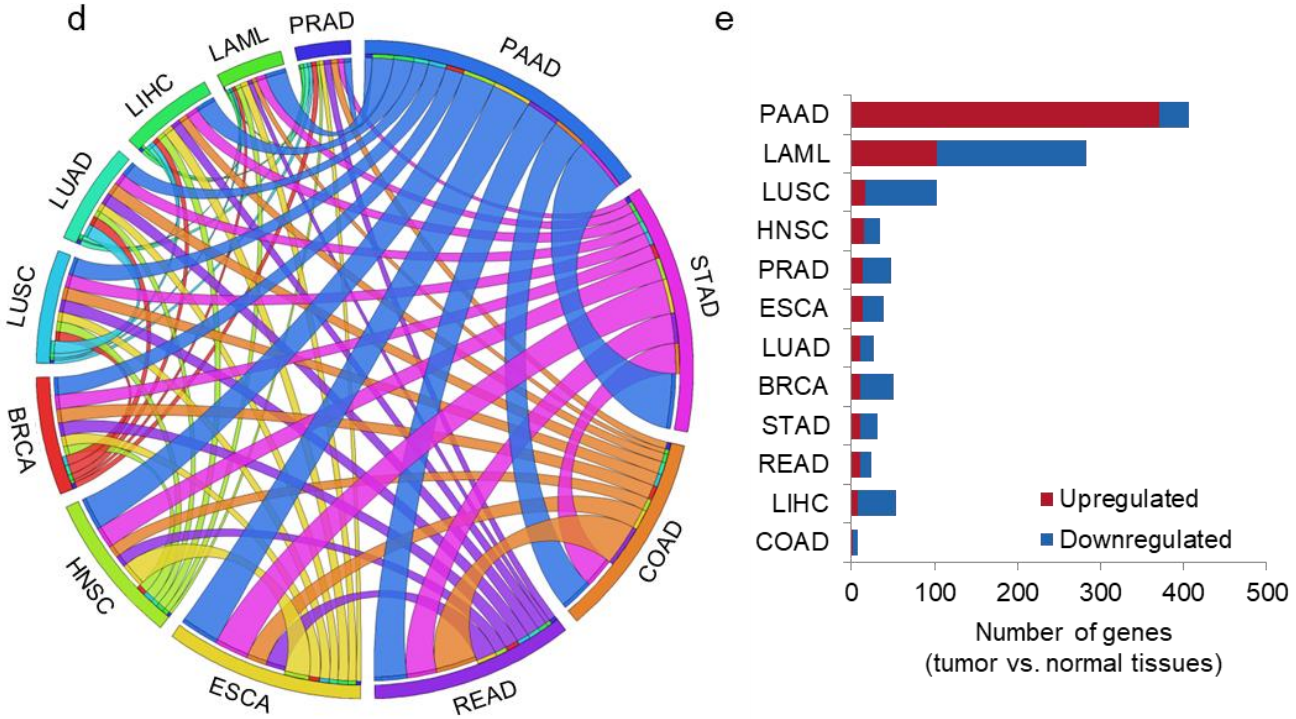

Fig. 1 Gene expression analysis of the secretome components in 12 TCGA tumor types compared with corresponding matched normal TCGA and GTEx tissues. a) Heatmap of the mean expression levels [log2 (TPM+1)] of secretome components in 12 tumor types compared with normal tissues. Both rows (secretome genes) and columns (tumor types) were clustered using Euclidian distance. Differential expression levels were calculated using the web-based tool Gene Expression Profiling Analysis (GEPIA, http://gepia.cancerpku.cn/)[32]. The resulting numbers of genes encoding predicted secreted proteins were filtered based on the Human Protein Atlas secretome data (https://www.proteinatlas.org/humanproteome/secretome)[27]. The upregulated and downregulated genes with absolute values of fold-change > 2.0 and q-value < 0.01 (ANOVA) are shown in red and blue, respectively. The pancreatic adenocarcinoma (PAAD) shows a clear enrichment of the upregulated secretome genes. **b)** Principal component analysis (PCA) of the secretome gene expression data in 12 tumor types compared with normal tissues. **c)** The total number of dysregulated secretome genes in each tumor type (TCGA) compared with corresponding matched normal tissues (TCGA and GTEx). d) The thickness of each link in the Circos plot represents the number of shared upregulated secretome genes among tumor types. e) Exclusive upregulated genes within tumor types. PAAD: Pancreatic adenocarcinoma; ESCA: Esophageal carcinoma; STAD: Stomach adenocarcinoma; HNSC: Head and neck squamous cell carcinoma; LUAD: Lung adenocarcinoma; LUSC: Lung squamous cell carcinoma; LIHC: Liver hepatocellular carcinoma; COAD: Colon adenocarcinoma; READ: Rectum adenocarcinoma; LAML: Acute myeloid leukemia; PRAD: Prostate adenocarcinoma; BRCA: Breast invasive carcinoma.

Secretome pathways with a potential role in cancer cachexia

Genes significantly deregulated in at least one tumor type were select to perform enrichment analysis using the KEGG pathways and Gene Ontology (GO) terms. Overall, we observed that pathways previously associated with cachexia are overrepresented in highly cachectic tumors (Fig. 2a). The upregulated genes enriched pathways associated with chemokine and cytokine in PAAD, STAD, ESCA, HNSC, COAD, and READ (Fig. 2, Supplementary Fig. 3). Terms previously associated with cachexia, such as lysosome, exocytosis, complement and coagulation cascade, ECM-receptor interaction, PI3K-Akt signaling, and leukocyte chemotaxis were strongly enriched for upregulated genes in PAAD, STAD, ESCA, and HNSC (Fig. 2). PAAD, STAD, ESCA, and HNSC presented a clear pattern of downregulated secretome genes that were less enriched for many pathways highly over-represented for the upregulated genes (Fig. 2a). The pattern of secretome pathways for LUAD and LUSC was distinct from tumors highly associated with cachexia, such as PAAD, STAD, ESCA, and HNSC (Fig. 2a). An enrichment for downregulated genes associated with ECM-receptor interaction, PI3K-Akt pathway, and protein digestion and absorption was detected in PRAD (Fig. 2a).

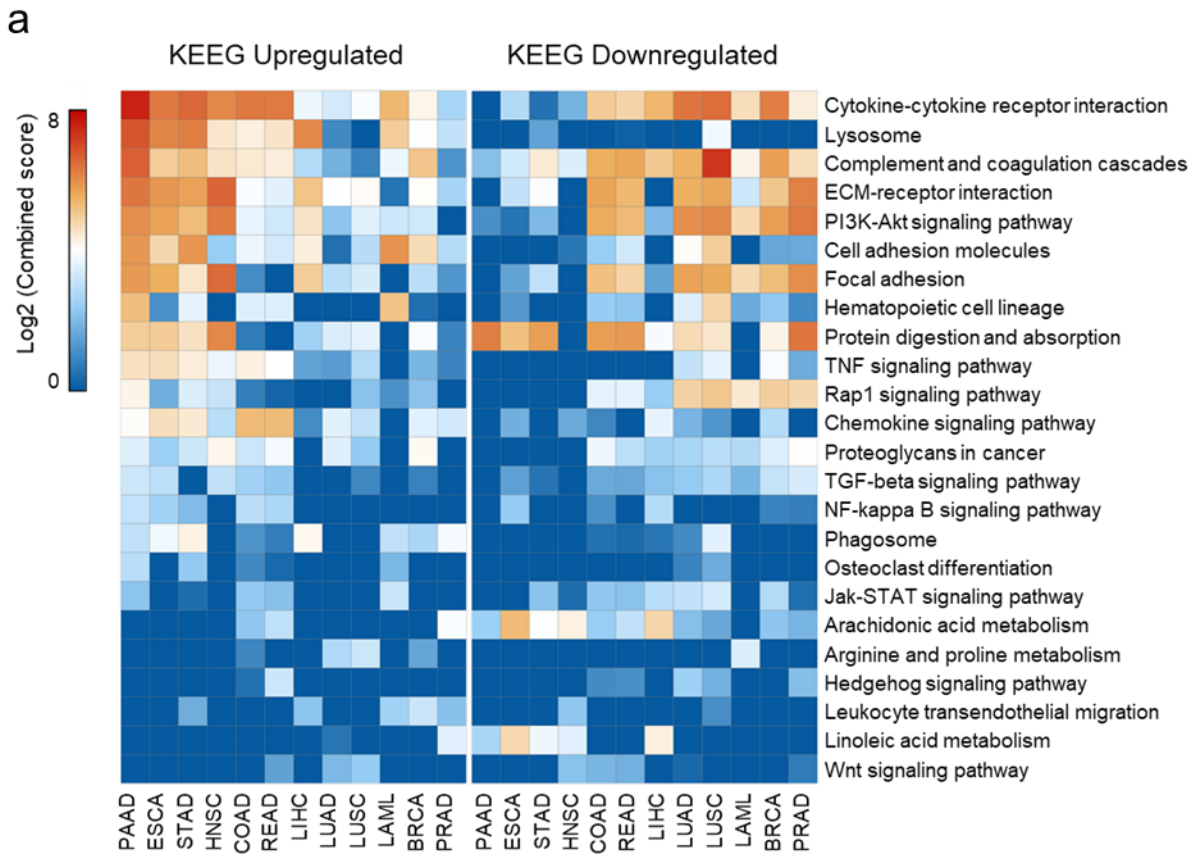

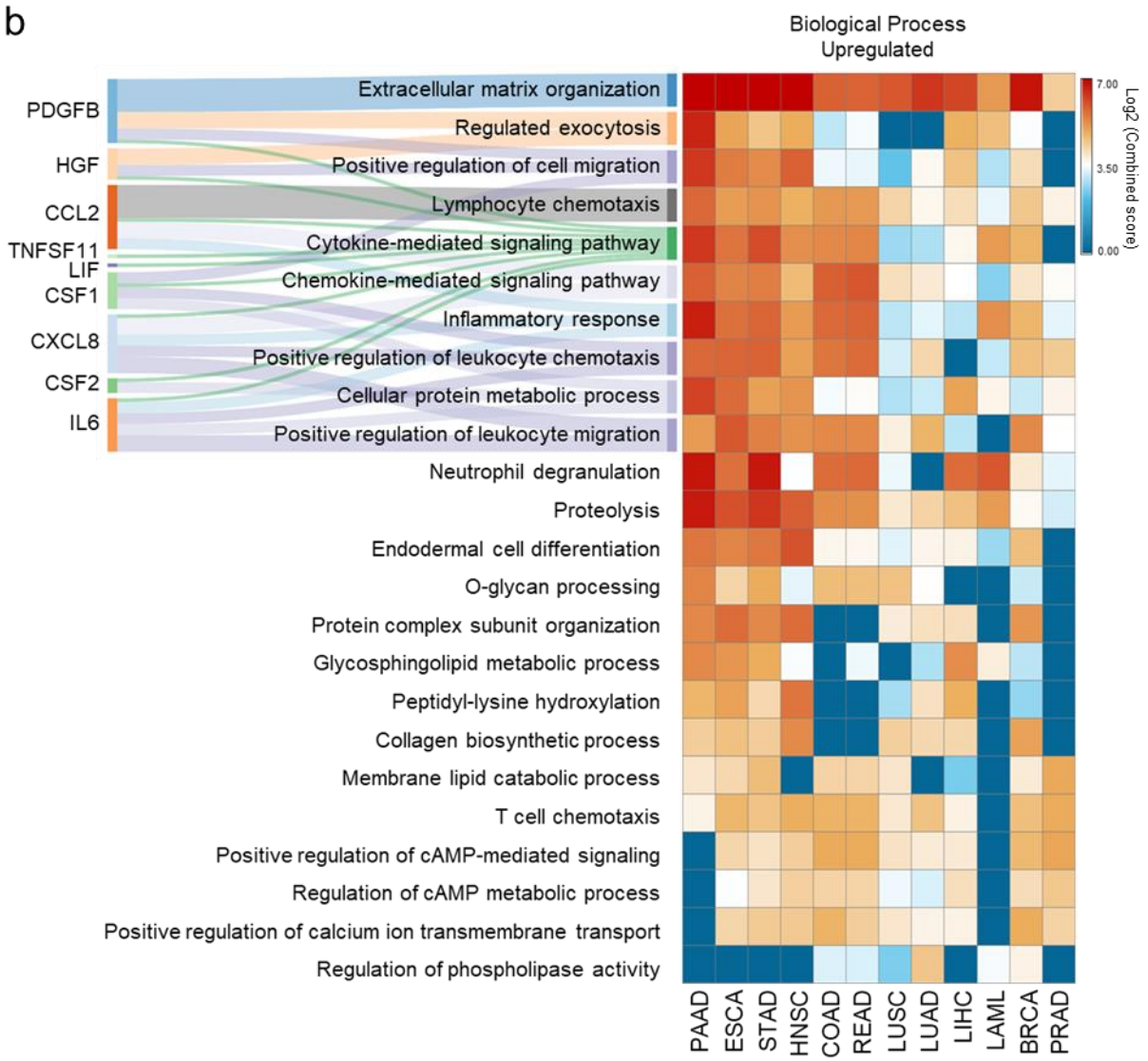

Fig. 2 Enriched pathways of the differentially expressed secretome genes. a) Top-ranked combined scores for The Kyoto Encyclopedia of Genes and Genomes (KEGG) pathways categories associated with upregulated (right panel) and downregulated (left panel) genes in tumor tissues vs. corresponding matched normal TCGA and GTEx tissues, computed by the gene set enrichment analysis tool EnrichR[36,37]. Pathways were included in the analysis when satisfying the criteria of over-representation (Log2 combined score > 2) in, at least, one tumor type (color intensity codes for combined score). Rows and columns were clustered based on Euclidean distance between Log2 combined score values. b) Right: Top-ranked combined scores for Gene Ontology (GO) categories associated with upregulated genes in tumor tissues vs. corresponding matched normal TCGA and GTEx tissues, computed by the gene set enrichment analysis tool EnrichR[36,37]. Left: Alluvial Diagram connecting the cachexia-inducing factors (CIF) predicted into those biological processes terms. PAAD: Pancreatic adenocarcinoma; ESCA: Esophageal carcinoma; STAD: Stomach adenocarcinoma; HNSC: Head and neck squamous cell carcinoma; LUAD: Lung adenocarcinoma; LUSC: Lung squamous cell carcinoma; LIHC: Liver hepatocellular carcinoma; COAD: Colon adenocarcinoma;

READ: Rectum adenocarcinoma; LAML: Acute myeloid leukemia; PRAD: Prostate adenocarcinoma; BRCA: Breast invasive carcinoma.

Tumor-specific expression profile of CIF is correlated with the prevalence of cachexia and weight loss

Considering that cytokine and chemokine pathways - enriched in tumors associated with cachexia - include known CIF (PDGFB, HGF, CCL2, TNFSF11, LIF, CSF1, CXCL8, CSF2, and IL6) (Fig. 2b), we further filtered the transcriptome data to 25 cytokines and growth factors. This same set of cachexia-inducing factors was previously used for protein blood screening in pancreatic cachectic patients[16]. The list of 25 factors is described in Supplementary Table 1.

We found that each tumor type shows a specific gene expression profile of CIF (Fig. 3a, Supplementary Fig. 4). PAAD presented the highest number (14) of upregulated CIF (*CXCL8*, *IL1B*, *HGF*, *TNFSF10*, *LIF*, *TGFA*, *TNFSF11*, *PDGFB*, *IL6*, *CCL2*, *CSF1*, *IL15*, *CSF2*, and *FGF2*), while PRAD showed no significant upregulated CIF. Other tumor types also presented upregulated pro-cachectic factors, such as breast invasive carcinoma (*IL1B* and *MMP13)*, LIHC (*PDGFB*), ESCA (*CXCL8*, *IL1B*, *LIF*, *PDGFB*, *IL6*, *CSF3*, and *MMP3*), HNSC (*CXCL8*, *IL1B*, *TNFSF10*, *PDGFB*, *CSF2*, *VEGFA*, and *MMP3*), and STAD (*CXCL8*, *TNFSF10*, *LIF*, *TGFAC*, and *TNFSF11*). LUSC and LUAD shared six downregulated CIF (*PDGFB*, *IL6*, *HGF*, *FGF2*, *CSF3*, and *CXCL12*), whereas only *TGFA* and *MMP13* were upregulated in both lung tumors. Although *IL1B, CXCL8* (also known as *IL8*), *TGFA*, and *LIF* were upregulated in at least five tumor types, five molecules (*IL10, CD40LG, IFNA1*, *IL4*, and *IL17A*) showed no alterations (Fig. 3a). Additionally, classic cachectic mediators were overexpressed, including *IL6* in PAAD and ESCA, and *TNF* in LAML. The transcripts abundance for these 25 CIF in the 12 tumor types revealed that *VEGFA*, *CCL2*, and *CXCL8* are expressed at high levels in many tumor tissues, while *IL4*, *IL17A*, and *CSF2* are expressed at low levels (Supplementary Fig. 5). Our data revealed potential cachexia biomarkers and mediators that are produced at high levels by the tumor tissues.

Using previously published data[8,11,12], we next investigated the total number of upregulated CIF for each tumor type and their correlation with the prevalence of cachexia and the percentage of weight loss. This dataset included the pancreatic, esophageal/gastric, head and neck, colorectal, lung, hematological, breast, and prostate cancers. These data have the potential to provide relevant correspondence in different cachexia studies, although they do not represent the full variation of cachexia for all the 12 cancer types. Remarkably, the number of upregulated CIF genes in tumor compared to normal tissues was strongly correlated with the prevalence of cachexia and weight loss (average percentage) in the majority of the tumor types available for this analysis (Fig. 3b). The only exception was lung cancers, but these results are also in accordance with the gene expression profiles that were detected for LUSC and LUAD, which are distinct from tumors more prominently associated with cachexia. These findings showed specific cachectic tumor-signatures with the potential to explain why specific cancer types are more likely to develop cachexia.

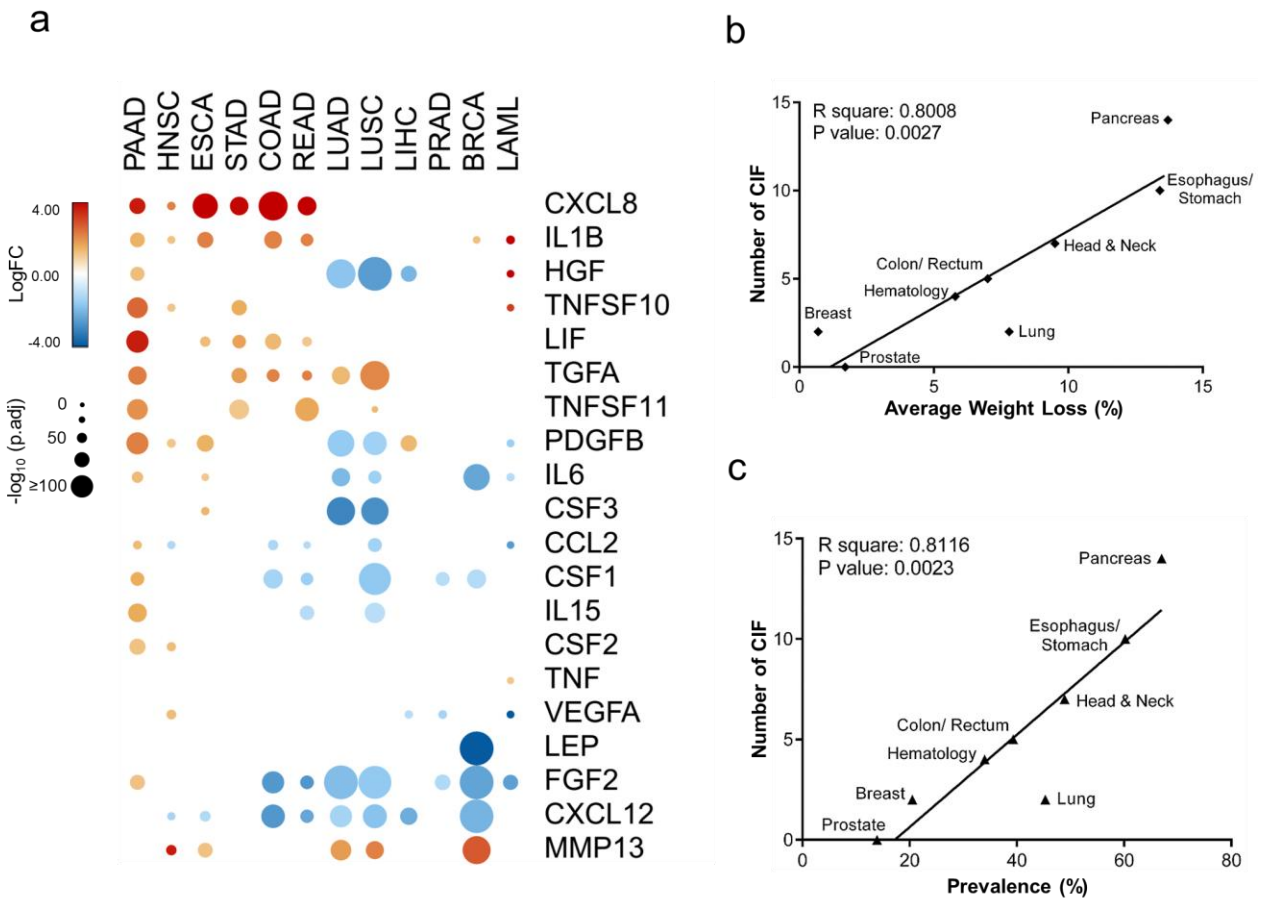

Fig. 3 Cachexia-inducing factors tumor-specific expression profiles strongly correlate with the prevalence of cachexia and weight loss in different tumor types. a) Schematic representation of the expression pattern of 25 cachexia-inducing factors (CIF) in different TCGA tumor types. Differential expression levels were calculated using the web-based tool Gene Expression Profiling Analysis (GEPIA, http://gepia.cancerpku.cn/)[32] from tumor tissues vs. matched normal TCGA and GTEx data. Upregulated and downregulated genes with

absolute values of fold-change > 2.0 and q-value < 0.01 (ANOVA) are shown in red and blue, respectively. Five molecules (*IL10, CD40LG, IFNA1, IL4,* and *IL17A*) showed no alteration and are not represented in the heatmap. b-c) Pearson's correlations coefficient (r) with corresponding p-values for the covariation between the number of differentially expressed CIF (y-axis) from TCGA datasets (tumor tissues vs. matched normal TCGA and GTEx data) and the percentage of weight loss (x-axis; b) or the percentage of cachexia prevalence (x-axis; c) for specific tumor types from relevant literature data[8,11,12]. Weight loss and prevalence of cachexia are strongly correlated with the number of CIF ($p < 0.01$). PAAD: Pancreatic adenocarcinoma; ESCA: Esophageal carcinoma; STAD: Stomach adenocarcinoma; HNSC: Head and neck squamous cell carcinoma; LUAD: Lung adenocarcinoma; LUSC: Lung squamous cell carcinoma; LIHC: Liver hepatocellular carcinoma; COAD: Colon adenocarcinoma; READ: Rectum adenocarcinoma; LAML: Acute myeloid leukemia; PRAD: Prostate adenocarcinoma; BRCA: Breast invasive carcinoma.

Expression profile of CIF is associated with tumor purity

Tumor microenvironment contains non-cancerous cells, including a diversity of immune cells that potentially contribute to the secretion of CIF. We then investigated the expression profile of these 25 CIF according to tumor purity (neoplastic cellularity and leukocyte fraction) in PAAD. This tumor type - known to present the highest prevalence of cachexia[12] and low tumor purity[38] - showed the highest number of upregulated secretome genes (Fig. 3a). We used previously published tumor purity data for PAAD[38], which is constituted by 74 "low-purity" samples (ABSOLUTE purity < 33%) and 76 "high-purity" samples (ABSOLUTE purity ≥ 33%). Using hierarchical clustering analysis, we observed that the expression profile of these 25 CIF discriminates high- and low-purity tumors, and most of these genes are overexpressed in low-purity tumors (Fig. 4). The overexpression of CIF in low-purity tumors was further associated with high leukocytes DNA methylation and low tumor cells DNA hypermethylation mode purity (Fig. 4). This data shows that leukocytes infiltration correlates with high expression of CIF in PAAD. Interestingly, no association was observed between the expression levels of cachexia-inducing factors and tumor grade (Fig. 4).

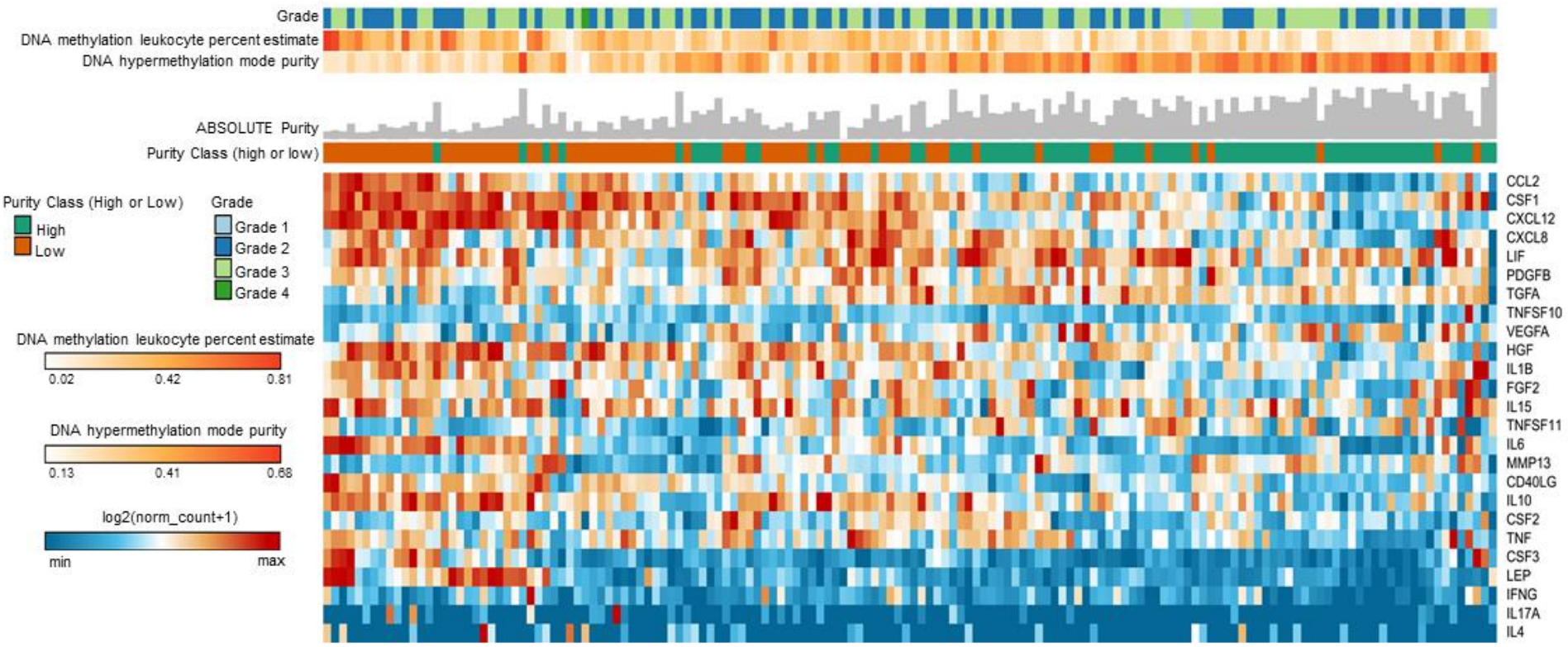

Fig. 4 Landscape of cachexia-inducing factors is associated with low tumor purity. Unsupervised hierarchical clustering of cachexia-inducing factors (CIF) is presented in a heatmap according to gene expression (Log2 norm_count+1). The integrated epigenomic data for PAAD samples, including DNA hypermethylation mode purity and DNA methylation leukocyte percent, are shown as tracks at the top together with the tumor grade. The absolute tumor purity data for each sample are shown as grey bars at the top. The percentage of patients classified as low or high purity **is** noted as orange and green tracks, respectively. Rows and columns were clustered based on Euclidean distance between Log2 norm_count+1 values.

The expression landscape of CIF predicts cancer outcome

Circulating levels of CIF such as IL6, CXCL8, IL1B, MCP-1 were previously correlated with cachexia development and poor prognosis in cancer[16–18,42–45]. Based on this evidence, we compared the tumor expression levels of CIF with patient prognosis using the platform SurvExpress[40]. Supplementary Table 12 summarizes the TCGA datasets used in our analysis. SurvExpress generated a prognostic index (risk score) based on the gene expression of 25 CIF and the survival of cancer patients for each of the 12 tumor types. Patients were divided into two groups, high- and low-risk, maximizing the number of patients into risk-groups by an optimization algorithm from the ordered prognostic index (Supplementary Table 12). More than 50% of CIF genes are overexpressed ($p < 0.05$) in high-risk groups in HNSC, READ, COAD, LIHC, and BRCA (Fig. 5a). This analysis also demonstrated the consistent overexpression of *IL4*, *INF-γ*, and *IL6* in at least eight different tumor types (Fig. 5a). The heatmap generated by clustering analysis differentiating patients into high- and low-risk demonstrated the enrichment of specific CIF in patients with low survival (high-risk group) in HNSC, LIHC, and BRCA (Fig. 5b). Examples of the CIF clustered in the heatmap and overexpressed in patients with low survival include: *LIF*, *IL6*, and *CSF3* (in HNSC); *TGFA, LIF, HGF, CXCL8,* and *FGF2* (in LIHC); and *LEP, FGF2, LIF, TGFA* (in BRCA) (Fig. 5b). It is also interesting that in PRAD, which is the less prone to developing cachexia, only *TGFA, IL15,* and *IL4* presented higher expression in patients with low survival, while *IL6, CSF3, LIF* clustered in the heatmap and were expressed at low levels in patients with high survival (Fig. 5b). The heatmaps for other tumor types are presented in Supplementary Fig. 6, and the relative expression levels of the 25 CIF in low- and high-risk groups of patients are shown in Supplementary Fig. 7. This variability in the expression profiles of CIF in patients with low and high survival may help to explain the heterogeneity in the clinical manifestation of cachexia in patients with different tumor types.

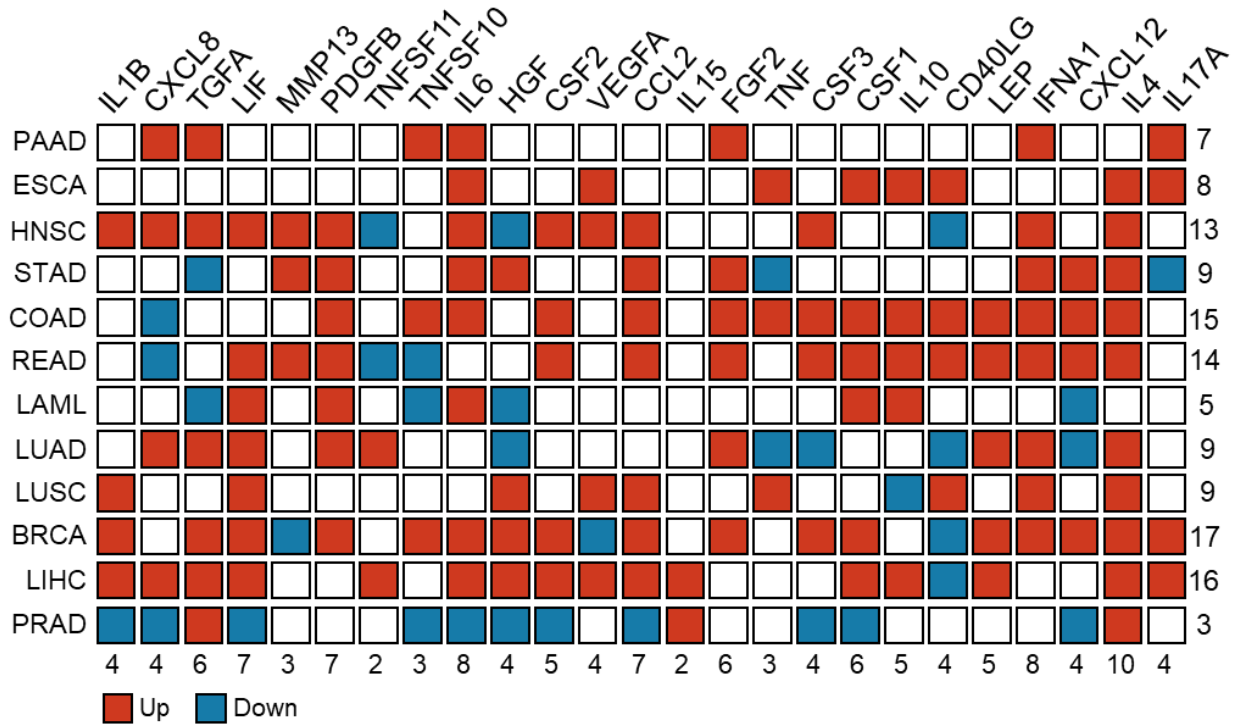

Fig. 5 High-risk groups are correlated with high expression of cachexia-inducing factors in tumor tissues. Schematic representation summarizing the expression pattern of 25 cachexia-inducing factors (CIF) in 12 TCGA tumor types. Differential expression levels were calculated in the web-based tool SurvExpress[40] by maximizing two risk groups (high-risk and low-risk) by prognostic index median and Cox fitting. The statistical difference for each mRNA expression between high- and low-risk groups was tested using the *t*-test. Upregulated and downregulated genes (high-risk vs. low-risk) with p-value < 0.05 are shown in red and blue, respectively. PAAD: Pancreatic adenocarcinoma; ESCA: Esophageal carcinoma; STAD: Stomach adenocarcinoma; HNSC: Head and neck squamous cell carcinoma; LUAD: Lung adenocarcinoma; LUSC: Lung squamous cell carcinoma; LIHC: Liver hepatocellular carcinoma; COAD: Colon adenocarcinoma; READ: Rectum adenocarcinoma; LAML: Acute myeloid leukemia; PRAD: Prostate adenocarcinoma; BRCA: Breast invasive carcinoma.

Finally, to evaluate whether the CIF genes have prognostic and predictive value in different cancer types, we used 12 TCGA datasets within SurvExpress to analyze the overall survival. Altered expression of CIF is associated with worse overall survival (Fig. 6 and Supplementary Table 12). The robustness of these 25 genes in stratifying with high confidence patients into two risk groups was consistently demonstrated by high hazard ratios in the 12 TCGA cohorts (Fig. 6). Using this list of 25 factors, we also detected differentially expressed genes that have higher relevance in predicting worse survival (Supplementary Table 13). Thus, these findings suggest that CIF genes are predictors of cancer survival outcomes.

Fig. 6 The expression landscape of cachexia-inducing factors predicts cancer outcome. Survival analysis based on the tumor mRNA expression of 25 cachexia-inducing factors (CIF). The data were calculated using the TCGA datasets of 12 tumor types in the web-based tool SurvExpress[40], which stratified the cancer patients in high- or low-risk groups (red and green, respectively). The adjusted hazard ratio (HR) with corresponding 95% confidence intervals, log-rank p-value (P), and the number of patients successfully stratified (N) determined by univariate Cox regression analyses are shown on each survival Kaplan–Meier curve. PAAD: Pancreatic adenocarcinoma; ESCA: Esophageal carcinoma; STAD: Stomach adenocarcinoma; HNSC: Head and neck squamous cell carcinoma; LUAD: Lung adenocarcinoma; LUSC: Lung squamous cell carcinoma; LIHC: Liver hepatocellular carcinoma; COAD: Colon adenocarcinoma; READ: Rectum adenocarcinoma; LAML: Acute myeloid leukemia; PRAD: Prostate adenocarcinoma; BRCA: Breast invasive carcinoma.

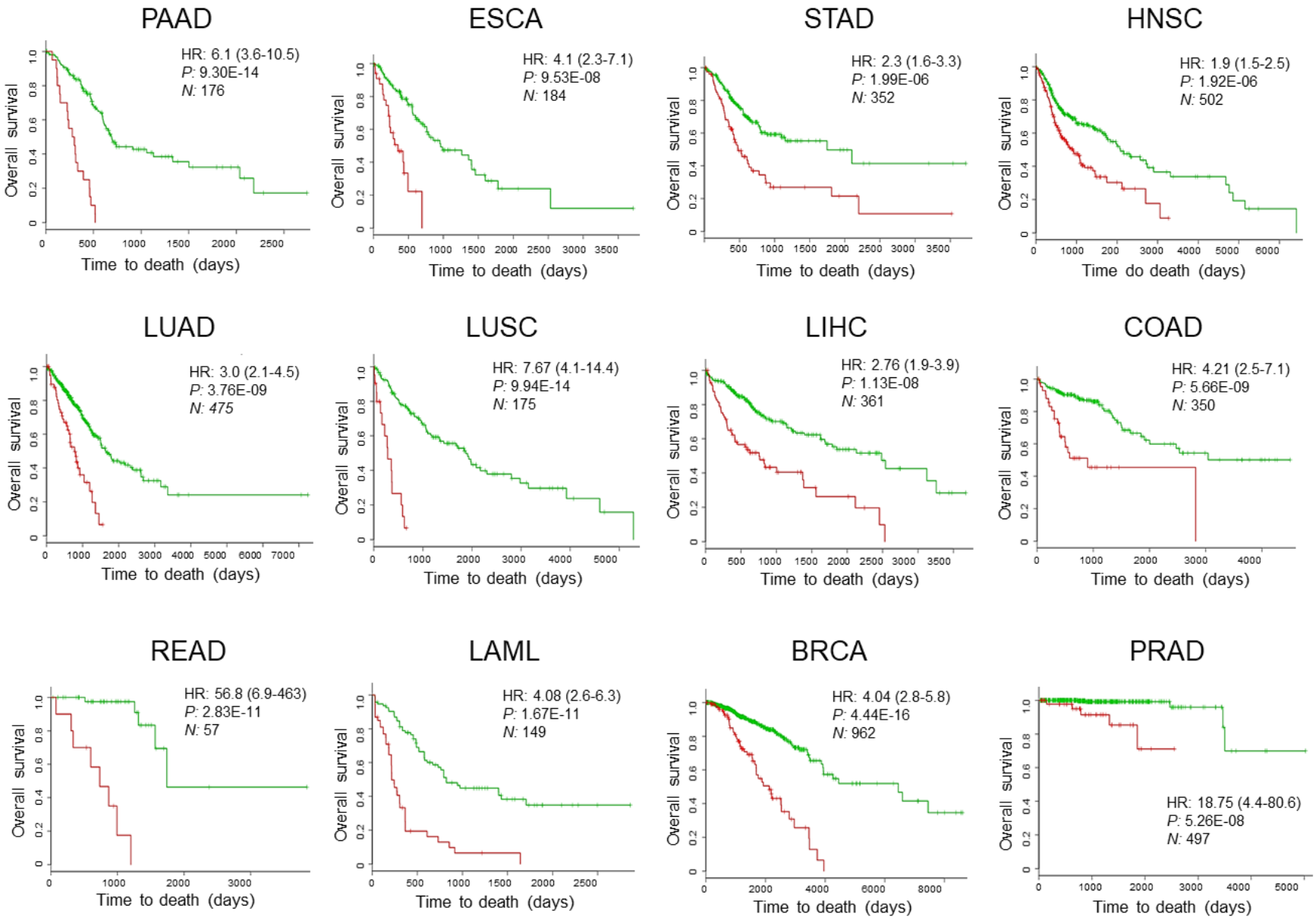
PAAD
HR: 6.1 (3.6-10.5)
P: 9.30E-14
N: 176
Overall survival
Time to death (days)
ESCA
HR: 4.1 (2.3-7.1)
P: 9.53E-08
N: 184
Overall survival
Time to death (days)
STAD
HR: 2.3 (1.6-3.3)
P: 1.99E-06
N: 352
Overall survival
Time to death (days)
HNSC
HR: 1.9 (1.5-2.5)
P: 1.92E-06
N: 502
Overall survival
Time do death (days)
LUAD
HR: 3.0 (2.1-4.5)
P: 3.76E-09
N: 475
Overall survival
Time to death (days)
LUSC
HR: 7.67 (4.1-14.4)
P: 9.94E-14
N: 175
Overall survival
Time to death (days)
LIHC
HR: 2.76 (1.9-3.9)
P: 1.13E-08
N: 361
Overall survival
Time to death (days)
COAD
HR: 4.21 (2.5-7.1)
P: 5.66E-09
N: 350
Overall survival
Time to death (days)
READ
HR: 56.8 (6.9-463)
P: 2.83E-11
N: 57
Overall survival
Time to death (days)
LAML
HR: 4.08 (2.6-6.3)
P: 1.67E-11
N: 149
Overall survival
Time to death (days)
BRCA
HR: 4.04 (2.8-5.8)
P: 4.44E-16
N: 962
Overall survival
Time to death (days)
PRAD
HR: 18.75 (4.4-80.6)
P: 5.26E-08
N: 497
Overall survival
Time to death (days)

Discussion

Cachexia prevalence and severity vary depending on tumor types. Pancreatic, esophageal, gastric, lung, and liver cancers have the highest prevalence, while breast or prostate cancers are not commonly associated with the syndrome[12]. The causes of such variations are still mostly unknown, and it is possible that each cancer type present tumor-specific biomarkers and mediators. We sought to characterize the molecular landscape of CIF in human cancers with different prevalence of cachexia, using the RNA-Seq dataset from TCGA and GTEx. Our results revealed tumor-specific secretome transcriptional patterns, potential mediators, and pathways associated with the syndrome. We also showed that a set of 25 CIF presented a tumor-specific expression profile, which was significantly associated with poor prognosis and correlated with the prevalence of cachexia and weight loss in cancer patients. In PAAD, these upregulated pro-cachectic factors were also associated with tumors that present low neoplastic cellularity and high leukocyte fraction. These correlations are plausible explanations of the variation found in the prevalence and severity of cachexia in human cancers and showed that specific therapeutic strategies, according to tumor types, must be considered to treat these patients.

Our comprehensive characterization of the secretome based on transcriptome revealed that the number of upregulated secreted protein-coding genes, compared to normal tissue, correlates with cachexia prevalence. PAAD presented the highest number of upregulated secretome genes (1,267) across all tumor types. This result is particularly expected for the pancreatic tissues, which presents more than 70% of the transcripts encoding secreted proteins in the normal tissues[27]. However, a substantial fraction of upregulated secretome genes in PAAD is also significantly increased in tumor types commonly associated with cachexia, such as STAD (515 genes), COAD (308 genes), READ (308 genes), ESCA (368 genes), and HNSC (305 genes) (Supplementary Fig. 1). The majority of these shared secretome genes include proteins associated with a cytokine-mediated signaling pathway, inflammatory response, cytokine-cytokine receptor interaction, and positive regulation of leukocyte chemotaxis. Several of these secreted proteins were previously investigated as potential blood biomarkers of cachexia in cancer patients[16–21]. For example, we found high expression levels of *CXCL8* in six tumor types with a high prevalence of cachexia (PAAD, STAD, COAD, READ, ESCA, and HNSC). This cytokine has been reported as an independent predictor of survival in pancreatic and colorectal cancer patients[42,46]. CXCL8 has also been positively associated with weight loss in pancreatic and gastric cancers[42,47,48]. Interestingly, *TNF* expression levels, a cytokine commonly associated with cancer cachexia[18], were not changed in cancer types with a high prevalence of the

syndrome. This result is similar to that found in resectable pancreatic cancer patients, in which cachexia was not associated with increased plasma levels of canonical pro-inflammatory cytokines[16].

Subsequently, we focused on the tumor expression profile of 25 potential CIF in 12 human cancers with different risks to develop cachexia. These factors have been previously investigated in pancreatic cancer cachexia[16]; however, the synergistic expression profile of these molecules in different tumor types needed to be clarified. Cancer literature data describing cachexia prevalence and weight loss[8,11] were associated with the number of these upregulated CIF. We found that CIF present a tumor-specific expression profile. Also, the number of CIF genes upregulated in the tumor is strongly associated with average weight loss and prevalence of cachexia. This is particularly clear in patients with pancreatic cancer, as they have a body weight loss of approximately 13.7 kg[11], which was correlated with the upregulation of 14 CIF (*CXCL8*, *IL1B*, *HGF*, *TNFSF10*, *LIF*, *TGFA*, *TNFSF11*, *PDGFB*, *IL6*, *CCL2*, *CSF1*, *IL15*, *CSF2*, and *FGF2*) that we found in PAAD. By contrast, prostate cancer patients have a body weight loss of around 1.7 kg[11], and PRAD does not upregulate CIF genes when compared to normal tissues. These findings suggest a simple explanation for the discrepancy in average weight loss and cachexia prevalence across cancer patients.

The prognostic value of the expression of these 25 selected pro-cachectic factors revealed an association with shorter overall survival for the predicted high-risk groups in the 12 cancer types. The molecular landscape of these CIF in each cancer type presented a distinct expression profile between high- and low-risk patients. Our TCGA data reanalysis showed that patients with shorter survival presented upregulation of a large number of CIF. A previous study showed that IL-6 increases gradually during the early stages of cachexia but then shows a sudden and steep rise just before death[49]. Thus, it is possible that other CIF present a temporal pattern of regulation that influences the course and severity of the syndrome.

Currently, the source of these cytokines into the tumor microenvironment (from tumor cells or from infiltrating immune cells) is unexplored. PAAD, the cancer type with the highest prevalence of cachexia, often demonstrates only 5–20% neoplastic cellularity (low purity tumors) and high leukocyte infiltration [38,50]. Thus, we hypothesized that the set of upregulated CIF in PAAD is associated with low-purity tumors. Our clustering analysis showed that CIF are highly expressed in low-purity tumors. Infiltrating immune cells have been associated with tumor growth, invasion, and metastasis in several cancer types [51]. However, this is the first study indicating the potential influence of infiltrating immune cells in a tumor type highly associated with cachexia. Further investigation of the source of these molecules will contribute to our understanding of cachexia and will allow us to probe specific and accurate therapeutic strategies for the syndrome.

Most studies focusing on in silico-based methods suffer from limitations. Tumor gene expression profiling of CIF for each tumor type presented herein should be experimentally validated in a larger cohort of cancer patients to circumvent these limitations. Furthermore, we were not able to validate the diagnostic of cachexia due to the absence of clinical data in several patients from the 12 TCGA tumor types. Thus, it remains to be tested whether tumor expression levels of CIF genes can stratify patients according to the cachectic status in these tumor types. However, it is challenging to obtain an independent cohort of individuals as used in our study, which is consisted not only by a high number of tumor samples but also by several non-diseased tissues (from TCGA and GTEx). Our strategy collectively analyzed TCGA and GTEx expression profiles adding higher precision, sensitivity, and robustness to our transcriptomic analysis. Further single-cell RNA-Seq investigation is an alternative to differentiate the specific contributions of different cell types in the tumor microenvironment to the tumor expression profile of cachectic patients. Despite such limitations, we used a systematic investigation to verify the expression of CIF genes in cancer cells using a large number of human samples and tumor types, allowing the identification of new potential biomarkers and mediators of cachexia. Overall, we provided insights that opening new perspectives in cancer cachexia scenario.

In conclusion, the synergic expression of the CIF in several tumor types highlights the importance of this group of soluble factors in cancer pathophysiology and presents a strong case for their targeting in specific anti-cachexia therapeutic development in different tumor contexts. Also, the tumor-specific profile of CIF will facilitate the development of better-targeted therapies for clinical decisions.

Acknowledgments

This study was supported by the São Paulo Research Foundation – FAPESP (grants #12/13961-6, #13/50343-1, #14/13941-0, and #18/19695-2). The results shown here are in whole based upon data generated by the TCGA Research Network (http://cancergenome.nih.gov/), and by the Genotype-Tissue Expression project (GTEx) (https://gtexportal.org/). The authors of this manuscript certify that they comply with the ethical guidelines for authorship and publishing in the Journal of Cachexia, Sarcopenia, and Muscle[52].

Conflict of interests

The authors Paula Paccielli Freire, Geysson Javier Fernandez, Diogo de Moraes, Sarah Santiloni Cury, Maeli Dal-Pai-Silva, Patricia Pintor dos Reis, Silvia Regina Rogatto, and Robson Francisco Carvalho declare that they have no conflict of interest.

References

1. Vaughan, V. C., Martin, P. & Lewandowski, P. A. Cancer cachexia: Impact, mechanisms and emerging treatments. *J. Cachexia. Sarcopenia Muscle* **4,** 95–109 (2013).

2. von Haehling, S., Anker, M. S. & Anker, S. D. Prevalence and clinical impact of cachexia in chronic illness in Europe, USA, and Japan: facts and numbers update 2016. *J. Cachexia. Sarcopenia Muscle* **7,** 507–509 (2016).

3. Dewys, W. D. *et al.* Prognostic effect of weight loss prior to chemotherapy in cancer patients. Eastern Cooperative Oncology Group. *Am. J. Med.* **69,** 491–7 (1980).

4. Martin, L. *et al.* Cancer cachexia in the age of obesity: Skeletal muscle depletion is a powerful prognostic factor, independent of body mass index. *J. Clin. Oncol.* **31,** 1539–1547 (2013).

5. Fearon, K., Arends, J. & Baracos, V. Understanding the mechanisms and treatment options in cancer cachexia. *Nat. Rev. Clin. Oncol.* **10,** 90–9 (2013).

6. Fearon, K. C. H., Glass, D. J. & Guttridge, D. C. Cancer cachexia: mediators, signaling, and metabolic pathways. *Cell Metab.* **16,** 153–66 (2012).

7. Harimoto, N. *et al.* Sarcopenia as a predictor of prognosis in patients following hepatectomy for hepatocellular carcinoma. *Br. J. Surg.* **100,** 1523–1530 (2013).

8. Pressoir, M. *et al.* Prevalence, risk factors and clinical implications of malnutrition in french comprehensive cancer centres. *Br. J. Cancer* **102,** 966–971 (2010).

9. Bozzetti, F. Screening the nutritional status in oncology: A preliminary report on 1,000 outpatients. *Support. Care Cancer* **17,** 279–284 (2009).

10. Segura, A. *et al.* An epidemiological evaluation of the prevalence of malnutrition in Spanish patients with locally advanced or metastatic cancer. *Clin. Nutr.* **24,** 801–814 (2005).

11. Hébuterne, X. *et al.* Prevalence of malnutrition and current use of nutrition support in patients with cancer. *J. Parenter. Enter. Nutr.* **38,** 196–204 (2014).

12. Baracos, V. E., Martin, L., Korc, M., Guttridge, D. C. & Fearon, K. C. H. Cancer-associated cachexia. *Nat. Rev. Dis. Prim.* **4,** 17105 (2018).

13. Tsoli, M. & Robertson, G. Cancer cachexia: malignant inflammation, tumorkines, and metabolic mayhem. *Trends Endocrinol. Metab.* **24,** 174–83 (2013).

14. Twelkmeyer, B., Tardif, N. & Rooyackers, O. Omics and cachexia. *Curr. Opin. Clin. Nutr. Metab. Care* **20,** 181–185 (2017).

15. Argilés, J. M., Stemmler, B., López-Soriano, F. J. & Busquets, S. Inter-tissue communication in cancer cachexia. *Nat. Rev. Endocrinol.* **15,** 9–20 (2018).

16. Talbert, E. E. *et al.* Circulating monocyte chemoattractant protein-1 (MCP-1) is associated with cachexia in treatment-naïve pancreatic cancer patients. *J. Cachexia. Sarcopenia Muscle* **9,** 358–368 (2018).

17. Penafuerte, C. A. *et al.* Identification of neutrophil-derived proteases and angiotensin II as biomarkers of cancer cachexia. *Br. J. Cancer* **114,** 680–687 (2016).

18. Lerner, L. *et al.* Plasma growth differentiation factor 15 is associated with weight loss and mortality in cancer patients. *J. Cachexia. Sarcopenia Muscle* **6,** 317–24 (2015).

19. Lerner, L. *et al.* MAP3K11/GDF15 axis is a critical driver of cancer cachexia. *J. Cachexia. Sarcopenia Muscle* **7,** 467–482 (2016).

20. Fukawa, T. *et al.* Excessive fatty acid oxidation induces muscle atrophy in cancer cachexia. *Nat. Med.* **22,** 666–71 (2016).

21. McLean, J. B., Moylan, J. S., Horrell, E. M. W. & Andrade, F. H. Proteomic analysis of media from lung cancer cells reveals role of 14-3-3 proteins in cachexia. *Front. Physiol.* **6,** 1–8 (2015).

22. Mukherjee, P. & Mani, S. Methodologies to decipher the cell secretome. *Biochim. Biophys. Acta - Proteins Proteomics* **1834,** 2226–2232 (2013).

23. Welsh, J. B. *et al.* Large-scale delineation of secreted protein biomarkers overexpressed in cancer tissue and serum. *Proc. Natl. Acad. Sci. U. S. A.* **100,** 3410–5 (2003).

24. Wang, Z., Gerstein, M. & Snyder, M. RNA-Seq: a revolutionary tool for transcriptomics. *Nat. Rev. Genet.* **10,** 57–63 (2009).

25. Da Costa Martins, P. a & De Windt, L. J. MicroRNAs in control of cardiac hypertrophy. *Cardiovasc. Res.* **93,** 563–72 (2012).

26. Ozsolak, F. & Milos, P. M. RNA sequencing: advances, challenges and opportunities. *Nat. Publ. Gr.* **12,** 87–98 (2010).

27. Uhlén, M. *et al.* Proteomics. Tissue-based map of the human proteome. *Science* **347,** 1260419 (2015).

28. Robinson, J. L., Feizi, A., Uhlén, M. & Nielsen, J. A Systematic Investigation of the Malignant Functions and Diagnostic Potential of the Cancer Secretome. *Cell Rep.* **26,** 2622–2635.e5 (2019).

29. Weinstein, J. N. *et al.* The Cancer Genome Atlas Pan-Cancer analysis project. *Nat. Genet.* **45,** 1113–20 (2013).

30. Lonsdale, J. *et al.* The Genotype-Tissue Expression (GTEx) project. *Nat. Genet.* **45,** 580–585 (2013).

31. Vivian, J. *et al.* Toil enables reproducible, open source, big biomedical data analyses. *Nat. Biotechnol.* **35,** 314–316 (2017).

32. Tang, Z. *et al.* GEPIA: a web server for cancer and normal gene expression profiling and interactive analyses. *Nucleic Acids Res.* **45,** W98–W102 (2017).

33. Aran, D., Sirota, M. & Butte, A. J. Systematic pan-cancer analysis of tumour purity. *Nat. Commun.* **6,** 8971 (2015).

34. Aran, D. *et al.* Comprehensive analysis of normal adjacent to tumor transcriptomes. *Nat. Commun.* **8,** 1–13 (2017).

35. Krzywinski, M. *et al.* Circos: an information aesthetic for comparative genomics. *Genome Res.* **19,** 1639–45 (2009).

36. Kuleshov, M. V *et al.* Enrichr: a comprehensive gene set enrichment analysis web server 2016 update. *Nucleic Acids Res.* **44,** W90–7 (2016).

37. Chen, E. Y. *et al.* Enrichr: interactive and collaborative HTML5 gene list enrichment analysis tool.

BMC Bioinformatics **14,** 128 (2013).

38. Raphael, B. J. *et al.* Integrated Genomic Characterization of Pancreatic Ductal Adenocarcinoma. *Cancer Cell* **32,** 185–203.e13 (2017).

39. Starruß, J., de Back, W., Brusch, L. & Deutsch, A. Morpheus: a user-friendly modeling environment for multiscale and multicellular systems biology. *Bioinformatics* **30,** 1331–2 (2014).

40. Aguirre-Gamboa, R. *et al.* SurvExpress: an online biomarker validation tool and database for cancer gene expression data using survival analysis. *PLoS One* **8,** e74250 (2013).

41. Metsalu, T. & Vilo, J. ClustVis: A web tool for visualizing clustering of multivariate data using Principal Component Analysis and heatmap. *Nucleic Acids Res.* **43,** W566–W570 (2015).

42. Hou, Y.-C. *et al.* Elevated Serum Interleukin-8 Level Correlates with Cancer-Related Cachexia and Sarcopenia: An Indicator for Pancreatic Cancer Outcomes. *J. Clin. Med.* **7,** 502 (2018).

43. Kuroda, K. *et al.* Interleukin 6 Is Associated with Cachexia in Patients with Prostate Cancer. *Urology* **69,** 113–117 (2007).

44. Zhang, D., Song, B., Wang, S., Zheng, H. & Wang, X. Association of interleukin-8 with cachexia from patients with low-third gastric cancer. *Comp. Funct. Genomics* **2009,** 1–6 (2009).

45. Richey, L. M. *et al.* Defining cancer cachexia in head and neck squamous cell carcinoma. *Clin. Cancer Res.* **13,** 6561–6567 (2007).

46. Xia, W. *et al.* Prognostic Value, Clinicopathologic Features and Diagnostic Accuracy of Interleukin-8 in Colorectal Cancer: A Meta-Analysis. *PLoS One* **10,** e0123484 (2015).

47. Song, B., Zhang, D., Wang, S., Zheng, H. & Wang, X. Association of Interleukin-8 with Cachexia from Patients with Low-Third Gastric Cancer. *Comp. Funct. Genomics* **2009,** 1–6 (2009).

48. Bo, S. *et al.* Association of interleukin-8 gene polymorphism with cachexia from patients with gastric cancer. *J. Interferon Cytokine Res.* **30,** 9–14 (2010).

49. Iwase, S., Murakami, T., Saito, Y. & Nakagawa, K. Steep elevation of blood interleukin-6 (IL-6) associated only with late stages of cachexia in cancer patients. *Eur. Cytokine Netw.* **15,** 312–6 (2004).

50. Wood, L. D. & Hruban, R. H. Pathology and molecular genetics of pancreatic neoplasms. *Cancer J.* **18,** 492–501 (2012).

51. Schreiber, R. D., Old, L. J. & Smyth, M. J. Cancer immunoediting: integrating immunity's roles in cancer suppression and promotion. *Science* **331,** 1565–70 (2011).

52. von Haehling, S., Morley, J. E., Coats, A. J. S. & Anker, S. D. Ethical guidelines for publishing in the journal of cachexia, sarcopenia and muscle: update 2017. *J. Cachexia. Sarcopenia Muscle* **8,** 1081–1083 (2017).

Supplementary Material

Note: The supplementary tables are found at:

https://drive.google.com/open?id=1nTPbQRLjWd08qbqhz05Yu4ffo88IuuIt

Supplementary Figures

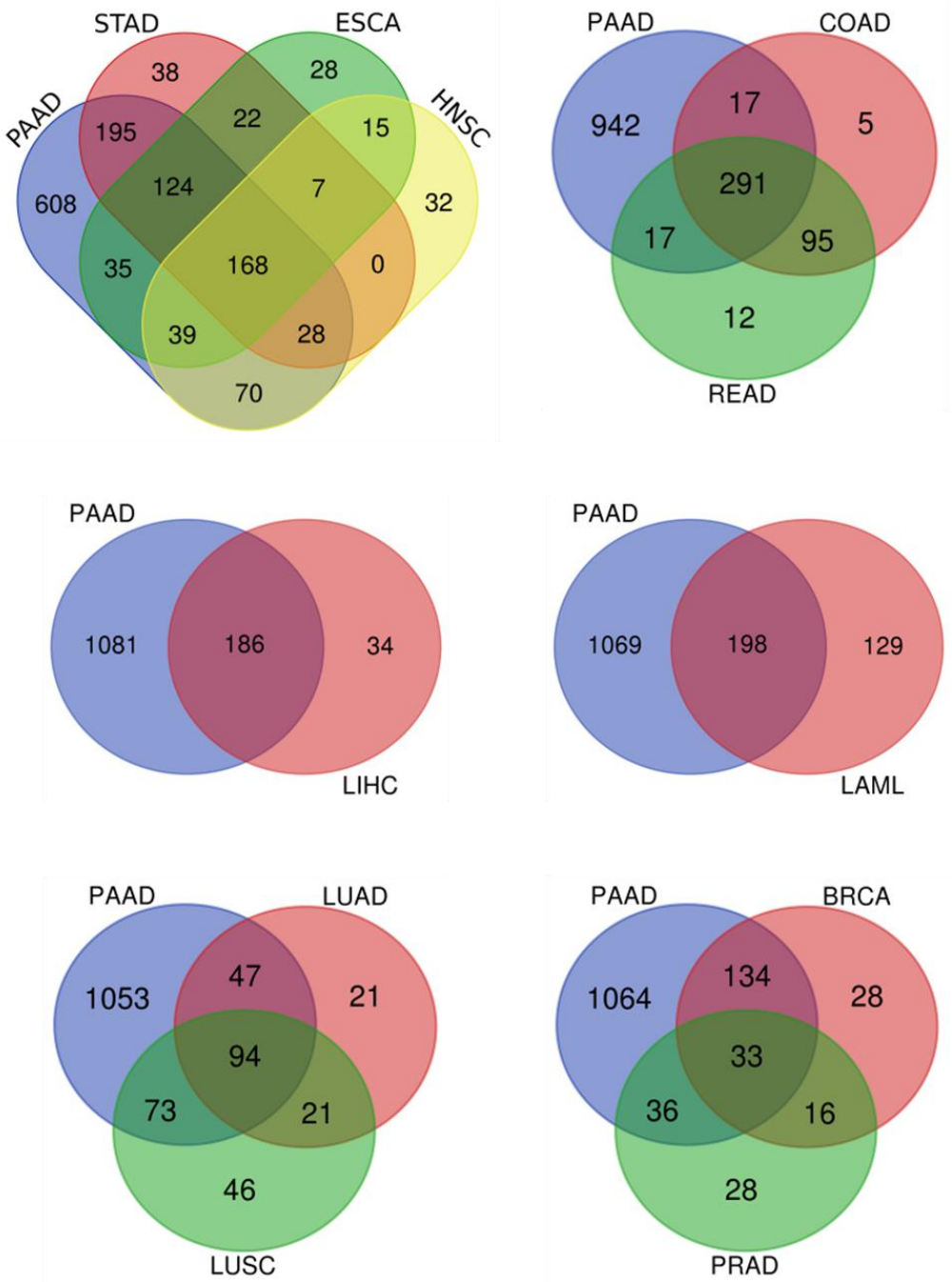

Supplementary Fig. 1 Upregulated genes shared among 12 tumor types. Venn diagrams showing shared upregulated secretome genes in 12 tumor types. Pancreatic adenocarcinomas (PAAD) presented the highest number of upregulated secretome genes and have the highest prevalence of cachexia[8,11,12]. Based on these data, PAAD was included in all comparisons. PAAD: Pancreatic adenocarcinoma; ESCA: Esophageal carcinoma; STAD: Stomach adenocarcinoma; HNSC: Head and neck squamous cell carcinoma; LUAD: Lung adenocarcinoma; LUSC: Lung squamous cell carcinoma; LIHC: Liver hepatocellular carcinoma; COAD: Colon adenocarcinoma; READ: Rectum adenocarcinoma; LAML: Acute myeloid leukemia; PRAD: Prostate adenocarcinoma; BRCA: Breast invasive carcinoma.

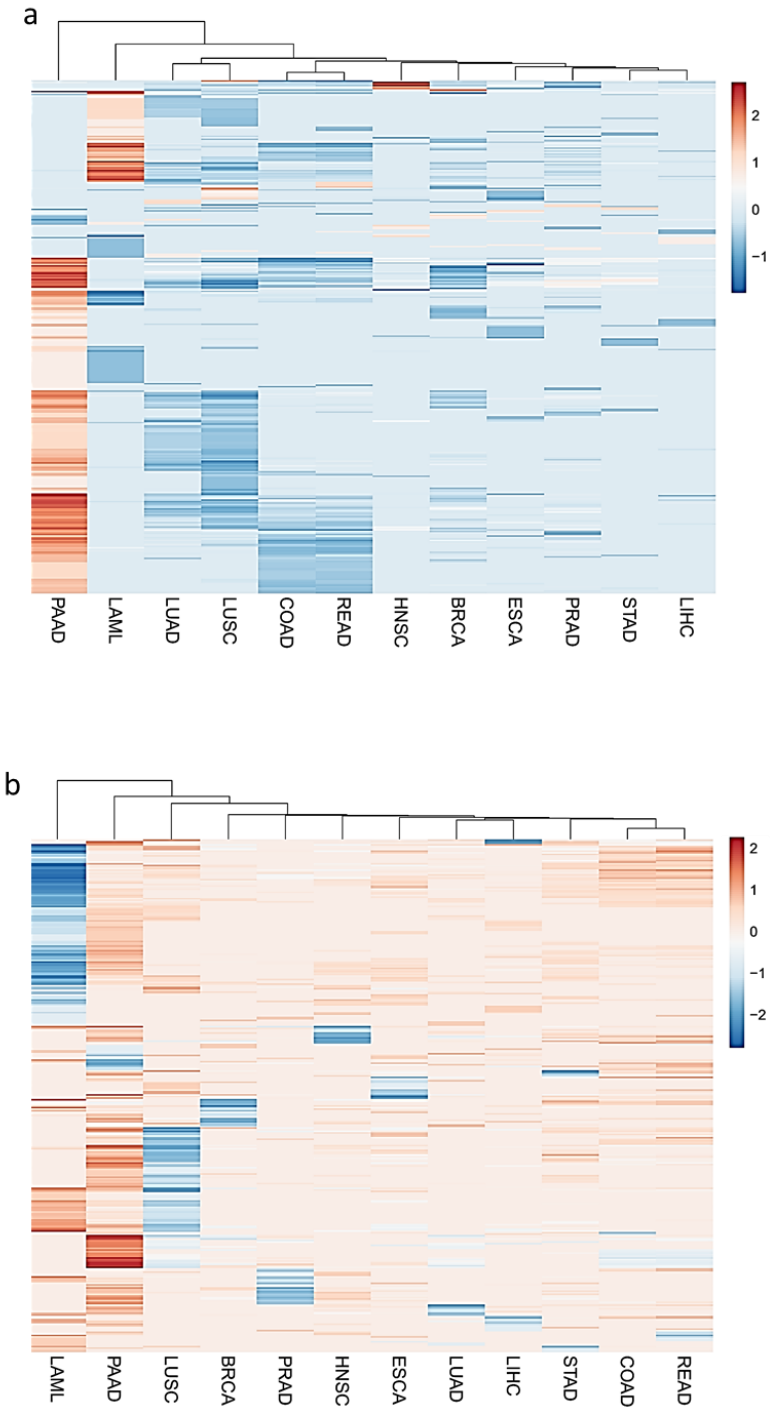

Supplementary Fig. 2 Exclusive upregulated genes within tumor types. Heatmap of the mean expression levels [log2 (TPM+1)] of specifically upregulated (a) or downregulated (b) secretome genes in each tumor type compared with corresponding matched normal TCGA and GTEx tissues. Differential expression levels were calculated using the web-based tool Gene Expression Profiling Analysis (GEPIA, http://gepia.cancerpku.cn/)32. The resulting numbers of genes encoding predicted secreted proteins were filtered based on the Human Protein Atlas secretome data27 (https://www.proteinatlas.org/humanproteome/secretome). Genes that are specifically upregulated or downregulated genes in one tumor type (absolute values of fold-change > 2.0 and q-value < 0.01; ANOVA) are shown in red and blue, respectively.

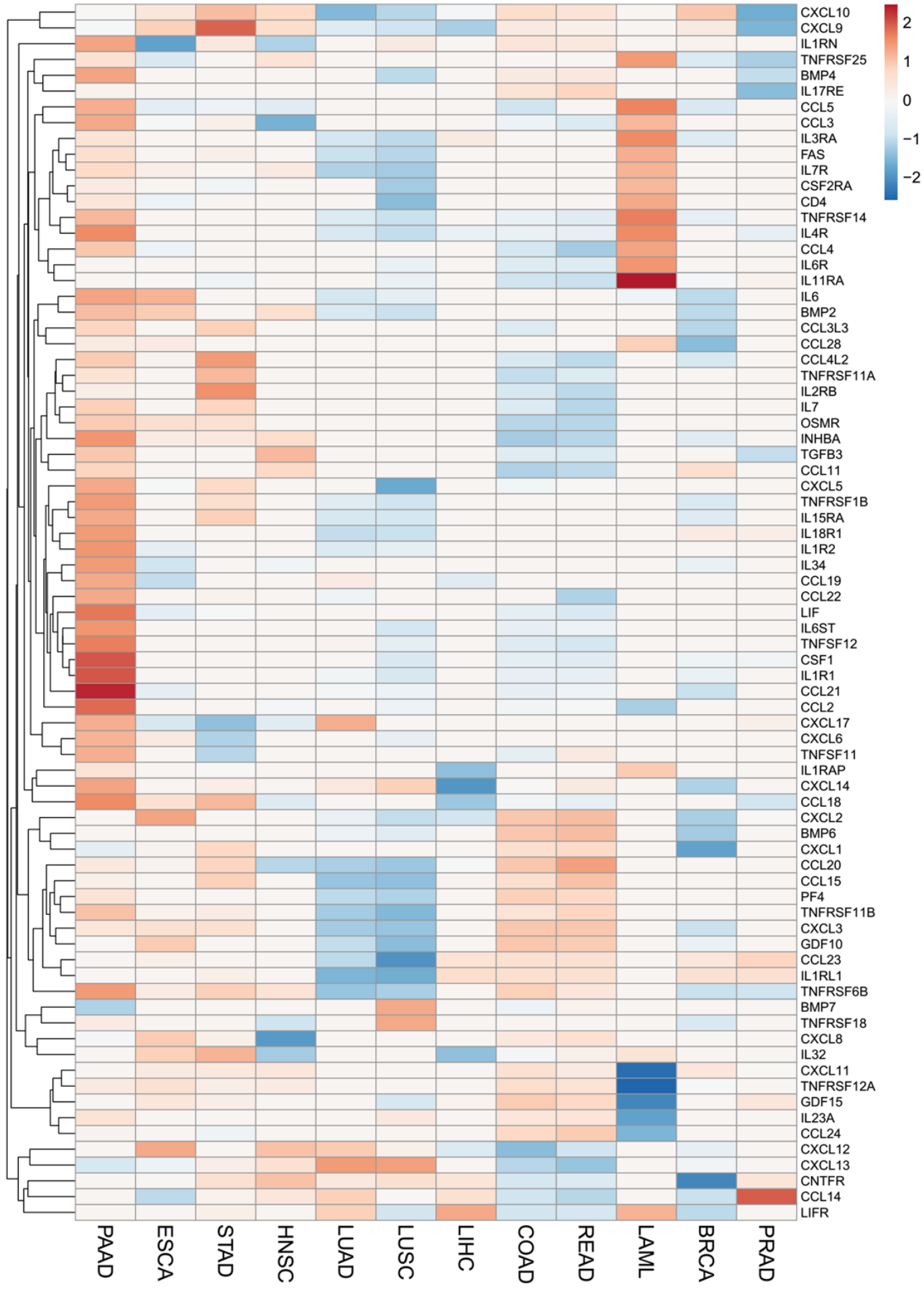
CXCL10
CXCL9
IL1RN
TNFRSF25
BMP4
IL17RE
CCL5
CCL3
IL3RA
FAS
IL7R
CSF2RA
CD4
TNFRSF14
IL4R
CCL4
IL6R
IL11RA
IL6
BMP2
CCL3L3
CCL28
CCL4L2
TNFRSF11A
IL2RB
IL7
OSMR
INHBA
TGFB3
CCL11
CXCL5
TNFRSF1B
IL15RA
IL18R1
IL1R2
IL34
CCL19
CCL22
LIF
IL6ST
TNFSF12
CSF1
IL1R1
CCL21
CCL2
CXCL17
CXCL6
TNFSF11
IL1RAP
CXCL14
CCL18
CXCL2
BMP6
CXCL1
CCL20
CCL15
PF4
TNFRSF11B
CXCL3
GDF10
CCL23
IL1RL1
TNFRSF6B
BMP7
TNFRSF18
CXCL8
IL32
CXCL11
TNFRSF12A
GDF15
IL23A
CCL24
CXCL12
CXCL13
CNTFR
CCL14
LIFR
2
1
0
−1
−2
PAAD
ESCA
STAD
HNSC
LUAD
LUSC
LIHC
COAD
READ
LAML
BRCA
PRAD

Supplementary Fig. 3 The cytokine-cytokine receptor interaction pathway is enriched in pancreatic adenocarcinoma. Heatmap of the mean expression levels [log2 (TPM+1)] of specifically upregulated (a) or downregulated (b) genes from the cytokine-cytokine receptor interaction pathway (The Kyoto Encyclopedia of Genes and Genomes, KEGG) in each tumor type (TCGA) compared with corresponding matched normal tissues (TCGA and GTEx). Differential expression levels were calculated using the web-based tool Gene Expression Profiling Analysis (GEPIA, http://gepia.cancerpku.cn/)[32]. Genes that are specifically upregulated or downregulated genes in each tumor type (absolute values of fold-change > 2.0 and q-value < 0.01; ANOVA) are shown in red and blue, respectively. PAAD: Pancreatic adenocarcinoma; ESCA: Esophageal carcinoma; STAD: Stomach adenocarcinoma; HNSC: Head and neck squamous cell carcinoma; LUAD: Lung adenocarcinoma; LUSC: Lung squamous cell carcinoma; LIHC: Liver hepatocellular carcinoma; COAD: Colon adenocarcinoma; READ: Rectum adenocarcinoma; LAML: Acute myeloid leukemia; PRAD: Prostate adenocarcinoma; BRCA: Breast invasive carcinoma.

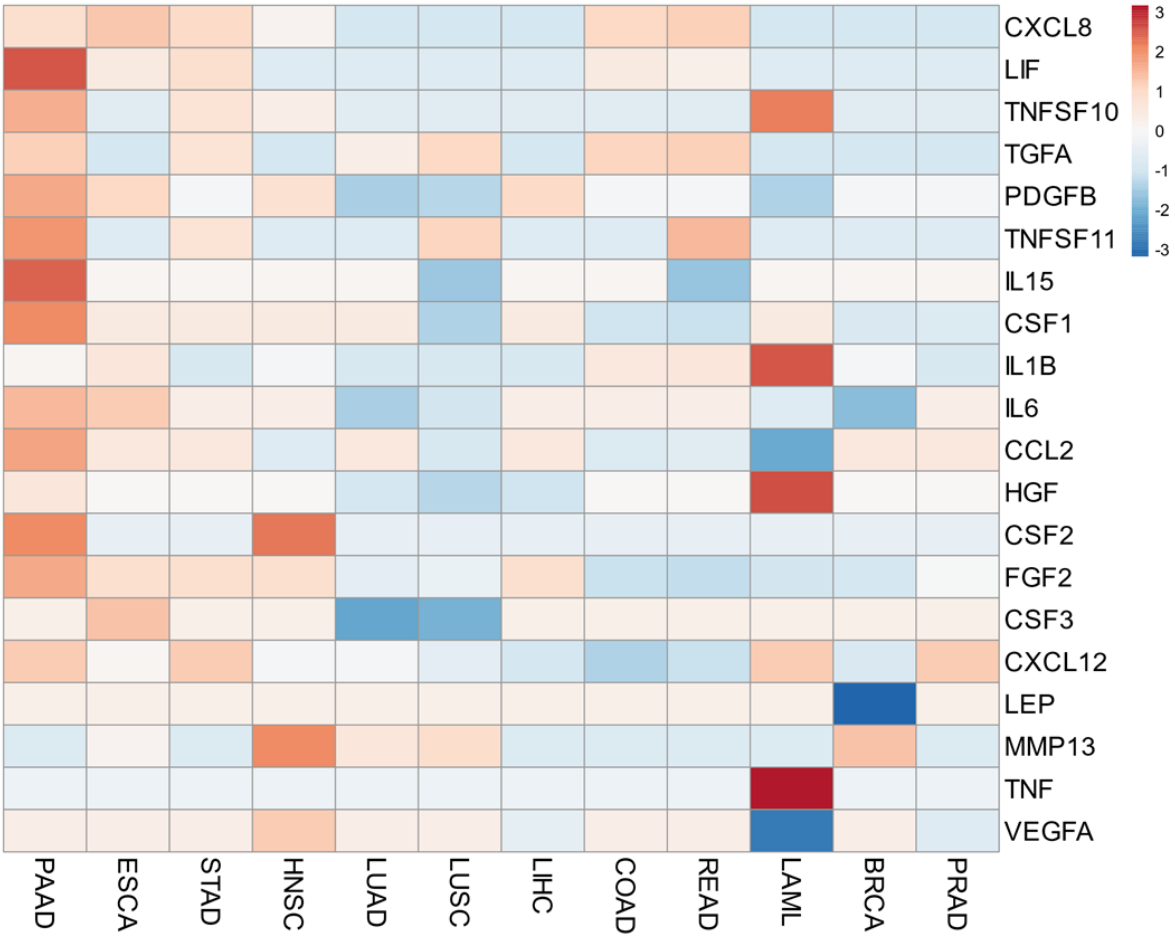

Supplementary Fig. 4 The expression landscape of cachexia-inducing factors in 12 tumor types. Heatmap of the mean expression levels [log2 (TPM+1)] of 25 cachexia-inducing factors (CIF) in 12 TCGA tumor types compared with corresponding matched normal tissues (TCGA and normal GTEx). Differential expression levels were calculated using the web-based tool Gene Expression Profiling Analysis (GEPIA, http://gepia.cancerpku.cn/)[32]. Genes that are specifically upregulated or downregulated genes in each tumor type (absolute values of fold-change > 2.0 and q-value < 0.01; ANOVA) are shown in red and blue, respectively. PAAD: Pancreatic adenocarcinoma; ESCA: Esophageal carcinoma; STAD: Stomach adenocarcinoma; HNSC: Head and neck squamous cell carcinoma; LUAD: Lung adenocarcinoma; LUSC: Lung squamous cell carcinoma; LIHC: Liver hepatocellular carcinoma; COAD: Colon adenocarcinoma; READ: Rectum adenocarcinoma; LAML: Acute myeloid leukemia; PRAD: Prostate adenocarcinoma; BRCA: Breast invasive carcinoma.

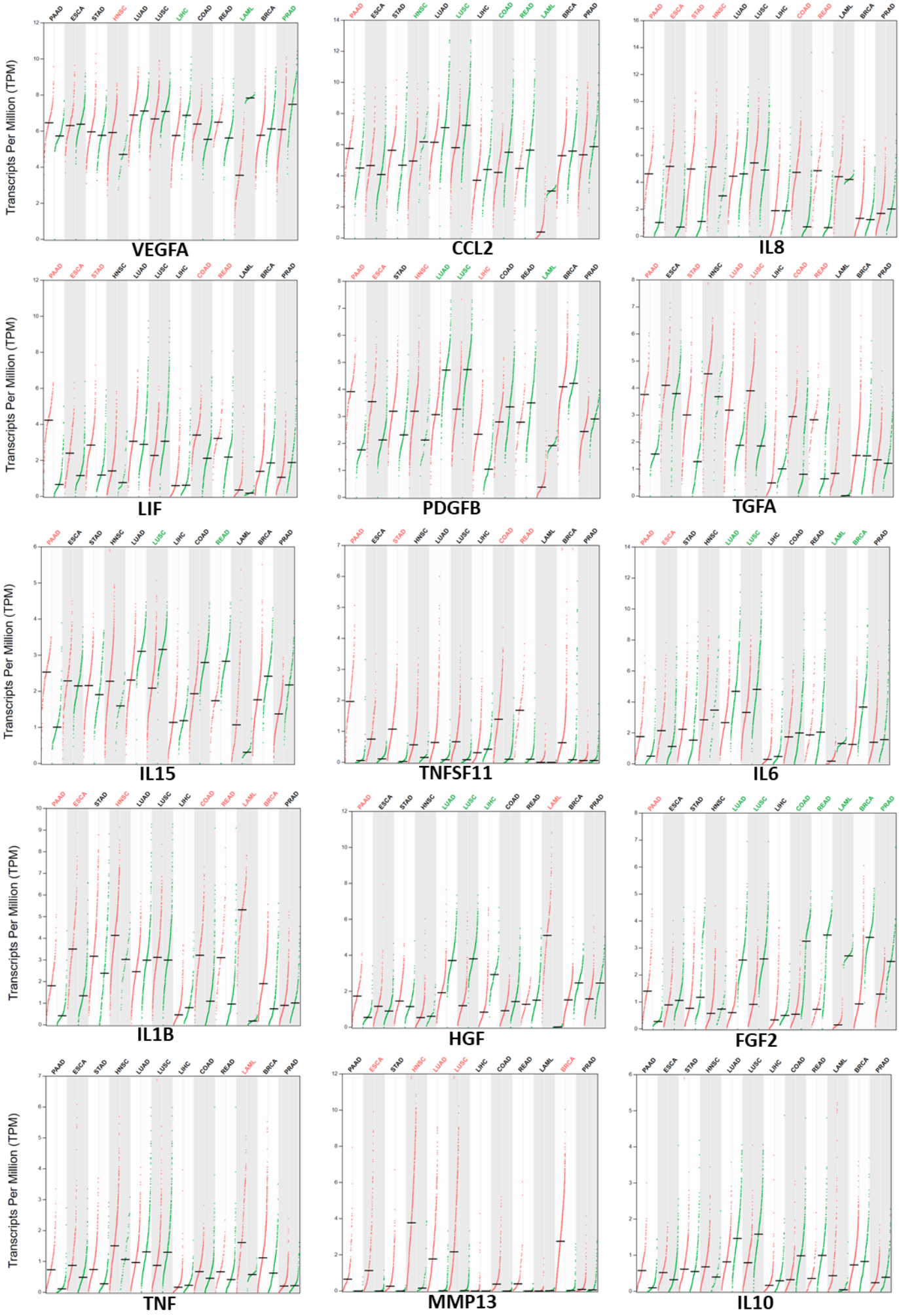
Transcripts Per Million (TPM)
PAAD ESCA STAD HNSC LUAD LUSC LIHC COAD READ LAML BRCA PRAD
VEGFA
CCL2
IL8
LIF
PDGFB
TGFA
IL15
TNFSF11
IL6
IL1B
HGF
FGF2
TNF
MMP13
IL10

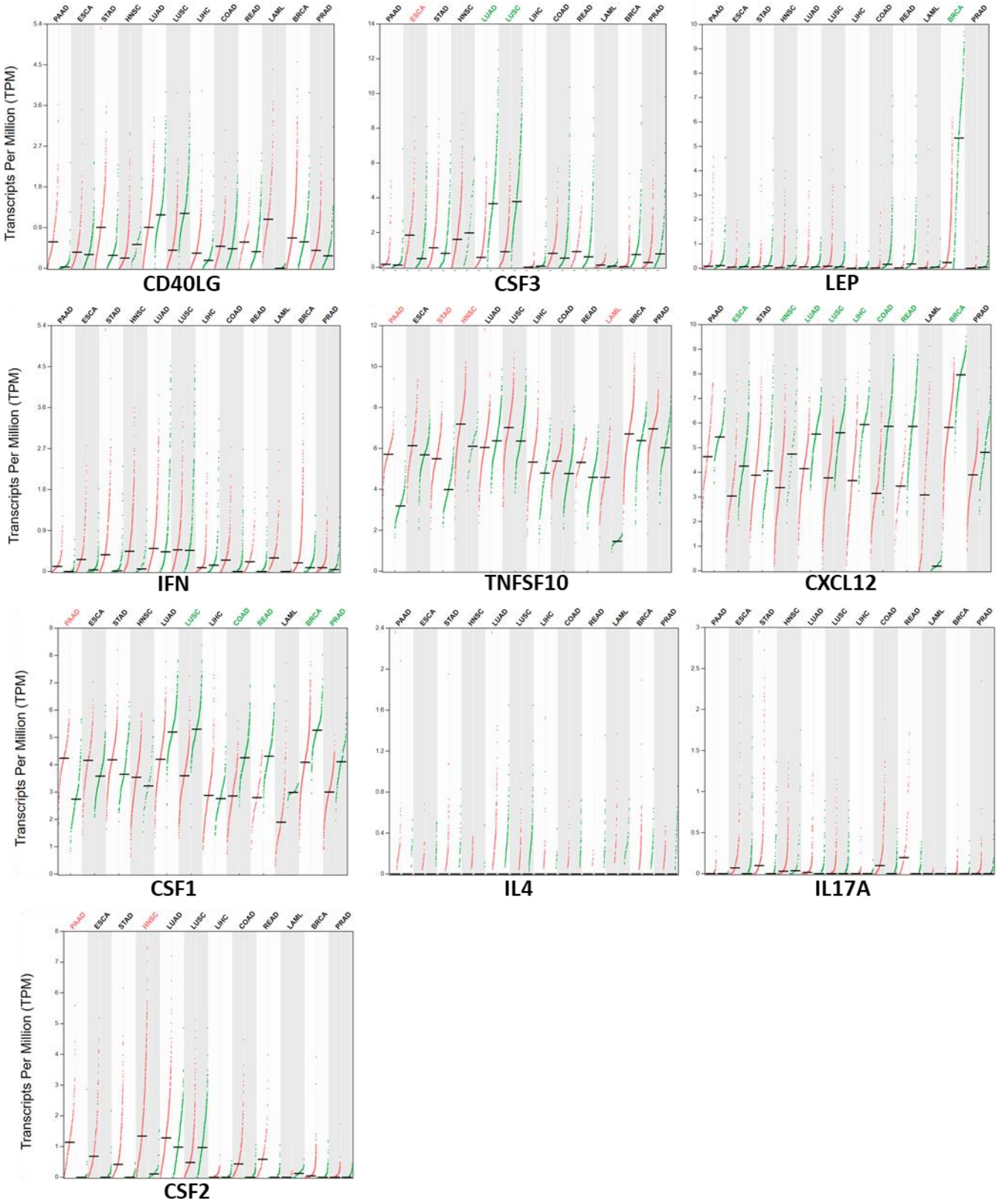

Supplementary Fig. 5 Gene expression profile of cachexia-inducing factors in 12 tumor types. Dot plots of the expression levels [log2 (TPM+1)] of 25 cachexia-inducing factors (CIF) in different 12 TCGA tumor types. Differential expression levels were calculated using the web-based tool Gene Expression Profiling Analysis (GEPIA, http://gepia.cancerpku.cn/)[32] from the tumor (TCGA; red dots) vs. matched normal (TCGA and GTEx; green dots) tissues. Upregulated and downregulated genes with absolute values of fold-change > 2.0 and q-value < 0.01 (ANOVA) are highlighted in red and green for the TCGA abbreviations, respectively.

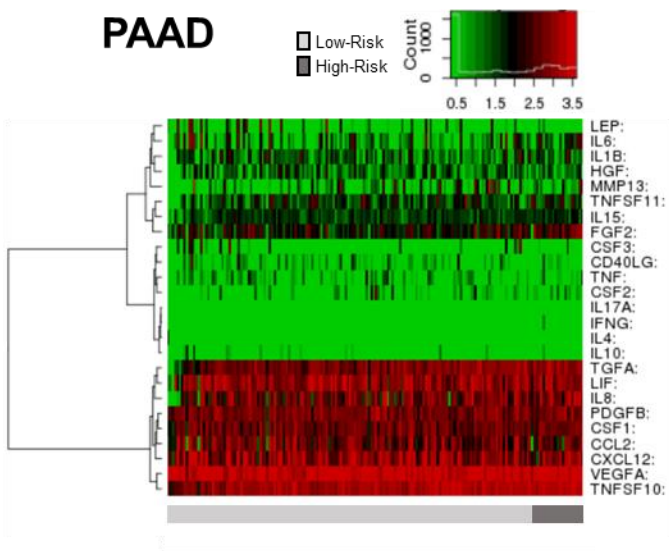
PAAD
Low-Risk
High-Risk
Count
0
1000
0.5 1.5 2.5 3.5
LEP:
IL6:
IL1B:
HGF:
MMP13:
TNFSF11:
IL15:
FGF2:
CSF3:
CD40LG:
TNF:
CSF2:
IL17A:
IFNG:
IL4:
IL10:
TGFA:
LIF:
IL8:
PDGFB:
CSF1:
CCL2:
CXCL12:
VEGFA:
TNFSF10:

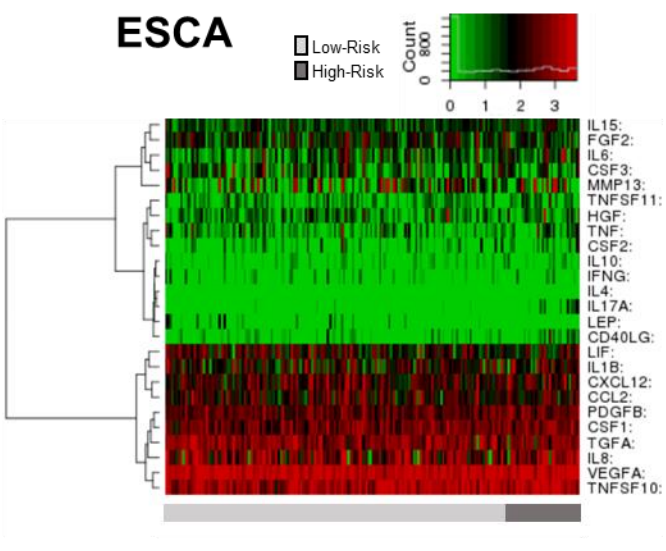
ESCA
Low-Risk
High-Risk
Count
0
800
0 1 2 3
IL15:
FGF2:
IL6:
CSF3:
MMP13:
TNFSF11:
HGF:
TNF:
CSF2:
IL10:
IFNG:
IL4:
IL17A:
LEP:
CD40LG:
LIF:
IL1B:
CXCL12:
CCL2:
PDGFB:
CSF1:
TGFA:
IL8:
VEGFA:
TNFSF10:

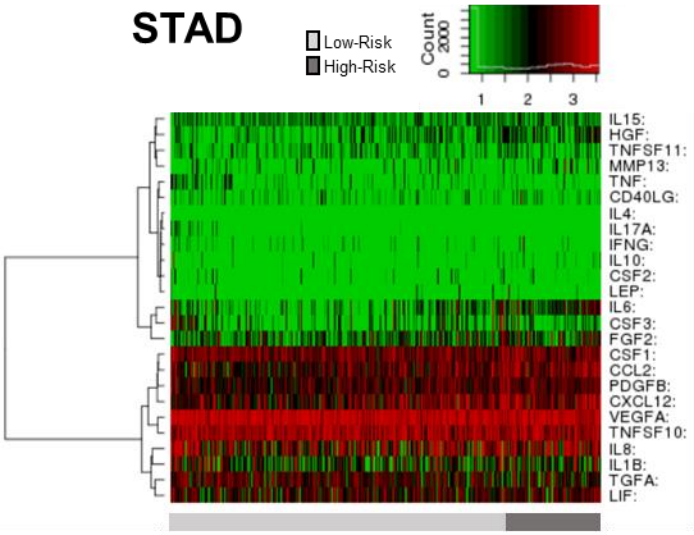
STAD
Low-Risk
High-Risk
Count
0
2000
1 2 3
IL15:
HGF:
TNFSF11:
MMP13:
TNF:
CD40LG:
IL4:
IL17A:
IFNG:
IL10:
CSF2:
LEP:
IL6:
CSF3:
FGF2:
CSF1:
CCL2:
PDGFB:
CXCL12:
VEGFA:
TNFSF10:
IL8:
IL1B:
TGFA:
LIF:

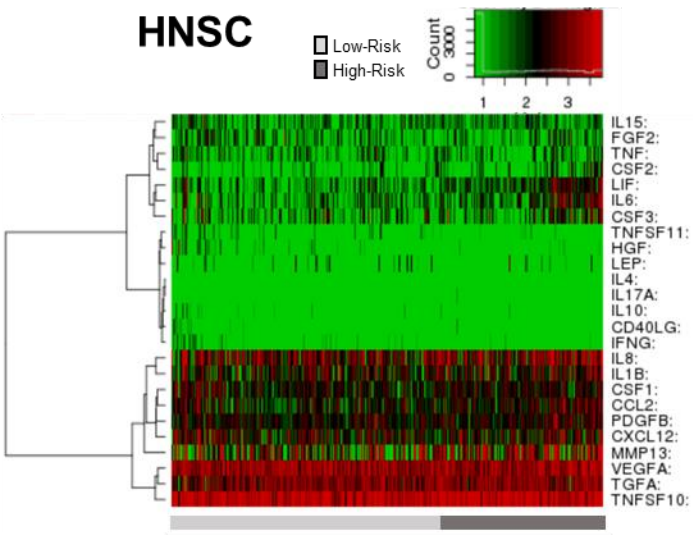
HNSC
Low-Risk
High-Risk
Count
0
3000
1 2 3
IL15:
FGF2:
TNF:
CSF2:
LIF:
IL6:
CSF3:
TNFSF11:
HGF:
LEP:
IL4:
IL17A:
IL10:
CD40LG:
IFNG:
IL8:
IL1B:
CSF1:
CCL2:
PDGFB:
CXCL12:
MMP13:
VEGFA:
TGFA:
TNFSF10:

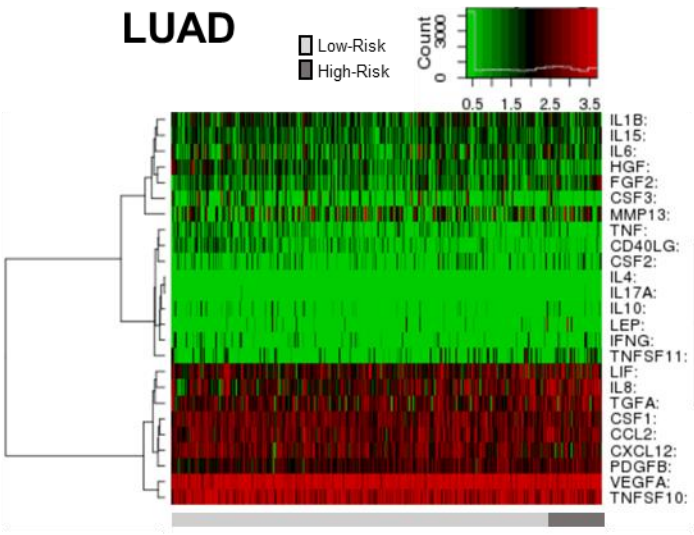
LUAD
Low-Risk
High-Risk
Count
0
3000
0.5 1.5 2.5 3.5
IL1B:
IL15:
IL6:
HGF:
FGF2:
CSF3:
MMP13:
TNF:
CD40LG:
CSF2:
IL4:
IL17A:
IL10:
LEP:
IFNG:
TNFSF11:
LIF:
IL8:
TGFA:
CSF1:
CCL2:
CXCL12:
PDGFB:
VEGFA:
TNFSF10:

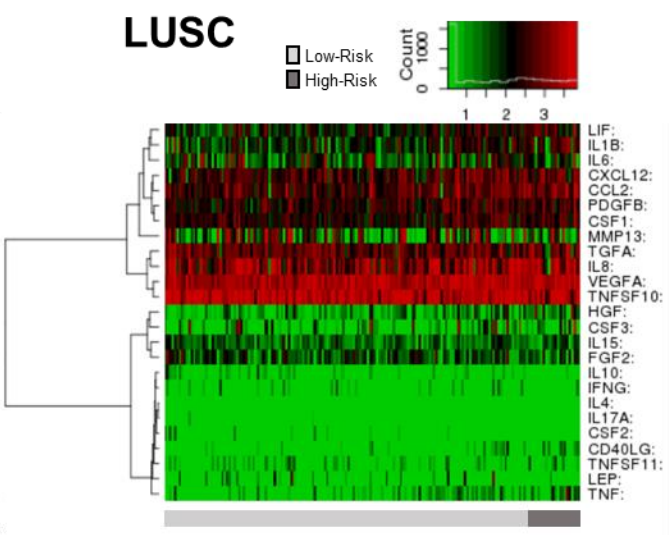
LUSC
Low-Risk
High-Risk
Count
0
1000
1 2 3
LIF:
IL1B:
IL6:
CXCL12:
CCL2:
PDGFB:
CSF1:
MMP13:
TGFA:
IL8:
VEGFA:
TNFSF10:
HGF:
CSF3:
IL15:
FGF2:
IL10:
IFNG:
IL4:
IL17A:
CSF2:
CD40LG:
TNFSF11:
LEP:
TNF:

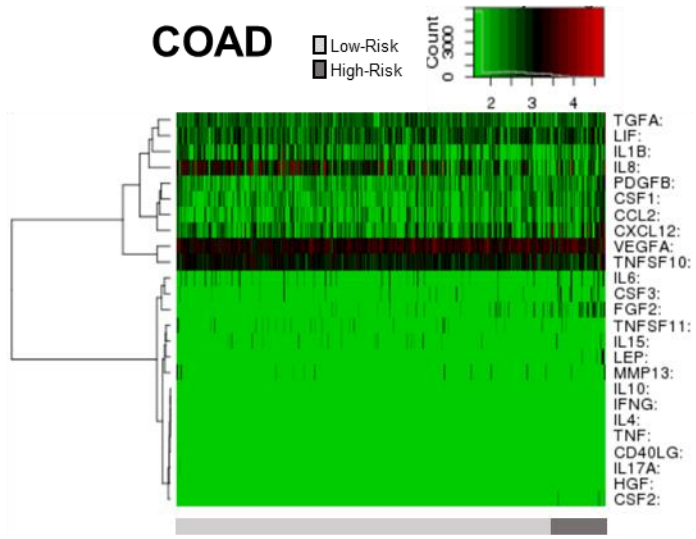
COAD
Low-Risk
High-Risk
Count
0
3000
2
3
4
TGFA:
LIF:
IL1B:
IL8:
PDGFB:
CSF1:
CCL2:
CXCL12:
VEGFA:
TNFSF10:
IL6:
CSF3:
FGF2:
TNFSF11:
IL15:
LEP:
MMP13:
IL10:
IFNG:
IL4:
TNF:
CD40LG:
IL17A:
HGF:
CSF2:

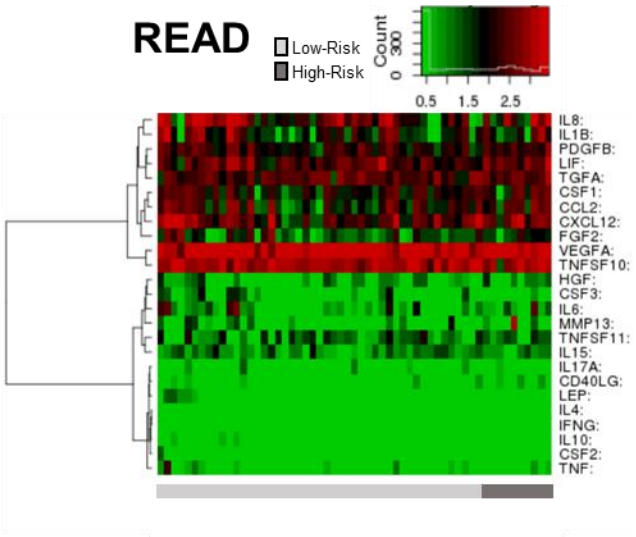
READ
Low-Risk
High-Risk
Count
0
300
0.5
1.5
2.5
IL8:
IL1B:
PDGFB:
LIF:
TGFA:
CSF1:
CCL2:
CXCL12:
FGF2:
VEGFA:
TNFSF10:
HGF:
CSF3:
IL6:
MMP13:
TNFSF11:
IL15:
IL17A:
CD40LG:
LEP:
IL4:
IFNG:
IL10:
CSF2:
TNF:

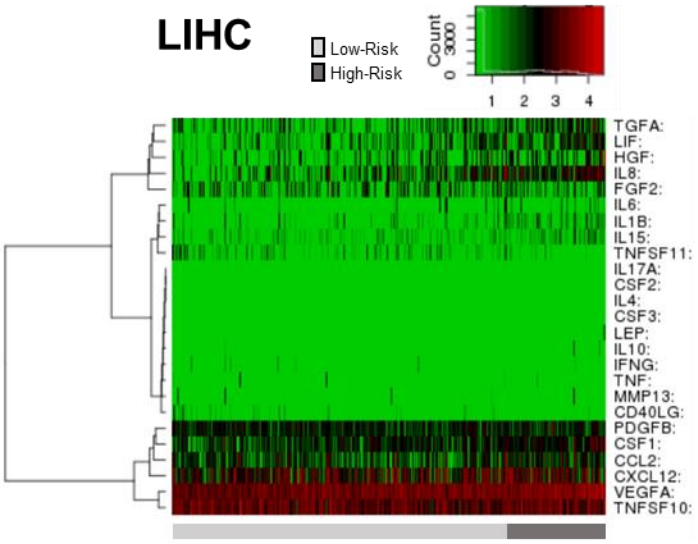
LIHC
Low-Risk
High-Risk
Count
0
3000
1
2
3
4
TGFA:
LIF:
HGF:
IL8:
FGF2:
IL6:
IL1B:
IL15:
TNFSF11:
IL17A:
CSF2:
IL4:
CSF3:
LEP:
IL10:
IFNG:
TNF:
MMP13:
CD40LG:
PDGFB:
CSF1:
CCL2:
CXCL12:
VEGFA:
TNFSF10:

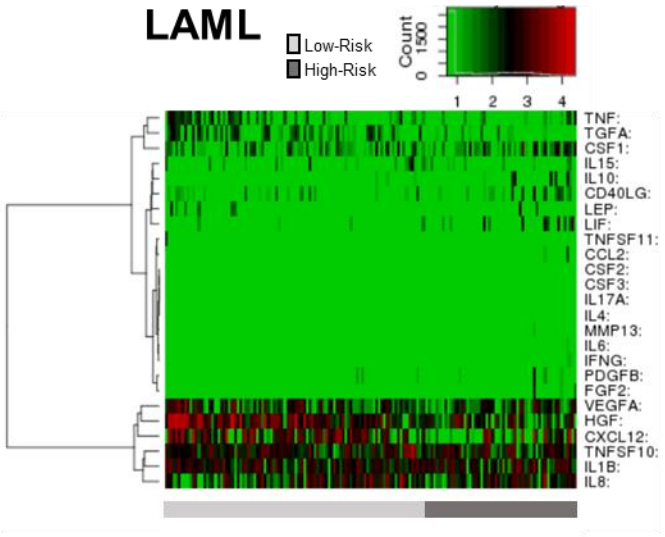
LAML
Low-Risk
High-Risk
Count
0
1500
1
2
3
4
TNF:
TGFA:
CSF1:
IL15:
IL10:
CD40LG:
LEP:
LIF:
TNFSF11:
CCL2:
CSF2:
CSF3:
IL17A:
IL4:
MMP13:
IL6:
IFNG:
PDGFB:
FGF2:
VEGFA:
HGF:
CXCL12:
TNFSF10:
IL1B:
IL8:

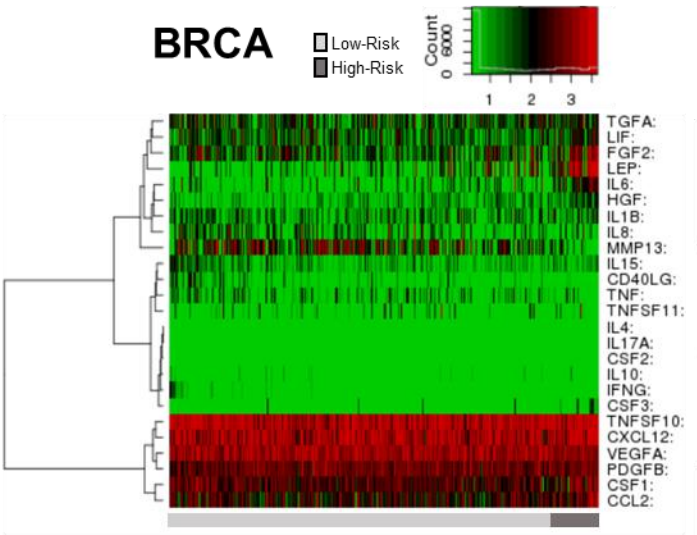
BRCA
Low-Risk
High-Risk
Count
0
6000
1
2
3
TGFA:
LIF:
FGF2:
LEP:
IL6:
HGF:
IL1B:
IL8:
MMP13:
IL15:
CD40LG:
TNF:
TNFSF11:
IL4:
IL17A:
CSF2:
IL10:
IFNG:
CSF3:
TNFSF10:
CXCL12:
VEGFA:
PDGFB:
CSF1:
CCL2:

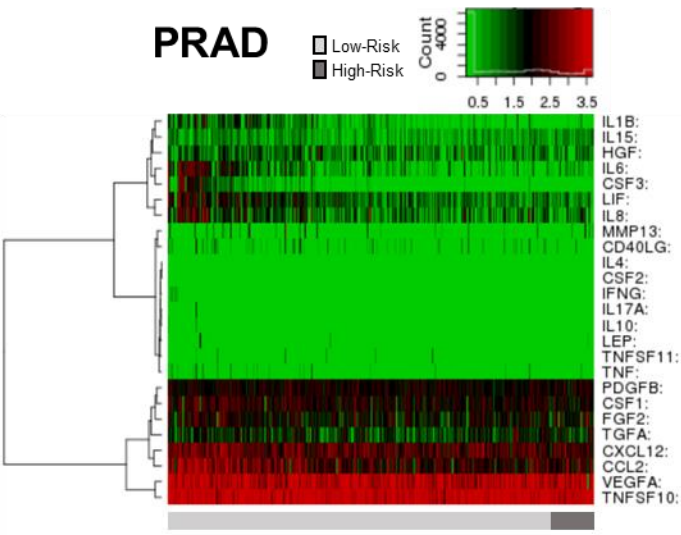
PRAD
Low-Risk
High-Risk
Count
0
4000
0.5
1.5
2.5
3.5
IL1B:
IL15:
HGF:
IL6:
CSF3:
LIF:
IL8:
MMP13:
CD40LG:
IL4:
CSF2:
IFNG:
IL17A:
IL10:
LEP:
TNFSF11:
TNF:
PDGFB:
CSF1:
FGF2:
TGFA:
CXCL12:
CCL2:
VEGFA:
TNFSF10:

Supplementary Fig. 6 Tumor-specific expression profile of cachexia-inducing factors stratified patients into low- and high-risk groups. Heatmaps are representing non-hierarchical clustering analysis of tumor mRNA expression of 25 cachexia-inducing factors (CIF) generated in SurvExpress[40], using 12 TCGA tumor types. The cancer patients were stratified into high- and low-risk groups, indicated below each heat map as dark-grey and light-grey bars, respectively. Risk groups were maximized based on the Prognostic Index assessed by gene expression values multiplied by beta coefficients. PAAD: Pancreatic adenocarcinoma; ESCA: Esophageal carcinoma; STAD: Stomach adenocarcinoma; HNSC: Head and neck squamous cell carcinoma; LUAD: Lung adenocarcinoma; LUSC: Lung squamous cell carcinoma; LIHC: Liver hepatocellular carcinoma; COAD: Colon adenocarcinoma; READ: Rectum adenocarcinoma; LAML: Acute myeloid leukemia; PRAD: Prostate adenocarcinoma; BRCA: Breast invasive carcinoma.

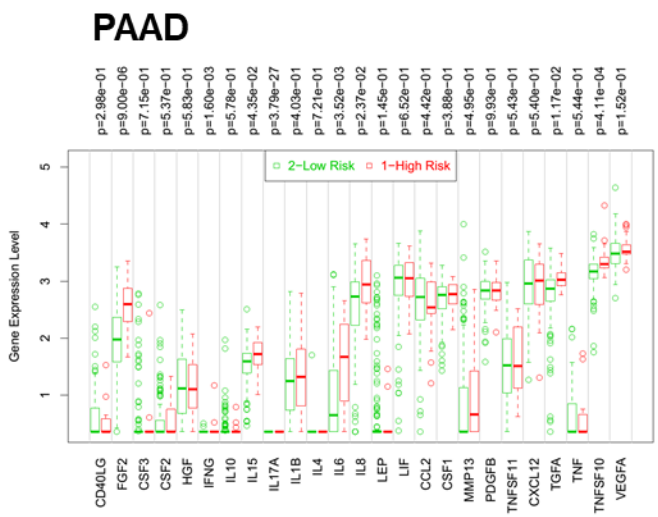
PAAD
p=2.98e−01 p=9.00e−06 p=7.15e−01 p=5.37e−01 p=5.83e−01 p=1.60e−03 p=5.78e−01 p=4.35e−02 p=3.79e−27 p=4.03e−01 p=7.21e−01 p=3.52e−03 p=2.37e−02 p=1.45e−01 p=6.52e−01 p=4.42e−01 p=3.88e−01 p=4.95e−01 p=9.93e−01 p=5.43e−01 p=5.40e−01 p=1.17e−02 p=5.44e−01 p=4.11e−04 p=1.52e−01
2−Low Risk
1−High Risk
Gene Expression Level
CD40LG FGF2 CSF3 CSF2 HGF IFNG IL10 IL15 IL17A IL1B IL4 IL6 IL8 LEP LIF CCL2 CSF1 MMP13 PDGFB TNFSF11 CXCL12 TGFA TNF TNFSF10 VEGFA

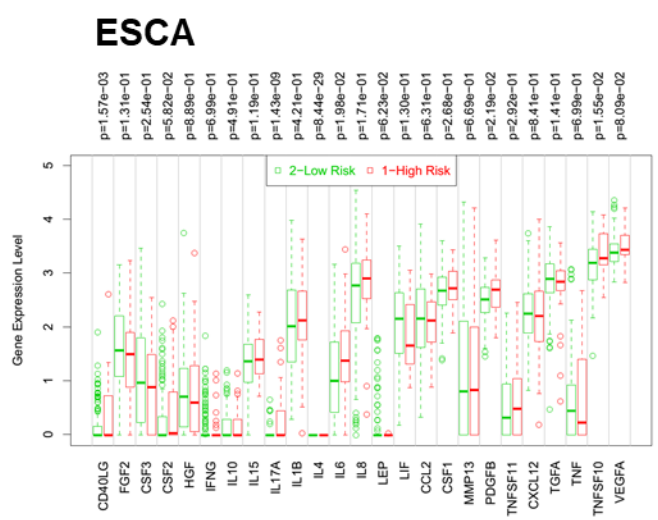
ESCA
p=1.57e−03 p=1.31e−01 p=2.54e−01 p=5.82e−02 p=8.89e−01 p=6.99e−01 p=4.91e−01 p=1.19e−01 p=1.43e−09 p=4.21e−01 p=8.44e−29 p=1.98e−02 p=1.71e−01 p=6.23e−02 p=1.30e−01 p=6.31e−01 p=2.68e−01 p=6.69e−01 p=2.19e−02 p=2.92e−01 p=8.41e−01 p=1.41e−01 p=6.99e−01 p=1.55e−02 p=8.09e−02
2−Low Risk
1−High Risk
Gene Expression Level
CD40LG FGF2 CSF3 CSF2 HGF IFNG IL10 IL15 IL17A IL1B IL4 IL6 IL8 LEP LIF CCL2 CSF1 MMP13 PDGFB TNFSF11 CXCL12 TGFA TNF TNFSF10 VEGFA

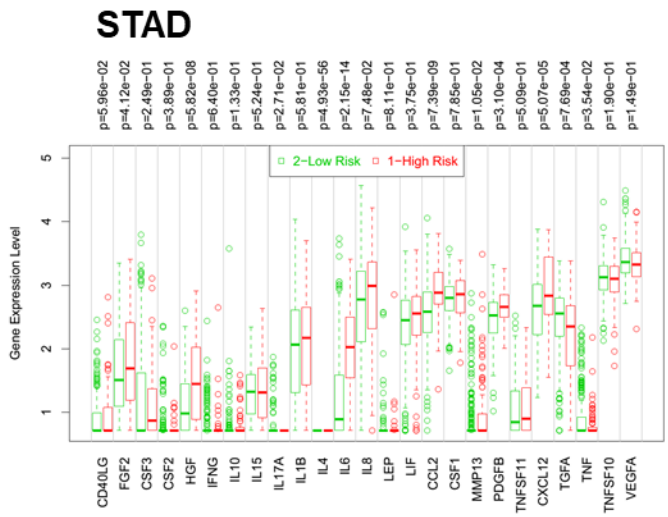
STAD
p=5.96e−02 p=4.12e−02 p=2.49e−01 p=3.89e−01 p=5.82e−08 p=6.40e−01 p=1.33e−01 p=5.24e−01 p=2.71e−02 p=5.81e−01 p=4.93e−56 p=2.15e−14 p=7.48e−02 p=8.11e−01 p=3.75e−01 p=7.39e−09 p=7.85e−01 p=1.05e−02 p=3.10e−04 p=5.09e−01 p=5.07e−05 p=7.69e−04 p=3.54e−02 p=1.90e−01 p=1.49e−01
2−Low Risk
1−High Risk
Gene Expression Level
CD40LG FGF2 CSF3 CSF2 HGF IFNG IL10 IL15 IL17A IL1B IL4 IL6 IL8 LEP LIF CCL2 CSF1 MMP13 PDGFB TNFSF11 CXCL12 TGFA TNF TNFSF10 VEGFA

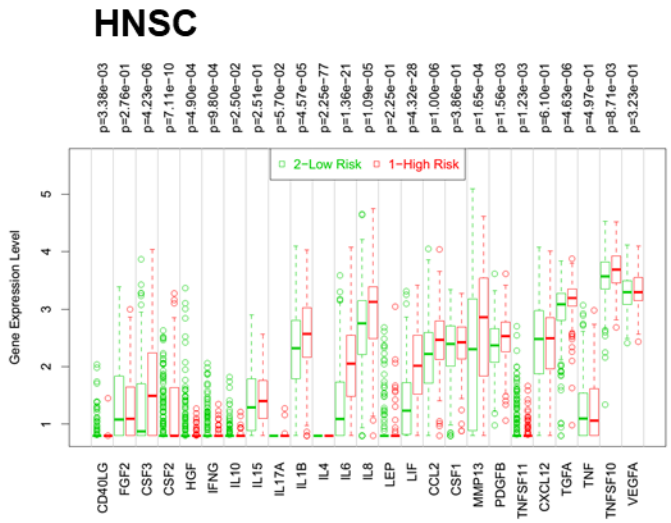
HNSC
p=3.38e−03 p=2.76e−01 p=4.23e−06 p=7.11e−10 p=4.90e−04 p=9.80e−04 p=2.50e−02 p=2.51e−01 p=5.70e−02 p=4.57e−05 p=2.25e−77 p=1.36e−21 p=1.09e−05 p=2.25e−01 p=4.32e−28 p=1.00e−06 p=3.86e−01 p=1.65e−04 p=1.56e−03 p=1.23e−03 p=6.10e−01 p=4.63e−06 p=4.97e−01 p=8.71e−03 p=3.23e−01
2−Low Risk
1−High Risk
Gene Expression Level
CD40LG FGF2 CSF3 CSF2 HGF IFNG IL10 IL15 IL17A IL1B IL4 IL6 IL8 LEP LIF CCL2 CSF1 MMP13 PDGFB TNFSF11 CXCL12 TGFA TNF TNFSF10 VEGFA

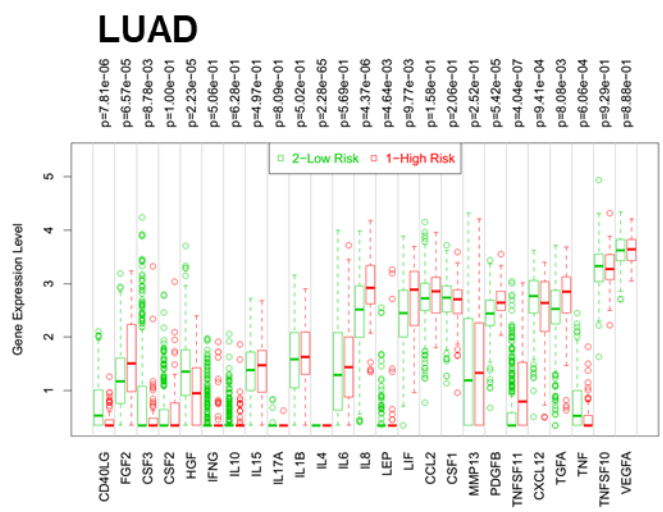
LUAD
p=7.81e−06 p=6.57e−05 p=8.78e−03 p=1.00e−01 p=2.23e−05 p=5.06e−01 p=6.28e−01 p=4.97e−01 p=8.09e−01 p=5.02e−01 p=2.28e−65 p=5.69e−01 p=4.37e−06 p=4.64e−03 p=9.77e−03 p=1.58e−01 p=2.06e−01 p=2.52e−01 p=5.42e−05 p=4.04e−07 p=9.41e−04 p=8.08e−03 p=6.06e−04 p=9.29e−01 p=8.88e−01
2−Low Risk
1−High Risk
Gene Expression Level
CD40LG FGF2 CSF3 CSF2 HGF IFNG IL10 IL15 IL17A IL1B IL4 IL6 IL8 LEP LIF CCL2 CSF1 MMP13 PDGFB TNFSF11 CXCL12 TGFA TNF TNFSF10 VEGFA

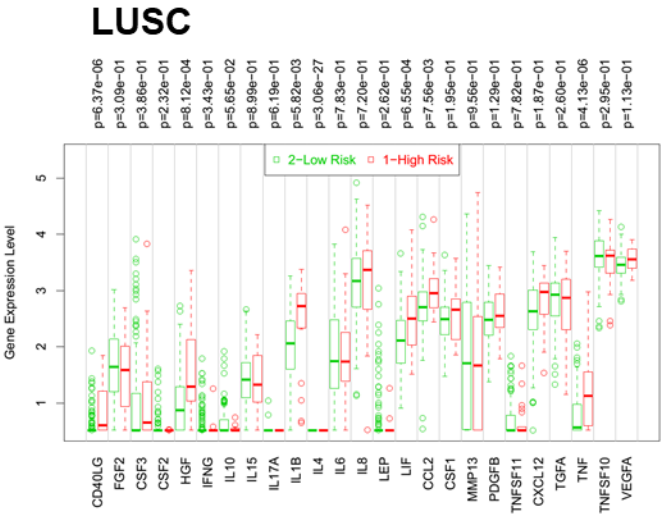
LUSC
p=6.37e−06 p=3.09e−01 p=3.86e−01 p=2.32e−01 p=8.12e−04 p=3.43e−01 p=5.65e−02 p=8.99e−01 p=6.19e−01 p=5.82e−03 p=3.06e−27 p=7.83e−01 p=7.20e−01 p=2.62e−01 p=6.55e−04 p=7.56e−03 p=1.95e−01 p=9.56e−01 p=1.29e−01 p=7.82e−01 p=1.87e−01 p=2.60e−01 p=4.13e−06 p=2.95e−01 p=1.13e−01
2−Low Risk
1−High Risk
Gene Expression Level
CD40LG FGF2 CSF3 CSF2 HGF IFNG IL10 IL15 IL17A IL1B IL4 IL6 IL8 LEP LIF CCL2 CSF1 MMP13 PDGFB TNFSF11 CXCL12 TGFA TNF TNFSF10 VEGFA

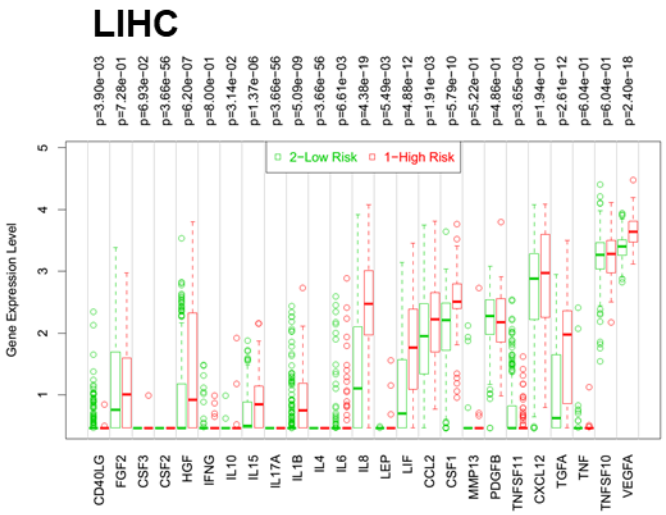
LIHC
p=3.90e−03 p=7.28e−01 p=6.93e−02 p=3.66e−56 p=6.20e−07 p=8.00e−01 p=3.14e−02 p=1.37e−06 p=3.66e−56 p=5.09e−09 p=3.66e−56 p=6.61e−03 p=4.38e−19 p=5.49e−03 p=4.88e−12 p=1.91e−03 p=5.79e−10 p=5.22e−01 p=4.86e−01 p=3.65e−03 p=1.94e−01 p=2.61e−12 p=6.04e−01 p=6.04e−01 p=2.40e−18
2−Low Risk
1−High Risk
Gene Expression Level
CD40LG FGF2 CSF3 CSF2 HGF IFNG IL10 IL15 IL17A IL1B IL4 IL6 IL8 LEP LIF CCL2 CSF1 MMP13 PDGFB TNFSF11 CXCL12 TGFA TNF TNFSF10 VEGFA

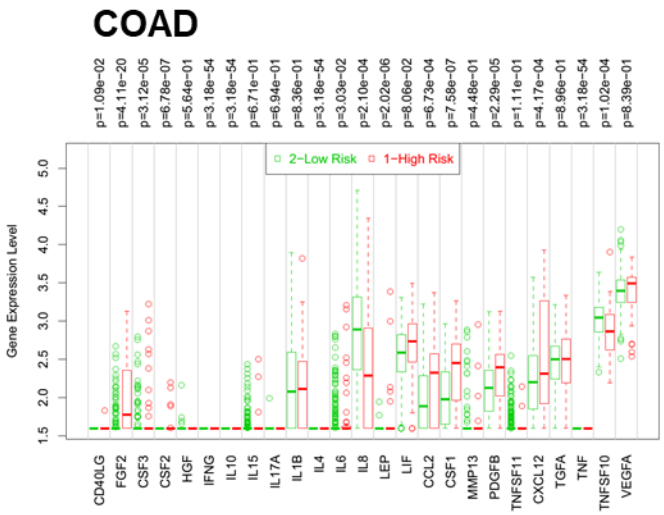
COAD
p=1.09e−02 p=4.11e−20 p=3.12e−05 p=6.78e−07 p=5.64e−01 p=3.18e−54 p=3.18e−54 p=6.71e−01 p=6.94e−01 p=8.36e−01 p=3.18e−54 p=3.03e−02 p=2.10e−04 p=2.02e−06 p=8.06e−02 p=6.73e−04 p=7.58e−07 p=4.48e−01 p=2.29e−05 p=1.11e−01 p=4.17e−04 p=8.96e−01 p=3.18e−54 p=1.02e−04 p=8.39e−01
2−Low Risk
1−High Risk
Gene Expression Level
CD40LG FGF2 CSF3 CSF2 HGF IFNG IL10 IL15 IL17A IL1B IL4 IL6 IL8 LEP LIF CCL2 CSF1 MMP13 PDGFB TNFSF11 CXCL12 TGFA TNF TNFSF10 VEGFA

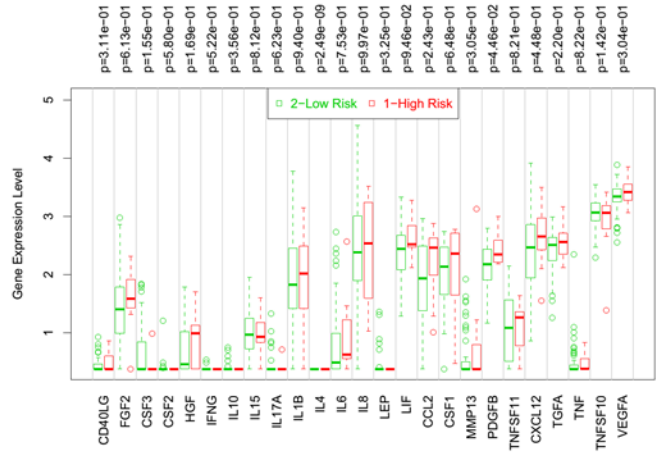
READ
p=3.11e−01 p=6.13e−01 p=1.55e−01 p=5.80e−01 p=1.69e−01 p=5.22e−01 p=3.56e−01 p=8.12e−01 p=6.23e−01 p=9.40e−01 p=2.49e−09 p=7.53e−01 p=9.97e−01 p=3.25e−01 p=9.46e−02 p=2.43e−01 p=6.48e−01 p=3.05e−01 p=4.46e−02 p=8.21e−01 p=4.48e−01 p=2.20e−01 p=8.22e−01 p=1.42e−01 p=3.04e−01
2−Low Risk
1−High Risk
Gene Expression Level
CD40LG FGF2 CSF3 CSF2 HGF IFNG IL10 IL15 IL17A IL1B IL4 IL6 IL8 LEP LIF CCL2 CSF1 MMP13 PDGFB TNFSF11 CXCL12 TGFA TNF TNFSF10 VEGFA

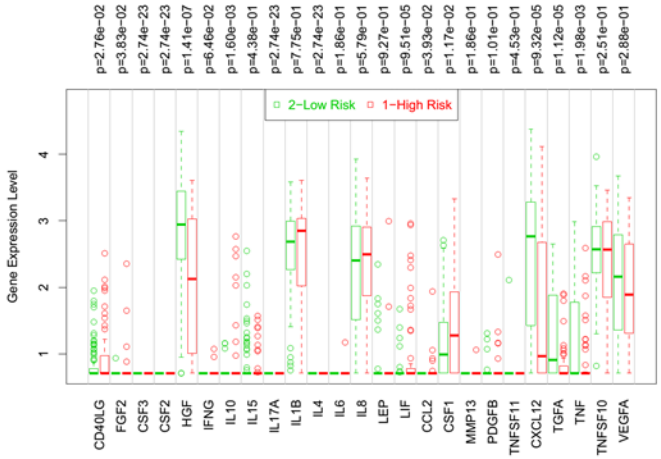
AML
p=2.76e−02 p=3.83e−02 p=2.74e−23 p=2.74e−23 p=1.41e−07 p=6.46e−02 p=1.60e−03 p=4.38e−01 p=2.74e−23 p=7.75e−01 p=2.74e−23 p=1.86e−01 p=5.79e−01 p=9.27e−01 p=9.51e−05 p=3.93e−02 p=1.17e−02 p=1.86e−01 p=1.01e−01 p=4.53e−01 p=9.32e−05 p=1.12e−05 p=1.98e−03 p=2.51e−01 p=2.88e−01
2−Low Risk
1−High Risk
Gene Expression Level
CD40LG FGF2 CSF3 CSF2 HGF IFNG IL10 IL15 IL17A IL1B IL4 IL6 IL8 LEP LIF CCL2 CSF1 MMP13 PDGFB TNFSF11 CXCL12 TGFA TNF TNFSF10 VEGFA

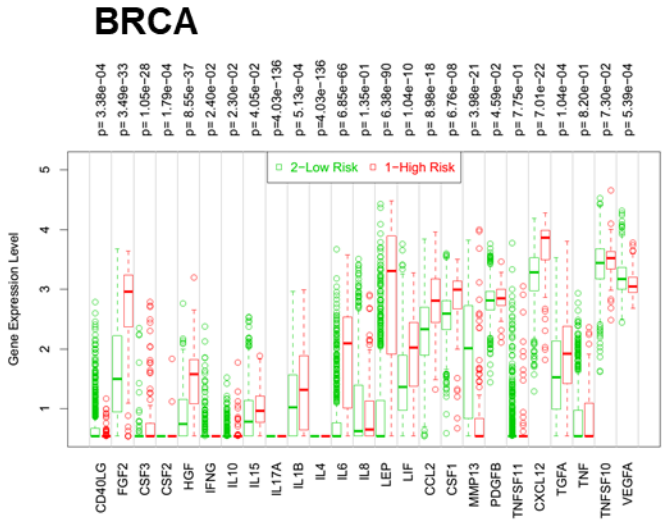
BRCA
p= 3.38e−04 p= 3.49e−33 p= 1.05e−28 p= 1.79e−04 p= 8.55e−37 p= 2.40e−02 p= 2.30e−02 p= 4.05e−02 p=4.03e−136 p= 5.13e−04 p=4.03e−136 p= 6.85e−66 p= 1.35e−01 p= 6.38e−90 p= 1.04e−10 p= 8.98e−18 p= 6.76e−08 p= 3.98e−21 p= 4.59e−02 p= 7.75e−01 p= 7.01e−22 p= 1.04e−04 p= 8.20e−01 p= 7.30e−02 p= 5.39e−04
2−Low Risk
1−High Risk
Gene Expression Level
CD40LG FGF2 CSF3 CSF2 HGF IFNG IL10 IL15 IL17A IL1B IL4 IL6 IL8 LEP LIF CCL2 CSF1 MMP13 PDGFB TNFSF11 CXCL12 TGFA TNF TNFSF10 VEGFA

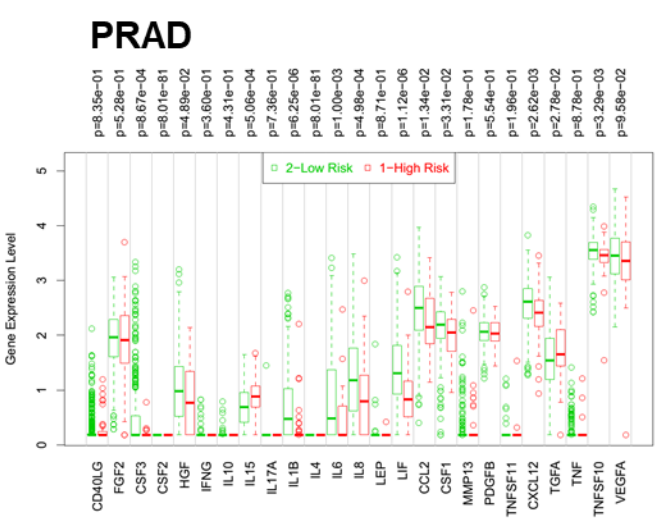
PRAD
p=8.35e−01 p=5.28e−01 p=8.67e−04 p=8.01e−81 p=4.89e−02 p=3.60e−01 p=4.31e−01 p=5.06e−04 p=7.36e−01 p=6.25e−06 p=8.01e−81 p=1.00e−03 p=4.98e−04 p=8.71e−01 p=1.12e−06 p=1.34e−02 p=3.31e−02 p=1.78e−01 p=5.54e−01 p=1.96e−01 p=2.62e−03 p=2.78e−02 p=8.78e−01 p=3.29e−03 p=9.58e−02
2−Low Risk
1−High Risk
Gene Expression Level
CD40LG FGF2 CSF3 CSF2 HGF IFNG IL10 IL15 IL17A IL1B IL4 IL6 IL8 LEP LIF CCL2 CSF1 MMP13 PDGFB TNFSF11 CXCL12 TGFA TNF TNFSF10 VEGFA

Supplementary Fig. 7 Cachexia-inducing factors tumor-specific expression profile from patients with low-risk and high-risk groups. Box plots representing tumor mRNA expression of 25 cachexia-inducing factors (CIF) generated by SurvExpress[40], using 12 TCGA datasets. The cancer patients were stratified into high- and low -risk groups, and are indicated as red and green, respectively. The statistical difference for each mRNA expression between high- and low-risk groups was tested using a *t*-test, and the resulting p-value is indicated. PAAD: Pancreatic adenocarcinoma; ESCA: Esophageal carcinoma; STAD: Stomach adenocarcinoma; HNSC: Head and neck squamous cell carcinoma; LUAD: Lung adenocarcinoma; LUSC: Lung squamous cell carcinoma; LIHC: Liver hepatocellular carcinoma; COAD: Colon adenocarcinoma; READ: Rectum adenocarcinoma; LAML: Acute myeloid leukemia; PRAD: Prostate adenocarcinoma; BRCA: Breast invasive carcinoma.

Conclusões Finais

Considerando os resultados obtidos a partir das três estratégias empregadas, este trabalho pode elucidar redes moleculares, mediadores e biomarcadores na caquexia associada ao câncer. A partir de dados de transcriptoma e microRNoma, identificamos vias moleculares envolvidas com a caquexia, como interações citocina-citocina, vias ativadas pela cascata JAK-STAT, respostas inflamatórias, vias de resposta à insulina e ciclo celular. Também identificamos novas interações mRNA-miRNA que estão envolvidas com o processo de atrofia muscular da síndrome, dentre elas destacamos as interações do miR-497 com transcritos que participam da via de sinalização IGF1-AKT-FOXO. Por fim, utilizando dados de transcriptoma, pudemos identificar um conjunto tumor-específico de mediadores de caquexia em 12 cânceres humanos com diferentes prevalências de caquexia. Dessa forma, esses resultados possibilitaram a obtenção de novas informações e melhor compreensão dos mecanismos moleculares e celulares que regulam o tecido muscular na caquexia. Além disso, os dados apresentados poderão ser úteis para o desenvolvimento de novas estratégias terapêuticas que minimizem a perda de massa muscular, aumentando assim a sobrevida e a melhora da qualidade de vida dos pacientes com caquexia.

Estágio no Exterior

Ago 2018 – Jan 2019 - **Harvard Medical School, Boston – USA**
PhD internship at Da-Zhi Wang's Laboratory
MicroRNA research in skeletal muscle cells and dystrophic knockout mice.
Supervisor: Da-Zhi Wang

Ago 2016 – Out 2016 - **BioGeM s.c.ar.l., Ariano Irpino – Italy**
Project: Experimental models for the study of human diseases
Regulomics Project

Atividades Docência

Aprimoramento didático;

Período: 03/2017 a 05/2017 (1º Semestre); 68 horas
Disciplina: Biologia Celular; Curso: Medicina
Responsável: Profa. Dra. Daniela C. dos Santos

Estágio Docência

Período: 05/2017 a 12/2017 (1º e 2º Semestre); 132 horas
Disciplina: Histologia; Curso: Medicina
Responsável: Prof. Dr. Luis Fernando Barbisan

Período: 02/2018 a 07/2018 (1º Semestre); 144 horas
Disciplina: Histologia e Biologia Celular; Curso: Medicina
Responsável: Prof. Dr. Luis Fernando Barbisan e Profa. Dra. Daniela C. dos Santos

Revisão de Periódico

2017 - FEBS Open Bio (IF: 1.95)

2019 - Journal of Cachexia, Sarcopenia and Muscle (IF:10.75)

2019 - Oncology Letters (IF:1.87)

2019 - Journal of Cellular and Molecular Medicine (IF:4.65)

Representação Discente

2017-2018**: Representante Discente do Conselho de Pós-Graduação – Programa de Genética**

Responsável pela interação entre coordenadores, professores e estudantes do programa de Pós-Graduação em Ciências Biológicas (Genética), além de participar da organização de eventos acadêmicos do Instituto de Biociências de Botucatu – IBB - UNESP Botucatu.

Artigos Publicados em Periódicos

Freire PP, Fernandez GJ, Cury SS, de Moraes D, Oliveira JS, de Oliveira G, Dal-Pai-Silva M, dos Reis PP, Carvalho RF. The Pathway to Cancer Cachexia: MicroRNA-regulated networks in muscle wasting based on integrative meta-analysis. Int J Mol Sci, 2019. (IF: 4.18)

Cury SS, de Moraes D, **Freire PP**, de Oliveira G, Marques DVP, Fernandez GJ, Dal-Pai-Silva M, Hasimoto ÉN, Dos Reis PP, Rogatto SR, Carvalho RF. Tumor transcriptome reveals high expression of IL-8 in non-small cell lung cancer patients with low pectoralis muscle area and reduced survival. Cancers. 2019. (IF: 6.16)

Vileigas DF, Harman VM, **Freire PP**, Marciano CLC, Sant'Ana PG, de Souza SLB, Mota GAF, da Silva VL, Campos DHS, Padovani CR, Okoshi K, Beynon RJ, Santos LD, Cicogna AC. Landscape of heart proteome changes in a diet-induced obesity model. Sci Rep. 2019. (IF: 4.01)

Scarano WR, Bedrat A, Alonso-Costa LG, Aquino AM, Fantinatti B, Justulin LA, Barbisan LF, **Freire PP**, Flaws J, Bernardo L. Exposure to an environmentally relevant phthalate misture during prostate development induces microRNA upregulation and transcriptome modulation in rats. Toxicol Sci 2019. (IF: 3.56)

Duran BOS, Góes GA, Zanella BTT, **Freire PP**, Valente JS, Salomão RAS, Fernandes A, Mareco EA, Carvalho RF, Dal-Pai-Silva M. Ascorbic acid stimulates the in vitro myoblast proliferation and migration of pacu (*Piaractus mesopotamicus*). Sci Rep, 2019. (IF: 4.01)

Silva-Gomes RN, Kuniyoshi MLG, Duran BOS, Zanella BTT, **Freire PP**, de Paula TG, Fantinatti BEA, Salomao RAS, Carvalho RF, Santos LD, Dal-Pai-Silva M. Prolonged fasting followed by refeeding modifies proteome profile and parvalbumin expression in the fast-twitch muscle of pacu (*Piaractus mesopotamicus*). PLoS One, 2019. (IF: 2.77)

Santos KC, Cury SS, Ferraz APCR, Corrente JE, Gonçalves BM, Machado LH, Carvalho RF, Nakamune ACMS, Fabro AT, **Freire PP**, Correa CR. Recovery of cardiac remodeling and dysmetabolism by pancreatic islet injury improvement in diabetic rats after yacon leaf extract treatment. Oxid Med Cell Longev, 2018. (IF: 4.86)

de Oliveira G, **Freire PP**, Omoto ACM, Cury SS, Fuziwara CS, Kimura ET, Dal-Pai-Silva M, Carvalho RF. Osteoglycin post-transcriptional regulation by miR-155 induces cellular architecture changes in H9c2 cardiomyoblasts. Gene, 2018. (IF: 2.63)

Cury SS, **Freire PP**, Martinucci B, Santos VC, Oliveira G, Ferretti R, Dal-Pai-Silva M, Pacagnelli FL, Delella FK, Carvalho RF. Fractal dimension analysis reveals skeletal muscle disorganization in mdx mice. Biochem Biophys Res Commun, 2018. (IF: 2.70)

Caldeira-Dias M, Luizon MR, Deffune E, Tanus-Santos JE, **Freire PP**, Carvalho RF, Bettiol H, Cardoso VC, Antonio Barbieri M, Cavalli RC, Sandrim VC. Preeclamptic plasma stimulates the expression of miRNAs, leading to a decrease in endothelin-1 production in endothelial cells. Pregnancy Hypertens. 2018. (IF: 1.99)

Ferreira JH, Cury SS, Vechetti-Júnior IJ, Fernandez GJ, Moraes LN, Alves CAB, **Freire PP**, Freitas CEA, Dal-Pai-Silva M, Carvalho RF. Low-level laser irradiation induces a transcriptional myotube-like profile in C2C12 myoblasts. Lasers Med Sci. 2018. (IF: 2.08)

Freire PP, Cury SS, Oliveira G, Moraes LN, Duran BOS, Fernandez GJ, Fuziwara CS, Ferreira JH, Kimura ET, Dal-Pai-Silva M, Carvalho RF. Osteoglycin inhibition by microRNA miR-155 impairs myogenesis. PLoS One, 2017. (IF: 2.77)

Moraes LN, Fernandez GJ, Vechetti-Júnior IJ, **Freire PP**, Souza RWA, Villacis RAR, Rogatto SR, Reis PP, Dal-Pai-Silva M, Carvalho RF. Integration of miRNA and mRNA expression profiles reveals microRNA-regulated networks during muscle wasting in cardiac cachexia. Sci Rep, 2017. (IF: 4.01)

Silva V, Ferron A, Cordeiro J, **Freire PP**, Campos DHS, Padovani CR, Sugizaki M, Cicogna AC, Lima-Leopoldo AP, Leopoldo AS. Moderate exercise training does not prevent the reduction of myocardial L-type Ca2+ channels protein expression at obese rats. Physiol Rep, 2017. (IF: 1.33)

Mazeto CFS, Campos DHS, **Freire PP**, Deus AF, Okoshi K, Padovani CR, Cicogna AC. Importance of Serca2A on early isolated diastolic dysfunction induced by supravalvar aortic stenosis in rats. Braz J Med Biol Res, 2017. (IF: 1.85)

Conti B, Santiago K, Cardoso E, **Freire PP**, Carvalho RF, Golim M, Sforcin JM. Propolis modulates miRNAs involved in TLR-4 pathway, NF-kappaB activation, cytokine production and in the bactericidal activity of human dendritic cells. J Pharm Pharmacol, 2016. (IF: 2.39)

Freire PP, Alves CAB, Deus AF, Lima-Leopoldo AP, Leopoldo AS, Silva DCT, Tomasi LCD, Campos DHS, Padovani CR, Cicogna A.C. Obesity does not Lead to Imbalance Between Myocardial Phospholamban Phosphorylation and Dephosphorylation. Arq Bras Cardiol, 2014. (IF: 1.68)

Lima-Leopoldo AP, Leopoldo AS, Silva DCT, Nascimento AF, Luvizotto RAM, Deus AF, **Freire PP**, Medeiros A, Cicogna AC. Long-Term Obesity Promotes Alterations in Diastolic Function Induced by Reduction of Phospholamban Phosphorylation Serine16 without Affecting Calcium Handling. J Appl Physiol (1985), 2014. (IF: 3.14)

Capítulo de Livro Publicado

Deus AF, Lima-Leopoldo AP, Leopoldo AS, Alves CAB, Mazeto CFS, Silva DCT, Campos DHS, Tomasi LCD, **Freire PP**, Cicogna AC. Sarcoplasmic reticulum calcium pump (SERCA) and Plasma membrane Ca2+ ATPase (PMCA). In: Calcium signaling: Biochemistry and Physiology Cell ed: Sarvier, 2012.

Artigos Aceitos para Publicação

Decreased myocardial type 1 collagen in obese rats is associated with increased of leptin and metalloproteinase-2 activity. Danielle T. Silva, Loreta D. Tomasi, Dijon H. Campos; Carlos A. B. Alves; Adriana F. Deus; **Paula P. Freire**; Carlos Padovani; Antonio C. Cicogna. Arquivos Brasileiro de Cardiologia. (Accepted for publication Jun 2019).

Artigos Submetidos

"The expression landscape of cachexia-inducing factors in human cancers", **Paula P Freire**, Geysson J Fernandez, Diogo de Moraes, Sarah S Cury, Maeli Dal-Pai-Silva, Silvia R Rogatto, Robson F Carvalho. *Journal of Cachexia, Sarcopenia and Muscle.* (Submitted Aug 2019)

"Control of myonuclear positioning and muscle function by skeletal muscle CIP protein", Jianming Liu, Zhan-Peng Huang, Mao Nie, Gang Wang, William J Silva, Qiumei Yang, **Paula P Freire,** Xiaoyun Hu, Huaqun Chen, Zhongliang Deng, William T Pu, Da-Zhi Wang. *PNAS.* (Submitted Dec 2019)

"MicroRNA-mRNA co-sequencing identifies transcriptional and post-transcriptional regulatory networks underlying muscle wasting in cancer cachexia", Geysson J Fernandez, Juarez H Ferreira, Ivan J Vechetti-Júnior, Leonardo N de Moraes, Sarah S Cury, **Paula P Freire**, Jayson Gutiérrez, Renato Ferretti, Maeli Dal-Pai-Silva, Silvia R Rogatto, Robson F Carvalho. *Scientific Reports*. (Submitted Jan 2020)

"An integrated meta-analysis of secretome and proteome identify potential biomarkers of pancreatic adenocarcinoma", Grasieli de Oliveira, **Paula P Freire**, Sarah S Cury, Diogo de Moraes, Jakeline S Oliveira, Maeli Dal-Pai-Silva, Robson F Carvalho. *Cancers* (Submitted Jan 2020)

We cannot solve our problems with the same thinking we used when we created them.

Albert Einstein